Investigating the Environmental Properties of Galaxies in the SDSS-MaNGA Survey

Thesis

The Open University

Investigating the Environmental Properties of Galaxies in the SDSS-MaNGA Survey

Ashley Spindler

Astronomy Discipline, School of Physical Sciences
The Open University

This thesis is submitted for the degree of
Doctor of Philosophy

May 2018

Abstract

This thesis presents a study of galaxy evolution in the local universe. I study how environments shape the structures of galaxies, and how internal and external processes affect star formation. I perform four investigations of galaxy properties: a study of the relations between size, mass and velocity dispersion of 124,524 galaxies from SDSS DR7; I estimate star formation rates using H_α and D_n4000 for galaxies in the MaNGA survey; a study of the spatial distribution of star formation in 1494 MaNGA galaxies; and finally, a study of 215 barred and 402 unbarred galaxies, to investigate how bars affect star formation.

I find that environment plays a key role in the evolution of galaxies, both structurally and in terms of their star formation. Using core velocity dispersion to study the effects of minor mergers and tidal/ram pressure stripping, I find that central galaxies are up to 30% larger and more massive than satellites. I suggest that minor mergers play a crucial role in the increase in size and mass of centrals. In addition, I find that satellites have a uniform radial suppression of star formation, compared to centrals, which may be due to the strangulation of their cold gas supplies.

I study the internal processes that affect star formation and find that specific star formation rate is suppressed at all radii for high mass galaxies. Massive galaxies are more likely to have suppressed star formation in their cores, which I determined is caused by a combination of morphological quenching and AGN feedback. Finally, I study the role of galaxy bars in regulating the cirumnuclear and disk star formation in late-type galaxies. I find that barred galaxies have lower star formation in their disks than unbarred galaxies, and that they are more likely to have enhanced star formation in their cores.

Dedicated to Sarah, for standing by me through it all …

Acknowledgements

Writing a thesis is a mammoth task, and no student has ever finished without the help and support of those around them. I would now like to acknowledge the people who made all of this possible, who kept me sane and on track, and who supported me when I needed them.

Firstly, I would like to thank my lead supervisor, David Wake. David's guidance and support in these three years were a vital part of my studies, without him I don't think I would have been able to finish. Importantly, David knew when to jump down a rabbit hole, and when to rein me in. I can't count the number of times David supported my wild ramblings on the next 'really cool thing' that I had found in my data, and gave me a push in the right direction to making said 'cool thing' into real science. I would also like to thank Stephen Serjeant, whose infectious enthusiasm and endless wisdom helped solve numerous challenges throughout my PhD.

To my fiancée, Sarah, I don't think a simple thank you is enough. You are the light of my life, and even in my darkest hours you have been a beacon which kept me going. I never would have gotten here without you.

A special thank you to Rhian Chapman, Amy Turner, Peter Woolman, George Pagomenos, Lawrence Bilton, George Jacobs, Laura Brooker and Rae James. The adventures we had were some of my favourite. We slew dragons, rescued kingdoms and escaped deadly dungeons. Perhaps it was all just an elaborate metaphor for finishing a Research Degree?

There are too many people to name that I want to thank in small ways, the students who shared the astronomy offices in Robert Hooke and K-block made coming into the office worth it. The weekly Cosmology Coffee meeting hosted by Stephen were often the highlights of my working week, and I wish everyone who attended all the best.

My final thank you goes out to the 'Nova Corps'. I started streaming on twitch.tv to pass away my free time, but what I didn't expect was the sense of community and great friends I got out of it. Thank you to those of you who supported me, by showing up and watching, talking in chat and giving me your subscriptions. Special thanks to the small few who even watched when I live streamed writing this thesis, and helped proofread my terrible grammar!

Table of contents

List of Publications

1. Spindler, A. and Wake, D. (2017). The differing relationships between size, mass, metallicity and core velocity dispersion of central and satellite galaxies. MNRAS, 468:333–345.

2. Spindler, A., Wake, D., Belfiore, F., Bershady, M., Bundy, K., Drory, N., Law, D. R., Masters, K., Sánchez-Gallego, J. R., Thomas, D., Westfall, K., and Wild, V. (2017). SDSSIV MaNGA: The Spatial Distribution of Star Formation and its Dependence on Mass, Structure and Environment. eprint arXiv:1710.05049. Accepted by MNRAS

List of figures

List of tables

1

Introduction

"A long time ago in a galaxy far, far away...."

– Star Wars, 1977

1.1 History

Astronomy is arguably the oldest form of science. Humans are inexorably drawn to the skies and our yearning to understand the nature of the heavens above is strong. In fact, evidence for humans studying the skies dates back thousands of years into pre-history. It is believed, for example, that the original purpose of the Stonehenge monument was an astronomical observatory (Baldwin et al., 1981; Gaffney et al., 2012), before the addition of the eponymous stones and the sites transforming into a place of predominantly religious worship (Baldwin et al., 1981; Gaffney et al., 2012; North, 1997).

Our drive as a species to understand our place in the cosmos has lead to many centuries of astronomers and scientists to categorise and classify the objects of the night sky. The earliest written records of astronomical observations trace back to the ancient Greeks, the works of Claudius Ptolemy, which categorised the motions of celestial objects in the 2nd Century CE. Ptolemy's cosmology (or model of The Universe) was a geocentric one, and remained the dominant and most influential model for 1200 years (Copernicus, 1543; Crowe, 1990)

It was in 964 CE that the Persian Astronomer Abd al-Rahman al-Sufi (Azophi) published his work the 'Book of Fixed Stars', which provided the first historical mention of a 'cloud' above the constellation of Pegasus. This cloud, later known as the Great Nebula of Andromeda and now referred to as the Andromeda Galaxy, was the first recorded observation of an object we now know to be outside of our own galaxy. Azophi also recorded the shapes

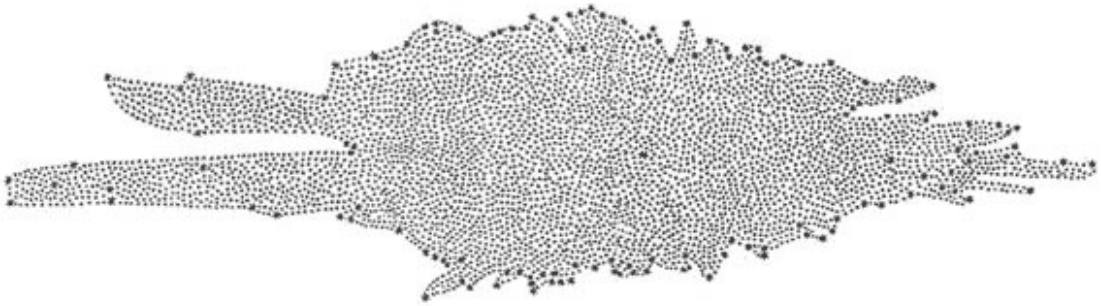

Fig. 1.1 The map of the Milky Way, as produced by William and Caroline Herschel, through the use of star counts. The solar system is the bold point near the centre of the image. From Herschel (1785).

of a number of star clusters and made reference to the Large and Small Magellanic Clouds, which are not in fact visible from his home in Iraq.

Since the invention of the telescope in the early 18th Century, many astronomers began to observe the nebulae and star clusters in detail. In 1771, French astronomer Charles Messier published his 'Catalog of Nebulae and Star Clusters', containing 103 nebulae and stellar clusters. Amusingly, Messier did not publish his list with the intention of studying the objects. He was a comet hunter and was frustrated by the similarities between nebulae and comet tails. His list was a list of objects that he wished to avoid when combing the night sky for new comets. In the 20th Century the list was added to, from observations of objects listed in Messier's notes, expanding to 110 in total.

Included in the Messier Objects are many clouds we now know to be distinct galaxies, such as Andromeda and the Triangulum Galaxy. When the catalog was published it was believed that these nebulae were clouds within the Milky Way, which was thought to be the only galaxy in the Universe. Studies of the Milky Way were underway at the time, with astronomers coming to realise the Galaxy itself was a flat disk. One such study was undertaken by Caroline and William Herschel, using Herschel's famous 20m telescope. The siblings mapped stars in all directions from Earth, and using some flawed assumptions attempted to map our own galaxy. Figure 1.1 shows the map that Herschel produced by counting stars in each direction. The map is of course inherently flawed, as Herschel had assumed that not only did every star have the same inherent brightness, but that the Galaxy was of uniform density, and that he could see the Galaxy's edge.

With the invention of photography in the 19th Century, astronomical research took to new heights. Astrophotography pioneer Isaac Roberts took the first long exposure photograph of the Great Nebula of Andromeda in 1888, which is shown in Figure 1.2. This photograph

Fig. 1.2 A long exposure photograph of the Great Nebula of Andromeda, captured by pioneering astrophotographer Isaac Roberts. From Roberts (1899)

was the first to reveal the spiral structure of the nebula, which was an unexpected feature. It was around this time that the term 'spiral nebulae' was coined, and much effort was made by astronomers to study the nature of these clouds. Of particular interest were the observations that revealed that the nebulae contained individual stars.

In the 1920's Edwin Hubble used the direct relationship between the luminosity of Cepheid variable stars and their distance to measure how far away the Andromeda nebula and other spiral nebulae were (Hubble, 1925). To the surprise of Hubble, and the astronomical community as a whole, the Andromeda nebula was found to be 700,000 light years from Earth, much further than the edge of the known Galaxy (Hubble underestimated this distance, however, as the true distance to Andromeda is 2.5 million light years). Further observations of spiral and elliptical nebulae confirmed this, showing that there existed more than one galaxy and that a new field of astronomy had been born: The Extra-Galactic.

While Hubble and his contemporaries were working on observational astronomy, a new field of science was being born in Germany. Albert Einstein was composing his General Theory of Relativity (Einstein, 1913). Einstein's formulation of gravity gave birth to the field of cosmology, the study of the very nature of the cosmos. Einstein, however, was a fan of the steady state theory of The Universe. He added in a cosmological constant to the mathematics

of his theory to prevent the expansion or collapse of The Universe (mathematically speaking), and vowed to find a physical interpretation of that constant.

Worlds collided when Hubble, now studying the spectral make up of the light from the exrta-galactic nebulae, discovered his next ground breaking findings. By measuring Doppler shifts, the shift in the colour of light due to relative motion, Hubble showed that most galaxies have been red shifted, proving that they are moving away from the Milky Way. This motion was found to occur in all directions, implying that all galaxies other than the most local are receding from each other. Einstein's cosmological constant was found to be in error, The Universe itself was expanding, not in a steady state.

These observations made up the basis of modern cosmology and extra-galactic astronomy. With the addition of dark matter, first hypothesised in the early 20th Century and confirmed by Vera Rubin and Kent Ford in the 1980s (Rubin et al., 1980), and dark energy in the 1990s (Riess et al., 1998), cosmology evolved once again. Baryonic matter took a back seat in the workings of the cosmos, making up only $\sim 5\%$ of energy in The Universe. The influence of dark matter in particular was of great interest to extra-galactic astronomy, as it not only explained the rotation curves of spiral galaxies, but provided a mechanism by which galaxy groups and clusters can form. The role of these groups and clusters in the evolution of galaxies makes up the inspiration of this work.

1.2 Modern Sky Surveys

In the late 1990s and the early 2000s the digital revolution hit astronomy in a big way. Gone were the days of photographic plates and observing individual objects one at a time. CCDs, spectrographs and other technologies allowed astronomers to begin mapping the skies in a way that had not happened before. Sky surveys, be they all sky redshift surveys, photometric surveys, deep imaging, or space based telescopic surveys, changed the way we looked at the skies. The tidal wave of data from these massive surveys revolutionised astronomy, as we were no longer limited to studying small samples of individual objects, but could study thousands to millions of objects statistically.

One such survey was the 2-degree Field Galaxy Redshift Survey (Colless et al., 2001, 2dFGRS), which began observations in 1997. The survey was carried out at the Australian Astronomical Observatory, formerly the Anglo-Australian Observatory, in New South Wales, using a multi-object spectrograph capable of taking spectra from 400 objects at once. Over 5 years of observations 2dFGRS measured the spectra from over 245,591 objects, including 232,155 galaxies. The survey's primary goals were in the realms of cosmology, and it contributed to the evidence in favour of the standard model of cosmology (ΛCDM) by

measuring baryonic acoustic oscillations, the density of non-relativistic matter and putting limits on the total mass of massive neutrinos.

While 2dFGRS was scanning the sky in optical wavelengths, the Two Micron All Sky Survey (Skrutskie et al., 2006, 2MASS) was mapping point sources across the entire sky in the infrared. Observations were made using a pair of 1.3m telescopes, one in Mount Hopkins, Arizona, and the other in Cerro Tololo, Chile. The survey used three infrared bands, (J (1220 nm), H (1630 nm), K_s (2190 nm)) and catalogued 471 million point sources and 1.6 million extended sources. Like 2dFGRS, the real strength of these surveys is not in their initial science results, but in the release of large catalogues of objects with measured properties to the public domain. Releasing this data allowed astronomers from around the world to access and study the cosmos without needing to re-observe to same objects.

Many sky surveys are performed from ground based telescopes, however this is not the only way to study the cosmos. Using space based telescopes it is possible to gain a unique perspective compared to the ground. Indeed, perhaps the biggest limitation of ground based observatories is the Earth's atmosphere itself. Refraction from the gases in our atmosphere and absorption from water vapour and other molecules limits not only the resolution possible in telescopes, but also the wavelengths that can be observed. From space, however, these limitations are not present. For example, the Wide-field Infrared Survey Explorer (Wright et al., 2010, WISE) mapped the sky in multiple near-infrared wavebands which are absorbed by atmospheric water vapour. WISE's all sky catalog is used to this day for a variety of extra-galactic studies, such as measuring star formation rates in dusty galaxies and studying Active Galactic Nuclei.

Perhaps the most influential sky survey, however, is the Sloan Digital Sky Survey (York and SDSS Collaboration, 2000, SDSS), which began observations in 2000 on the 2.5-meter Sloan Foundation Telescope at Apache Point Observatory in New Mexico (Gunn et al., 2006). SDSS began by capturing images in 5 bands from over 8000 square degrees, and measured the spectra of 800,000 galaxies. Until 2009 the telescope operated in both imaging and spectroscopic mode, but since then has operated purely as a spectrographic observatory. As SDSS evolved over the years more projects were added, such as the APO Galactic Evolution Experiment (APOGEE) and Baryon Oscillation Spectroscopic Survey (BOSS), which aimed to study everything from the evolution of the Milky-Way to the very cosmological constants which define The Universe.

SDSS has played a major role in the study of extra-galactic astronomy, releasing public databases of millions of categorised galaxies. Multiple Value Added Catalogues (VACs) have been released which study the reduced SDSS data and provide catalogues of many frequently used galaxy properties. For example the New York University Value Added Catalog (Blanton

et al., 2005b, NYU-VAGC) compiles spectroscopic and photometric measurements from SDSS galaxies and cross-matches them with other surveys, such as 2dFGRS and 2MASS. The MPA-JHU catalog, alternatively, provides measurement of galaxy properties such as stellar mass, star formation and emission line fluxes for 818,333 unique objects.

The Fourth Sloan Digital Sky Survey (Blanton et al., 2017) began operations in 2014, and includes three seperate projects. APO Galactic Evolution Experiment 2 (APOGEE-2) which continues the Galactic stellar survey programs of previous Sloan surveys, the extended Baryon Oscillation Spectroscopic Survey (Dawson et al., 2016, eBOSS) which studies the properties of quasars and galaxies at high redshift in a cosmological survey, and Mapping Nearby Galaxies at Apache Point Observatory (Bundy et al., 2015, MANGA) which is an integral field spectroscopy survey studying 10,000 nearby galaxies to measure spatially resolved spectra.

The work in this thesis is based on single fibre spectroscopy from the Data Release 7 of SDSS (Abazajian et al., 2009, DR7), and MaNGA IFU spectroscopy from Data Release 14 (Abolfathi et al., 2017, DR14). The technical details of the MaNGA survey are summarised in Section 1.4.

1.3 Galaxy Evolution and the Role of Environment

1.3.1 Galaxy Structure

Since Hubble identified that the spiral and elliptical nebulae were in fact galaxies in their own right in the 1920s there has been much effort into understanding their structure, composition, and evolution. Hubble himself constructed a view of galaxy structure and evolution using a technique now referred to as 'Hubble's Tuning Fork Diagram' (Hubble, 1926).

'Early type' galaxies make up the left side of the fork; these are galaxies which have a smooth, featureless distribution of stars and are typically elliptical or lenticular in shape. The right side of the fork is split into two groups, the barred and unbarred spirals, which are together referred to as 'late types'. Late types have disk like morphologies, which may include spiral arms, bars, rings or bulges. It is important to note, however, that the early and late type names are something of a misnomer, as they do not in fact refer to any assumption based on the evolution of these galaxies. Hubble himself said of the names:

> The nomenclature, it is emphasized, refers to position in the sequence, and temporal connotations are made at one's peril. The entire classification is purely empirical and without prejudice to theories of evolution.
>
> *Hubble (1927).*

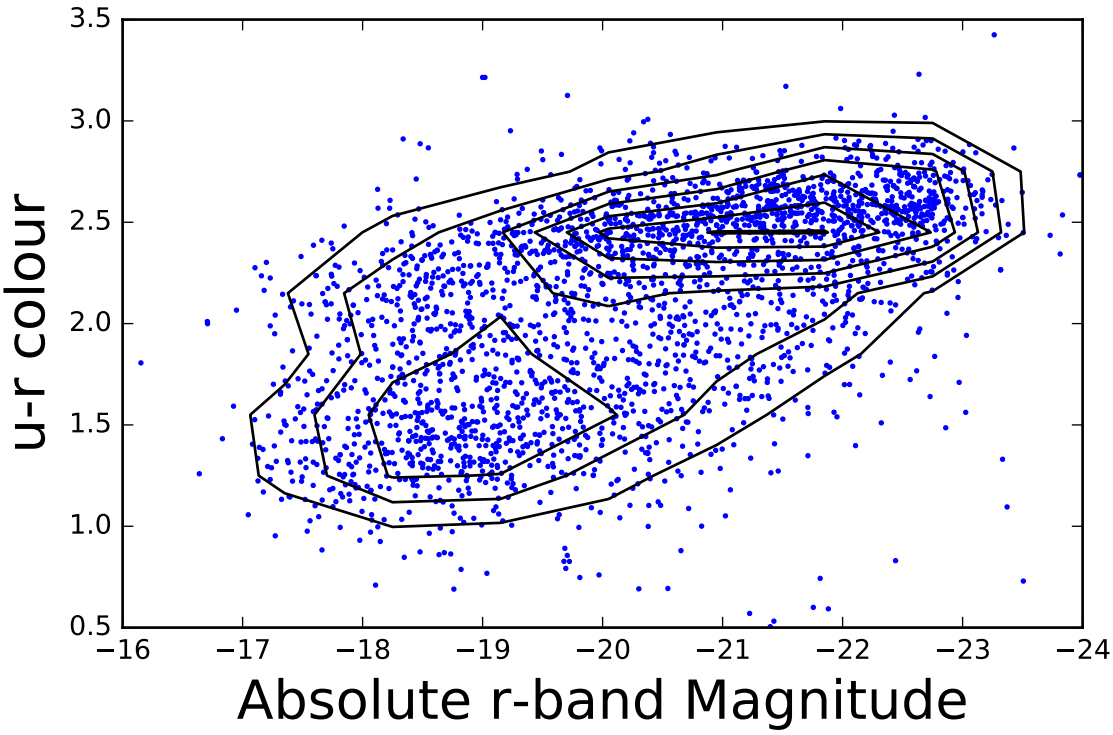

Fig. 1.3 The absolute *r*-band magnitude of galaxies in the MaNGA target catalog, against their *u*-*r* colour. The absolute magnitude on the x-axis goes from dim galaxies on the left to bright galaxies on the right. On the y-axis, galaxies go from blue at the bottom to red at the bottom. The contours show the density of points, illustrating the red sequence and the blue cloud.

In the modern view, galaxy populations are often described in terms of scaling relations, such as the 'Colour-Magnitude Relation', 'Size-Mass Relation' and the 'Fundamental Plane'. Among many other relationships, these correlations provide vital insights into the structure and evolution of galaxies.

The relationship between a galaxy's colour and its brightness, referred to as the 'Galaxy Colour-Magnitude Diagram', is perhaps the most important relationship when discussing classifications of galaxies (Baldry et al., 2006, 2004; Balogh et al., 2004; Blanton and Moustakas, 2009; Brammer et al., 2009; Chester and Roberts, 1964; Kodama and Arimoto, 1997; Strateva et al., 2001; Visvanathan, 1981; Visvanathan and Griersmith, 1977). The diagram, shown in Figure 1.3 using galaxies from MaNGA, demonstrates the bimodality of galaxy populations. Galaxies lie in two groups, the red sequence and the blue cloud. Between the two groups is the transition region, referred to as the green valley. These groups contain galaxies with many similar properties.

Red sequence galaxies are dominated by early type morphologies, higher stellar masses, more compact sizes, older stellar populations and less ongoing star formation. Blue cloud

galaxies have more spiral type shapes, larger radii and are dominated by young stellar populations due to the ongoing formation of new stars. Finally, green valley galaxies are often thought to be galaxies transitioning from the blue cloud to the red sequence, with intermediate morphologies and star formation rates.

The properties of green valley galaxies is a field of active study, with many authors now suggesting that there are multiple pathways of evolution from the blue cloud to the red sequence. Schawinski et al. (2014) use data from SDSS, the Galaxy Evolution Explorer (Martin et al., 2005, GALEX) and Galaxy Zoo 2 (Willett et al., 2013) to show that while early-type galaxies move very quickly across the green valley, late-type galaxies transition from star forming to quiescent very slowly.

Another important galaxy scaling relation is the 'Size-Mass relation', which relates a galaxies stellar mass to its size, usually measured by the radius that contains half the galaxies light (the half-light radius) (Carlberg, 1984; Cimatti et al., 2008; Furlong et al., 2017; Huertas-Company et al., 2013; McLure et al., 2013; Rees and Ostriker, 1977; Shankar et al., 2014; Spindler and Wake, 2017). As one might expect, more massive galaxies are larger than low mass galaxies, however this is not strictly true in all cases. Early-type galaxies tend to be more compact than late-type galaxies of the same mass.

In fact, for early-type galaxies, the size-mass relation is a projection of the 'Fundamental Plane', which describes the relationship between stellar mass, size and the velocity dispersion of stars in a galaxy. Galaxies typically lie on a flat plane in the 3D parameter space (Bernardi et al., 2003; Bezanson et al., 2015; Hou and Wang, 2015). The fundamental plane shows how early-type galaxies are supported by the random motion of their stars. Late-type galaxies, however, are supported by rotation and have their own scaling relation between mass and velocity dispersion called the 'Tully-Fisher Relation' (Bell and de Jong, 2001; Mocz et al., 2012; Tully and Fisher, 1977).

Through out this section I have focussed on the properties of galaxies in the local Universe. However, it is important to note that the scaling relations and properties of galaxies have varied greatly over the last 13 Gyrs. For example, in the early Universe the global star formation rate was increasing, and peaked around $z \sim 2$, this was coupled with the evolution of galaxies as they slowly used up available gas supplies (Behroozi et al., 2013; Hopkins and Beacom, 2006; Madau and Dickinson, 2014). There are more galaxies which have ceased forming stars in the local Universe than at higher redshifts (O'Mill et al., 2008).

These relations come together to describe the modern model of galaxy evolution. Galaxies form via the hierarchical collapse of gas and dark matter (White and Frenk, 1991). The first stars formed into globular clusters, but their gravity quickly caused further collapse into irregular spheroids. To conserve angular momentum as the inner regions collapse to form a

bulge the outer stars and gas are pushed outwards to form a disk. Early disk galaxies had high rates of star formation, which we see today as Ultra- and Hyper-Luminous Infrared Galaxies (Eisenhardt et al., 2012; Riechers et al., 2017; Tran et al., 2001; Vieira et al., 2013, ULIRGs & HLIRGS). Although the exact mechanisms are still debated, as these disk galaxies grow they begin to form structures such as spiral arms and bars. Spiral arms are likely formed due to density wave mechanics, which result from the gas and dust bunching up into the arms as they rotate around the galaxy and causing star formation to occur inside the wave (Dobbs and Baba, 2014; Goldreich and Lynden-Bell, 1965; Hart et al., 2017; Vorobyov and Basu, 2005). Bars form due to non-axisymmetric instabilities in a galaxy which causes material to bunch up around resonant orbits towards the galactic centre. These instabilities may be an inevitable consequence of galaxy formation, but may also be induced by environmental events like harassment and mergers (Athanassoula and Misiriotis, 2002; Barnes and Hernquist, 1991; Bournaud and Combes, 2002; Combes and Sanders, 1981; Zana et al., 2018).

Galaxies will continue to form new stars as long as they have a supply of cold gas that can accrete onto the galaxy. Most galaxies have halos of hot gas surrounding them, which slowly accretes onto the galaxy as it cools and relaxes (Bianchi, 2011; Kennicutt, 1998a; Sánchez Almeida et al., 2014). Other sources of star forming material are galaxy interactions, such as minor and major mergers that deposit gas and dust. Mergers can trigger extreme bouts of star formation called starbursts (Athanassoula et al., 2016; Brooks et al., 2009; Ciotti et al., 2007). Over time a galaxy's gas supply will run out, causing star formation to cease. When this happens, the hot blue stars that dominate a young stellar population's colour die off and the galaxy transitions from the blue cloud into the red sequence. This transition is often accompanied by morphological changes, such as the fading of spiral arms or dramatic transformations into early-type galaxies due to major mergers (Ciotti et al., 2007; Kormendy et al., 2009).

1.3.2 Galaxy Environments

Galaxies are not born in isolation; the space they exist in is dynamic and populated by other galaxies, intergalactic dust and the ever present dark matter. The theory of hierarchical clustering has largely been accepted as the 'go to' model for the formation of large scale structure (Navarro et al., 1997; Ouchi et al., 2005; Springel et al., 2001; White and Frenk, 1991). In this model, after the inflationary periods of the very early Universe, the gravity of dark and baryonic matter remained the dominant force in The Universe for some time (Berezhiani et al., 2001). The differences in the density of matter, which had been amplified by inflation, caused the dark matter and baryonic matter to begin to fall in on itself. The baryonic matter fell to the centres of the dark matter clouds, which due to the lack of self-

interaction forms gravitationally bound spheroidal structures called 'Dark Matter Haloes'. It is in these first haloes that galaxies began to form (White and Frenk, 1991).

This was not the end of the process however, as the massive dark matter haloes were not isolated from each other and began to fall towards and merge with their neighbours. Small haloes would merge, forming larger gatherings of dark matter and galaxies with them. Eventually, many haloes would grow to vast sizes, containing the matter from many smaller sub-haloes and many galaxies (Frenk et al., 1996; Nagai and Kravtsov, 2005). We refer to this collections of galaxies as groups and clusters, though the delineation between these classifications is not well defined. For example, The Milky Way exists in the 'Local Group', along with our neighbouring galaxies Andromeda and the Triangulum Galaxy and their associated satellites with a dark mass mass of $M_h \sim 10^{12} M_\odot$ (Carlesi et al., 2017; González et al., 2014). Alternatively, there is the 'Coma Cluster', which is a collection of gravitationally bound galaxies numbering over 1000, approximately 99 Mpc from Earth that has a dark matter halo mass of $M_h \sim 10^{15} M_\odot$ (The and White, 1986).

Galaxy environments have been shown to have strong effects on the evolution of galaxies. For example, the 'Morphology-Density Relation', first shown by Dressler (1980), describes how with increasing galaxy density the fraction of E-type and S0 galaxies increases, while there is a corresponding decrease in the fraction of spiral galaxies. This very strong trend points to mechanisms which shape galaxies in different environments, causing them to more rapidly evolve from late types into early types, compared with more sparse regions of space.

In addition to the changes in morphology, there are many relationships between environment and internal galaxy properties. Galaxies in denser regions of space tend to be more massive, for example, with redder colours and less star formation. While galaxies in low density regions, such as small groups or isolated galaxies, tend to have lower masses, higher star formation rates and bluer colours (Bamford et al., 2009; Cooper et al., 2007; Cucciati et al., 2006).

There are many mechanisms that can affect a galaxy due to its environment, which have been well studied. Perhaps most important are galaxy mergers, both minor mergers, which occur when one galaxy is much larger than another, and major mergers between two similar size galaxies, which have been shown to be more common in high density regions of The Universe (de Ravel et al., 2011). This is to be expected, of course, as a higher density means more galaxies which can interact and merge. Mergers not only drive the transformation from late to early type, but also trigger massive star bursts which can rapidly use up the available star forming material (Athanassoula et al., 2016; Brooks et al., 2009; Ciotti et al., 2007,?; Kormendy et al., 2009).

Apart from mergers, galaxies can be subject to a number of processes that can strip gas and stars. Ram pressure stripping, first discussed in Gunn and Gott (1972), refers to the removal of gas due to the fluid drag force between the galaxy and the intracluster medium. Tidal stripping refers to the removal of stars and gas due to the tidal gradient across a galaxy caused by the galaxy not being in the centre of the dark matter halo (Kravtsov et al., 2004; Mandelbaum et al., 2006; Merritt, 1984). Finally, harassment occurs when two or more galaxies interact but do not merge, which destabilises the structures and can cause stars and gas to escape into the intracluster medium or be exchanged by the galaxies (Moore et al., 1996, 1998; van den Bosch et al., 2008a).

One complication in the study of galaxy environments however, is how to define them. Many studies use different, often unique measurements of environment based on the specific dataset in use, which can lead to difficulty in interpreting the results in the context of the entire field. One example is the 'Local Density', which is often defined by the distance to the 'nth nearest neighbour galaxy' (Beers and Tonry, 1986; Ulmer et al., 1992). For example, Balogh et al. (2004) use the 5th nearest neighbour density, which they define as $\log_{10}(\Sigma) = 0.5 * \log_{10}(\Sigma_4) + 0.5 * \log_{10}(\Sigma_5)$, where $\Sigma_N = N/(pi * d_N^2)$ and d_N is the distance to the Nth nearest neighbour. However, this sample uses galaxies from SDSS, and is limited to a magnitude of $M_r < -20$. Compared to Schaefer et al. (2017), who use galaxies from the Galaxies and Mass Assembly (GAMA) survey, which calculates the environment density using galaxies with a limiting magnitude of $M_r < --18.5$. By probing dimmer galaxies, Schaefer et al. (2017) finds higher densities for galaxies in the same environments.

Some studies, such as Smethurst et al. (2017), use the distance of a galaxy from the centre of its group, compared the to virial radius of the dark matter halo (r_{200}) as a measure of environment. This distance not only gives an estimate of the density, galaxies closer to the cluster core are in higher density regions, but also a measure of how long the galaxy has been in the cluster since the initial in fall (Tully and Shaya, 1984). The trouble with this method, and methods which compare galaxies based on dark matter halo mass, is that measuring the size and mass of the halo is very difficult. In rare cases, x-ray observations of the intracluster gas and studies of weak gravitational lensing can be used to infer dark matter halo masses (Böhringer et al., 1994; Kaiser and Squires, 1993). More commonly however, clustering algorithms are used to define which galaxies are asscociated with a single group and halo masses assigned based on the total luminosity or mass of the galaxies in the group (Yang et al., 2009). It is also necessary to define the cluster centre in some way, which can be simple for small groups where one galaxy is much larger than the others, but is more difficult in a groups and clusters with many high mass galaxies in the cluster core. Yang et al. (2009)

define the centrals as the brightest or most massive galaxies, however in some cases (Skibba et al., 2011) the brightest cluster galaxy may be a satellite instead.

In this work, I choose to use the Central/Satellite classifications for our investigations of environment. In this model a clustering method called a 'Friends of Friends Algorithm' is used to find candidate galaxy groups, the groups are iterated over until no new galaxies are added to them. As described above, these groups are assigned a dark matter halo mass based on the total luminosity of the group's galaxies. In each group, the brightest (or most massive) galaxies are tagged as the Central, while all other galaxies are tagged as Satellites. The advantage of using such a model, over measurements of local density, is that it divides galaxies based on what environmental processes they may be subject to. As the satellites are moving through the group, they are subject to environmental processes such as ram pressure and tidal stripping, as well as harassment. Centrals, however, do not experience stripping, but are much more likely to be subject to minor and major mergers, and experience shock heating from the halo (Abadi et al., 1999; Bluck et al., 2016; Dekel et al., 2003; Oman and Hudson, 2016; White et al., 2007; Zheng et al., 2007).

1.3.3 Star Formation in Galaxies

The formation of new stars plays a vital role in galaxy evolution. From driving the growth of a galaxy, to using up its supply of cold gas, generating interstellar dust and increasing the galaxy's supply of metals, galaxies would not look the same if it weren't for the ongoing production of new stars. The process of star formation itself is still an active area of research, however the bulk of this topic falls out of the scope of this thesis. I will, however, provide a brief explanation to provide context to the subject.

Star formation occurs when clouds of cold gas, i.e. gas which is not supported by the kinetic energy of its constituent particles, begins to collapse under its own gravity. This collapse can be triggered in many ways, such as a collision with another nebula, a shock front from a nearby supernova, or due to pressure from the motion of the parent galaxy through the intergalactic medium, and may even occur without outside stimulus. As the cloud collapses it will fragment into smaller pieces, which given enough mass will continue to fall in on themselves. At the centre of these fragments the gas will begin to form into a protostar and protoplanetary disk. Eventually, enough gas will fall onto the protostar by accretion that it will have enough mass to generate the high temperatures and pressures needed in its core to begin fusing hydrogen into helium, and a star is born.

An important aspect of star formation for this work, is the 'Initial Mass Function' (IMF), which describes the number density of stars at different stellar masses that should be formed in an episode of star formation. The most famous and widely used IMF is from the work

of Salpeter (1955), though many more IMFs have been developed in the ensuing decades, taking into account recent discoveries into star formation. It is generally assumed, though in some opinions contentiously, that the IMF is a universal property, which allows astronomers to use the same models for most galaxies (Chabrier, 2003; Kroupa, 2001). Recently, however, there has come mounting evidence that the IMF may in fact be variable. Cappellari et al. (2012), for example, use dynamical models of galaxies to show a strong dependance on the stellar mass-to-light ratios for IMFs of early type galaxies. this implies that the IMF may be intimately tied to a galaxy's formation history (Conroy et al., 2014, 2017; van Dokkum et al., 2017).

One of the key results of the past few decades has been from the study of the star formation history of The Universe. It appears from studies of samples of galaxies, out to the earliest times in the cosmos, that the global star formation rate is decreasing, having peaked 10 Gyr ago at a redshift of $z = 1.9$ (Baugh et al., 1998; Heavens et al., 2004; Hopkins and Beacom, 2006; Madau and Dickinson, 2014; Schaye et al., 2010).Since the peak, the global star formation rate has decreased exponentially, meaning that half of todays stellar mass was formed by $z = 1.3$, and just 25% was formed after $z = 0.7$. The decrease in star formation at the global scale can largely be attributed to the reduction of available cold gas, compared to earlier times in The Universe (Schaye et al., 2010).

As I have previously described, scaling relations provide key insights into galaxy evolution. As star formation is such an important aspect for the ongoing growth of galaxies, I also wish to construct relationships between ongoing star formation and galaxy properties. The most popular relation is the so-called 'Main Sequence of Star Formation', which compares a galaxy's stellar mass to its current star formation rate. The main sequence, however, is a misnomer, as it seems to imply that galaxies evolve along this sequence (similar to how stars evolve along the Main Sequence). The Mass-SFR relation however is more like the colour-magnitude diagram, seperating two classes of galaxies, with a transition region between them.

The main sequence is made up of galaxies with active ongoing star formation, while galaxies that fall below the main sequence are considered to be 'quiescent'. Star forming galaxies are closely related to blue cloud galaxies, and share much overlap in properties, tending to have late type morphologies and blue colours. Quiescent galaxies, however, are related to the red sequence, having redder colours, more compact sizes and early type shapes. The movement of a galaxy from star forming and blue, to quiescent and red is an active region of research and makes up a significant portion of this work.

Star formation can shut down in many ways, and the exact processes and the physics behind them are still widely debated. It is generally accepted that the shut down can happen

in two ways, via slow secular processes, or via rapid processes. The slow processes are generally related to the internal properties of a galaxy, such as its stellar mass, morphology or the presence of an AGN. More rapid processes, sometimes called 'Quenching', tend to be related to external factors, such as star bursts caused by major mergers or ram pressure stripping of cold gas supplies. For a detailed discussion of the processes involved in the shut down of star formation, see the Introduction of Chapter 4.

1.3.4 Measuring Star Formation

There are many ways to measure the star formation of a galaxy, each with it's own advantages and disadvantages. Some of these methods rely on measuring as much of a galaxy's light as possible, while others depend on single imaging bands or emission lines. Most of these methods, however, rely on measuring the light emitted from O and B type stars, with stellar masses greater than $10M_{\odot}$ and temperatures greater than $10,000K$. These massive stars are very short lived, so detecting them means that the stellar population must be young. For a given IMF, it is possible to calculate the age of a stellar population from the number of high mass stars compared to low mass stars (Kennicutt, 1998a). These indirect measures of the stellar population and star formation rate are extremely popular among the extragalactic astronomy community due to their ease of use and need for only small amounts of data, compared to full stellar population modelling that often requires measurements of a full galaxy spectrum or multiple bands of light to perform an Spectral Energy Distribution (SED) fit Brinchmann et al. (2004); Salim et al. (2016, 2007).

The main difference between the light output by massive stars and low mass stars is the contribution to the UV end of the spectrum. Stars with $T > 10,000k$ output large amounts of UV light, but lower mass stars produce almost none, due to black body physics. Because of this, measuring the UV output of a galaxy or star cluster (using GALEX, for example) allows for a direct measure of how many young, hot stars are present in the galaxy (Buat et al., 1989; Kennicutt, 1998a; Leitherer et al., 1995; Steidel et al., 1996). For example, the relation between UV luminosity and SFR from Madau et al. (1998) converted to a Salpeter (1955) IMF is:

$$SFR(M_{\odot}\ yr^{-1}) = 1.4 \times 10^{-28} L_{\nu}(\text{ergs s}^{-1}\ \text{Hz}^{-1}) \tag{1.1}$$

The main advantage of using UV to measure star formation is that it is directly tied to the emission from the young stellar population, not the secondary emission of emission lines or infrared light. However, it is very sensitive to the assumed IMF, since you have to extrapolate

the population of stars with $M_* < 4M_\odot$. In addition, extinction plays an important role, as the UV light is easily blocked by dust, which can be patchy and difficult to calibrate.

One alternative to using the UV continuum is to instead rely on the H_α emission line. Emitted by HII regions when they are excited by high energy radiation, H_α can act as a tracer for star formation. The UV light from the young stars excites nearby HII regions, which leads to the emission of the 656.28 nm line, which is the first emission line in the Balmer series. Because only the shortest lived stars contribute to the flux of H_α it provides a near instantaneous measure of the star formation, unaffected by the previous star forming history. The advantages of this method are that it is very sensitive, can be used to map the SFR of nearby galaxies at high resolutions even with small telescopes, and can also be detected at high redshifts. Like the UV emission, the H_α SFRs are sensitive to the choice of IMF and estimation of extinction. The extinction is often modelled in a simple way, by assuming a foreground dust screen and calculating the Balmer Decrement using the H_β line. These SFRs are also limited by the assumption that all massive star formation can be traced by nebula emission, when in reality there is always some fraction of emission that escapes.

Thermal infrared is another tracer of star formation, as a significant amount of the light from stars is absorbed and remitted at wavelengths of $10 - 300\mu m$. As the absorption cross section of insterstellar dust is peaked in the UV, it leads that the FIR light can be a sensitive probe of young stellar populations. The use of the FIR is a hotly debated subject however, as the contribution to the dust heating can come from many sources. In blue galaxies it is most often associated with young stars, but in redder galaxies the dust heating from older stars can be very important. It is also important to consider any infrared cirrus emission, which is related to the interstellar radiation field. The efficacy of using FIR to measure star formation is largely dependent on the type of galaxy being studied. In late-type galaxies, the FIR spectrum is well correlated with other tracers of star formation, such as the UV continuum and H_α luminosities. However, in early-type galaxies, the contribution to the FIR emission from older stars is much more dominant and as such the UV and H_α flux is often quite low compared to the FIR.

One final method, though certainly not the only other method, is to fit the galaxy's light to a stellar population synthesis model. This could be done using spectral fitting of the optical wavelengths, such as in Brinchmann et al. (2004), or by SED fitting using light from multiple bands, such as in Salim et al. (2007). Like the previous methods, this technique is dependent on the form of IMF chosen, and the estimation of extinction. Stellar population fitting is also computationally intensive, and requires much more data to be collected than other methods of measuring star formation. The benefit however is that by modelling the stellar population, you can learn much more about the make up of the galaxy, including the star formation

history and stellar mass. This type of modelling is also dependent on what data is available, for example without including data from the UV continuum the contribution to the SED from AGN or LINER regions may be underestimated (Salim et al., 2016).

1.4 MaNGA - Mapping Nearby Galaxies at Apache Point Observatory

Mapping Nearby Galaxies at Apache Point Observatory (MaNGA) is one of the three core programs in the Fourth Sloan Digital Sky Survey. This project began operations in 2015 and over its 6-year running time will observe 10,000 galaxies using a technique known as Integral Field Spectroscopy (IFS). IFS is used to measure the spectra of light at every spatial point in the target field of view. This is achieved by using Integral Field Units (IFUs), small bundles of optical fibres which are fed into a multi-object spectrograph. Each optical fibre produces a spectrum from the light gathered in the target spatial region.

While many studies have been carried out with spectroscopic surveys, they have a significant limitation that they only cover small spatial regions of galaxies. These small regions, or in some cases simple 1D gradients, are then used to infer integrated properties about galaxies. Often the intricate and complex internal structure is missed completely because the spectra are taken from the galactic centre only. IFS, however, allows us to capture the full 2D distribution of the galaxy's light. This crucial extra dimension means that information regarding the distribution of emission lines and spectral indices can be mapped, and that kinematics and angular momentum can be studied in the separate galaxy components. This technique can then ultimately allow for the study of how, for example, the spiral arms contribute to the star formation in the galaxy, or how the central bulge was constructed over cosmic time.

MaNGA is the next step in a long line of IFS surveys. The past two decades has seen much pioneering work completed, such as the SAURON (de Zeeuw et al., 2002) and ATLAS^{3D} (Cappellari et al., 2011) that observed 72 E/S0/Sa and 260 E/S0 galaxies, respectively. DiskMass studied 146 face-on disk galaxies, with a high spectral resolution ($R \sim 10,000$, Bershady et al., 2010). These studies showed the strength of IFU observations in different approaches, SAURON focussed on the kinematic and dynamical properties of galaxies, while DiskMass examined internal stellar mass and mass-to-light ratios.

Recent advances have allowed improvements in both spatial and spectral resolution, and large increases in sample size. CALIFA (Sánchez et al., 2012), will observe 600 galaxies at a spatial resolution of $1kpc$ and a wavelength coverage of 3750 to 7000Å. Perhaps the

N_{fibres}	Number per plate	Diameter (in fibers)	Diameter (arcsec)
19	2	5	12.5"
37	4	7	17.5"
61	4	9	22.5"
91	2	11	27.5"
127	5	13	32.5"

Table 1.1 Science IFU complement of the MaNGA survey

most direct comparison to MaNGA is the recently launched SAMI survey (Allen, 2015; Bryant et al., 2015). SAMI aims to observe 3400 galaxies, using a multi-plexed IFU on the Australian Astronomical Observatory (Croom et al., 2012). SAMI has so far studied; the nature of gas outflows and shocks (Ho et al., 2014); star formation and its variation with environment (Schaefer et al., 2017); and the relationship between kinematic classes, such as fast and slow rotators, and projected galaxy density (Fogarty et al., 2014).

In MaNGA the IFS technique is combined with the SDSS plug-plate methodology, which allows multiple galaxies to be observed at once. The plug-plate is an aluminium disk which is placed in the focal plane of the Sloan 2.5m telescope (Gunn et al., 2006). Holes are drilled into the plates to match the on sky position of the target galaxies and stars. Fibre optic cables or IFU hexabundles are then plugged into the holes and fed into the BOSS spectrographs (Smee et al., 2013), with a wavelength range of $3600-10,000$Å. There is some variation in the spectral resolution in the spectrographs, with the resolving power ($R = \lambda/\Delta\lambda$) on the blue side rising from $R \sim 1400$ at 4000Å to $R \sim 2100$ at 6000Å. On the red side, the resolving power is $R \sim 2600$ at 9000Å, and $R \sim 1800$ around 6000Å.

There are 17 science fibre-bundles in MaNGA, which are used over the 3 degree field of view of the Sloan telescope. The fibres have a close-packed hexagonal design, with a 54% live fill factor (Bundy et al., 2015; Drory et al., 2015). The fibre-bundles range from 19 to 127 fibres, with diameters of 12" to 32", with each fibre having a diameter of 2". The different size bundles allow galaxies with varying on-sky angular sizes to be covered to the same effective radii, with smaller IFUs being used for smaller or more distant galaxies. Table 1.1 shows the IFU complement of each plate. There are 92 single fibres which are associated with the science bundles for sky measurements and a further 12 7-fibre mini-bundles which are used for spectro-photometric calibration (Law et al., 2016; Yan et al., 2016b).

Since each IFU bundle has a fill factor of 54%, it is necessary to perform a dithering pattern and take multiple exposures of each plate. By dithering the IFU three times in a 1.44" equilateral triangle, the IFU can be used to fully cover the area of the target galaxy (Law et al., 2015). Each dithered observation is taken over 15 minutes, and it is required that all three

ditherings are taken within an hour of each other to maximise the quality of the combined data cube. Wavelength dependent refraction is a serious cause for concern in the survey, this can cause up to a 1" difference in where the extreme ends of the wavelength range hit the IFU. By ensuring that each set of observations are all taken within an hour of each other, it is possible to minimise the change in refraction over the course of the integration. The three dithered exposures make up the minimum observation unit, which is repeated until the signal-to-noise ratio reaches 5Å^{-1} per fiber in the *r*-band continuum at a surface brightness of 23 AB arcsec^{-2} (Bundy et al., 2015; Law et al., 2015; Yan et al., 2016a,b).

By 2020 the MaNGA survey will observe 10,000 galaxies selected in a way that ensure the goals of the survey can be met. The survey has a sky coverage of $\sim 4000 deg^2$ and a redshift range of $0.01 < z < 0.15$, with an average redshift of $z \sim 0.03$. With the goal of a volume limited sample in mind, the galaxies are chosen such that the stellar mass distribution is flat above $M_* > 10^9 M_\odot$. Figure 1.4 shows the selection cuts, based on *i*-band magnitude and redshift. *i*-band magnitude is used as a proxy for stellar mass in the sample selection as it is model independent.

As can be seen in Figure 1.4, the sample is split into two sub-samples. The Primary sample, which contains ~ 5000 galaxies, are targeted such that the IFU provides a spatial coverage of $1.5r_e$. The Primary sample is however deficient in high mass blue galaxies and low mass red galaxies, as such there is a colour enhancement added to make up for this, which adds ~ 1700 galaxies the Primary to make the Primary+ sample. The Secondary sample instead achieves a spatial coverage of $2.5r_e$, by targeting galaxies at a higher redshift, and contains ~ 3300 galaxies. The sample contains no cuts in galaxy size or inclination and has a spatial sampling of $\sim 1-2$ kpc, depending on M_i ($1.2kpc$ for $M_* < 10^{10} M_\odot/h^2$, 3.8 kpc for $M_* > 10^{11} M_\odot/h^2$).

The two samples have slightly different scientific motivations. The Primary+ sample is selected so that there is high SNR and spatial resolution in the inner regions of the galaxies, as this is where the majority of the stellar mass in contained. The Secondary sample, however, is more driven by a desire to study the regime where dark matter dominates and the delve into the uncharted territory of the galactic outskirts of shocks and outflows. Finally, the sample is designed to be as simple as possible, depending on just three observables: redshift, *i*-band magnitude and (for the Colour-Enhanced supplement) $NUV - i$ colour.

Recall from before that the final goal for MaNGA is for the sample to be volume-limited, but the above selection criteria do not meet this requirement. The sample is chosen so that there are an equal number of high and low luminosity galaxies, but this would bias any studies as a function of any property except M_i. For example, even in a narrow bin of stellar mass the mass-to-light ratio can vary more than the stellar mass for a given volume limited

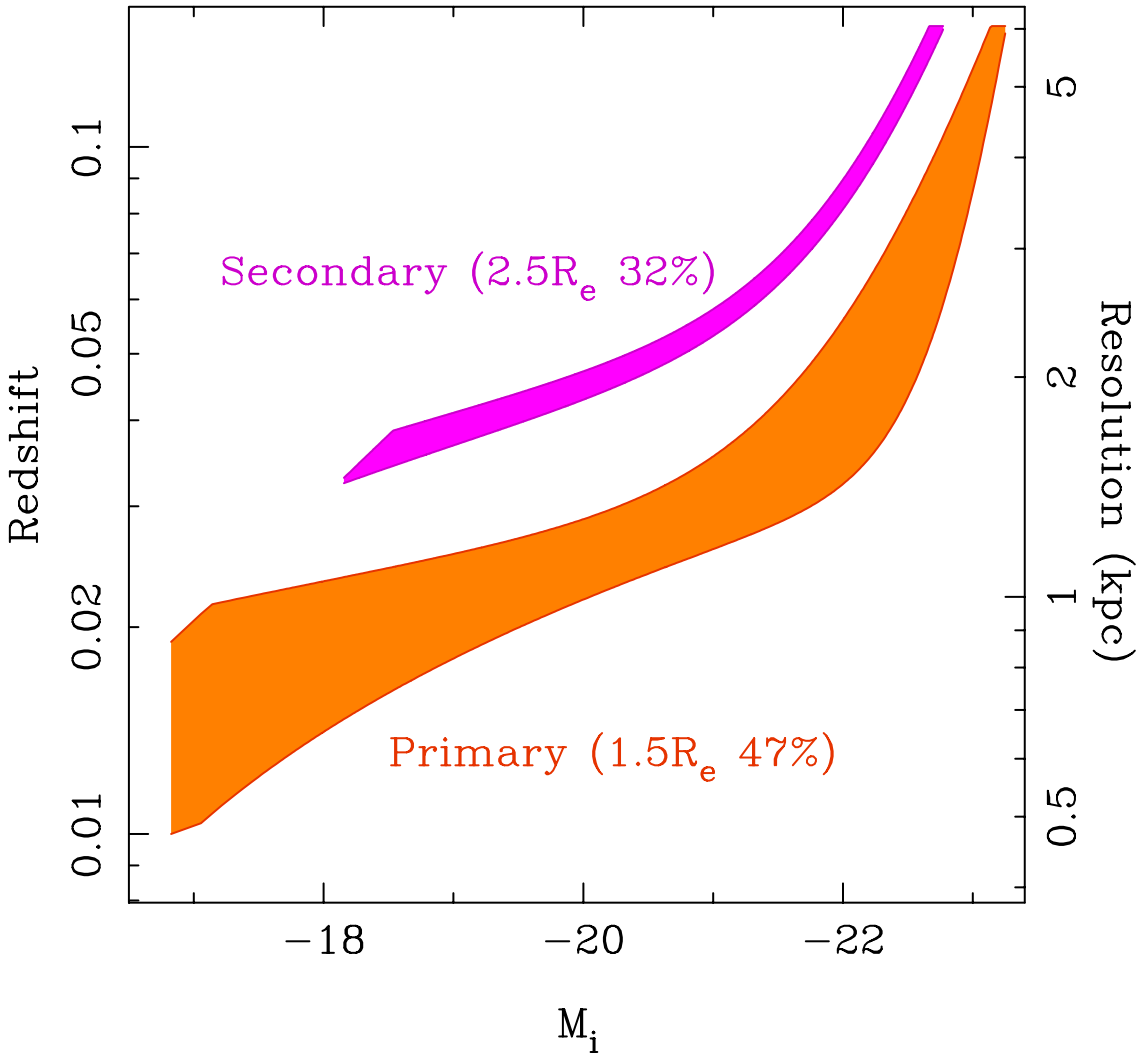

Fig. 1.4 The sample cuts in redshift and *i*-band magnitude. Figure 8 from Bundy et al. (2015). The aim is to target all galaxies in the cut out regions, which are defined by a smooth function in *i*-band magnitude. The sample design is such that it maintains a constant spatial coverage of $1.5r_e$ in the Primary+ sample and $2.5r_e$ in the Secondary sample. The right hand axis shows the expected spatial resolution, assuming a FWHM of 2.5". The percentages are modified to allow for 10% of the galaxies to be part of ancillary projects.

sample. To correct for this, a set of volume weights have been calculated for the samples. Fortunately, as we know the full redshift range over which any galaxy could be selected, it is easy to calculate the required volume weight. For each galaxy, the redshift range is simply $z_{min}(M_i) < z < z_{max}(M_i)$. However, this volume varies with M_i and as such the volume weight is therefore dependent on just M_i (or M_i and $NUV - i$ colour for the Primary+ sample).

The raw signal from the BOSS spectrographs is reduced by the Data Reduction Pipeline (Law et al., 2016, DRP,), which produces reduced data products in the forms of Row Stacked Spectra (RSS) and Datacubes. The DRP first performs the extraction of the raw signal, a sky subtraction and flux calibration on each individual exposure. The second stage of the DRP then combines together the individual frames while accounting for differences in atmospheric conditions to create a calibrated fibre spectra. One important stage in the atmospheric calibration is correction for the wavelength dependent refraction, which causes a given fibre to receive light from different parts of a galaxy at blue and red wavelengths. Each target galaxy then has all its spectra coadded to produce the final data products.

The sky subtraction is vitally important, especially compared to previous SDSS surveys which focussed on the bright cores of galaxies. In MaNGA the target galaxies are sampled out to radii where their brightness is decreasing rapidly, compared to the sky background, and so noise and emission lines from the atmosphere (such as from OH radicals) can begin to dominate the signal. The sky subtraction is designed to reduce this noise to the Poisson-limited levels, so that spectra can be stacked without the sky lines and background noise overcoming the galaxy signal. To achieve this, MaNGA has 96 sky-fibres, which are placed in areas of the plug plates which are determined to be 'blank sky' objects, within 14 arcmin of their associated science IFU.

Flux calibration is performed using the 12 7-fibre mini-IFU bundles, which are allocated to standard stars within the plates field of view. A best-fit point spread function (PSF) is estimated using the relative fluxes between the mini-IFUs, the position of the target star in the IFU, the scale of the measured PSF from the IFU, and the scale and rotation of the expected differential atmospheric refraction. Using the PSF, the aperture loss fraction can be calculated and the total flux from the standard star can be estimated. Next, the system response is calculated as a function of wavelength based on a grid of theoretical spectra, normalised to the observed SDSS broadband magnitudes. Finally, the corrections from each individual star are averaged to obtain the best throughput correction of the system, and applied to each science IFU.

The final datacubes are constructed from the row stacked spectra, organised into 4563 wavelength channels (for the logarithmically sampled data). Using the astrometric solutions, x and y coordinates are calculated for each wavelength channel, which describe the position

of the centre of each fibre based on fractional pixel coordinates and a chosen origin.. The datacubes have a spatial pixel size of 0.5 arcsec pixel^{-1}. The wavelength channels are assembled into a thee-dimensional cube with a spatial size a little bigger than the dithered footprint of the science IFU. Each slice of the cube in the z-axis contains the rectified image of the galaxy in a particular wavelength channel. Also included in the cube are inverse variances and a 3D data quality mask.

Finally, the Data Analysis Pipeline (DAP, Westfall et al. (in prep)) performs a number of analysis programs on the reduced data. The DAP uses a custom built pipeline which fits the stellar continuum, emission lines and spectral features using pPXF (Cappellari, 2012). The final DAP data products include stellar kinematics, measurements of emission lines with total flux, equivalent width and gas velocities and measurments of the Lick, D_n4000, TiO, and IMF spectral indices. All of these analyses are performed in a variety of spatial bins, including individual spectral pixels (spaxels) and Voronoi binning to $S/N > 10$.

To perform the analysis, the DAP goes through the following steps. First, the pixel signal-to-noise (S/N) is calculated between 5600.1Å and 6750.0Å, which is the FWHM of the r-band filter. Next, the spatial binning takes place, which currently provides four binning methods: Unbinned analysis of each spaxel, Voronoi binning based on creating bins with a S/N of 10 (Cappellari and Copin, 2003), NRE bins the data into two radial bins of 0-1 and 1-2 r_e and all spaxels combined into a single spectrum. Once the binning is complete, the DAP uses pPXF to fit the stellar continuum, primarily to measure the stellar kinematics (both velocity and dispersion). Once the continuum has been fit, the best-fit model can be subtracted and the gas emission lines measured. A Gaussian emission line model is used, wherein each emission line is fit with a Gaussian distribution and a constant baseline within a 50Å window. These lines are fit independently and provide both line fluxes and equivalent widths, and gas kinematics with fitted velocities and dispersions. Finally the spectral indices are fit, in the version of the MaNGA data used in this thesis only $D4000$ and D_n4000 are fit. $D4000$ is defined as the ratio between the average flux density in ergs s^{-1} cm^{-2} Hz^{-1} between 4050 and 4250 Å and the flux density between 3750 and 3950 Å (Bruzual A., 1983; Poggianti and Barbaro, 1997). D_n4000 is measured over a smaller window of wavelengths og $3850-3950$Å and $4000-4100$Å, the advantage of using D_n4000 is that it is less sensitive to dust absorption, due to the smaller windows (Balogh et al., 1999; Vergani et al., 2008).

MaNGA is a powerful survey, with a considerably larger sample size than previous IFU surveys, very good spectral coverage across optical wavelengths and uniform spatial coverage across its target galaxies. The science goals of the survey are numerous and varied, with over 100 projects posted to the SDSS-IV project page. The science outcomes of the project are summarised in the following key science questions:

MaNGA's Key Science Questions:

1. How are galaxy disks growing at the present day and what is the source of the gas supplying this growth?

2. What are the relative roles of stellar accretion, major mergers, and secular evolution processes in contributing to the present-day growth of galactic bulges and ellipticals?

3. How is the shutdown of star formation regulated by internal processes within galaxies and externally driven processes that may depend on environment?

4. How is mass and angular momentum distributed among different components and how has their assembly affected the components through time?

Bundy et al. (2015)

This thesis is predominantly concerned with answering the third question, by studying the spatial distribution of star formation and how it varies with galaxy properties such as mass, structure and environment.

1.5 This Work

This thesis is structured through four science chapters. The overarching theme is the role of environment in the evolution of galaxies and the processes that lead to the shut down of star formation in the local Universe. The scientific aims of this thesis can be summed up as:

1. How are galaxies shaped by their environment? What processes drive the structural evolution of central and satellite galaxies?

2. What are the roles of internal, secular processes in the shutdown of star formation?

3. What are the roles of external, environment processes in the shutdown of star formation?

In Chapter 2 I study a large sample of galaxies from SDSS Data Release 7 (Abazajian et al., 2009), while Chapters 3 to 5 study galaxies using the MaNGA survey data from Data Release 14 (Abolfathi et al., 2017). I make concluding remarks and look to future work in Chapter 6. Throughout this thesis I consider a standard ΛCDM cosmology with the following parameters: $H_0 = 100\,h$ km s^{-1}, $\Omega_0 = 0.3$ and $\Omega_\Lambda = 0.7$.

1.5.1 Chapter 2 - The Differing Relationships Between Size, Mass, Metallicity and Core Velocity Dispersion of Central and Satellite Galaxies

I study the role of environment in the evolution of central and satellite galaxies with the Sloan Digital Sky Survey. I begin by studying the size-mass relation, replicating previous studies, which showed no difference between the sizes of centrals and satellites at fixed stellar mass, before turning our attention to the size-core velocity dispersion (σ_0) and mass-σ_0 relations. Under the assumption that σ_0 is invariant to environmental processes, I study how the median size and mass of galaxies varies between centrals and satellites. I then follow-up this investigation of sizes and masses by looking at the radial distribution of stellar mass for galaxies at fixed σ_0. This Chapter focuses on my first science question, and explores how galaxies are affected structurally by evironmental processes, such as minor mergers, ram pressure stripping, and tidal stripping.

1.5.2 Chapter 3 - A Two-Source Star Formation Rate Model for MaNGA Galaxies

I develop a data analysis pipeline to predict the ongoing, specific and surface density star formation rates for galaxies in the SDSS-MaNGA Survey. Galaxies are classified by their location on the BPT diagram and resolved BPT maps are created using the H_α, H_β, N[II] and O[III] emission lines. Star formation rates are initially predicted using the well known relationship between H_α emission and instantaneous star formation, after I correct for dust attenuation by using H_β and the Balmer Decrement.

Due to contaminated emission from AGN and Low-Ionization (Nuclear) Emission-line Regions (LI(N)ER), I only use H_α to calculate star formation rates in spaxels which have star forming emission based on the BPT diagram. To avoid biasing our results towards star forming galaxies without AGN/LI(N)ER emission I construct an empirical relationship between the D_n4000 spectral index and the specific star formation rate. This relationship is used to fill in the star formation rate maps where the BPT diagram finds AGN/LI(N)ER like emission. I then turn our attention to testing the global properties of the galaxies in the MaNGA sample and comparing our SFRs to those found in previous surveys of the same galaxies.

This Chapter sets the stage for the following Chapters to answer the second two science questions posed above, by providing a suite of data products which allow for the investigation of the spatial distribution of star formation.

1.5.3 Chapter 4 - The Spatial Distribution of Star Formation and its Dependence on Mass, Central Velocity Dispersion and Environment

I study the spatially resolved star formation of 1494 galaxies in the SDSSIV-MaNGA Survey. The galaxy sample is selected to include star forming, composite and AGN/LI(N)ER type galaxies, identified using the BPT diagram, which have specific star formation rates above $log_{10}(SSFR) > -11.5$. I investigate the shapes of the radial profiles of specific star formation rate, with respect to different measures of a galaxy's internal an external properties. I study how galaxies vary with mass and central velocity dispersion, which give insights to how the formation and growth of bulges affects the specific star formation rate in the cores of galaxies. I use the BPT classification of these galaxies, and their morphological stucture as measured by the Sérsic index, to infer the roles of AGN feedback and morphological quenching in the galaxy cores. Finally, I examine the role of environment in regulating the specific star formation and whether the stripping of star forming material or strangulation play a major role in shaping satellites.

1.5.4 Chapter 5 - The Role of Bars in Suppressing and Enhancing Star Formation

I study the role of galaxy bars in the regulation of star formation at the local scale. Using a sample of morphologically selected galaxies from Galaxy Zoo 2 and MaNGA, I investigate the spatially resolved specific star formation rate, $4000-$Å break and equivalent width of H_α. Our sample consists of 215 galaxies with strong and weak bars, and 402 disk galaxies with no bars. I study how the radial profiles of SSFR vary with stellar mass for the barred and unbarred galaxies, to find how the presence of a bar affects both the core and disk star formation rates. By constructing ratios of inner and outer star formation, I study how the bars drive gas into the cores of galaxies to drive circumnuclear star formation and starve the galaxy disk. I also investigate the role of environment in barred galaxies, by studying the central and satellite classifications of these galaxies. This Chapter is particularly focussed on the second key science question posed previously, on the internal processes dominating star formation, but also attempts to shed more like on external processes.

2

The Differing Relationships Between Size, Mass, Metallicity and Core Velocity Dispersion of Central and Satellite Galaxies

"The sky above the port was the color of television, tuned to a dead channel."
– William Gibson, *Neuromancer, 1984*

2.1 Introduction

The effect of environment on galaxy evolution has been an area of much study in recent times. Large surveys such as the Sloan Digital Sky Survey (SDSS, Abazajian et al., 2009; York and SDSS Collaboration, 2000) provide astronomers with sufficient data to study galaxies statistically in a variety of environments. It is largely accepted that galaxies are situated in dark matter haloes which grow hierarchically over time, such that smaller haloes infall towards and merge with larger ones. These dark matter haloes play host to individual galaxies, but also to groups and clusters made up of pairs, tens or even thousands of galaxies (Kravtsov and Borgani, 2012; Navarro et al., 1997).

Galaxies in different haloes and at different positions within those haloes have varying properties, which are related to the properties of, and location within, their host haloes. For example satellite galaxies experience lower levels of star formation than central galaxies due

This work in this Chapter was presented in Spindler and Wake (2017), which was published in MNRAS.

to quenching mechanisms, which predominantly act on those satellites (Baldry et al., 2006; Kauffmann et al., 2004; Weinmann et al., 2009; Wetzel et al., 2013). Indeed, two very similar galaxies could evolve in significantly different ways if placed in different environments; for example if one were to become a satellite galaxy while the other remains a central or isolated galaxy.

Scaling relations can tell us much about the evolution of galaxies and help constrain models of that evolution. The size-mass relation of early-type galaxies has been shown to be invariant with environment by a number of authors. Huertas-Company et al. (2013) showed that the size-mass relation of early type galaxies is the same for central and satellite galaxies, implying no environmental dependance. Shankar et al. (2014) found no environmental dependance of bulge-dominated galaxy sizes at fixed mass in contrast to state-of-the-art semi-analytic models of galaxy formation which predicted a $\sim$1.5-3 times increase in size from low to high mass haloes. Shankar et al. (2014) describes a number of mechanisms within the models that predict an environmental dependance, such as violent disk instabilities which can lead to bulge growth (Bournaud et al., 2011a,b; Dekel et al., 2009), minor mergers which happen up to $\sim$4 times more often in high mass haloes in some models (Hirschmann et al., 2013; McCavana et al., 2012), gas dissipation following mergers which would more effectively shrink galaxies in less massive haloes and finally satellite evolution which could stunt the growth of central galaxies from mergers if satellite star formation is quenched in a fast manner as opposed to a slow one.

In addition to the size-mass relation Mocz et al. (2012) showed that the Tully-Fisher relation for disk galaxies is largely unaffected by environment, finding only a small steepening with increasing local density. Hou and Wang (2015) find a significant environmental dependance on the fundamental plane coefficients of early-type central galaxies in SDSS DR7 (Data Release 7), but find no dependance on environment for the same coefficients of satellite galaxies.

The preservation of the size-mass relation for centrals and satellites is an important test of environmental processes in galaxy formation models, however it does not completely rule out environmental processes modifying the size and mass for a given galaxy. Previous studies have compared centrals and satellites at fixed stellar mass in an attempt to control for the strong dependency of many galaxy properties on mass, trends which are largely independent of environment (van den Bosch et al., 2008b). However, to investigate how the evolution of a galaxy differed as a result of its host halo being accreted onto a more massive halo, we must compare central and satellite galaxies that were the same before the satellites were accreted. Many of the physical processes that may be applied to a galaxy once it has become a satellite, such as stripping of its hot halo gas, ram pressure stripping of its cold gas, tidal stripping

of its stars, and a modified merger rate, would affect its stellar mass evolution (Abadi et al., 1999; Balogh et al., 2004; Dekel et al., 2003; Gunn and Gott, 1972; Larson et al., 1980; Pasquali, 2015; van den Bosch et al., 2008a). As such, comparing centrals and satellites at fixed stellar mass will be unlikely to lead to a direct comparison of galaxies that were similar before the satellites became satellites. In many cases the physical processes that we wish to understand are exactly those processes that may affect the stellar mass evolution.

These physical processes could be acting in a way which preserves the size-mass relation, in essence hiding their effects from studies looking at this relation. For example, central galaxies are much more likely to experience minor mergers than satellites; this could have a 'puffing up' effect by adding mass predominantly to the outer regions of the galaxy making them larger and more massive at the same time (Naab et al., 2009; van Dokkum et al., 2010). Satellites on the other hand can either have their star formation quickly halted by quenching, leading to no further growth or have their mass stripped away by tidal interactions with their dark matter halo and harassment by nearby galaxies.

Similar problems exist when comparing galaxy populations at different epochs, which have also typically been studied at fixed stellar mass. Recently a number of groups have tried to more directly study progenitor and descendant populations at differing masses by using fixed cumulative stellar mass number density selections (e.g Lundgren et al., 2014; Papovich et al., 2011; Patel et al., 2013; van Dokkum et al., 2010; Wake et al., 2008; White et al., 2007), matched galaxy population from halo modelling and subhalo abundance matching (SHAM) (e.g. Behroozi et al., 2013; Conroy et al., 2008; Conroy and Wechsler, 2009; Moster et al., 2013; Wake et al., 2008; White et al., 2007; Zheng et al., 2007), or by comparing populations at fixed core velocity dispersion (Bezanson et al., 2012). Of these techniques, number density selection cannot be applied to the central satellite comparison. Halo modelling (assigning dark matter halos using clustering simulations) and SHAM (assigning a halo mass based on a galaxy's luminosity or stellar mass by matching their abundances) has been used to remove the effect of differing stellar mass growth when comparing centrals and satellites in the work of Wetzel et al. (2013).

In this Chapter I will make comparisons at fixed core velocity dispersions (σ_0) for central and satellite galaxies. Core velocity dispersion is largely invariant to growth by minor mergers (e.g. Bezanson et al., 2012; Loeb and Peebles, 2003) and internal processes that could significantly change σ_0, such as major bursts of star formation or puffing up via mass loss from quasars (Fan et al., 2008), are rare at the redshifts of this study. Indeed Torrey et al. (2015) show that in the Illustris simulation the core velocity dispersion of the most massive progenitors of z=0 galaxies has hardly changed on average since $z \sim 1.5$. Furthermore, since the cores of the galaxies are shielded from the environment by their outer regions, σ_0 should

remain largely unaffected by the possible mechanisms which could drive or prevent growth such as minor mergers, star formation, or tidal stripping. I compare the sizes and masses of central and satellite galaxies selected from the Sloan Digital Sky Survey and study the radial mass distribution of the galaxies, relative to the core velocity dispersion.

In Section 2.2 I describe the data sample and the cuts made. In Section 2.4 I revisit the size-mass relation for satellite and central galaxies, and investigate the size-σ_0 and mass-σ_0 relations. I also study the mass distributions of the central and satellite galaxies in bins of core velocity dispersion and discuss the implications of these results. Finally in Section 2.6 I discuss and summarise our results. Throughout the Chapter I consider a standard cosmology with the following parameters: $H_0 = 100\,h$ km s^{-1}, $\Omega_0 = 0.3$ and $\Omega_\Lambda = 0.7$.

2.2 Data

The galaxies used in this analysis come from the main sample of the SDSS Data Release 7 (DR7, Abazajian et al., 2009). I combine the Large Scale Structure Sample of the New York University Value Added Galaxy Catalog (VAGC, Blanton et al., 2005b), the MPA/JHU catalog (Brinchmann et al., 2004; Kauffmann et al., 2003b; Salim et al., 2007), the UPenn SDSS PhotDec Catalog (UPenn, Meert et al., 2015) and the Yang Group Catalog (Yang et al., 2009). The catalogs have a coverage of 7966 sq degrees, a r-band magnitude range of $-23.5 < M_r < -19.5$. I apply a redshift cut of $0.01 < z < 0.1$, which leaves 291,042 galaxies in the sample.

From the VAGC I take the fibre measurements for the Velocity Dispersion (σ) and the redshifts (Z). The velocity dispersions from the VAGC are taken from inside the 3 arc second fibre of SDSS and need to be corrected to represent the core velocity dispersion of the galaxy. To do this I corrected σ to be within one-eighth of the r_e of the galaxy using the following relationship from Cappellari et al. (2006): $\sigma_0 = \sigma_{ap}(8r_{ap}/r_e)^{0.066}$. This is the mean power-law relation, $\sigma_R \propto R$, of 25 E/S0 type galaxies from the SAURON survey. The relation was fitted using a Tukey Biweight and agrees well with previous studies of the relation from Jorgensen et al. (1995) and Mehlert et al. (2003). In this study it applies an average correction of $12 \pm 1\%$. Due to the resolution of SDSS spectra σ_0 has large errors at low values, in addition the population is poorly sampled at high values of σ, considering this I only include galaxies with $70 kms^{-1} < \sigma < 300 kms^{-1}$ and $\Delta\sigma < 15\%$.

From MPA/JHU catalog I use the specific star formation rates ($sSFR = SFR/M_*$), which are calculated using the technique described in Brinchmann et al. (2004).

The UPenn PhotoDec Catalog uses two component fits of the photometry to estimate a variety of galaxy properties, as opposed to the single component fits of earlier catalogs, I use

the best fit for each galaxy which may be a single component or a combination of Sérsic, exponential and De Vaucouleurs profiles. I use the total r and g-band magnitudes to calculate new stellar masses from the best fits of the catalog. In addition I use the best fit half-light radii; galaxies with $r_e > 30$ kpc are cut from the sample due to poor sampling and large errors above this radius. I also use the axis ratios from this catalog to cut out edge-on spirals, as the rotational velocity of these galaxies can contaminate their core velocity dispersion and cause it to appear higher than it would otherwise be. To achieve this I remove galaxies with a b/a ratio < 0.1. Finally I use the Sérsic indices from the best single component fits and the total stellar mass estimates.

I calculate the maximum volume, V_{max}, over which a galaxy could be observed using the flux limit of SDSS, the mass of the galaxy, the redshift limit and the mass completeness limits as derived from Wake et al. (2012). This process corrects for the fact that many low brightness galaxies are not picked up by SDSS as they fall below the flux limit, which would skew the results at higher redshifts to high luminosity galaxies.

I use the total r and g-band magnitudes and the stellar masses from the UPenn catalog. From these properties I find the mean stellar mass-to-light ratio at fixed $g-r$ colour for the galaxies in the sample. I then use this ratio to calculate stellar mass profiles from the radial profiles of r and g magnitude from the SDSS photometry. While using a fixed stellar mass-to-light ratio for a certain colour does not accurately portray each individual galaxy, I expect the variations between galaxies to average out when looking at mean radial profiles of stellar mass.

In this Chapter I use a variety of subsamples, which include the central and satellite galaxies described in Section 2.3, and the star forming and quiescent galaxies defined in 2.4. I find that there are no differences in the redshift distributions of these subsamples and as such there is no effect on the results that such a difference may introduce.

Applying the cuts laid out in this section gives a final sample of 124,524 galaxies. The majority of the galaxies not included in our final sample are disqualified by the stellar mass completeness limit and velocity dispersion cuts.

2.3 Defining Central and Satellite Galaxies

To define central and satellite galaxies I primarily use the Yang Group Catalog (Yang et al., 2009), which uses an iterative group finding algorithm to construct dark matter haloes from the SDSS galaxies. Starting with a simple friends-of-friends algorithm, tentative groups are found and assigned properties based on their characteristic luminosities. Using the properties of these tentative groups the algorithm decides whether or not to add galaxies from the

nearby redshift space. If new galaxies are added to the group, the dark matter properties are recalculated based on the new group luminosity. The group finder iterates over this process until no changes to the groups are made.

The Yang Catalog has two definitions for the centrals and satellites, which are based on the stellar mass and luminosity of the galaxies in each halo. In these definitions the most massive or brightest galaxy in each group is designated the central and the rest of the galaxies satellites. I choose to use the mass rather than luminosity definition for our centrals, but take some further steps to mitigate any bias that this definition may introduce into our analysis. As I have selected centrals to be more massive, this could introduce a small bias into the mass-σ_0 relation (and by extension the size-σ_0 relation), making the central galaxies more massive at fixed σ_0. Consider a halo where the two most massive galaxies have identical central velocity dispersions; the most massive galaxy will be designated the central and the least massive the satellite. As a result central galaxies may appear more massive than satellite galaxies at fixed σ_0 simply as a result of the central/satellite definition. This definition could also introduce other similar biases for any galaxy property that depends on stellar mass.

To mitigate this potential bias I consider throughout the Chapter two additional central/satellite definitions. The first chooses to use the galaxy with the highest σ_0 as the central in all haloes. This leads to approximately 2500 centrals (5% of the groups in the sample) being swapped with a satellite from their halo that has a higher dispersion. The second combines the mass and σ_0 definitions by randomly selecting which galaxy (the highest mass or the highest dispersion) will be the central, resulting in roughly 1250 centrals being swapped with satellites. I use this random sampling method to define the main sample throughout this work, but I also show the results for both the mass and dispersion samples for reference. I note that whilst the three definitions of central galaxies produce slightly different results in the manner that I expected, using any of them would result in the same conclusions for all the trends that I study. The same is true for the most conservative method of only using haloes where the central galaxy has both the highest stellar mass and σ_0, although I do not make use of this definition since it removes a large number of galaxies from our sample.

2.4 Results

2.4.1 The Size-Mass Relation

I begin by comparing the size-mass relation of the central and satellite galaxies. In Figure 2.1 I plot the median r_e of the centrals and satellites at fixed mass in 20 stellar mass bins, each of which has the same number of satellite galaxies. The top row is the size-mass relation and

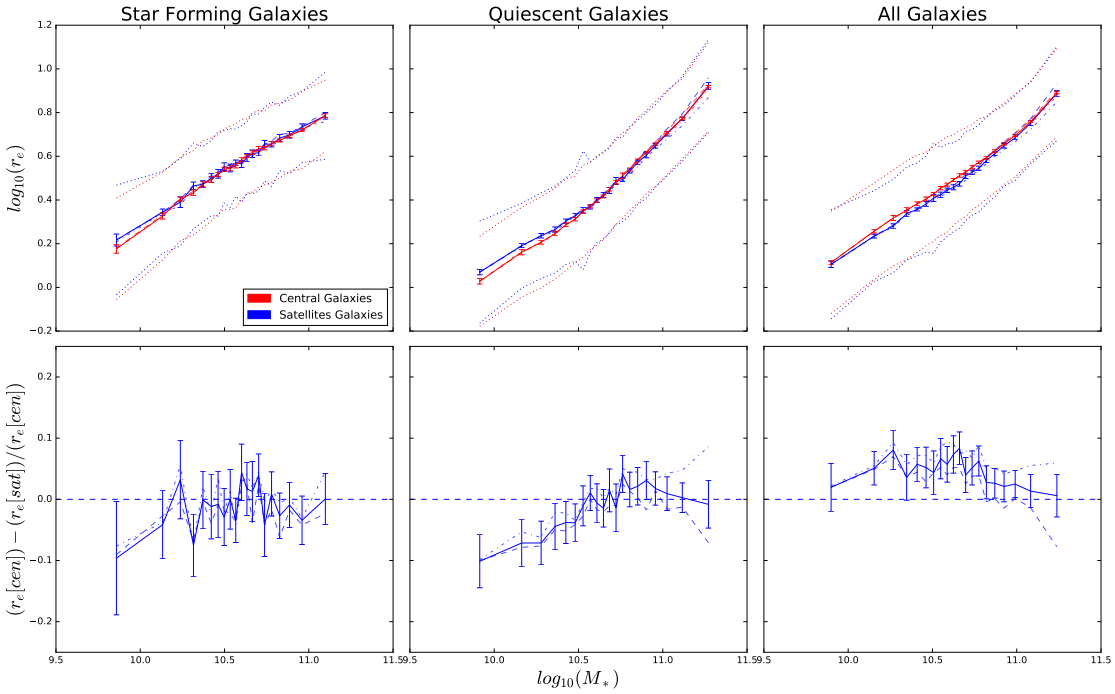

Fig. 2.1 (Top) Comparison of the median half-light radius at fixed mass of central (red line) and satellite (blue line) galaxies. Left is the star forming population, centre is the quiescent and right is the entire population. The dotted lines represent the 1σ scatter. The solid lines represent the random central/satellite split, the faint dot-dashed lines represents the mass split and the faint dashed lines represent the σ_0 split (see the main text for details). (Bottom) The fractional difference in median radius at fixed mass for central and satellite galaxies. I see that for the star forming and quiescent population the size-mass relation is almost the same for centrals and satellites. For all galaxies the centrals are slightly larger than the satellites, but this is predominantly due to the different quiescent fractions in the central and satellite populations (see text).

the bottom row is the difference between the centrals and satellites. The errors are calculated from 1000 bootstrap resamplings. In all cases I weight by V_{max}. The panels from left to right show relations for star forming galaxies, quiescent galaxies, and all galaxies. I split the galaxies into star forming and quiescent populations by applying a cut at $log_{10}(sSFR) = -11$, which sits at the minimum between the two peaks in the bimodal sSFR distribution (e.g. Wetzel et al., 2012).

I apply this sSFR cut for two reasons. Firstly, as is visible in Figure 2.1, star forming galaxies typically have larger r_e than quiescent galaxies at the same mass (or σ_0) although, the difference decreases at higher masses and dispersions. This difference most likely results from extended luminous star forming disks in the star forming galaxies increasing the r-band r_e. If I ignored this dependence on star formation, mean differences in the sizes of centrals and satellite galaxies could result from differences in the quiescent fractions, which are known to be higher in satellite galaxies at all masses (e.g. Wetzel et al., 2012). Secondly, since a central galaxy is more likely to be star forming than a satellite, I would like to separate out the effects of ongoing star formation, which would preferentially produce more massive central galaxies, from processes like tidal stripping of stars and minor mergers, which act on SF or quiescent galaxies alike.

The solid lines in Figure 2.1 represent the random central/satellite sample, while the faint dot-dashed and dashed lines represent the samples with centrals defined by mass and dispersion respectively. The three different central definitions show very similar relationships with the largest divergence at the high mass end. This plot mimics those found in Huertas-Company et al. (2013) (and others), that the size-mass relation is largely the same for centrals and satellites.

Even though there is very little difference between the central and satellite size-mass relations for either star forming or quiescent galaxies there is a small difference in size for the full galaxy population, with central galaxies being larger at all masses. This larger difference is a result of the differing quiescent fractions of central and satellite galaxies. The higher fraction of quiescent satellites at all masses results in smaller sizes relative to the centrals, which are more likely to be star forming.

The fact that the size-mass relation does have very little dependence on environment is an interesting result in and of itself (e.g. see Shankar et al. (2014) for comparisons to semi-analytic galaxy formation model predictions), but it does not tell us how the sizes and masses of individual galaxies may be being changed by their transition from central to satellite relative to those that remain centrals. It only tells us that if the masses and sizes are changing for centrals and satellites these changes must be linked. For example, if mass is lost then the galaxy must shrink in r_e, and if mass is gained then the galaxy must expand in

r_e, such that the size-mass relation remains unchanged. Another way to put this is that the stellar mass density of the centrals and satellites remains constant and satellites are no more or less compact than their central counterparts.

Minor mergers and ongoing star formation provide mechanisms for growth that predominately apply to central galaxies and which could increase the size of galaxies in a way which preserves the size-mass relation. However, tidal stripping and harassment mainly affect satellites and could lead to reduced sizes and masses, again in a way which could preserve the size-mass relation. Wetzel et al. (2013) estimate that as a result of the quenching of their star formation quiescent satellite galaxies are 10-20% less massive than they would have been had they remained centrals. Tidal stripping could further reduce the mass of satellites galaxies by 10% on average, depending on the halo mass Bahe et al. (2016). For these reasons comparing galaxies at fixed mass may not be the best way to approach studying environmental effects on galaxies. Instead I want to be able to compare central and satellite galaxies that were the same or similar prior to a satellites accretion onto a new dark matter halo.

2.4.2 Size and Mass comparisons at fixed σ_0

To determine how the growth of satellites and centrals differ, I consider a variable which is not likely to be affected by the environmental processes experienced by a galaxies whether they are a central or satellite. I choose to investigate the relationships of M_* and r_e with the core velocity dispersion, σ_0, which, as already discussed, I expect to remain largely unchanged by the physical processes acting on centrals and satellites.

Figure 2.2 shows the V_{max} weighted median half-light radius of central and satellite galaxies in the top row and the difference between the medians in the bottom row as a function of σ_0. I use the same method as in Figure 2.1 to split the sample into bins of σ_0. As with Figure 2.1 the solid lines represent the random central/satellite split and the faint dot-dashed and dashed lines represent the mass and dispersion based samples respectively.

For the star forming galaxy sample I see that there is no difference in the size-σ_0 relation for the random central/satellite split. The centrals from the mass definition are slightly larger than the satellites, but this is likely due to the bias mentioned in Section 2.2. When I use the dispersion based sample, the satellites become slightly larger than the centrals at dispersions above $\sigma_0 = 125 kms^{-1}$. However, I could in fact be introducing the opposite bias here as I have deliberately decided against classifying the more massive, larger galaxies as centrals in some haloes.

Unlike the star forming sample, the quiescent galaxies show a large difference in size between the centrals and satellites in all three central/satellite splits. For the randomly defined sample the fractional difference increases with σ_0 from $4 \pm 7\%$ at $\sigma_0 = 90 km/s$, to $32 \pm 4\%$

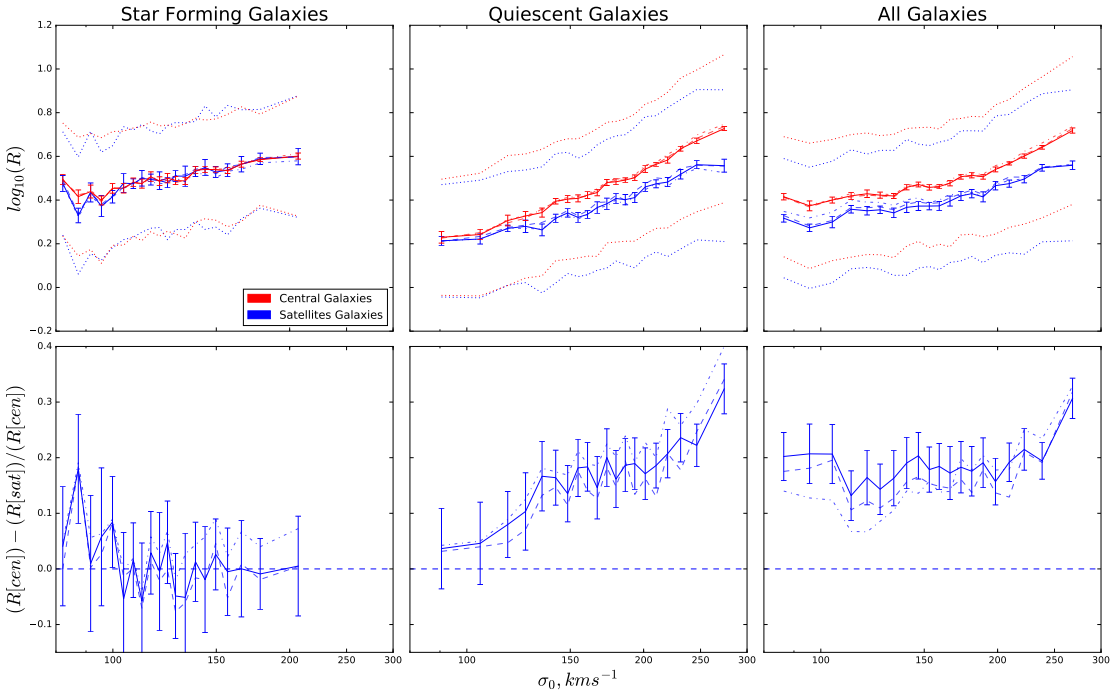

Fig. 2.2 (Top) Comparison of the median half-light radii of central (red) and satellite (blue) galaxies. Left is the star forming population, centre is the quiescent population and right is the entire population. The dashed lines represent the 1σ scatter. The solid lines represent the random central/satellite split, the faint dot-dashed lines represents the mass split and the faint dashed lines represent the σ_0 split (see the main text for details). (Bottom) The fractional difference in median radius at fixed σ_0 for central and satellite galaxies. For the star forming population I see no difference in size at fixed central dispersion, but for quiescent galaxies I see that the centrals become increasingly larger at higher dispersions than for satellites. For all galaxies there is a constant difference in size.

at $\sigma_0 = 270 km/s$ with an average difference of 16%. In the mass defined sample I see that the σ_0 dependance is stronger, with the difference in size reaching $40 \pm 4\%$, with an average difference of 19%. The dispersion defined sample shows a lower maximum size difference of only 25% and an average difference of 13%.

In the full galaxy population the difference in size remains relatively constant at all values of σ_0 with an average difference of 16%. The relation is fairly constant for the random and dispersion defined samples, but has a small σ_0 dependance in the mass defined sample.

Given that the central and satellite size-mass relations are the same and the size-σ_0 relations are not, I would expect to find a difference in mass at fixed dispersion between centrals and satellites. In Figure 2.3 I plot the median stellar mass in bins of velocity dispersion. As with the size-σ_0 relation I see that there is a mass deficit in the satellite galaxies. The star forming galaxies exhibit an average difference of 5% in mass for the random central definition sample, the difference in slightly higher at 8% for the mass defined sample and disappears completely for the dispersion defined sample.

Quiescent central galaxies show a consistently higher mass at fixed dispersion than quiescent satellite galaxies. The relation is relatively flat for the randomly defined sample, with an average difference of 17%. The average difference is lower for the dispersion defined sample at 14%. For the mass defined sample there is a stronger dependance on σ_0 with the fractional difference reaching 32% in the highest dispersion bin, and with an average difference of 20%.

2.4.3 Radial Profiles

If I assume that σ_0 is invariant with environment then the satellite and central galaxies were originally similar galaxies which have followed different evolutionary pathways. Our results indicate that this different evolution has either caused the centrals to continue growing, most likely through some combination of star formation and minor mergers, or that the satellites have been stunted by processes such as quenching, tidal stripping, and harassment. To investigate further I use the radial colour profiles in the *g* and *r* bands from SDSS to identify if there is a change in the mass distribution of the galaxies. If the environment is indeed playing a role in shaping the mass and size of the galaxies then I could see a difference in the mass profiles of the centrals and satellites. One might expect to see that the galaxy cores remain the same for centrals and satellites, indicating that the core and therefore the core velocity dispersion has not been affected by the environment. However, in the outskirts of the galaxies one might expect that the satellites will have less mass than the centrals, due to the satellites losing mass and the centrals gaining mass from the environment. I will investigate the mean radial profiles of surface mass density and total stellar mass.

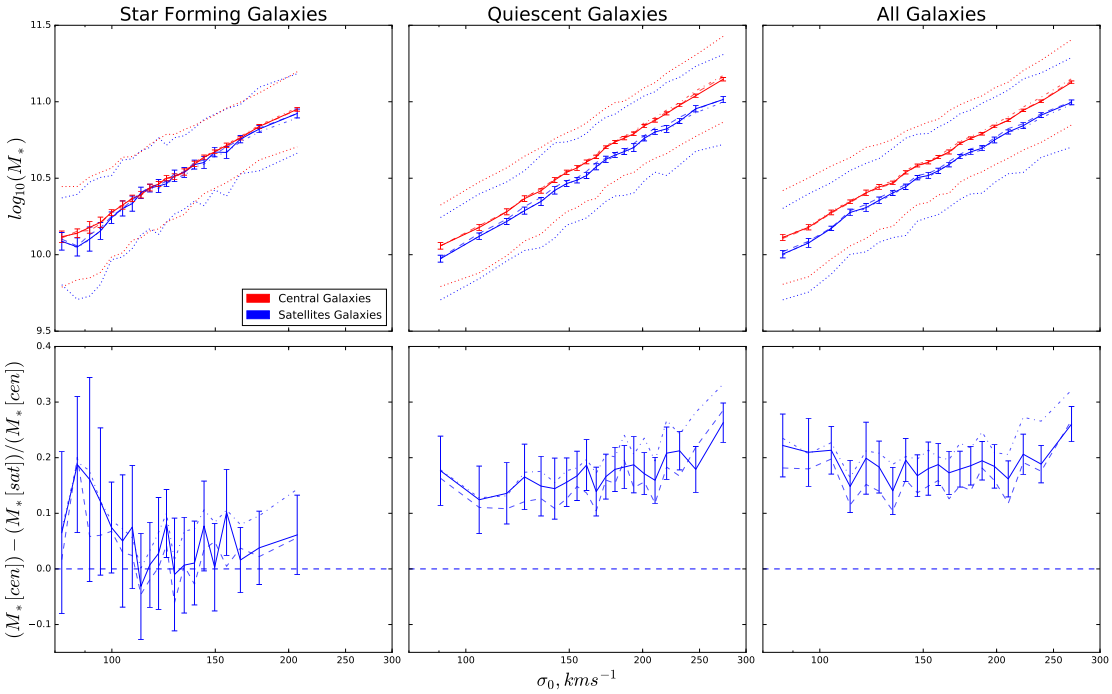

Fig. 2.3 (Top) Comparison of the median stellar mass of central (red) and satellite (blue) galaxies. Left is the star forming population, centre is the quiescent group and right is the entire population. The dashed lines represent the 1σ scatter. The solid lines represent the random central/satellite split, the faint dot-dashed lines represents the mass split and the faint dashed lines represent the σ_0 split (see the main text for details). (Bottom) The fractional difference in median mass at fixed σ_0 for central and satellite galaxies. The star forming population shows a small difference in mass at fixed dispersion and the quiescent population has a larger difference in mass, which increases with higher dispersion. For all galaxies the difference in mass remains roughly constant.

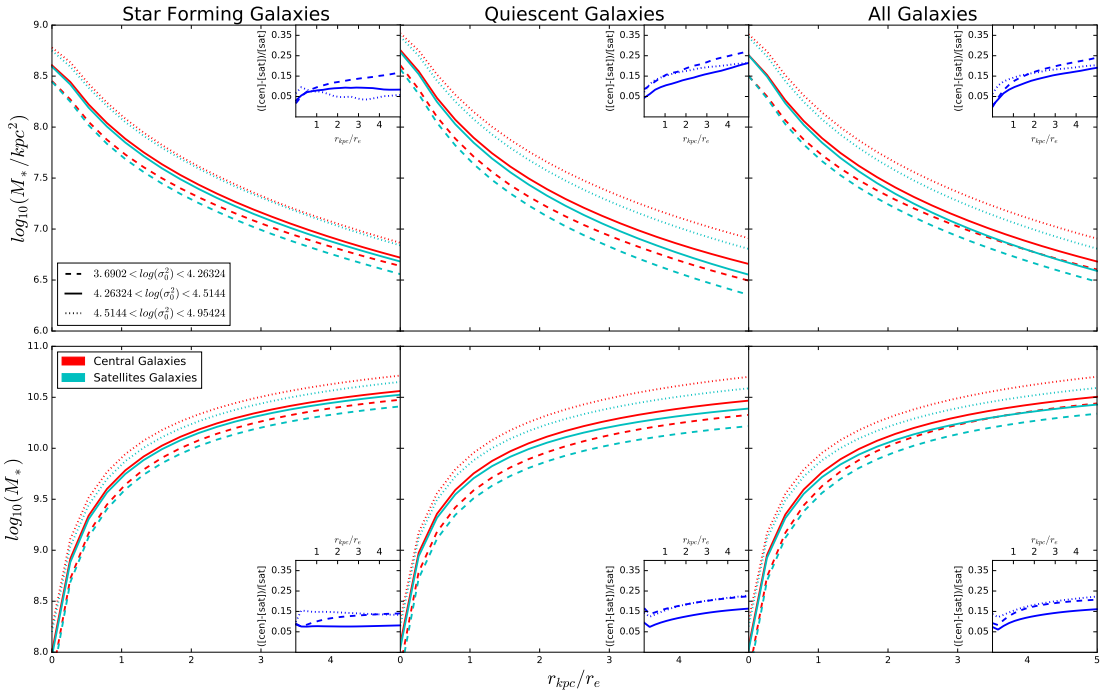

Fig. 2.4 (Top) The mean surface mass density at fixed radius of the star forming, quiescent and full galaxy populations. (Bottom) The cumulative mean mass at fixed radii. The dashed, solid and dotted lines represent increasing bins of velocity dispersion, while the red lines are the central galaxies and the blue lines are the satellite galaxies. The inset figures show the fractional differences in mass density and cumulative mass at fixed radii. In the core regions of the galaxies I see that the centrals and satellites have the same mass density, indicating that the cores are largely unaffected by the environment. However in the outer regions of the galaxies the mass density begins to diverge, with centrals having more mass at larger radii. This relationship is stronger for quiescent galaxies than for star forming galaxies, which mirrors our previous results. I only consider the random central/satellite split in this Figure.

I measure the radial mass profiles using the *r*-band and *g*-band profiles from SDSS. The magnitudes are k-corrected using the values from NYU-VAGC to a common redshift of $z = 0.1$. To convert the magnitude profiles into mass profiles I require a mass-to-light ratio, which I estimate using the stellar masses of the galaxies and *g*- and *r*-band magnitudes from the UPenn catalog. I fit a linear relation to the observed $g-r$ colour and the stellar mass to *r*-band light ratios of all the galaxies in the sample. I fit the radial $g-r$ colour profiles of each galaxy to this relation to find the mass-to-light ratios in each of the radial bins. Finally, I use these mass-to-light ratios to convert the *r*-band magnitude profiles into stellar mass profiles.

In Figure 2.4 I plot the mean surface mass densities in units of $log_{10}(M_*)$ per square kiloparsec and cumulative mass profiles in units $log_{10}(M_*)$ for galaxies split in to three bins of velocity dispersion and into the three star formation rate populations. For a given star formation class surface mass density increases as the velocity dispersion increases. For a given dispersion the quiescent galaxies have higher surface mass densities than the star forming galaxies. I see the same trend in the cumulative mass profiles (bottom panels of Figure 2.4), with the higher dispersion bin being the most massive and the quiescent galaxies being more massive than star forming galaxies.

In each of the surface mass density plots I see that the centrals and satellites have very similar core densities. However, at larger radii the mass density of the centrals becomes higher than the satellites. Once again I see that the difference between the centrals and satellites is larger for the quiescent galaxies than for the star forming galaxies. The difference in density is also greater in the highest dispersion bin for quiescent galaxies, as was seen in the previous section. These results are reflected in the cumulative mass profiles. For a given bin in dispersion the satellite core masses are very close to the central core masses, but I see that most of the mass difference is in the outer regions of the galaxies.

2.4.4 The Stellar Metallicity Relations

Pasquali et al. (2010) found that satellite galaxies had lower stellar metallicity than centrals with the same stellar mass and that this metallicity difference increased as the stellar mass decreased. They argued that this could be being caused by mass stripping from the satellites, so that the satellites had the higher stellar metallicity of the higher mass galaxies they were before being stripped[1]. The same result would also occur if the centrals were increasing in mass without changing their metallicity (e.g. from minor mergers), while the satellites

[1] Pasquali et al. (2012) argue that this is not in fact the mechanism responsible based on gas phase metallicity measurement.

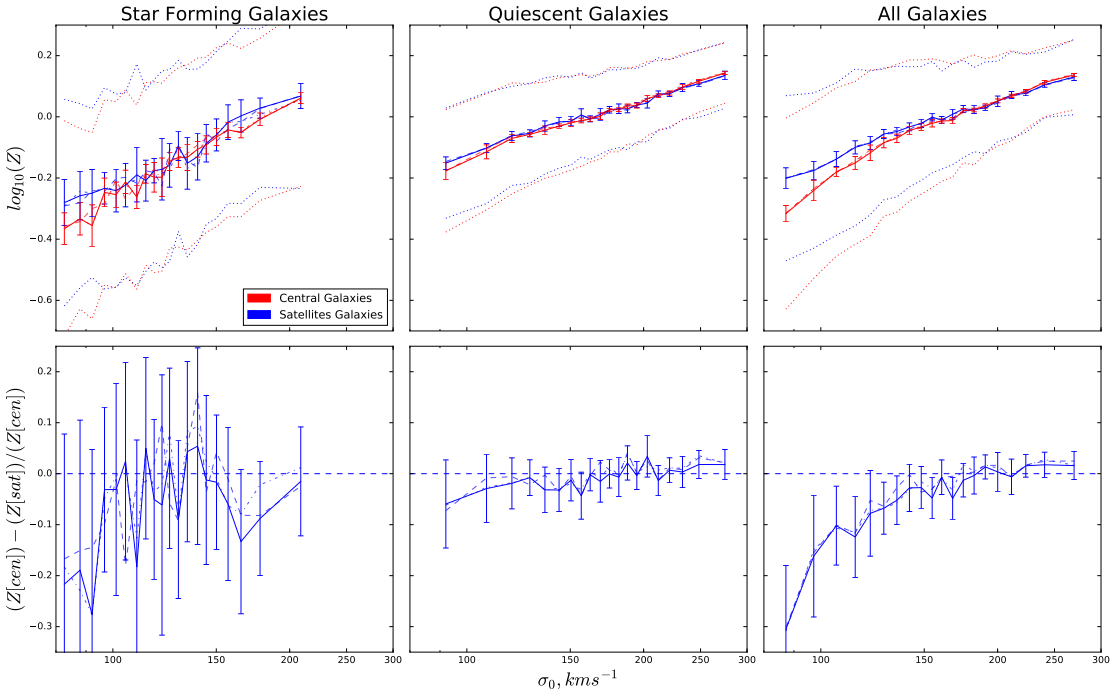

Fig. 2.5 (Top) Comparison of the median stellar metallicity at fixed σ_0 of central (red line) and satellite (blue line) galaxies. Left is the star forming population, centre is the quiescent and right is the entire population. The dashed lines represent the 1σ scatter. The solid lines represent the random central/satellite split, the faint dot-dashed lines represents the mass split and the faint dashed lines represent the σ_0 split (see the main text for details). (Bottom) The fractional difference in median stellar metallicity at fixed σ_0 for central and satellite galaxies. I see that for the star forming and quiescent population the metallicities for centrals and satellites are largely the same, except at very low dispersions for the star forming sample. Contrary to this, the all galaxy sample shows a strong trend with σ_0 in the difference in metallicity, where low dispersion centrals have lower metallicity than low dispersion satellites, this is however due to the relative mixing of star forming and quiescent centrals and satellites at different dispersions.

remained unchanged. I revisit this relation and include results for the metallicity at fixed σ_0 and for galaxies split by star formation rate as before.

In Figures 2.5 and 2.6 I show the difference between central and satellite metallicity for SF, quiescent and all galaxies as a function of σ_0 and mass, respectively, in the same way as I have previously. I have used the stellar metallicity measurements of Gallazzi et al. (2005) as were used by Pasquali et al. (2010). One important aspect of these measurements is that the size of the SDSS fibre insures that the metallicity is being measured in the central part of the galaxy (typically within one r_e) and therefore should be largely unaffected by environmental processes in the same way σ_0 is unaffected, in particular minor mergers depositing metal poor stars on the outskirts of central galaxies.

One can see in Figure 2.5 that for both SF and quiescent galaxies there is almost no difference between the metallicity of central and satellite galaxies at fixed σ_0. At fixed mass there is a small difference ($\sim$5%) with central galaxies having lower metallicities than the equivalent satellites. In both cases there is a very weak trend such that the higher the mass or σ_0 of the centrals the smaller their deficit in metallicity relative to the satellites, with the highest σ_0 centrals actually being more metal rich. The $\sim$5% difference in metallicity between centrals and satellites at fixed mass is consistent with the difference in mass measured at fixed σ_0 (Figure 2.3) and the central mass-metallicity relation. In other words it is consistent with the central metallicity remaining unchanged between galaxies that become satellites or remain centrals and either central galaxies gaining mass and/or the satellite galaxies losing mass. The absence of any real difference in metallicity at fixed σ_0 further supports our tenet that σ_0 is unaffected by environmental processes.

It is worth pointing out a couple of other interesting aspects of Figure 2.5. Since SF and quiescent galaxies are considered separately, central and satellite galaxies show very little difference in metallicity at fixed mass or σ_0. The larger difference for the full galaxy population shown in the right hand panel of Figures 2.5 and 2.6, and previously found by Pasquali et al. (2010), is largely being driven by differing fractions of SF and quiescent galaxies within the central and satellite population. There is a larger fraction of quiescent galaxies in the satellite population, which typically have higher metallicities than SF galaxies of the same mass or σ_0, causing the median metallicity of the satellites within the whole galaxy population to be higher. The increase in the difference between the central and satellite metallicity as mass or σ_0 decreases is caused by the combination of two effects; both the difference in metallicity between SF and quiescent galaxies and the difference in the fraction of quiescent galaxies between centrals and satellites increase as mass or σ_0 decrease.

It is also worth noting that the lack of much of a difference in the stellar metallicity of central and satellite galaxies when split in SF and quiescent is at odds with the recent

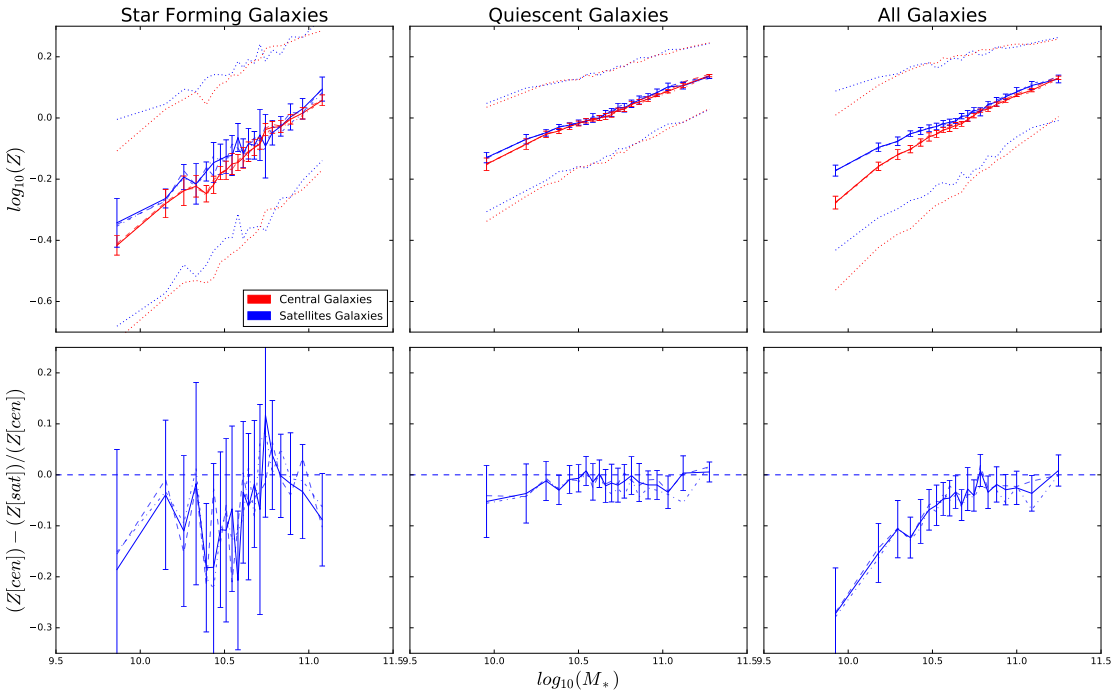

Fig. 2.6 (Top) Comparison of the median stellar metallicity at fixed stellar mass of central (red line) and satellite (blue line) galaxies. Left is the star forming population, centre is the quiescent and right is the entire population. The dashed lines represent the 1σ scatter. The solid lines represent the random central/satellite split, the faint dot-dashed lines represents the mass split and the faint dashed lines represent the σ_0 split (see the main text for details). (Bottom) The fractional difference in median stellar metallicity at fixed mass for central and satellite galaxies. As with the fixed σ_0 case I see little difference in the metal content of the centrals and satellites for the quiescent sample, and a small difference in the metal content of star forming centrals and satellites. As with the σ_0 there is a strong dependance on mass for the difference in metal content for the full galaxy population.

measurements from the EAGLE simulation (Bahe et al., 2016), which show a much larger difference in all star forming groups. The differences between these results are likely due to the fact that the EAGLE metallicity measurements encompass the entire galaxy, not just the central 3 arcsec for SDSS spectra. Bahe et al. (2016) show that satellites in EAGLE accrete much less of their stellar mass than field galaxies due to a lower merger fraction, which partly explains the differences in metallicities. If as I have described previously, this accreted mass is predominantly at larger radii, the difference in metallicity would not show up in the SDSS aperture. However, in agreement with the results presented here, Bahe et al. (2016) do show that satellite mass loss cannot explain the increase in metallicity that they see.

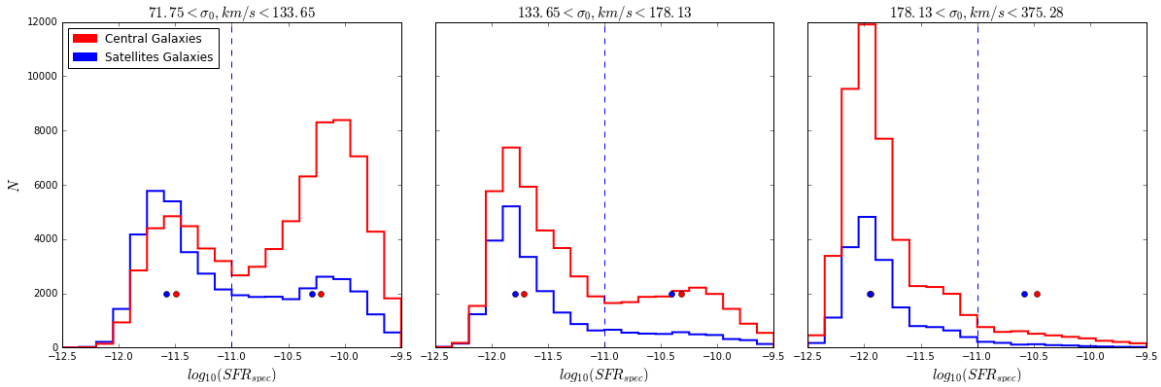

Fig. 2.7 I show the distributions of Specific Star Formation Rate in three bins of core velocity dispersion. The Figure shows central galaxies in red and satellite galaxies in blue and the $log_{10}(sSFR) = -11$ cut for quiescent and star forming galaxies as the blue dashed line. I also mark the median sSFR for the centrals and satellites in both star formation groups with solid circles. I see that the distributions are similar, but the centrals have a higher median sSFR in most of the bins.

2.5 Systematics

In this section I investigate whether other correlations between galaxy properties that are independent of environment could be responsible for the observed differences between central and satellite galaxy size and mass, including the star formation rate and morphology distributions.

2.5.1 The Effect of Ongoing Star Formation

Throughout, I have split our sample into two separate groups by specific star formation rate, by applying a cut at $log_{10}(sSFR) = -11$. The purpose of this cut was to separate the effect of ongoing star formation within the centrals and satellites, which could lead to a difference in size and mass. As demonstrated by Figures 2.1 and 2.2 the star forming galaxies are larger than their quiescent counterparts and so there is a relationship between size and sSFR at fixed mass or σ_0. As a result, I want to be sure that within the two sets of galaxies there is not a residual difference in the star formation rates between the central and satellite galaxies, which may be responsible for the size and mass[2] difference between centrals and satellites. For example, if the median specific star formation rate of quiescent galaxies was $10^{-11.5} yr^{-1}$ and the median for satellites was $10^{-12} yr^{-1}$ the central galaxies could be larger simply due to correlation between size and sSFR.

In Figure 2.7 I compare the distributions of specific star formation rates for central and satellite galaxies, in bins of core velocity dispersion. I also mark on the median sSFR rates in

[2]Star forming galaxies also have higher mass at fixed σ_0 e.g. Bezanson et al. (2015), Figure 2.3

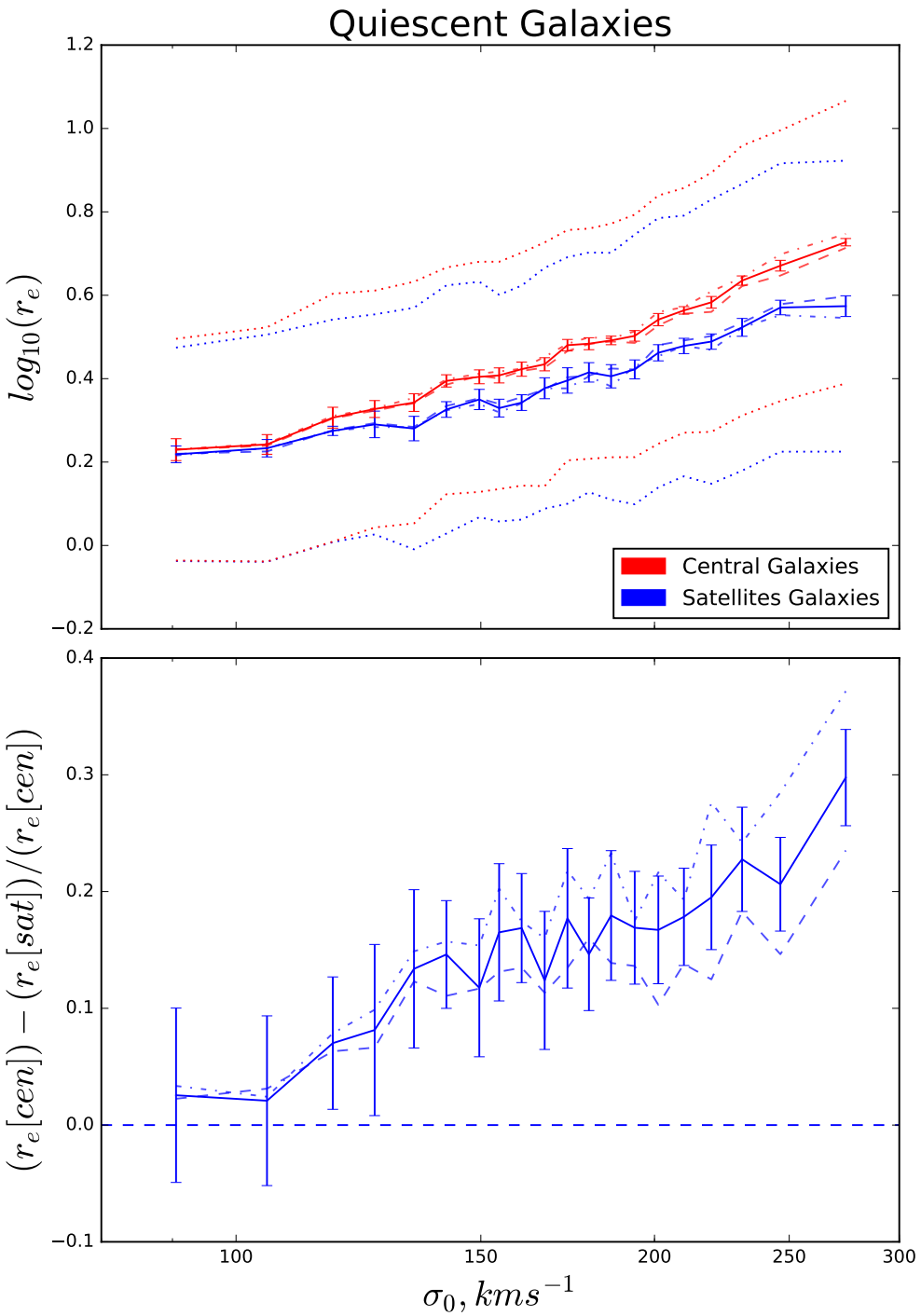

Fig. 2.8 (Top) Comparison of the median half-light radii of central (red) and satellite (blue) galaxies in the quiescent group weighted by their relative specific star formation rate distributions (see the main text for details). The dashed lines represent the 1σ scatter. The line styles are the same as in previous figures. (Bottom) The fractional difference in median radius at fixed σ_0 for central and satellite galaxies. I see that there is little difference between these weighted results and the results from Figure 2.2, indicating that differences between the central and satellite sSFR distributions are not responsible for the differences between central and satellite size and mass.

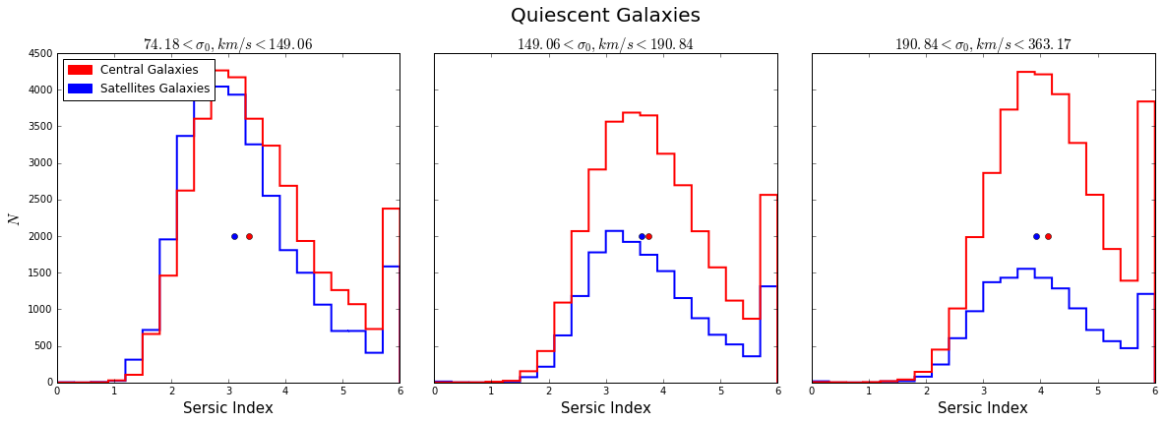

Fig. 2.9 I show the distributions of Sérsic Index in three bins of core velocity dispersion. The central galaxies are shown in red and satellite galaxies in blue. I also mark the median Sérsic Index for the centrals and satellites in both star formation groups with solid circles. I see that the distributions are similar, but the centrals have a higher median Sérsic Index in all of the bins. Note that there are a large number of galaxies in the Sérsic Index = 6 bin as this is the maximum index assigned by the UPenn catalog.

the star forming and quiescent groups. This figure shows that whilst the shapes of the sSFR distributions are similar, the central galaxies have a slightly higher median sSFR rate than the satellites. To make sure that these differences are not responsible for any of the previously observed trends I can weight each satellite galaxy in such a way as to make the central and satellite sSFR distributions identical. To do this I weight the satellites in each sSFR bin by the fractional difference between the number of satellite and central galaxies in that bin. I can then add these weights back into our calculations of the differences in size and mass from Section 2.4.

I show the weighted results for the size-σ_0 relation for quiescent galaxies in Figure 2.8, which shows that the sSFR weights do not significantly alter the relation or the fractional difference in size, which ranges from 3% at low dispersion to 29% at high dispersion. I do not show the star forming galaxies or the mass-σ_0 relation, but neither of these are significantly affected by the sSFR weights either. These results indicate that despite the central galaxies having slightly higher sSFR than the satellites, even when split into star forming and quiescent subsamples, and there being a correlation between sSFR and size at σ_0, the differing sSFRs are not contributing to the observed difference in the size or mass of central and satellite galaxies at fixed σ_0.

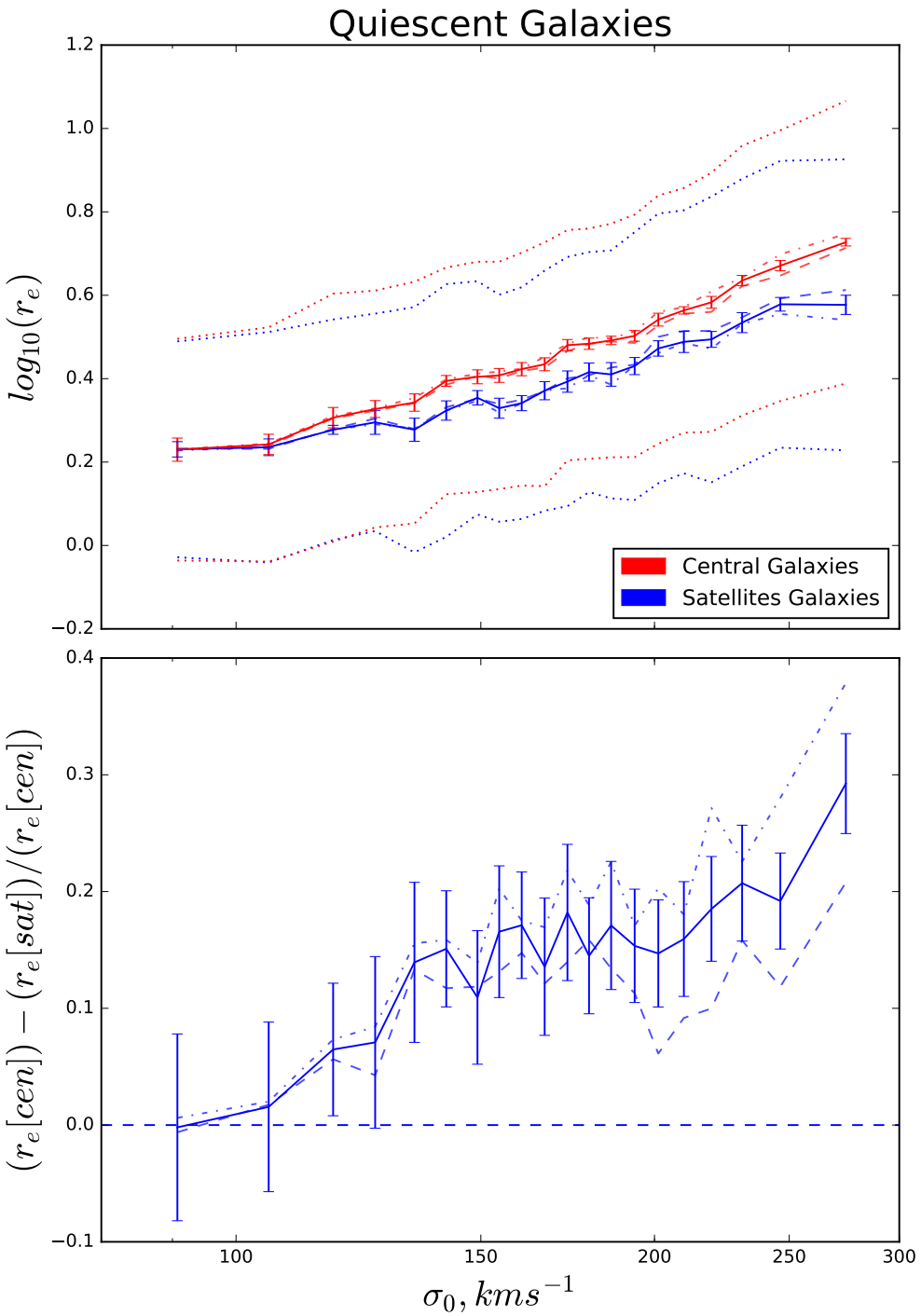

Fig. 2.10 (Top) Comparison of the median half-light radii of central (red) and satellite (blue) galaxies in the quiescent group weighted by their relative Sérsic Index distributions (see the main text for details). The dashed lines represent the 1σ scatter. The line styles are the same as in previous Figures. (Bottom) The fractional difference in median radius at fixed σ_0 for central and satellite galaxies. I see that the difference in size has decreased only slightly from the results in Figure 2.2, indicating that differences between the central and satellite morphology distributions are not responsible for the differences between central and satellite size and mass.

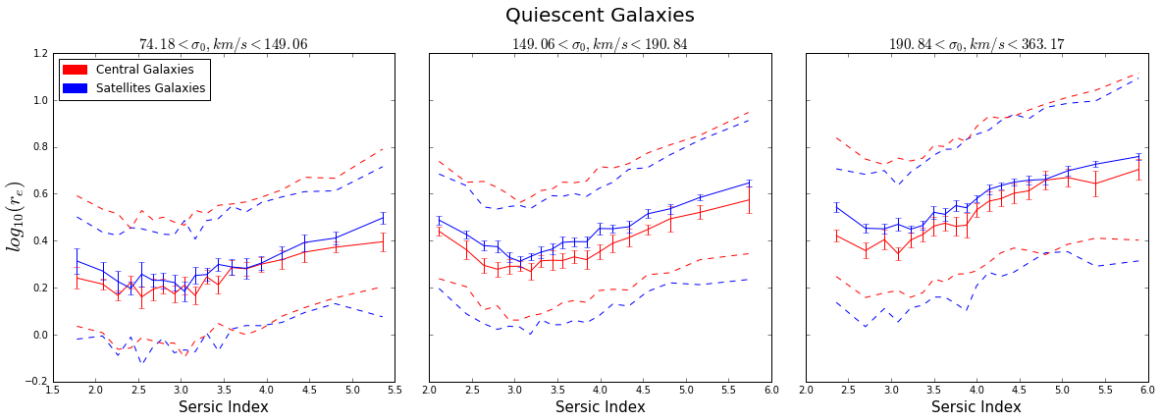

Fig. 2.11 I show the Sersic index-size relations for quiescent central and satellite galaxies in three bins of σ_0. The error bars are the standard deviation of the medians from 1000 bootstrap resamplings and the dashed lines represent the 1σ scatter. These plots show that both central and satellite galaxies are typically larger at higher Sersic Index, which is responsible for the effect of the weights on the size-σ_0 relation shown in Figure 2.10.

2.5.2 Differing Morphologies of Centrals and Satellites

While it is generally true that star forming galaxies are mostly late-type spirals, and quiescent galaxies are predominantly early-types, there may be a difference in the distribution of these morphologies between the centrals and satellites. For instance one could imagine a larger fraction of late-type galaxies amongst quiescent satellites than quiescent centrals as the star formation is halted in satellite galaxies. As morphological late-type galaxies are typically larger at fixed mass and higher mass at fixed σ_0 than early-type galaxies (both among star forming and quiescent populations e.g. Bezanson et al. 2015) it would follow that, much like in Section 2.5.1, any difference in the morphological distribution between central and satellites could be contributing to the observed difference in the size-σ_0 or mass-σ_0 relations.

I study this in the same way as I did for the ongoing star formation rates by analysing the Sérsic indices of the central and satellite galaxies at fixed σ_0. In Figure 2.9 I show the distributions of morphologies in three bins of σ_0 for the quiescent galaxies. The satellite galaxies have lower median Sérsic indices, indicating that they are on average more disk like. Paradoxically, this would actually indicate that the satellites should be larger at fixed mass than the centrals, though the effect may be small enough that it is simply washed out by the environmental signal. The Sérsic Index is most different for low dispersion galaxies, the difference drops for medium dispersion galaxies and rises again for the high dispersion galaxies.

Much like in the previous section, I wish to test how much the difference in galaxy shape can affect the relations I have found. I build a set of weights for the satellite galaxies by

finding the fractional difference between the number of satellites and centrals in each Sérsic index bin. I apply these weights to the satellite galaxies and recalculate the differences in size and mass at fixed σ_0. In Figure 2.10 I show the median size at fixed σ_0 for quiescent centrals and satellites and the difference in size between those galaxies. Comparing to Figure 2.2, I see that the difference in size has decreased slightly, to $0 \pm 8\%$ at the lowest σ_0 to $29 \pm 4\%$ in the highest σ_0 bin for the random sample. The average difference in size drops to 17% for the mass selected central sample, 16% in the randomly selected central sample and 13% in the σ_0 selected sample. Interestingly, this is the opposite effect that might be expected. Since satellites are more disk-like one would have expected them to made them larger at fixed σ_0 and thus the difference in size smaller before I corrected for the difference in morphologies. However, as I show in Figure 2.11 the higher Sérsic index galaxies are in fact larger and since they receive larger weights from the correction the satellites are made larger, thus the difference in size decreases.

The largest change in the difference in size happens in the lowest dispersion bin which drops from 5% to almost no difference at all. This is also where the difference in median Sérsic index is largest in Figure 2.9. The smallest changes happen at medium dispersions and the change increases again at high dispersion, this mirrors the differences in median Sérsic Index between central and satellite galaxies.

2.6 Summary & Discussion

I have analysed the properties of central and satellite galaxies in a sample of 130,000 galaxies, from Data Release 7 of the SDSS. I use derived quantities from the NYU-VAGC, the MPA/JHU Catalog and the UPenn Photodec Catalog. I split our galaxies into star forming and quiescent groups and then divide them into centrals and satellites using the Yang et al. (2009) group catalog.

I began by revisiting the size-mass relation of central and satellite galaxies. Using the median half-light radius in bins of fixed stellar mass I observed that for star forming and quiescent galaxies the size-mass relation does not depend on whether a galaxy is a central or a satellite, echoing the results of previous studies (for example, Huertas-Company et al., 2013). However I posit that comparing galaxies at fixed mass could be failing to capture the importance of environment in a galaxy's evolution, as mass evolution can also be changed by environmental processes. With mergers affecting central galaxies more often than satellites and satellites being subject to tidal and ram pressure stripping, galaxy harassment and quenching, the net effect will result in central galaxies being more massive than satellites. Therefore, by comparing galaxies at fixed mass I are not comparing galaxies that were similar

prior to a satellite's accretion onto a new dark matter halo and thus I are not capturing the effect of the environments they are being accreted onto. To mitigate these differences, I choose to study the size and mass of galaxies at fixed core velocity dispersion, as events that can change σ_0 (e.g. major mergers) are rare on the timescales of satellite infall.

I study the size-σ_0 and mass-σ_0 relations by finding the median half-light radii and stellar masses within bins of core velocity dispersion. I find that at fixed σ_0 the central galaxies are consistently larger and more massive than their satellite counterparts by $\sim$15% on average. In Section 2.5 I show that this difference in size and mass is not due to a residual difference in ongoing star formation or morphology between satellites and centrals despite quiescent and star forming satellite galaxies having lower median sSFR and Sersic indices than their central counterparts.

For star forming galaxies I find that there is very little difference in the size or mass of central and satellite galaxies at fixed σ_0. Centrals are just a few percent more massive and show almost no size difference except at the lowest dispersions. The lack of much environmental difference is likely the result of star forming satellites having spent a relatively short amount of time as satellites, they are yet to be quenched. A short time as a satellite in a halo means that a galaxy will have continued to form stars at broadly the same rate as an equivalent star forming central galaxy and will be much less likely to have experienced any tidal stripping or disruption. For quiescent galaxies I do see a significant difference between both the size and mass of central and satellite galaxies with central galaxies being both larger and more massive at fixed σ_0. I also find that there is a strong dependence of the size difference on σ_0, with low σ_0 centrals being just a few percent larger and high σ_0 centrals being 30% larger, on average, than equivalent satellites. The mass difference also shows a trend with σ_0 although it is much weaker.

I have measured the radial mass profiles the central and satellite galaxies at fixed σ_0. These profiles show that at fixed dispersion, and in all the star formation rate groups, the cores of the central and satellite galaxies are almost identical. However, at larger radii the galaxies begin to differ, and in the outskirts of the galaxies I begin to see larger differences in total mass and stellar mass density. As with the size-σ_0 and mass-σ_0 relations, the differences in mass and mass density are greatest for the quiescent galaxies and there is a larger difference for the high dispersion galaxies. These profiles are clear evidence that the satellites have less mass at larger radii than the centrals, while the cores of the galaxies are being preserved against any environmental processes.

Finally, I study the mass-metallicity and σ_0-metallicity relations of central and satellite galaxies. I find that when split by star formation rate there is almost no difference in the σ_0-metallicity relations for central and satellite galaxies and at most a 5% difference in

the mass-metallicity relation such that satellites are more metal rich. The small observed difference between central and satellite metallicity at fixed mass is entirely consistent with the difference in mass measured at fixed σ_0 and the central galaxy mass-metallicity relation. This is consistent with the picture that both the central metallicity and σ_0 are unaffected by any processes operating differently on central and satellite galaxies whereas the stellar mass is changing.

Under the assumption that σ_0 is largely conserved when a galaxy becomes a satellite there are a number of ways that the results I have found could occur. Firstly, quiescent central galaxies could continue to accrete mass onto their outskirts whereas their satellite counterparts do not. Alternatively, quiescent satellite galaxies (that were either accreted as quiescent or SF centrals) are being stripped down in size and mass from the outside in. Finally, star forming central galaxies that become quiescent after becoming satellites have different masses and sizes at fixed σ_0 than quiescent centrals. These processes (or their combination) not only need to produce larger and more massive centrals than satellites but also the variation in those differences with σ_0.

I expect that all three processes must occur to some degree. Quiescent centrals experience minor mergers which deposit mass preferentially on to the outskirts. As a result of the shape of the stellar-to-halo-mass relation, the more massive (higher σ_0) the galaxy the more mass they accrete in this way and the larger the fraction of the mass comes from minor mergers. The larger the merger ratio the more the size of a galaxy is expected to increase per unit mass deposited (Naab et al., 2009), and so this naturally explains the increasing size and mass difference between central and satellites as σ_0 increases. I expect more mass to be accreted onto higher σ_0 centrals with a larger fraction coming from minor mergers causing a relatively larger size difference. This effect may also be revealed in the size-mass (or size-σ_0) relation for quiescent galaxies. The slope is steeper at high mass (σ_0) and shallow at low mass (σ_0), so for a given change in mass a galaxy grows more at high mass (σ_0) and less at low mass (σ_0).

Tidal stripping of stellar mass from satellite galaxies is responsible for the intra-cluster and group light that makes up a significant fraction of stellar mass in groups and clusters. Estimates of the fraction of mass stripped from simulations range from just a few percent up to $\sim$20% with the amount of mass stripping decreasing with stellar mass and increasing with halo mass (Bahe et al., 2016). The typical fraction of mass lost to stripping is in reasonable agreement with the typical mass difference I observe ($\sim$15%) and the stripping is expected to occur from the outside in, again consistent with our observed mass profiles. However, I see no dependence of central-satellite mass difference on σ_0, which appears inconsistent with the expected mass dependent stripping fraction from the models.

Our final mechanism that could contribute to the difference in the size and mass difference of quiescent central and satellite galaxies is the possibility that there are differing relationships between σ_0 and stellar mass or size for galaxies that become quiescent while centrals and galaxies that become quiescent while satellites. Quiescent satellites will consist of galaxies that became quiescent as centrals before becoming satellites, and galaxies that became quiescent as a result of becoming satellites. Figures 2.2 and 2.3 show that quiescent centrals are $\sim$30% smaller and less massive than SF centrals with the same σ_0. If galaxies that become quiescent as satellites evolve more like the SF population of centrals than the quiescent population at fixed σ_0, continuing to form stars for some time after accretion (e.g. Oman and Hudson, 2016; Wetzel et al., 2013), they may be more like their SF central counter parts than their quiescent central ones, i.e. more massive and larger. This would tend to counter act any effect of tidal stripping of satellites or central growth from minor mergers. Since the fraction of satellite galaxies that were SF when they became satellites will increase as σ_0 decreases, a result of the strong correlation between quiescence and σ_0 (e.g. Bluck et al., 2016; Wake et al., 2012), I would expect any difference in size and mass at fixed σ_0 between satellite galaxies that became quiescent as satellites, rather than as centrals, to mainly affect the lower σ_0 population. I anticipate that the corrections I have applied for the small differences in SFR and Sérsic index between the central and satellite quiescent galaxies in Section 2.5 would mitigate these effects, but it remains possible that the differing quenching mechanisms and/or timescales could mean that satellites quenched as satellites could still be larger and more massive than satellites quenched as centrals, even when their SFRs and Sérsic indices are matched.

Taken together, these considerations seem to point to the continued growth of central galaxies by minor mergers being largely responsible for the mass and size differences between quiescent central and satellite galaxies at fixed σ_0, particularly at high σ_0, with tidal stripping playing a minor role that increases as σ_0 decreases. Since at high σ_0 almost all galaxies are quiescent (Bluck et al., 2016; Wake et al., 2012), and tidal stripping is expected to be minimal, it is reasonable to assume that essentially all the difference in size (25%) and mass (20%) of central and satellite galaxies is caused by minor mergers on to the centrals that have occurred over the average time that the satellites have been satellites ($\sim$3 Gyr Wetzel et al., 2013).

3

A Two-Source Star Formation Rate Model for MaNGA Galaxies

"... to boldly go where no one has gone before."
– Captain Jean-Luc Picard, *Star Trek: The Next Generation, 1987-1994*

3.1 Introduction

Perhaps the most important properties of a galaxy are its stellar mass and star formation rate (SFR). Strong correlations exist between these properties and other vital statistics of galaxies, such as morphology, colour and age (Baldry et al., 2006, 2004; Bezanson et al., 2015; Blanton and Moustakas, 2009; Blanton et al., 2005b; Brinchmann et al., 2004; Courteau et al., 2014; Gallazzi et al., 2005; Kauffmann et al., 2003b; Kennicutt, 1998a; Lundgren et al., 2014; Renzini and Peng, 2015). It is necessary then, when new surveys are conducted, to develop techniques and data products that predict and describe these parameters. Integral Field Spectroscopy (IFS) surveys indeed provide a new challenge: what are the best ways to estimate these properties at the spaxel level, as opposed to calculating integrated properties from the combined light of the entire galaxy?

The estimation of integrated galaxy properties goes back to the 1970s, with Faber (1972) presenting their quadratic programming approach to population synthesis. They studied the nuclei of M31, M32 and M81 using 32-band colour data, along with 10-colour data from elliptical galaxies, fitting stellar populations that allowed for accurate estimation of line strengths. However, it was found that mass-to-light ratios could not be well constrained

This model was presented briefly in Spindler et al. (2017) which has been accepted by MNRAS for publication.

without a way to discriminate between M-dwarf stars and M-giant stars (Faber, 1972). Further works by Searle et al. (1973), Tinsley and Gunn (1976) and Larson and Tinsley (1978) went on to improve the methodology of early synthesis modelling and estimated more parameters such as star formation rates and histories.

Advances in the 1980s lead to more detailed stellar population synthesis (SPS) models (Bruzual A., 1983; Guiderdoni and Rocca-Volmerange, 1987; Renzini and Buzzoni, 1986), such as from Guiderdoni and Rocca-Volmerange (1987), who derived model populations of stars to predict the colours and magnitudes of galaxies at all redshifts, including cosmological effects and intrinsic galaxy evolution. The model included a variable star formation rate and a uniform initial mass function (IMF), which allowed for good fits to far-UV and visible spectra from nearby galaxies across the Hubble sequence.

The biggest step forward came with the adoption of isochrone analysis in the early 1990's (Bruzual A. and Charlot, 1993), which has become the standard in modern SPS models (Bruzual and Charlot, 2003). An isochrone represents the evolutionary track on the Hertzsprung-Russell (HR) diagram of a star with a given mass and metallicity (Bertelli et al., 1994; Bruzual A. and Charlot, 1993; Charlot and Bruzual, 1991; Conroy, 2013). Isochrones are constructed using stellar evolution codes, which are sampled over different masses and time-scales Modern SPS models combine grids of isochrones with stellar spectra, a star formation history and an initial mass function to generate a potential stellar populations that describe how many stars of different masses are present. The resulting model SED can be modified by a dust attenuation curve and a chemical evolution model (Bruzual and Charlot, 2003; Conroy, 2013).

SPS models have become the foundation of integrated property estimation, but it has also allowed for many simpler methods to be developed. Using SPS models, it is possible to calibrate simple relationships between single spectral features, such as UV flux or H_α emission line luminosity, and a galaxy's star formation rate (Calzetti, 2013; Kennicutt, 1983, 1998a,b; Kennicutt et al., 1994). There are also calibrations used to convert from broadband colours to stellar masses (Bell and de Jong, 2001; Courteau et al., 2014). These relations are calculated by averaging over whole galaxy populations and so by design do not account for all of the complexities, such as dust attenuation and stellar metallicites. However, they do provide a fairly easy way of calculating the base properties of a galaxy, without having to model their populations using SED fitting. In fact, SED fitting with only optical data is often unreliable, as it is necessary to include UV information to accurately calculate a star formation rate for a galaxy (Salim et al., 2016).

Perhaps the most popular method for calculating star formation rates is using the flux of the H_α emission line (Kennicutt, 1998a). H_α is the first spectral line in the Balmer series,

emitted by hydrogen atoms when an electron falls from the third energy level to the second, with a wavelength of 656.28 nm. In space H_α emission is found in HII regions, which have been excited by UV emission from some nearby high energy source. Most often, this source of UV light comes from O and B type stars, which are massive and hot ($M_* > 10M_\odot$, $T > 10,000K$, Kennicutt, 1998b). As such measuring the UV flux (or some processed product of the UV flux such as H_α or infra-red flux) acts as a measure for the number of massive stars that are present. For a given IMF the number of these massive stars, in relation to lower mass stars, gives an estimate of the population age and by extension the star formation rate. The age estimate comes from the fact that the hottest stars are very short lived, so any flux measure from them tells us they must have been recently formed.

One of the great benefits of large scale surveys with public datasets is the legacy data products and value added catalogues which compile numerous galaxy properties. Using a variety of techniques and datasets astronomers have a wide range of publicly available catalogues. For SDSS, there are many catalogues of galaxy properties available: such as the MPA/JHU catalog (Brinchmann et al., 2004), which provides SED based stellar masses and star formation rates; the GALEX-SDSS-WISE Legacy Catalog (GSWLC, Salim et al., 2016), which expands on the work of the MPA/JHU and improves the SED fitting by including UV flux measurements from GALEX; the New York University Value Added Catalog (NYU-VAGC, Blanton et al., 2005b), containing positions and ID numbers of galaxies found in multiple galaxy catalogs, and derived properties such as Sérsic profiles and velocity dispersions; or the University of Pennsylvania Photometric Decomposition catalog (Meert et al., 2013, 2015, 2016), which provides bulge-disk decompositions of SDSS galaxies, including stellar mass estimates of the different galaxy components.

With the recent advent of large scale IFS surveys, such as Mapping Nearby Galaxies at APO (MaNGA, Bundy et al., 2015), the Calar Alto Legacy Integral Field Area Survey (CALIFA, Sánchez et al., 2012) and Sydney-Australian-Astronomical-Observatory Multi-object Integral-Field Survey (SAMI, Schaefer et al., 2017), it is necessary to apply the techniques used in integrated property estimation to the spatially resolved data from the Integral Field Units (IFUs), which comes with its own set of difficulties. For example, signal-to-noise in individual spaxels is often lower than for single-fibre surveys, so it may not be possible to perform reliable SED fitting. Often spaxels are binned together to some minimum signal to noise ratio to ensure good quality fits, in this case the spectra from multiple spaxels are stacked together and used as the input for the SSP codes (Cappellari, 2009; Cappellari and Copin, 2003). Bins can either be group together radially, as is the case in the Pipe3D fitting pipeline for MaNGA (Sánchez et al., 2016b), or grouped to minimise the distance

between spaxels in the bin as in the MaNGA Data Analysis Pipeline (Westfall et al. (in prep)) [1].

In this Chapter I discuss the two-source star formation rate model that was developed for galaxies observed as part of the MaNGA survey. In Section 3.2 I introduce the MaNGA data used in this survey, including the Pipe3D-MaNGA stellar population cubes and the data cubes from the Data Analysis Pipeline, I also describe the supplementary catalogs used throughout the Chapter that include properties calculated using SDSS single fibre spectroscopy and photometry for our sample galaxies. Section 3.3 describes the diagnostics used to classify galaxies using the Baldwin-Phillips-Terevich diagram (Baldwin et al., 1981). The star formation rate calculations are described in Section 3.4; I split this into two stages for the H_α SFRs and the SSFR-D_n4000 model, and I describe the construction of the final data cubes to be used for analysis. Section 3.5 presents the results of analysing the global properties of galaxies; I investigate the SFR main sequence, and compare our total SFRs to the MPA/JHU catalog and the GALEX-SDSS-WISE Legacy Catalog. Finally, I conclude our findings in Section 3.6.

3.2 Data

I study galaxies from SDSS Data Release 14 (DR14, Abolfathi et al., 2017), which includes a total of 2791 galaxies. I make use of three of the products from the DAP, the ALL binned data that combines the flux from all the spaxels in the data cube for maximum signal to noise, the VOR10 data that bins the spaxels into SNR>10 Voronoi bins and the NONE binned data that includes all of the spaxels in the data cubes individually, with an angular size of 0.5 arcsec. The ALL binned data is used in the Baldwin-Phillips-Terevich (BPT) diagnostics in Section 3.3 and for calculating the total Star Formation Rates and Specific Star Formation Rates. I use the Voronoi binned data to calibrate our D_n4000-SSFR model, as the high signal to noise allows us to go to lower specific star formation rates (SSFR). The final data products will be used in Chapters 4&5.

3.2.1 Supplementary Data Catalogs

I use a number of additional catalogs in the analysis of our star formation rate pipeline, these include: the NASA-Sloan Atlas (NSA), the MPA/JHU catalog (Brinchmann et al., 2004; Kauffmann et al., 2003b; Salim et al., 2007) and the GSWLC (Salim et al., 2016).

[1] Note, the DAP is not an SSP code but a spectral fitting pipeline

The NASA-Sloan Atlas is a collection of images and galaxy parameters from surveys in the optical, ultraviolet and infra-red. The NSA uses data from the Sloan Digital Sky Survey (Aihara et al., 2011; York and SDSS Collaboration, 2000) and the Galaxy Evolution Explorer (GALEX, Martin et al., 2005) and forms the parent catalog from that the MaNGA target catalog is chosen from. I use the stellar mass in the NSA to validate the Pipe3D-MaNGA data explained in Section 3.2.2.

With over 1400 citations on the main Brinchmann et al. (2004) article, the MPA/JHU is possibly the most used catalog of galaxy properties for SDSS studies. The star formation rate model derived in Brinchmann et al. (2004) serves as the main inspiration for our own model. The catalog uses Bayesian statistics to derive star formation rates from galaxies using stellar population fitting to a variety of emission lines and spectral properties. Galaxies that are contaminated with emission from AGN and LI(N)ER like emission instead have their star formation rates calculated using a model based on the strength of the $4000-$ Å break (D_n4000). I compare our total star formation rates to this catalog in Section 3.5.3.

The GALEX-SDSS-WISE Legacy Catalog provides physical properties (stellar mass, star formation rates and dust attenuations) for 700,000 galaxies in the SDSS. This catalog uses Bayesian SED fitting with data from GALEX and SDSS to find star formation rates for galaxies and also provides SFRs derived from mid-IR measurements from the Wide-field Infra-red Survey Explorer (WISE, Wright et al., 2010). I compare our total SFRs to those found in the GSWLC in Section 3.5.4.

3.2.2 Pipe3D-MaNGA Data

In addition to the DAP analysed data, I make use of the Pipe3D-MaNGA Value Added Catalog. Pipe3D is an IFU based analysis pipeline that explores the stellar population and ionised gas properties of galaxies in recent IFU surveys (CALIFA, MaNGA, SAMI) and is discussed in Sánchez et al. (2016a) and Sánchez et al. (2016b). I make use of the Pipe3D data products applied to the MPL-5 galaxies.

I use the Single Stellar Population (SSP) data products for MPL-5 galaxies, from which I take the maps of stellar mass density ($log_{10}(M_{\odot})/arcsec^2$). Pipe3D uses a different spatial binning scheme than the DAP, so I re-sample the datacube such that it matches the spatial binning in the VOR10 data cubes and the NONE binned data cubes from MPL-5. I find the per spaxel stellar mass in each of the Pipe3D bins, and then sum the new spaxels in each of the MPL-5 voronoi bins.

To test for the consistency of the data, I show the total masses of each galaxy using Pipe3D and their stellar masses given in the NASA-Sloan Atlas in Figure 3.1. I have adjusted for the differences in the Salpeter and Chabrier IMFs used in the NSA and Pipe3D respectively by

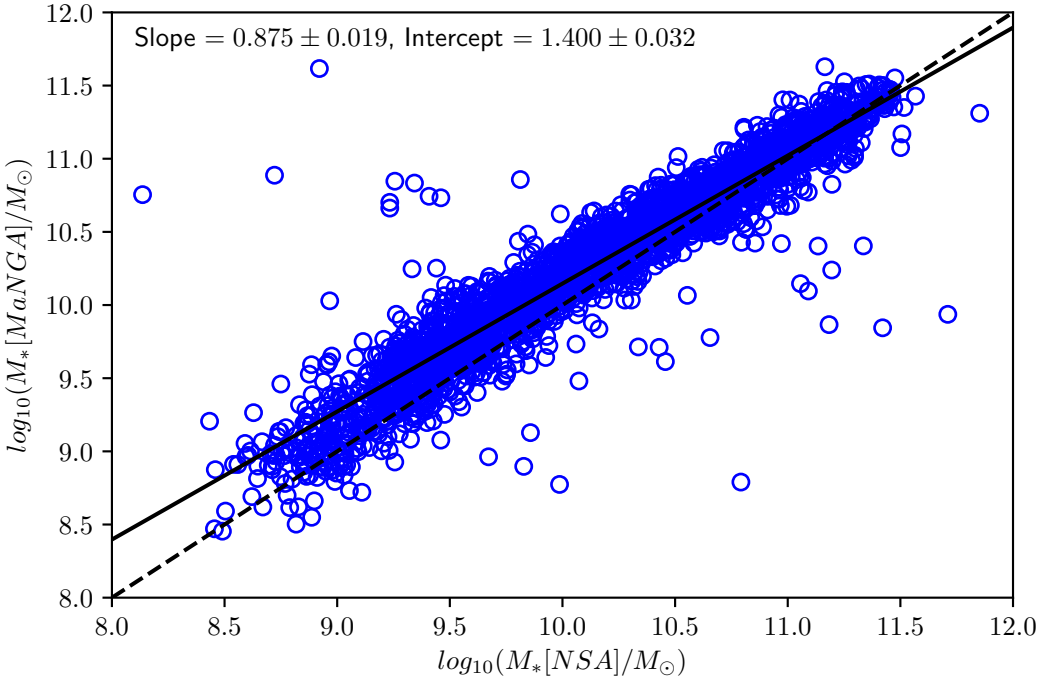

Fig. 3.1 The Stellar masses from the NASA-Sloan Atlas compared with the total masses from the Pipe3D-MaNGA products. The Pipe3D-MaNGA masses have been adjusted by 0.24 dex to account for the differences in cosmologies and IMFs used. The dashed line shows the 1-1 relation and the solid line is a linear fit to the data.

applying a $0.24dex$ offset to the integrated Pipe3D stellar masses. The masses agree very well, with only a small number of galaxies falling outside of the $2-\sigma$ scatter. The reasons for some galaxies having very large offsets is not yet known, however flags are provided for these galaxies and as such I do not use them within our final sample, removing 16 galaxies.

3.3 BPT Diagnostics

The techniques I use to investigate star formation rates rely heavily on the emission lines from galaxies. In most cases these emission lines can be traced back to the UV emission from young stellar populations that contain OB type stars, however in some cases these emission lines become contaminated. A significant source of contamination is from Active Galactic Nuclei (or AGN), which are a source of UV and x-ray emissions as their super massive black hole heats and consumes gas from its accretion disk (Baldwin et al., 1981). This emission goes on to excite cold gas clouds in the same way as the emission from OB stars, which leads

to an excess in the emission line flux. In addition to AGN there are Low Ionisation (Nuclear) Emission Regions (or LI(N)ERS), which have lower intensities than AGN and have been shown to be associated with galaxy cores as well as old stellar populations with post-AGB stars and regions with shocked gas (Belfiore et al., 2016; Heckman, 1980). These emission sources are harder than those associated with OB-stars and as such lead to higher levels of excitation in heavier gases such as oxygen and nitrogen.

Baldwin et al. (1981), devised the diagnostic diagram shown in Figure 3.2, which compares the ratios $log_{10}([OIII]/H_\beta)$ and $log_{10}([NII]/H_\alpha)$. I use the DAP ALL binned data, which sums the emission over the entire galaxy to find their position in the BPT diagram. Galaxies that have more [OIII] and [NII] with respect to H_β and H_α are more likely to be hosts of AGN and LI(N)ER emission. In Kauffmann et al. (2003a) galaxies from Data Release 4 were studied and a demarcation between star forming galaxies and AGN/LI(N)ER galaxies was empirically defined. Further to this, in Kewley et al. (2001), a theoretical upper limit for the emission lines in starburst galaxies was calculated, I show the definitions of both these lines in Equations 3.1 & 3.2.

$$log([OIII]/Hb) = 0.61/(log([NII]/Ha) - 0.05) + 1.3 \tag{3.1}$$

$$log([OIII]/Hb) = 0.61/(log([NII]/Ha) - 0.47) + 1.19 \tag{3.2}$$

Using these two demarcation lines, shown in Figure 3.2 as the solid and dashed lines, I can define galaxies as being Star Forming if they fall below the Kauffmann line, Composite if they fall between the Kauffmann and Kewley lines and AGN/LI(N)ER if they fall above the Kewley line. Composite galaxies are those that have a contribution from both star formation and AGN/LI(N)ER like sources and AGN/LI(N)ER galaxies have emission that is dominated by emission from those types of sources. It is possible to identify galaxies as AGN/LI(N)ER with just the H_α and [NII] lines, so if in those lines the $SNR > 3$, and $log_{10}([NII]/H_\alpha) > 0.05$ I can define low SNR AGN. Finally, there are the galaxies that do not fit any of these definitions, which we term 'lineless' galaxies. Strictly speaking, these galaxies do not completely lack emission lines, in most cases they are deficient in just one line. There are a number of ways the classification system can fail, which results in a galaxy being labelled lineless. First, if the H_α or [NII] lines have $SNR < 2$ the galaxy is unclassifiable. Second, the galaxy could have H_β or [OIII] lines with $SNR < 2$ and H_α or [NII] lines have $SNR < 3$. Third, the H_β or [OIII] lines could have $SNR < 2$, while the H_α or [NII] lines have $SNR > 3$ but $log_{10}([NII]/H_\alpha) < 0.05$, the opposite of the low SNR AGN

class. Of these, the most common appears to be undetectable H_α, which accounts for 415 of the lineless galaxies.

In total there are 1049 star forming galaxies, 435 composite galaxies, 428 AGN/LI(N)ER, 22 low SNR AGN galaxies and 719 Lineless galaxies.

Once I have classified galaxies using their integrated light to define our sample, I then need to consider the spatially resolved nature of the MaNGA datacubes. Instead of using the total light from a galaxy, I can instead study the emission sources on a spaxel by spaxel basis. Using the datacubes, I can identify regions of the galaxy that have emission from star formation and regions of the galaxy that are contaminated by other emission sources. The purpose of this being that I can then use H_α to calculate the star formation in star forming spaxels and D_n4000 everywhere else.

I use the Kauffmann et al. (2003a) line to calculate each individual spaxel's location on the BPT diagram for each galaxy in the survey. Following on from the integrated data, I designate each spaxel as Star Forming, AGN/LI(N)ER or Lineless. I do not use a composite designation in the spatially resolved data as I would not treat composite data differently to AGN/LI(N)ER spaxels, i.e. they are still contaminated and I cannot use H_α in those regions. In Figure 3.3 I show examples of this technique for 6 galaxies in the MaNGA survey. I show the SDSS g-r-i images with the MaNGA IFU hexagon superimposed, the spatially resolved BPT maps, the $log_{10}(H_\alpha Flux)$ map, the map of the D_n4000 spectral index and the SNR map of each galaxy. I also state the plate and IFU numbers for each galaxy and the BPT designation from their integrated light.

In the Figure 3.3 the blue spaxels are star forming, the red spaxels are AGN/LI(N)ER like emission and the yellow spaxels are lineless. Note that the AGN/LI(N)ER like emission is not restricted to the cores of galaxies, as might be suggested by the 'Nuclear' terminology used. For example, Belfiore et al. (2016) showed that the LI(N)ER emission can be related to shocked gas and ageing stellar populations, in addition to nuclear emission from super massive black holes. In the H_α maps I apply a signal-to-noise cut at $SNR < 2$. In the D_n4000 map I apply a cut based on the error at $D_n4000/\Delta(D_n4000) < 15$.

In Figure 3.3, galaxy 7957-12702 is a spiral galaxy and has been classified as star forming by its integrated light. The BPT map shows very little contamination of AGN/LI(N)ER like emission, which is restricted to the outskirts. The H_α map shows that there is increased emission in the galaxy's core and in some regions of the disk, however it is broadly uniform. The D_n4000 map is also very uniform, suggesting little difference in the stellar population age throughout the galaxy. Galaxy 7495-12703 is also a star forming spiral galaxy, however there is slightly more AGN/LI(N)ER contamination at the edge of this galaxies map, suggesting perhaps that there is some shocked gas or an old stellar population in that region of the

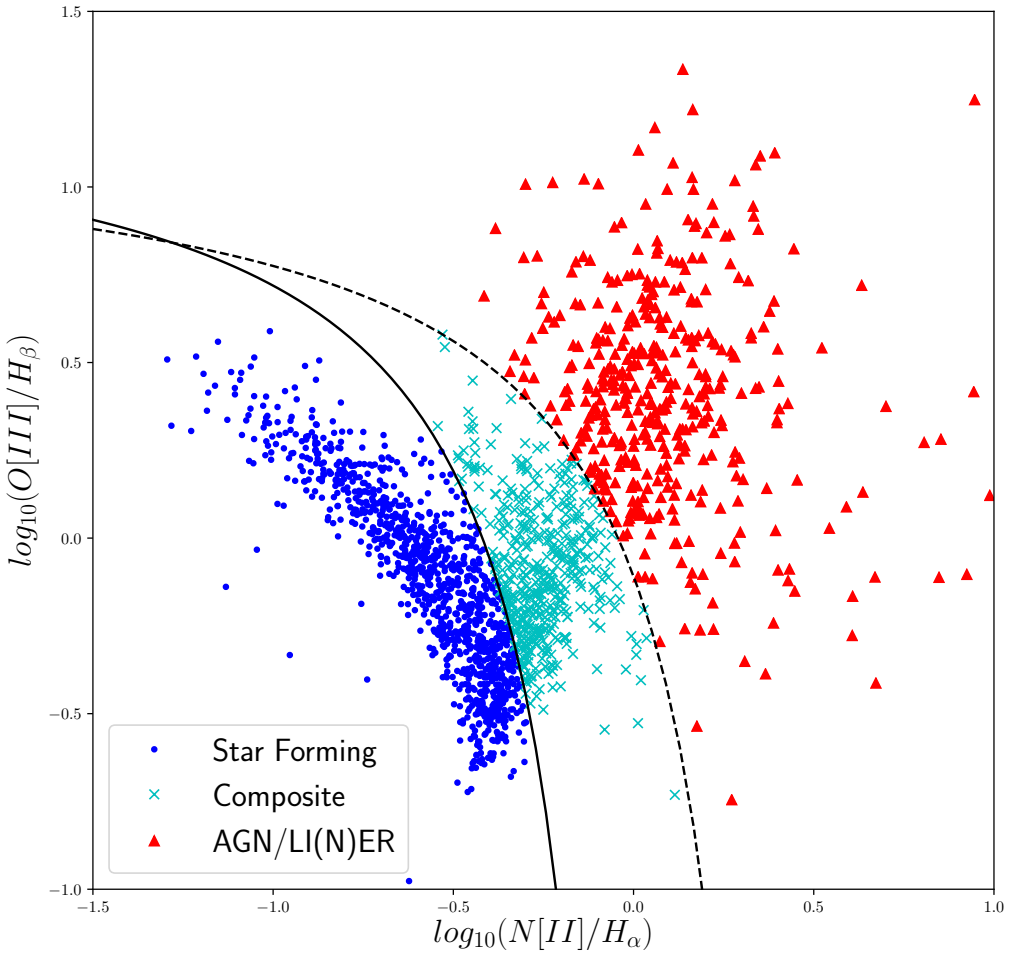

Fig. 3.2 The BPT Diagram for galaxies in the MaNGA survey. The positions of galaxies are calculated from the ALL binned DAP products. Blue dots are the Star Forming Galaxies, cyan crosses and the composite galaxies and the red triangles are the AGN/LINER galaxies. The solid line is the relation from Kauffmann et al. (2003a) and the dashed line is from Kewley et al. (2001).

galaxy. The H_α emission in this galaxy is not as high as in 7957-12702, and is mainly in the disk. This is also visible in the D_n4000 map that shows an increase towards the galaxy bulge, possibly indicating an older stellar population.

Galaxy 8082-12703 is a composite disk galaxy, The bulk of the disk has star forming type emission, however there is a large amount of contaminated emission in the outskirts of the galaxy. This emission may be due to the gas being excited by old stellar populations or the gas being heated by the galaxy's environment via ram pressure or some other mechanism. Galaxy 8317-12704 is an AGN type disk galaxy: the centre of the galaxy has a large region of AGN contamination, the outskirts have a mix of AGN/LI(N)ER emission and lineless spaxels that are likely due to older stellar populations, and there is a small amount of star forming spaxels around the central AGN region. Galaxy 8086-12705 is an AGN type elliptical galaxy, which exhibits almost purely AGN spaxels in the high signal-to-noise regions, however, there are a few small star forming regions in the outskirts of the galaxy that are surrounded by lineless regions. Finally, galaxy 8602-12703 is a lineless elliptical galaxy, there are no discernible features in the BPT map, and the D_n4000 map is also very limited by signal-to-noise.

3.4 Star Formation Rates

In this Section I will present our method for producing spatially resolved maps of star formation. I use a two-source model, which calculates star formation rates from H_α emission in the first instance in spaxels that are classified as star forming in the BPT diagram. These SFRs are used to model the dependence of specific star formation rate on the strength of the 4000 Å break (D_n4000). I then use this model to find the SFRs in spaxels with AGN and LINER contamination, and spaxels that are lineless, which would otherwise be excluded in a model that relies only on H_α emission. I use star forming spaxels from both star forming and composite galaxies. This is to ensure that I include spaxels from galaxies that contain contaminated spaxels. This method is inspired by the work of Brinchmann et al. (2004) in the star formation estimations in the MPA/JHU DR7 catalog and allows us to expand our analysis to galaxies with AGN and LI(N)ER emission, which have previously been discarded by other authors (Belfiore et al., 2017b; Schaefer et al., 2017).

The final model will be applied to the DAP maps with no spatial binning, however it is important to begin with high signal-to-noise data as this allows us to go to much lower SFRs using low amounts of H_α. As such I will begin my analysis using the Voronoi binned DAP products, which bins the spaxels into spatial regions that have a total r-band signal-to-noise ratio per bin > 10.

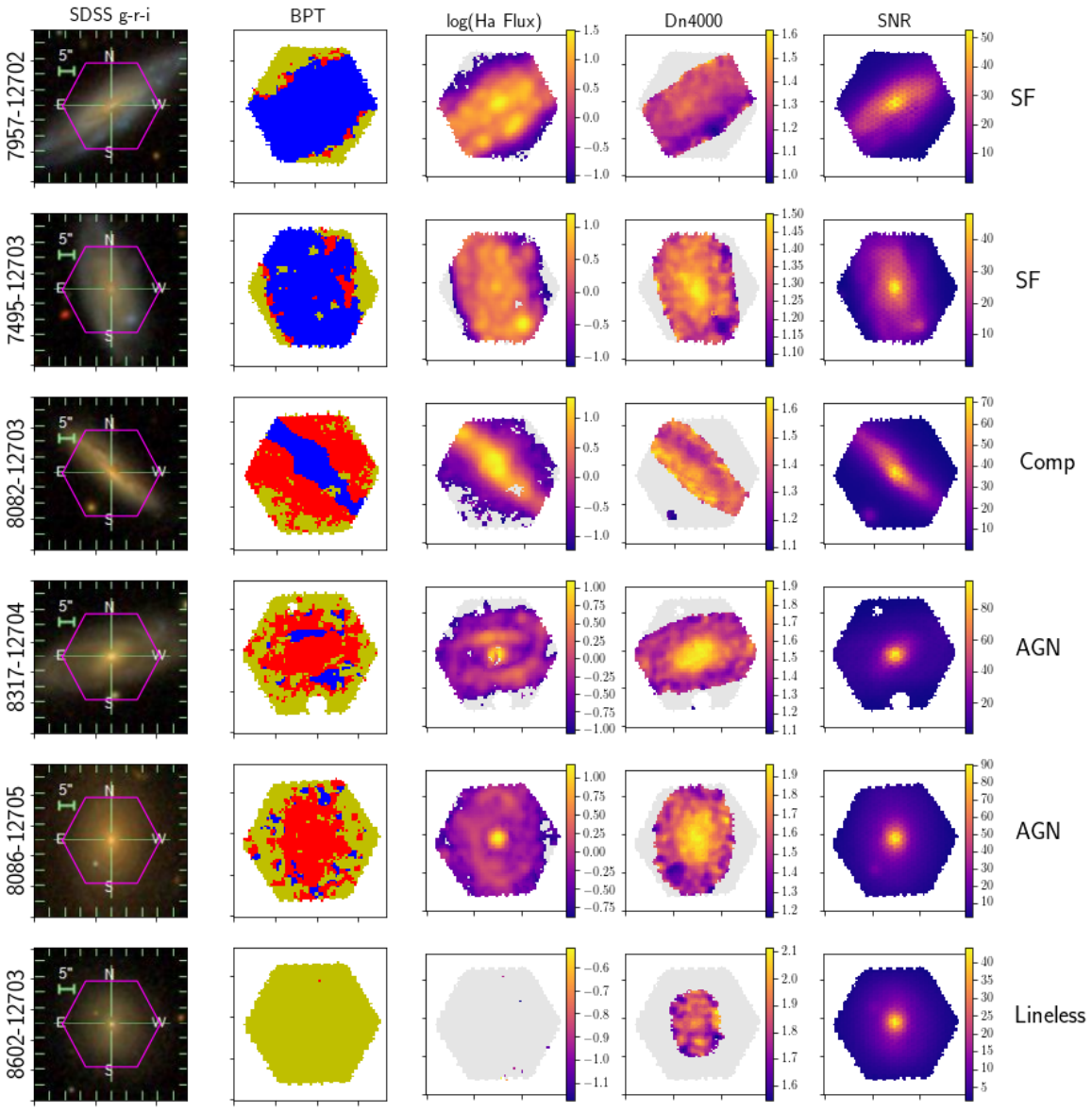

Fig. 3.3 I show six example galaxies with their SDSS g-r-i image, resolved BPT map, H_α flux map, D_n4000 map and Signal-to-Noise Ratio map. In the SDSS images, the blue hexagon represents the foot print of the MaNGA IFU. All the galaxies chosen here have 127-fibre IFUs. In the BPT maps, the blue spaxels are Star Forming, the red spaxels are identified as AGN/LI(N)ER and the yellow spaxels are Lineless. In the Ha maps the grey spaxels fall below the $SNR < 2$ limit and in the D_n4000 map the grey spaxels fall below the error limit of $D_n4000/\Delta(D_n4000) < 15$. I indicate the plate and IFU number of each galaxy on the right and the BPT classification of the integrated flux on the left.

Using the maps from Section 3.3, the star forming bins from the Voronoi maps have their star formation estimated using H_α, as detailed in 3.4.1, I then produce the model detailed in 3.4.2 using these SFRs. The unbinned maps are then treated in the same way, with star forming spaxels using dust corrected H_α to estimate their SFRs and the AGN/LI(N)ER, low SNR and lineless spaxels estimated using the D_n4000 model.

3.4.1 $H\alpha$ Star Formation Rates

Measuring star formation relies on two components, an Initial Mass Function that tells the stellar mass distribution of a new population of stars, and the lifetime of hot blue stars. O-type stars with masses in excess of $10M_\odot$ have lifespans of less than 10^7 years, and emit large amounts of radiation in the UV. Thus, by detecting the UV directly or as a function of processed light (emission lines or infra-red) I can have a good idea about how many O-type stars are present. For a given IMF, I can predict the content of the stellar population at other masses, and thus the total stellar mass formed in that burst of star formation (Kennicutt, 1998a).

A conversion factor can be calculated between the observed ultraviolet, emission line or infra-red flux using stellar population synthesis modelling (Kennicutt, 1998a). For the ultraviolet continuum, sampling the wavelength range from $1500-2800$Å covers a region of the spectrum that is dominated by the light from young populations of stars, but does not include absorption from the Lyman-Alpha forest. Observations of this kind have been carried out mostly by space based telescopes, such as GALEX and many calibrations have been published regarding converting UV luminosities to SFR (Buat et al., 1989; Cowie et al., 1997; Deharveng et al., 1994; Leitherer et al., 1995; Madau et al., 1998; Meurer et al., 1995). For example, the Madau et al. (1998) calibration, converted to a Salpeter (1955) IMF with mass limits of $0.1M_\odot$ to $100M_\odot$ yields (as presented in Kennicutt, 1998a):

$$SFR(M_\odot yr^{-1}) = 1.4\times10^{-28}L_\nu(ergs^{-1}Hz^{-1}). \tag{3.3}$$

However, ultraviolet light is not readily observable from ground based observatories, as it is largely absorbed by the Earth's atmosphere. For optical observations we instead look for the emission line fluxes, which are emitted from nebulae excited by the UV emission from hot, young stars. As I have stated previously in this Chapter, the most common emission line used in star formation calibrations is the H_α line. H_α flux is readily absorbed and reprocessed by dust in the interstellar medium however, and this absorption must be corrected for. In this work I correct for dust attenuation by assuming a foreground dust screen and using the Cardelli et al. (1989) extinction law to calculate the Balmer decrement:

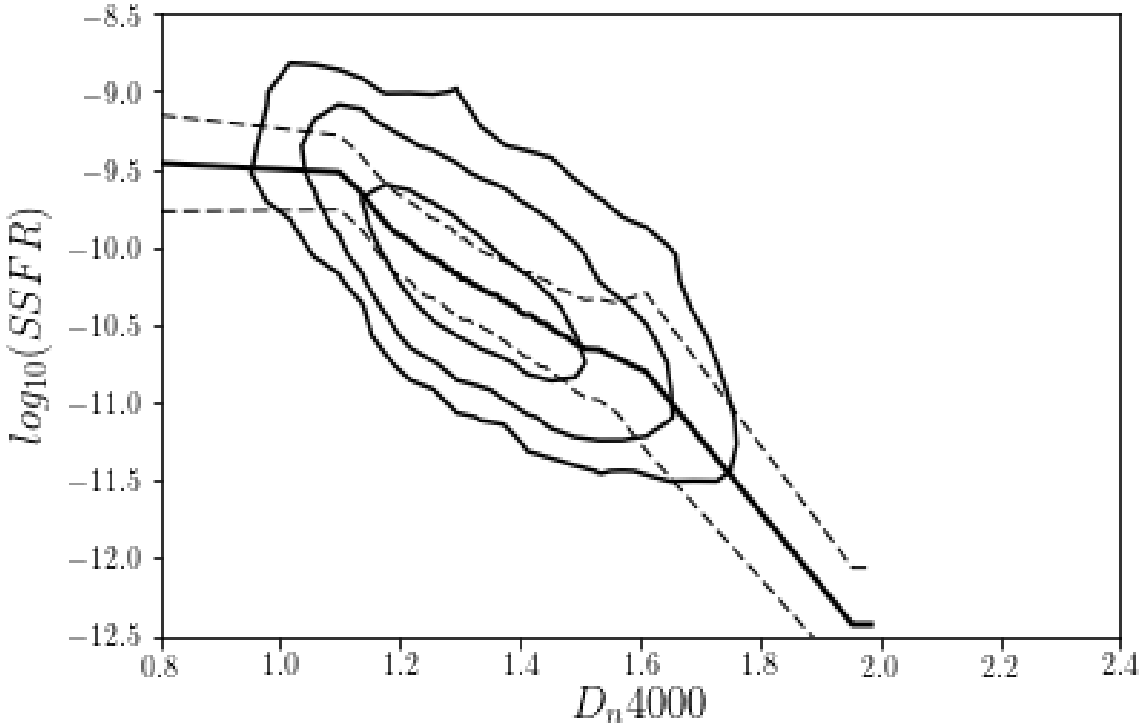

Fig. 3.4 I show the model for D_n4000 specific star formation rates, based on the SSFRs calculated using H_α. I have included only bins that are star forming in the BPT diagram. The contours show the $1-$, $2-$ and $3-\sigma$ levels. the solid black line shows the median SSFR at fixed D_n4000 and the dashed lines show the $1-\sigma$ scatter from the median. This model uses bins from the VOR10 binning scheme that also have a $SNR > 20$.

$$L_{H_\alpha}(Corrected) = L_{H_\alpha}((L_{H_\alpha}/L_{H_\beta})/2.8)^{2.36} \tag{3.4}$$

This correction assumes a case B recombination and corrects the deviation from the theoretical ratio between the H_α and H_β luminosity. The corrected H_α luminosity is converted into a SFR using the relation from Kennicutt (1998a), for a Salpeter (1955) IMF:

$$SFR(L_{H_\alpha}) = L_{H_\alpha}/10^{41.28}(M_\odot yr^{-1}) \tag{3.5}$$

3.4.2 D_n4000 Star Formation Rates

In areas of the galaxy where there is contamination of AGN, LI(N)ER, old stellar populations and shocked gas, I need a different estimator of Star Formation Rate, as these regions have contaminated H_α emission. I also cannot simply ignore these portions of the galaxies,

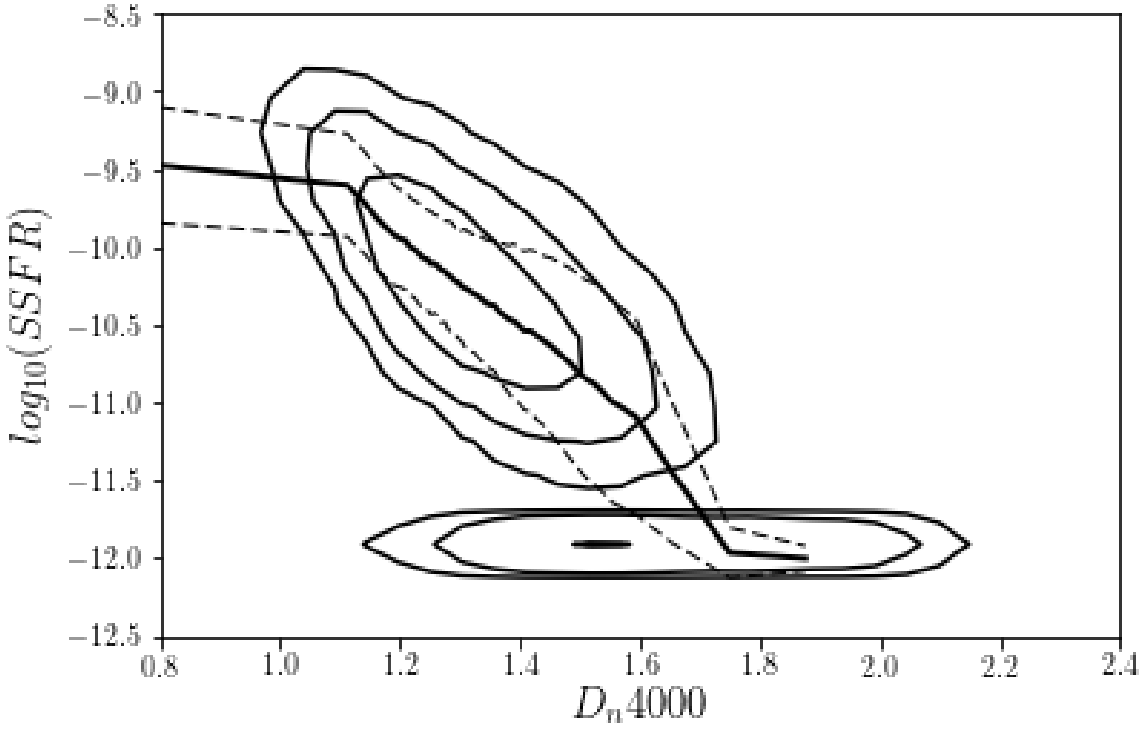

Fig. 3.5 I show the model for D_n4000 specific star formation rates, based on the SSFRs calculated using H_α. I use bins that are star forming in the BPT diagram, and bins that are classified as Lineless have been included at a fixed upper limit of $log_{10}(SSFR) = 11.5$. The contours show the $1-$, $2-$ and $3-\sigma$ levels. the solid black line shows the median SSFR at fixed D_n4000 and the dashed lines show the $1-\sigma$ scatter from the median. This model uses bins from the VOR10 binning scheme that also have a $SNR > 10$.

as the excess emissions often take place in important structures such as the bulge or bar. Brinchmann et al. (2004) showed that D_n4000 could be used to estimate the SFRs of galaxies in DR4 and later DR7 of the Sloan Digital Sky Survey, by first building a model based on the H_α SSFRs of the SF galaxies and their D_n4000 values.

For this model I choose to use the Voronoi binned data as the high r-band signal to noise allows us to detect low levels of H_α emission and thus low levels of star formation. Each bin in the Voronoi data cubes has a minimum r-band SNR of 10, however I can also be selective and restrict the minimum SNR to reduce the overall scatter in the data while maintaining the quality of the data. I present the first model in Figure 3.4, which includes the SSFRs in star forming voronoi bins from SF and Composite galaxies, with a minimum r-band SNR of 20. The contours show the $1-$, $2-$ and $3-\sigma$ levels in the data, the solid line shows the mean SSFR at fixed D_n4000 and the dashed lines show the standard deviation in the mean.

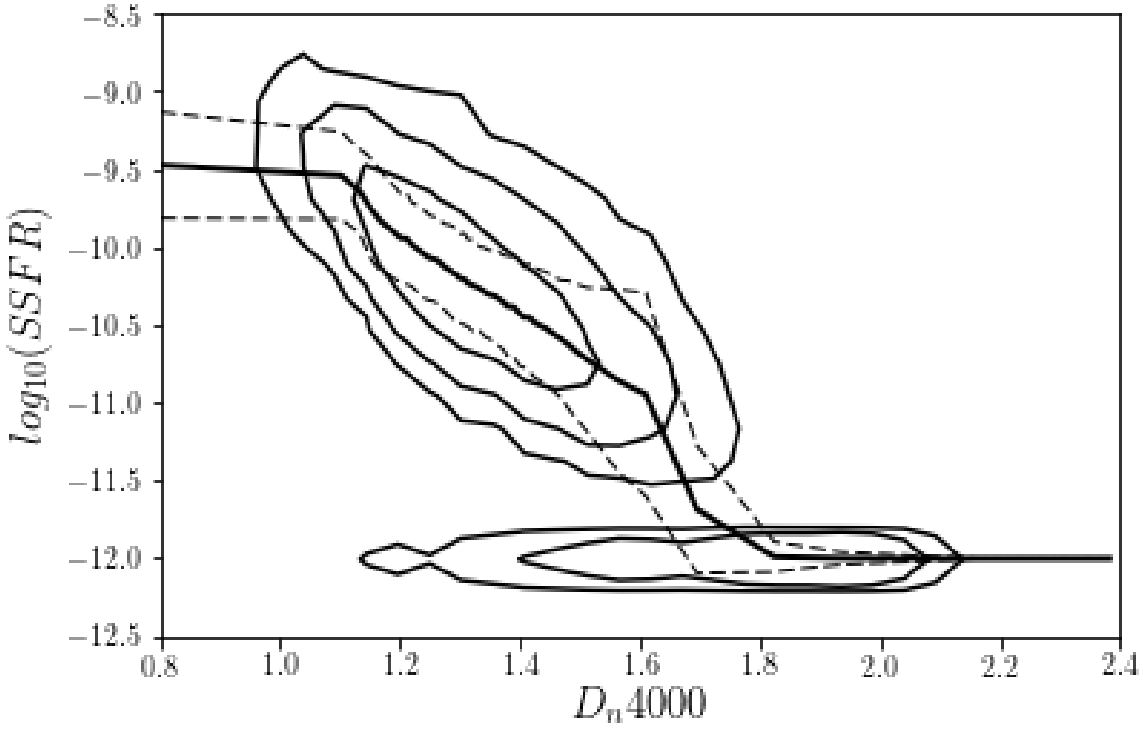

Fig. 3.6 I show the model for D_n4000 specific star formation rates, based on the SSFRs calculated using H_α. I use bins that are star forming in the BPT diagram, and bins that are classified as Lineless have been included at a fixed upper limit of $log_{10}(SSFR) = 11.5$. The contours show the $1-$, $2-$ and $3-\sigma$ levels. the solid black line shows the median SSFR at fixed D_n4000 and the dashed lines show the $1-\sigma$ scatter from the median. This model uses bins from the VOR10 binning scheme that also have a $SNR > 20$.

The bulk of the data is confined to the $1.1 < D_n4000 < 1.7$ region. This model is fairly well constrained around the most common values of D_n4000, with a scatter of around 0.25 dex.

There is a significant problem, however, at high values of D_n4000. By opting only star forming regions I have eliminated the high D_n4000 bins from the sample. If I were to use the model as is, the star formation rates in high D_n4000 regions of the galaxies would likely be overestimated and are poorly constrained due to the lack of data in this region. To compensate for this, I choose to create a new set of models that include the lineless bins as "effectively quenched". The lineless bins are added into the model with a fixed $log_{10}(SSFR) = -12$, to represent regions of the galaxy where star formation is effectively shut down. This is justified as if there were any star formation occurring in these regions, I would be able to detect it via its emission lines, if the region is lineless then there must be no or incredibly low levels of star formation. This limit then, defines the zero level of star formation in our model, if whole

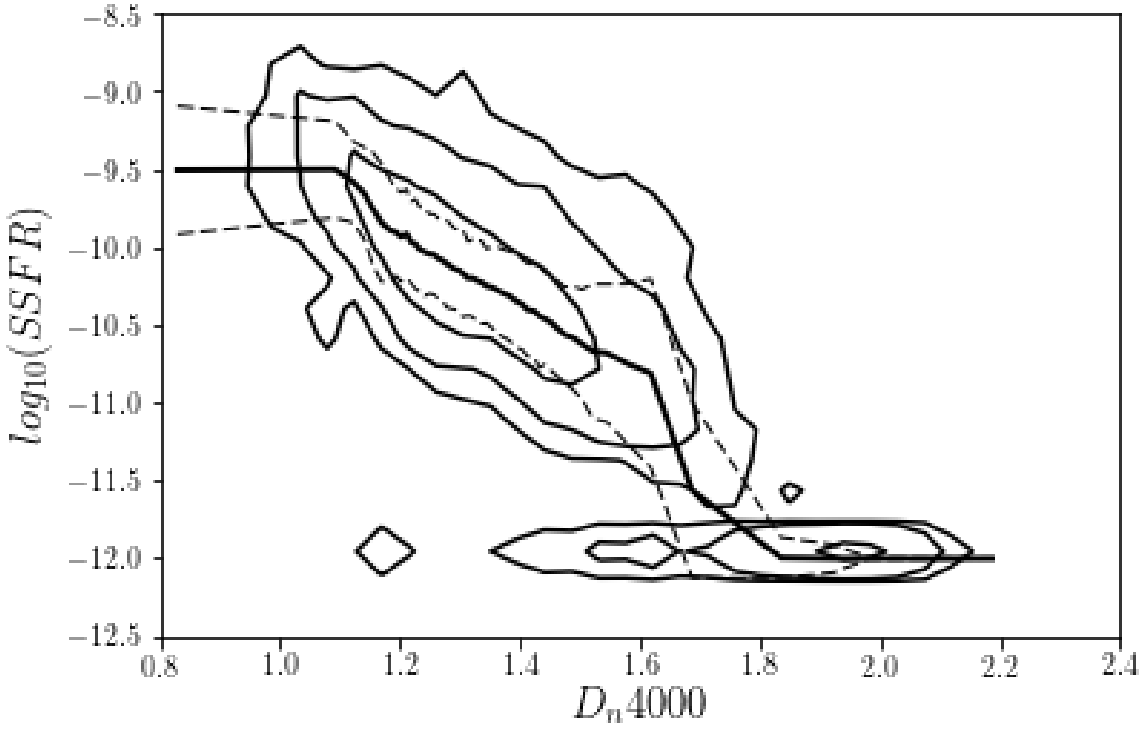

Fig. 3.7 I show the model for D_n4000 specific star formation rates, based on the SSFRs calculated using H_α. I use bins that are star forming in the BPT diagram, and bins that are classified as Lineless have been included at a fixed upper limit of $log_{10}(SSFR) = 11.5$. The contours show the $1-$, $2-$ and $3-\sigma$ levels. the solid black line shows the median SSFR at fixed D_n4000 and the dashed lines show the $1-\sigma$ scatter from the median. This model uses bins from the VOR10 binning scheme that also have a $SNR > 30$.

galaxies, bins or individual spaxels have SSFRs that approach this value, I know they are effectively quenched.

In Figures 3.5, 3.6 and 3.7 I show three potential models for the SSFR-D_n4000 relation with the lineless bins included at the minimum SSFR and minimum SNRs of 10, 20 and 30, respectively. The lineless bins are predominantly distributed between $1.6 < D_n4000 < 2.0$, their introduction allows for the SSFR to decrease over the span of $1.6 < D_n4000 < 1.8$. Overall the three models look very similar. The slope down to the minimum SSFR is perhaps the gentlest in the $SNR > 10$ model, however the larger spread in D_n4000 values means that more scatter is introduced to the median value compared to the $SNR > 20$ model. The $SNR > 30$ has a sharp drop off at D_n4000 1.6 and at $D_n4000 < 1.1$ the median actually drops instead of rising. I choose to use the $SNR > 20$ model for our final data cubes and analysis.

3.4.3 Data Product Construction

In this section I will outline the practical steps taken to produce the final star formation rate maps. To produce the final maps I use the data products from the DAP and Pipe3D. The data analysis is coded in the Python programming language, using the *Numpy* (van der Walt et al., 2011), *SciPy* (Jones et al., 2001) and *Astropy* (Astropy Collaboration et al., 2013) packages. Galaxies were analysed in parallel using the Python *multiprocessing* module.

For each galaxy, the analysis process is as follows. I import the redshift (z), axis ratio (b/a) and half-light radius (r_e, arcsec) from the *drpall* target file, which lists all the galaxies in the sample. From the redshift I calculate the conversion between angular size to physical size, in kiloparsecs, using the Astropy.cosmology module. The FITS files containing the DAP and Pipe3D products are loaded in and the individual maps extracted, I use the maps for H_α, H_β, $[OIII]$, $[NII]$, and D_n4000 from the DAP and the stellar masses from Pipe3D. I also use the inverse variance maps for each emission line and D_n4000. Finally I import the elliptical radius map, which projects the elliptical distance in arcsec from the centre of the galaxy using the inclination and position angle of the galaxy, additional radius maps are produced with units of kiloparsecs and r/r_e. To calculate the physical size, I use the *Astropy* cosmology package with the standard cosmology described in Chapter 1.

The next step is to construct the signal-to-noise masks. For the emission lines, spaxels are masked where $[LineFlux]/\sqrt{1/[InverseVariance]} < 2$ and for D_n4000 I mask spaxels where $[D_n4000]/\sqrt{1/[InverseVariance]} < 15$. Note that the D_n4000 cut is quite high due to an issue in their calculation in the MPL-5 version of the DAP, it corresponds roughly to an r-band SNR of 5. Following the SNR masks, I produce the spatially resolved BPT diagram for the given emission lines as outlined in 3.3.

Star formation rates in SF regions are found using the dust-correct H_α measurements as detailed in 3.4.1. Specific star formation rates are calculated by dividing the SFR map by the mass map and I produce a star formation rate surface density ($\Sigma_{SFR}, M_* yr^{-1} kpc^{-2}$) map by dividing each spaxel's SFR by the area of the spaxel in kpc^2.

For all other spaxels, I interpolate the measured value for D_n4000 with the SSFR-D_n4000 model and multiply those values by the stellar mass in each spaxel to find a SFR. I also calculate Star Formation Rate Surface Densities as above. The final structure of the data products will be presented in Appendix A.

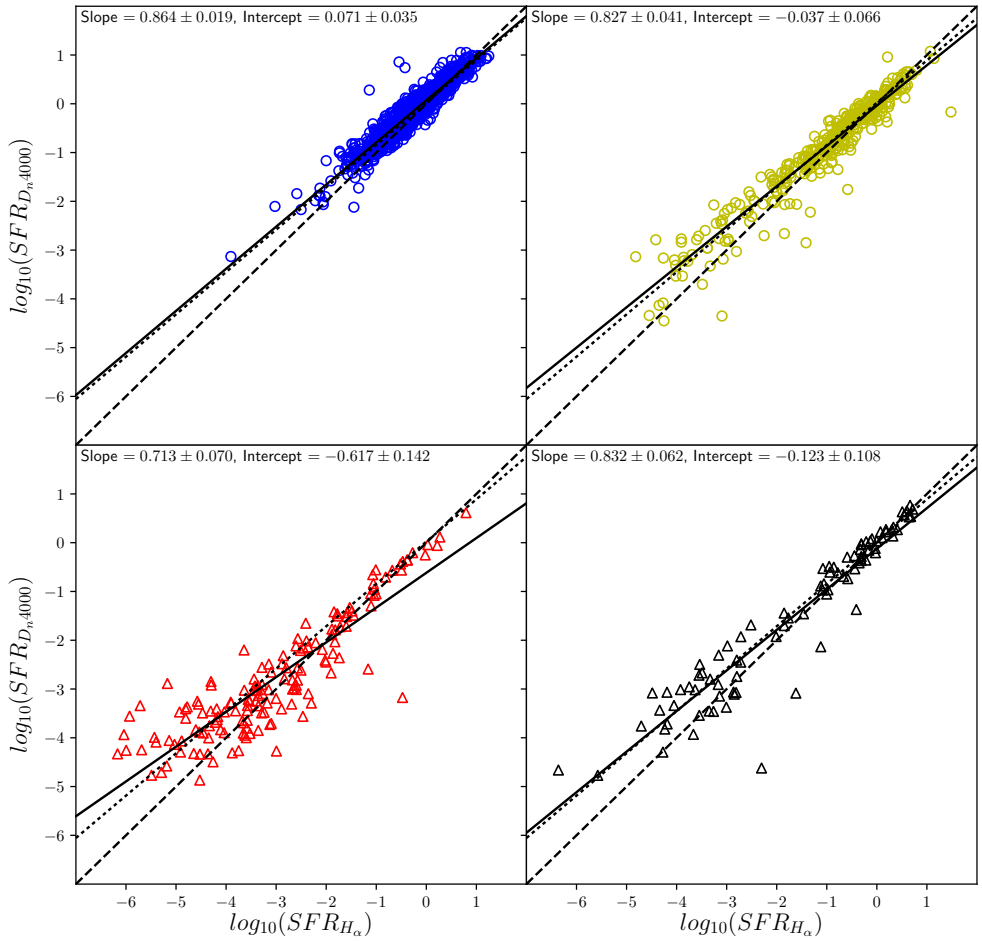

Fig. 3.8 For each galaxy, I compare the combined star formation rates from H_α to the combined SFR from D_n4000, in spaxels that are defined as star forming. The top left panel shows star forming galaxies, the top right composite, the bottom left AGN/LI(N)ER hosts and bottom right lineless galaxies. I show a linear fit calculated with a orthogonal distance regression in each panel as a solid line, with the parameters of each fit in the top left. The dashed line shows the 1-to-1 relation. The dotted line shows the linear fit to the whole sample.

3.5 Results

3.5.1 Comparison of H_α and D_n4000 Star Formation Rates

Before I can compare our SFRs to those calculated using previous surveys I need to confirm that the H_α and D_n4000 SFRs are internally consistent. I compare the SFRs predicted in the star forming spaxels for each galaxy using H_α and D_n4000 in Figure 3.8. These are not total SFRs, as they do not include the entire galaxy, I sum the SFRs from only the spaxels which are classified as star forming and have good signal-to-noise in both H_α and D_n4000. The top left panel shows the results for star forming galaxies, the top right shows composites, the bottom left AGN/LI(N)ER galaxies and lineless galaxies in the bottom right. In each panel I indicate the 1-to-1 relation with the dashed line, and the linear fit to the full sample with the dotted line. The solid line in each panel shows the linear fit to the galaxies in that panel, for which the parameters of the fit are shown in the top left of each panel.

Above $\log_{10}(SFR) = -2$ I find a very good agreement between the H_α and D_n4000 SFRs with a scatter of just 0.24 dex for the full sample. However, at lower SFRs I see there is a disagreement between the H_α and D_n4000 values, particularly for AGN/LI(N)ER galaxies that have the lowest SFRs. At low SFR, the D_n4000 values are found to be higher than the H_α values. There is a simple explanation for this, it is caused by the upper limit in the SSFR-D_n4000 model. At high values of D_n4000 the spaxels are assigned a fixed value, as I cannot reliably use the measure to go below this point, as such a spaxel with a higher mass will exhibit a higher SFR than a low mass spaxel. The upper limit in the SSFR-D_n4000 model is of course the limiting factor in the technique I have chosen to employ, as it will over predict the star formation rates in galaxies that are largely quiescent.

Interestingly, we find lineless galaxies which have high star formation rates, as high as some composite galaxies and nearly as high as some star forming galaxies. Upon inspection, these galaxies have high H_α, but are missing one of the other emission lines needed to classify them using the BPT diagram, as described in Section 3.3. In the case of these high SFR lineless galaxies, they lack the SNR in the $[NII]$ line, or have high enough SNR in $[NII]$ but have $log_{10}([NII]/H_\alpha) < 0.05$.

3.5.2 SFR relations with Mass and Environment

The relationships between the stellar mass of a galaxy and its star formation rate are well established, with the literature often referring to the so-called “Main Sequence of Star Formation” (Noeske et al., 2007). The main sequence refers to the fact that star forming galaxies have a proportional relationship between $\log_{10}(SFR)$ and $\log_{10}(M_*)$ with a small

amount of scatter. Non-star forming galaxies however lie below the main sequence in the "red sequence" and "green valley" regions. The distribution of galaxies is overall bimodal, with most galaxies lying in the main sequence or the red cloud, with a smaller number of galaxies occupying the green valley (Brammer et al., 2009; Elbaz et al., 2011; Lee et al., 2015; Michałowski et al., 2012; Schreiber et al., 2015; Tacconi et al., 2013).

To investigate the relationships between global SFR and stellar mass, I show the Mass-SFR distribution in Figure 3.9. I mark galaxies based on their classification type in the BPT-diagram; blue circles represent the star forming galaxies, yellow circles are the composites, red triangles are the AGN/LI(N)ER galaxies and black triangles are lineless.

I have performed a linear fit to the star forming galaxies in order to measure the properties of the star formation main sequence. This is plotted in Figure 3.9 along with the fits from Belfiore et al. (2016) and Renzini and Peng (2015). The main sequence for our sample of galaxies is steeper Belfiore and Renzini lines, with a slope of $m = 0.83 \pm 0.9$, compared to $m = 0.73 \pm 0.02$ and $m = 0.76 \pm 0.01$ for Belfiore and Renzini, respectively. The differences between the sequences is due to the different IMFs assumed. Belfiore and Renzini both assume a Chabrier (2003) IMF, while our work uses the Salpeter (1955) IMF assumed in the Pipe3D analysis.

Figure 3.9 shows that there is a dichotomy in the star formations rates of star forming galaxies and AGN/LI(N)ER or lineless galaxies. Naturally, the star forming galaxies lie predominantly in a linear relationship with stellar mass, while the AGN/LI(N)ER and lineless galaxies are in the "red sequence". It is important to note that the majority of the AGN/LI(N)ER and lineless galaxies have upper limit star formation rates, due to their high D_n4000 values and they receive the SSFR limit of $log_{10}(SSFR) = -12$ in the two-source star formation rate model. As such they do not lie in a single linear sequence as is seen in Figure 3.9 but rather in a cloud.

The composite galaxies however fill out the green valley region and the higher mass end of the main sequence. The location of the composite galaxies is particularly interesting, as the green valley is often interpreted as the home of galaxies that are transitioning from the star forming regime into quiescent galaxies (Belfiore et al., 2017b; Schawinski et al., 2014).

3.5.3 Comparison with the MPA/JHU catalog

The most often used catalog galaxy star formation rates for the SDSS galaxies comes from the work of Brinchmann et al. (2004) in the MPA/JHU catalog. This work utilised the stellar population synthesis codes from Bruzual and Charlot (2003) to build a Bayesian statistics model from the SDSS single fibre spectroscopy. The MPA/JHU star formation rates are found using a number of techniques based on the BPT-classification of the galaxies. For star

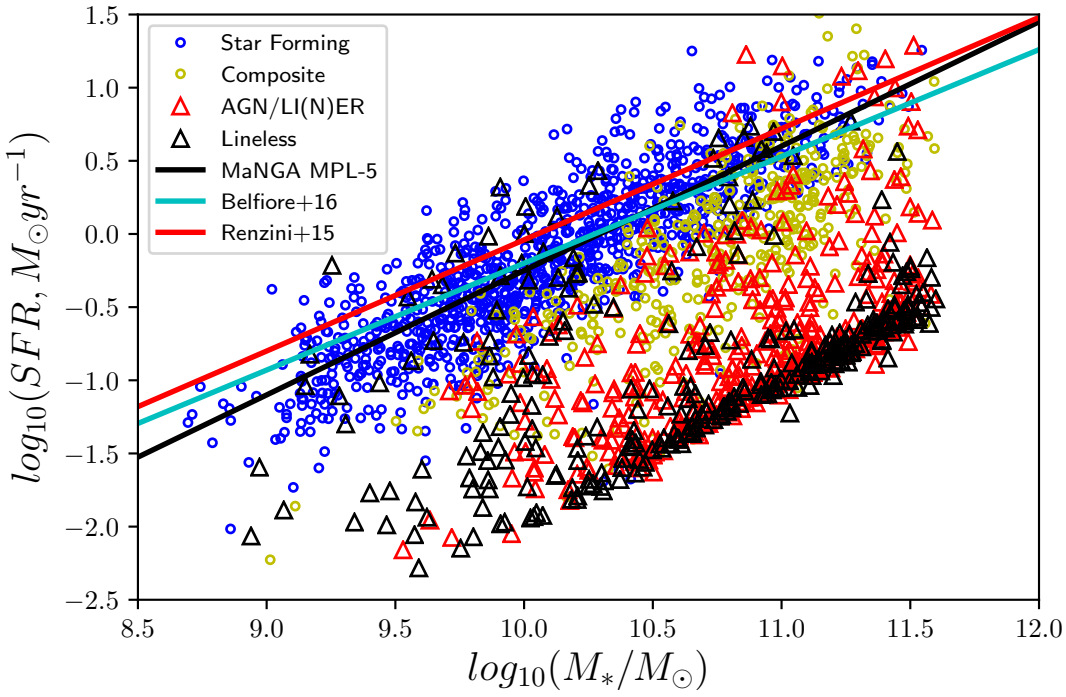

Fig. 3.9 The Mass-SFR distribution for MPL-5, using the SFRs calculated in this chapter and the Pipe3D-MaNGA stellar masses. Blue circles are star forming galaxies, yellow circles are composite galaxies, red triangles are AGN/LI(N)ER and black triangles are Lineless galaxies. the black dashed line is a linear fit to the 'Main Sequence of Star Forming Galaxies'. The black line indicates the main sequence fit for our data, while the cyan and red lines refer to the relationships from Belfiore et al. (2016) and Renzini and Peng (2015), respectively.

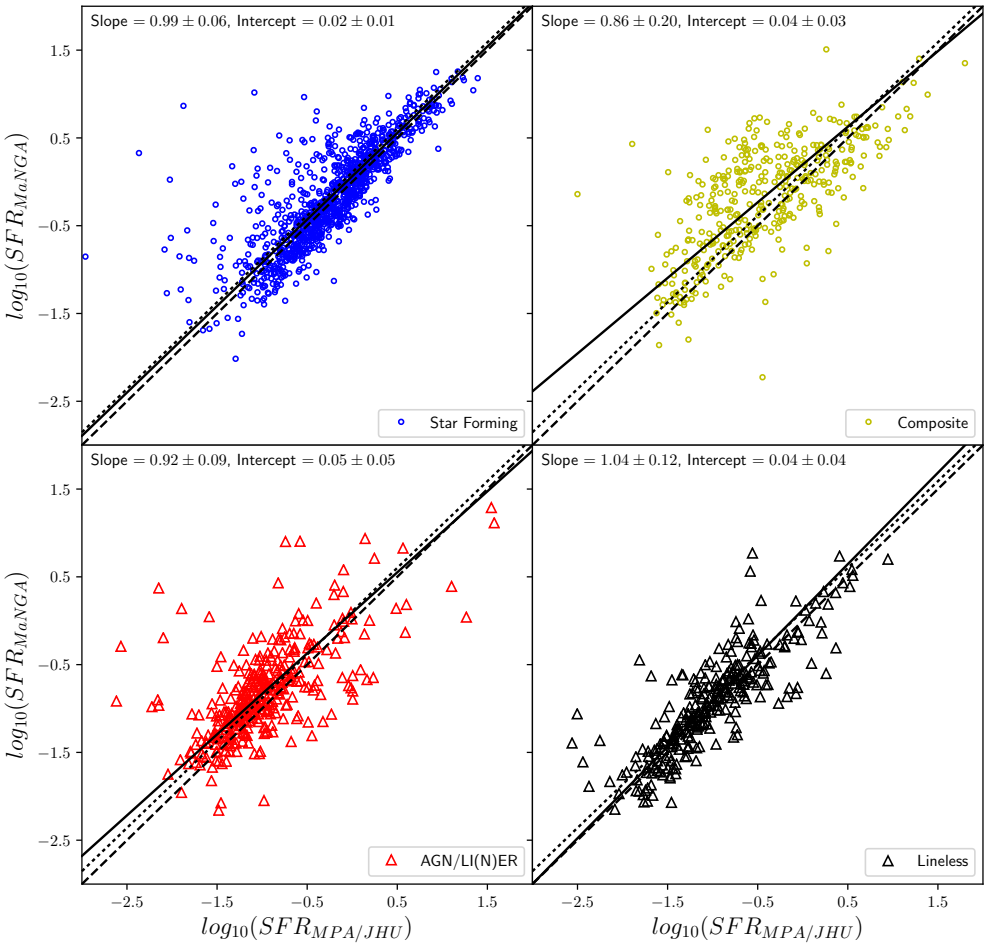

Fig. 3.10 I compare the total star formation rates from the MPA/JHU catalog with those calculated with MaNGA. The top left panel shows Star Forming galaxies, the top right composite, the bottom left AGN/LI(N)ER hosts and bottom right Lineless galaxies. I show a linear fit calculated with a orthogonal distance regression in each panel as a solid line, with the parameters of each fit in the top left. The dashed line shows the 1-to-1 relation. The dotted line shows the linear fit to the whole sample.

forming galaxies, the full emission line data is used to fit the galaxies to a model grid of stellar populations to find the star formation rates with the highest Bayesian likelihood. From these star forming galaxies, a relationship between the SFRs and H_α luminosity is found, this is used to calculate the star formation rates in galaxies that are not contaminated by AGN and LINER emission but do not have sufficient signal-to-noise in their full emission line spectra to be fit using the model grid.

Further to this, Brinchmann et al. (2004) found a relationship between SSFR and D_n4000, which was used to model the star formation rates of composite, AGN/LI(N)ER and lineless galaxies. This model is more in depth than the one used in this work, as it relies on the model grids found using the Bruzual and Charlot (2003) codes and Bayesian statistics. As the MPA/JHU values are calculated from the measurements inside the SDSS 3" fibres, they do not represent the star formation in the entire galaxy but rather just the small region inside the fibre. For this reason Brinchmann et al. (2004) calculates an aperture correction using the resolved SDSS images, this attempts to correct the fibre based SFR measurements to a total star formation rate based on the colours of the galaxy in the SDSS *ugriz* bands.

Due to the prevalence of this data catalog, its extensive crossover with the MaNGA dataset and the similarities in the techniques used, this is the perfect catalog to compare star formation rates with MaNGA.

Figure 3.10 shows the comparison between the SFRs calculated using the MaNGA IFUs and those from the MPA/JHU catalog. The four panels show galaxies split by their BPT classification, with star forming galaxies in the top left, composites in the top right, AGN/LINER galaxies in the bottom left and lineless galaxies in the bottom right. I show the orthogonal distance regression fit to the complete sample as the dotted line in each panel, it has the parameters:

$$\log_{10}(SFR_{MPA/JHU}) = 0.97 \pm 0.01 \times \log_{10}(SFR_{MaNGA}) + 0.09 \pm 0.01 \tag{3.6}$$

The full sample has a $1-\sigma$ scatter of $0.38dex$. For star forming and lineless galaxies the results agree fairly well, with close to 1-to-1 relations and each having a scatter of $0.34dex$. But for the composite and AGN/LI(N)ER galaxies, however, I see that our SFRs are generally higher than the MPA/JHU, especially at lower SFRs, and with scatters of $0.50dex$ and $0.45dex$ respectively. The reason for this scatter and offset can be traced back to the aperture corrections. Consider, for example, a galaxy with high D_n4000 in its centre indicating low SSFR but with a disk that is still actively forming stars. In the MPA/JHU the 3" fibre from SDSS would only measure the low SSFR in the centre of the galaxy; this low SSFR would then be adjusted by the aperture correction to give a global estimate. However, the aperture correction may not fully take into account the higher star formation rates in the

disk, which would be measured in the MaNGA IFUs. Galaxies such as these (which I show are present in the sample in Chapter 4) would explain why the MaNGA global estimates are higher than the MPA/JHU.

3.5.4 Comparison with the GALEX-SDSS-WISE Legacy Catalog

For a long time the MPA/JHU was the only publicly available catalogue of stellar masses and star formation rates for the SDSS main galaxy sample, and it is certainly the most widely used dataset for those measurements. While the MPA/JHU could be described as an emission line/D4000/SED hybrid method of finding star formation rates, the GALEX-SDSS-WISE Legacy Catalog uses state-of-the-art SED fitting of UV and optical fluxes (Salim et al., 2016). In this section I will give a short description of the methodology used in the GSWLC and then present comparisons of the SFRs with the integrated MaNGA SFRs.

The main stellar masses and star formation rates in the GSWLC are calculated using data from the GALEX (Martin et al., 2005) surveys and the SDSS main galaxy sample (MGS). The catalogue covers 90% of the footprint of the SDSS MGS with shallow GALEX observations ($t \sim 100s$) and 49% of the MGS with medium GALEX observations ($t \sim 1500s$). These samples make up the GSWLC-A and GSWLC-M catalogues, there is also a GSWLC-D catalogue, however this only covers 7% of the MGS with deep GALEX observations ($t \sim 30,000s$) (Salim et al., 2016). The comparisons made in this chapter use the GSWLC-M catalogue, which covers 70% of the MaNGA MPL-5 sample.

The GSWLC uses SED fitting with the Code Investigating GALaxy Emission (CIGALE) software (Noll et al., 2009). CIGALE is a code that produces grids of model SEDs and performs SED fitting. The model SEDs produced with CIGALE include UV/optical/near-IR stellar emission, and optionally dust and nebula emission. The GSWLC utilises the Bruzual and Charlot (2003) stellar population synthesis models, which allow for the fitting of nebular emission lines.

CIGALE then performs a Bayesian SED fitting regime to the UV photometry from GALEX, and the optical photometry from SDSS ModelMags (Stoughton et al., 2002). This fitting practice generates a probability distribution for the physical parameters by assigning probabilities to each model spectrum at the specified redshift, based on the goodness of fit between the model and the broadband SEDs.

Two star formation histories were tested for the GSWLC, a two-component model that includes two exponentially declining functions with their own starting times and e-folding times, and a delayed start exponential model that starts at zero star formation, peaks at some specified time and then decreases exponentially. The delayed exponential SFH is given by:

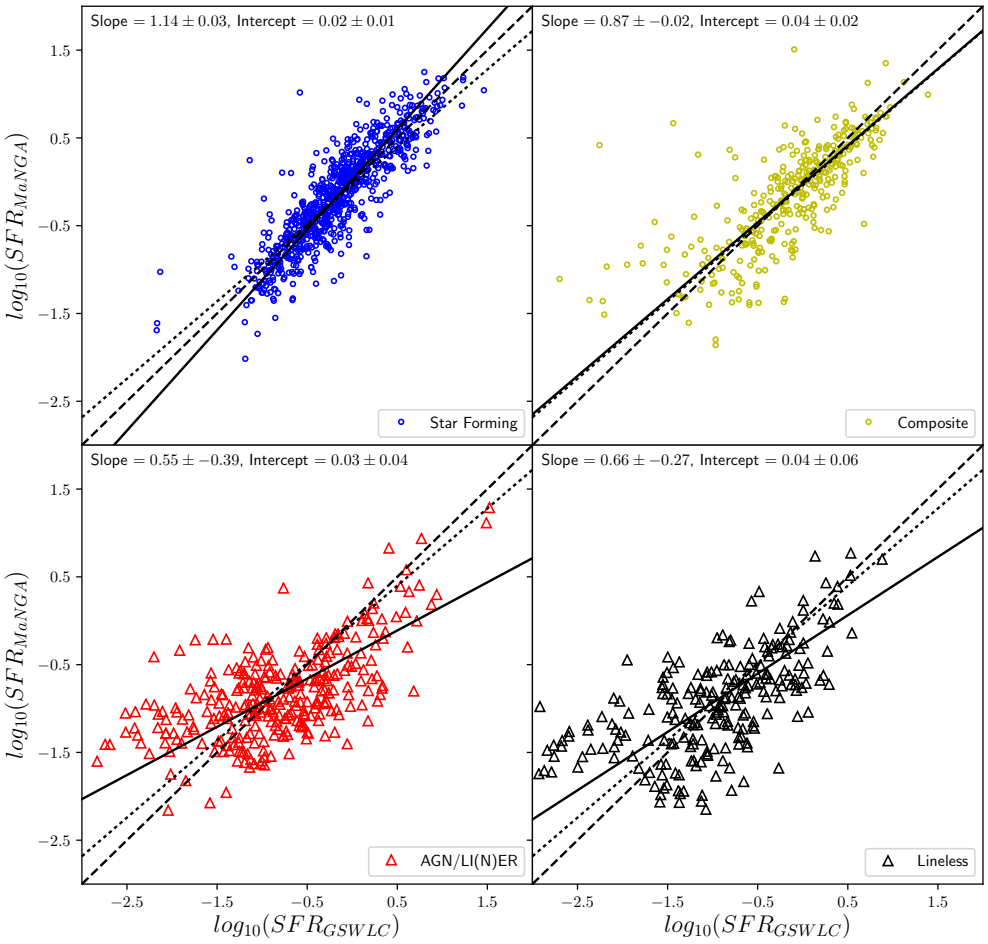

Fig. 3.11 I compare the total star formation rates from the GSWLC catalog with those calculated with MaNGA. The top left panel shows Star Forming galaxies, the top right composite, the bottom left AGN/LI(N)ER hosts and bottom right Lineless galaxies. I show a linear fit calculated with a orthogonal distance regression in each panel as a solid line, with the parameters of each fit in the top left. The dashed line shows the 1-to-1 relation. The dotted line shows the linear fit to the whole sample.

$$SFR \propto \frac{t}{\tau^2} e^{-t/\tau} \tag{3.7}$$

It was found that both models find similar stellar masses and SFRs, with no systematic differences between low SFR galaxies and only a 0.1 dex difference between actively star formation galaxies. However, the two-component SFH model provided a better goodness-of-fit, possibly due to the their non-smooth shape replicating the bursty nature of star formation in low mass galaxies (Weisz et al., 2011).

The catalogue uses a dust attenuation model that is a modified Calzetti et al. (2000) curve, which includes an additional bump in the UV range. It was found that this curve achieves a much better quality fit than a standard Calzetti curve.

In Figure 3.11 I compare the star formation rates of galaxies classified between the GSWLC-M catalogue and the integrated MaNGA data, with the galaxies split by the BPT classification in separate panels. I have performed a Orthogonal Distance Regression to fit a linear relationship between the two catalogues and provide the parameters of the fit with their standard errors in the top left corner of each panel. The linear fit is shown with the solid line and the 1-to-1 relation with the dashed line. The integrated MaNGA SFRs agree very well with the GSWLC for star forming and composite galaxies, with a slopes close to 1-to-1 and a scatter of just 0.25 dex and 0.4 dex, respectively. There are no systematic differences in the SFRs present for the star forming galaxies, however composite galaxies with low SFRs do show some bias towards higher star formation rates in MaNGA.

For the AGN/LI(N)ER hosts and Lineless galaxies, I see that there is a systematic difference between the GSWLC SFRs and MaNGA. At the low end of SFR, I find that the MaNGA SFRs are generally much higher than the GSWLC, this is a consequence of the SSFR-D_n4000 limit that prevents us from measuring very low SFRs. Above $\log_{10}(SFR_{GSWLC}) = -1.5$, however, I find that the MaNGA SFRs are consistently lower for AGN and Lineless galaxies. Similar discrepancies were found between the GSWLC and the MPA/JHU AGN and lineless galaxies. The additional star formation in the AGN galaxies was attributed to the inclusion of the UV bands from GALEX, which when removed reduced the AGN SFRs to be more in line with the MPA values. For the lineless galaxies, however, it was suggested that many of these galaxies with intermediate SFRs may in fact be post-starburst or 'E+A galaxies' (Dressler and Gunn, 1983; Goto, 2007) and that these galaxies are very sensitive to the assumed dust model. When using a Calzetti dust model instead of the modified dust law, it was found that the SFRs from the SED fits were an order of magnitude lower, however the reduced chi-squared parameter was much higher, implying that the modified dust law better predicted the SFRs of these galaxies.

3.6 Conclusions

In this chapter I have used data from SDSSIV-MaNGA to develop predictions of star formation rate in 2791 local galaxies observed with Integral Field Spectroscopy. I have constructed data cubes that provide spatially resolved star formation rates, specific star formation rates and star formation surface densities based on estimates from the dust corrected H_α emission line and the strength of the 4000Å break.

In order to fully sample the star formation from an individual galaxy I required a map that designated which estimator to use. For this, I developed spatially resolved BPT maps for each galaxy in the sample. Using the relationships from Kauffmann et al. (2003a) and Kewley et al. (2001) spaxels in the galaxy maps were designated 'Star Forming', 'Composite', 'AGN/LI(N)ER' or 'Lineless'. I also calculated a total BPT designation for each galaxy, which is used for further sample selection and when comparing galaxy properties to other catalogs.

For star forming spaxels, I use the dust corrected flux of the H_α emission line to estimate start formation rate, using the relation from Kennicutt (1998a). The H_α flux is related to the UV emission from young giant blue stars, which have a short lifetime after a burst of star formation. However, H_α is readily absorbed by the interstellar dust within galaxies, and so I need to correct for this absorption. To correct for the dust I use the flux from the H_β to calculate the Balmer decrement, assuming a Cardelli et al. (1989) extinction law and a case B recombination at $T \sim 10,000$K.

In non-star forming spaxels, the H_α flux has been contaminated by flux from a source other than young stars, for example Active Galactic Nuclei or emission from shocked gas. Alternatively, there may simply be no emission in those spaxels, due to low signal to noise or a very old, stable population of stars. In these cases, I require a different measure of star formation. I decided to follow the example laid out in the MPA/JHU catalog and calculate specific star formation rates using a model based on the D_n4000 spectral index. I tested a number of variations of the model, the minimum signal to noise was varied to find a balance between total number of data points and the lowest detectable SSFR, the final model uses the VOR10 binning scheme datacubes, with bins that have $SNR > 20$. It was found that using only star forming bins meant the model was incomplete at values of $D_n4000 > 1.8$, as such I included lineless bins with an upper limit specific star formation rate at $\log_{10}(SSFR) = -12$.

An initial test was carried out to ensure the D_n4000 model correctly matched the H_α SFRs. The total star formation rates from star forming spaxels, calculated using the two methods, were compared for each galaxy. I found a good agreement between the two methods for all galaxy classifications in the BPT diagram.

An important scaling relation of galaxy properties is the so-called 'Main Sequence of Star Formation', which relates a galaxy's stellar mass with its star formation rate. I have compared the stellar masses and SFRs of galaxies in the MaNGA sample and found that star forming galaxies do indeed lie in a linear relationship between mass and SFR. Composite galaxies were found to generally occupy the high mass end of the main sequence and the 'green valley'. AGN/LI(N)ER galaxies and Lineless galaxies predominantly occupy the quiescent regions of the mass-SFR plane. I compared our linear fit of the main sequence of star formation and found that it was steeper than the main sequences from Renzini and Peng (2015) and Belfiore et al. (2017b), however this differences is likely due to the differences in the assumed IMFs.

I compared our total star formation rates with the values calculated in the MPA/JHU catalog, the most widely used catalog of star formation rates for SDSS galaxies. I find very good agreement with MPA values, with a linear fit close to 1-to-1 and a scatter of $0.38 dex$. Star forming and lineless galaxies have the best fits with the MPA data, which the scatter is greater for composite and AGN/LI(N)ER galaxies. I believe that the combination of both sources of star formation in the MaNGA maps and the differences between the total IFU star formation and the aperture corrected total are responsible for the larger scatter.

Finally, I compared our values for total star formation rates with the GALEX-SDSS-WISE Legacy Catalog, which uses an updated SED fitting technique that utilises UV data from GALEX and optical data from SDSS to calculate SFRs. I find good agreements for star forming and composite type galaxies, however the AGN and Lineless galaxies are typically assigned higher SFRs in MaNGA than in the GSWLC due to the upper limit in the D_n4000 model.

The data products constructed in this chapter allow for the exploration of the spatial distribution of star formation in local galaxies. I can study galaxies in a variety of classifications using the BPT diagram and compare the distribution of star formation against a range of galaxy properties, such as total stellar mass, morphological parameters or using proxies for environment.

4

The Spatial Distribution of Star Formation and its Dependence on Mass, Central Velocity Dispersion and Environment

"Everything starts somewhere, although many physicists disagree."
– Terry Pratchett, *Hogfather, 1996*

4.1 Introduction

In the last two decades, large scale spectroscopic surveys, such as SDSS, GAMA and zCOSMOS (Driver et al., 2011; Lilly et al., 2007; York and SDSS Collaboration, 2000), have been a driving force in extragalactic astronomy. One of the principal results of these surveys is the characterisation of the bimodality in galaxy populations across a variety of galaxy properties. Morphological type, colour, star formation rate, stellar population age and gas content have all been shown to be strongly bimodal (Baldry et al., 2006, 2004; Balogh et al., 2004; Blanton et al., 2005a, 2003; Blanton and Moustakas, 2009; Peng et al., 2010a). Broadly, galaxies can be split into two groups; star forming galaxies which are typically low density, disk-like in shape and blue in colour, and quiescent galaxies, which are more compact than star forming galaxies, generally do not host spiral shapes and are red in colour.

The results from this Chapter are presented in Spindler et al. (2017) which has been accepted by MNRAS for publication.

Quiescent galaxies also typically contain older stellar populations than star forming galaxies (Blanton and Moustakas, 2009; Thomas et al., 2005). Faber et al. (2007) found that while the number density of blue galaxies has remained constant since $z \sim 1$, the number density of red galaxies has increased. These observations suggest then that there are physical processes that move galaxies from the Star Forming type to the Quiescent type. In this Chapter I explore the shut down of star formation, or 'quenching' in local galaxies. I explore processes that shut down star formation at the local and global scale, and which act on different time scales.

In recent years, a new generation of integral field spectroscopy (IFS) surveys have been employed to study the evolution of galaxies and by extension the process of quenching. These IFS surveys (such as CALIFA, Sánchez et al. 2012, MaNGA, Bundy et al. 2015, and SAMI, Bryant et al. 2015) use monolithic or multi-object spectrographs, and fibre optic bundles (or integral field units, IFUs) to observe galaxies both spatially and spectrally. The resulting data cubes provide spatially resolved information about the spectral make-up of the galaxy, allowing astronomers to study the spatial distribution of galaxy properties such as star formation, metallicity, kinematics and stellar age.

It has been suggested for some time that there are multiple channels by which galaxies can quench. Broadly speaking, there has been some consensus in the literature to divide processes into two channels, those dependent on stellar mass and those that rely on environment (Belfiore et al., 2017b, 2016; Mendel et al., 2013; Peng et al., 2010b; Rees and Ostriker, 1977; Schawinski et al., 2014; Silk, 1977; Smethurst et al., 2015). Mass-quenching refers to the mechanisms that shut down star formation due to the intrinsic properties of the galaxy, such as radio-mode feedback from AGN, morphological quenching, bar quenching and halo-shock heating (Belfiore et al., 2017b, 2016; Bower et al., 2006; Fabian, 2012; Gavazzi et al., 2015; Heckman and Best, 2014; Masters et al., 2011; Page et al., 2012; Schawinski et al., 2007). Environmental-quenching refers to the mechanisms related to the extrinsic properties of a galaxy, these include ram pressure stripping, tidal stripping, galaxy harassment and strangulation (Abadi et al., 1999; Balogh et al., 2000; Bialas et al., 2015; Font et al., 2008; Gunn and Gott, 1972; Gupta et al., 2017; Lewis et al., 2002; McCarthy et al., 2008b; Peng et al., 2015; van den Bosch et al., 2008a). This split between processes is slightly crude, however, as there is some overlap between the groups as there is with any binary split in astronomy. For example: the mass loss due to tidal and ram pressure stripping is in part tied to the stellar mass of the galaxy, with lower mass galaxies losing more material than high mass ones; one could also consider AGN quenching to be partly affected by environment, as one of the favoured mechanisms is for the AGN to heat the surrounding intra-cluster medium and prevent accretion of new star forming material.

Interestingly however, it has been shown by some authors that mass and environment quenching may in fact be part of the same mechanism. For example Knobel et al. (2015) found that central galaxies in groups also respond to the environmental processes that are typically only associated with satellites, they go on to suggest that the differences in apparent mass dependences of satellite and central quenching occur because the properties that determine satellite quenching (e.g., dark matter halo mass, group centric distance, local overdensity) are independent of satellite stellar mass. Carollo et al. (2016) and Smethurst et al. (2017) both suggest that environmental processes work in tandem with mass and morphological quenching mechanisms in driving the evolution of satellite galaxies in groups.

There are a number of physical processes which act on galaxies in dense environments, which have been widely studied in the literature. Ram pressure stripping refers to the removal of gas from a galaxy due to the drag force exerted from motion through the intracluster medium (Cayatte et al., 1994; Cortese et al., 2011; Forman and Jones, 1982; Giovanelli and Haynes, 1985; Gunn and Gott, 1972; Markevitch et al., 2000; Solanes et al., 2001). Ram pressure stripping leads to a confinement of star formation to the centres of galaxies, as it predominantly acts on the outer disk of later type galaxies (Cortese et al., 2012; Koopmann and Kenney, 2004a,b). Similarly, galaxies may be subject to tidal harrassment from the surrounding dark matter halo and neighbouring galaxies, which affects star formation by removing gas from the disks or driving it into the galaxy bulges (Hernquist, 1989; Moreno et al., 2015).

If a galaxy's outer halo of gas is stripped away, it will lose the ability to replenish the gas it uses in star formation, causing an eventual shut down in star formation often referred to as starvation or strangulation (Larson et al., 1980; McCarthy et al., 2008b; Peng et al., 2015). Interestingly, strangulation is predicted to have a different spatial pattern than gas stripping, occurring uniformly over the entire galaxy instead of preferentially shutting down star formation in the disks or bulges of galaxies. One possible outcome of this is anaemic spirals, disk type galaxies which are deficient in HI gas and star formation compared to other disks, but which still have a spiral structure (Elmegreen et al., 2002; van den Bergh, 1991).

The existence of mass-based and secular quenching has been widely established in the literature, but the understanding of the underlying physics on the other hand is not. Bell et al. (2012); Cheung et al. (2012); Franx et al. (2008); Pasquali et al. (2012); Wake et al. (2012) and Bluck et al. (2014) all point out the strong link between the presence of a large bulge and the likelihood that a galaxy will be quenched. Martig et al. (2009) showed that the build up of a spheroidal components from mergers or other processes can stabilise the gas in a galaxy against collapse and fragmentation. This prevents star formation and causes early type galaxies to become red and dead. Smethurst et al. (2015) found that quenching

time-scales are correlated with galaxy morphology. Bars have also been linked to low the shut down of star formation in galaxies, both on a global scale and with the central few kpc of the galaxy core (Gavazzi et al., 2015; Masters et al., 2011)

The large bulges in quenched galaxies lead to the assumption that supermassive black holes may play a role in quenching, as the black hole mass is well correlated with bulge mass (Häring and Rix, 2004; Marconi and Hunt, 2003; McConnell and Ma, 2013). It has been shown that radio-mode AGN are capable of heating the intracluster medium, which could play an important role in regulating star formation and gas accretion (Fabian, 2012; Gaspari et al., 2012; McCarthy et al., 2008a; Mittal et al., 2009; Rafferty et al., 2008). However, no link has been found between the presence of a radiative mode AGN and a suppression of star formation (Carniani et al., 2015; Cicone et al., 2014; Maiolino et al., 2012).

It appears then, from the mechanisms that drive mass based and environment based quenching, that they should provide opposing signals in galaxies. So-called 'inside-out' and 'outside-in' quenching has been discussed in the literature (Li et al., 2015; Tacchella et al., 2015). The environment channel may demonstrate an outside-in signal, whereby the cold gas is stripped from the outer disks or driven into the centre by tidal interactions, which would present enhanced star formation in the galaxy cores with respect to the outskirts. Mass quenching, if driven by AGN feedback or bulge growth, would instead demonstrate an inside-out quenching pattern, as the AGN quenches the star formation in the galaxy bulges first.

Thanks to the next generation integral field spectroscopy surveys we can now study the effects of quenching at spatially resolved scales and identify the signals for both the mass based and environment based quenching mechanisms. Belfiore et al. (2017b) have already shown the presence of inside-out quenching with their study of "central low ionisation emission region" (cLIER) galaxies, which they show could be green valley galaxies in the process of quenching. The outside-in process, instead, has been observed in MaNGA through stellar population analysis by Goddard et al. (2017b) who find slightly positive age gradients in early-type galaxies pointing towards outside-in progression of star formation. This pattern was found to be independent of environmental density in Goddard et al. (2017a) and Zheng et al. (2017). Schaefer et al. (2017), used the Sydney-AAO Multi-Object Integral Field Spectrograph (SAMI), to show that increasing local density correlated with reduced star formation in the outskirts of galaxies. Conversely, Brough et al. (2013) found no evidence of environmental quenching on a sample of galaxies studied using their H_α profiles, however this sample size was much smaller than Schaefer et al. (2017) with only 18 galaxies in the former and 201 galaxies in the latter. Narrow band imaging of H_α has been used to study the environmental dependence of star formation in dense environments. In the Virgo

cluster Koopmann and Kenney (2004a) showed that approximately half of their sample of 84 galaxies had truncated star formation, and 10% had star formation rates which were uniformly suppressed. In the Calar Alto Legacy Integral Field Area survey (CALIFA) Pérez et al. (2013) showed that massive galaxies grew their mass inside-out by using stellar population spectral sysnthesis to find spatially and time resolved star formation histories. González Delgado et al. (2017) also studied spatially resolved star formation histories of a morphologically diverse sample of galaxies and found that galaxy formation happens very rapidly and in the past it was the central regions of early type galaxies where star formation was at its most intense. In addition, Lin et al. (2017) found evidence of bar induced star formation in the centres of so-called 'turnover galaxies', which exhibit a rejuvenated stellar populations in their cores.

In this Chapter I use a large sample of 1368 Star Forming and Composite AGN/Star Forming galaxies from the Fourth Sloan Digital Sky Survey Mapping Nearby Galaxies at APO (SDSSIV-MaNGA, Blanton et al., 2017; Bundy et al., 2015) survey to study the spatial distribution of star formation and its dependence on stellar mass, core velocity dispersion, morphology and environment. I investigate the shapes of the galaxy's specific star formation rate profiles, and whether there is an inside-out or outside-in suppression of star formation with respect to galaxy's internal and external properties.

This work is complemented by a parallel paper Belfiore et al. (2017a), which studies the sSFR profiles in the Green Valley and in central LIER galaxies.

This work is structured as follows. In Section 4.2 I discuss the MaNGA survey and our sample selection criteria. In Section 4.3 I show our results for the specific star formation rate profiles and their dependence on a variety of galaxy properties, then in Section 4.4.1 I split the galaxy sample in galaxies which are centrally quenched or star forming. In Section 4.4 I discuss our results in the context of a variety of quenching mechanisms, including AGN feedback, morphological quenching and strangulation. Finally I conclude in Section 4.6. I make use of a standard ΛCDM cosmology with $\Omega_m = 0.3$, $\Omega_\Lambda = 0.7$ and $H_0 = 70 km^{-1} s^{-1} Mpc^{-1}$.

4.2 Data

4.2.1 Sample Selection

DR14 contains 2791 galaxies across the primary, secondary, colour enhanced and ancillary samples. In this work I begin with the full MaNGA sample, with galaxies from the Primary, Secondary and Colour-Enhanced Samples.

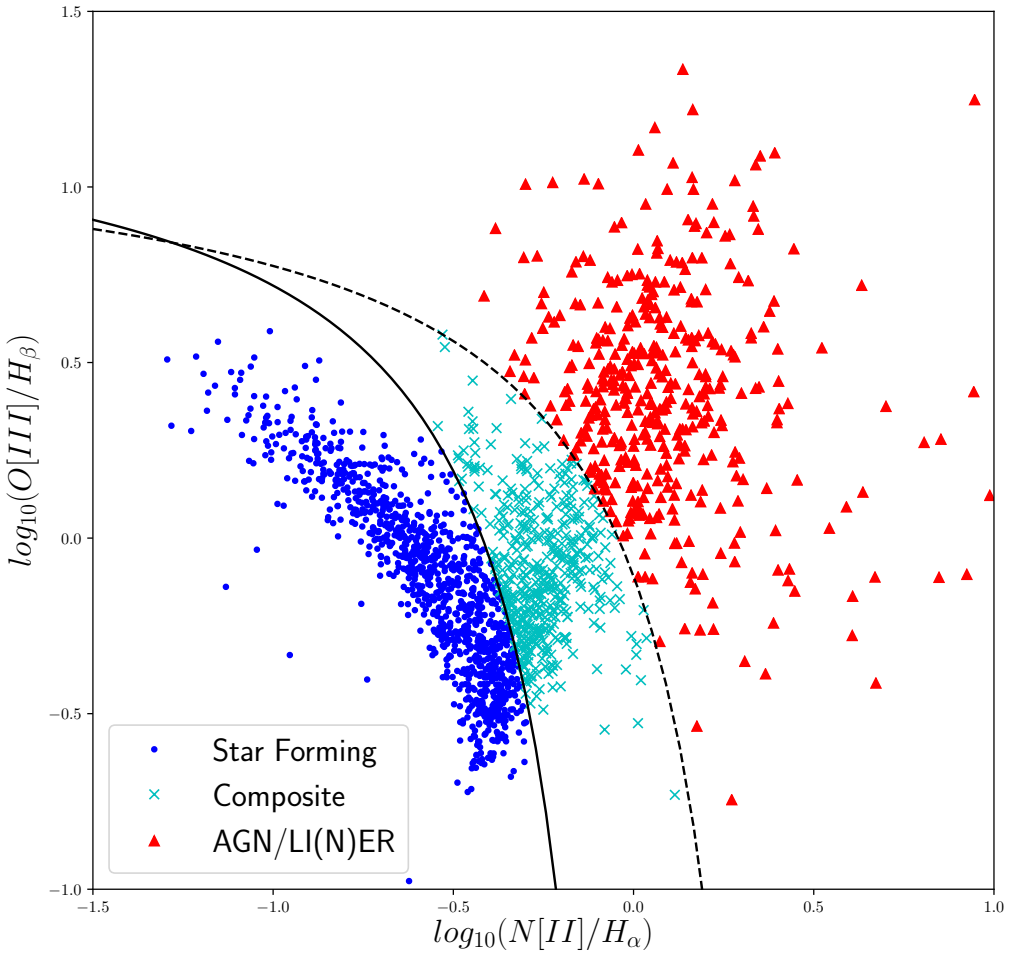

Fig. 4.1 The BPT Diagram for galaxies in the MaNGA survey. The positions of galaxies are calculated from the integrated flux over the entire IFU. Blue dots are the Star Forming Galaxies, cyan crosses and the composite galaxies and the red triangles are the AGN/LINER galaxies. The solid line is the relation from Kauffmann et al. (2003a) and the dashed line is from Kewley et al. (2001).

I remove IFUs which contain two or more galaxies from the sample, which were identified by eye in the SDSS g-r-i imaging of the MaNGA galaxies, which cuts 153 fibre bundles from the sample. I do this to eliminate the need to calculate centres for both galaxies in order to find individual SFR profiles.

Throughout this work I wish to study galaxies which are dominated by different forms of ionising radiation, such as from star formation, Active Galactic Nuclei (AGN) and Low-Ionization (Nuclear) Emission Regions (LI(N)ER), or galaxies which are a composite of these emission types. As such, I measure the line intensities of H_α, H_β, $[NII]$ (6585nm) and $[OIII]$ (5008nm) in the integrated fluxes of the DR14 data cubes and calculate the positions of these galaxies on the Baldwin-Phillips-Terlevich (BPT, Baldwin et al., 1981) diagram. I require that the emission line SNR in each of these lines be > 2 to accurately calculate their positions on the BPT diagram, the limiting factors in the signal-to-noise are the strengths of the H_β and $[OIII]$ lines. I divide the galaxies into five groups: Star Forming for galaxies which fall below the Kauffmann et al. (2003a) line, Composite for galaxies between the Kauffmann and Kewley et al. (2001) lines, AGN/LI(N)ER for those above the Kewley line, Low SNR AGN for galaxies with low SNR in the H_β and$[OIII]$ lines but with integrated $SNR > 3$ in H_α and $[NII]$ with $\log_{10}(H_\alpha/NII) > 0.47$ and finally Lineless galaxies for those galaxies with low SNR in all four diagnostic lines. I find 1049 Star Forming galaxies and 435 Composite galaxies which I examine in the main bulk of this Chapter, in addition there are 428 AGN/LI(N)ER and 22 low SNR AGN galaxies which I study in Section 4.4.3, and 719 Lineless galaxies which I discard from the sample. The BPT diagram for the DR14 sample is shown in Figure 4.1 and shows the separations used in this sample selection. Finally, I remove from the sample galaxies which have total Specific Star Formation Rates (calculated using the model described in Chapter 3) of $\log_{10}(SSFR) < -11.5$.

The above classifications are different to Belfiore et al. (2017a), in which I use a spatially resolved BPT classifications. While the above work is interested in the roles of central Low-Ionisation Emission-line Regions (cLIER) galaxies and their transition through the green valley, in this work I are interested in the much broader trends across the entire population. In this case I find that using the integrated flux to calculate the BPT class suits our needs, especially with the inclusion of the composite class which includes galaxies with star forming disks and AGN/LI(N)ER central regions which may be confused with only a SF-AGN/LI(N)ER cut. An alternative classification system in which I measured the BPT classification in the central 3" of each galaxy was tested, however I found that the majority of the galaxies which have different classes in this system were AGN/LI(N)ERs and lineless galaxies which are otherwise already removed from the sample due to low SSFRs.

A final cut is applied to the sample based on galaxy axis ratio. Edge-on disks with a $b/a < 0.3$ are removed from the sample, as I have found that their radial profiles are poorly resolved. A total of 128 galaxies are removed based on this cut. The final sample is then composed of 1494 galaxies, 1016 of which are star forming, 364 are composite and 114 are AGN/LI(N)ER.

In addition to the core MaNGA data products I make use of the SDSS-MaNGA-Pipe3D (Pipe3D, Sánchez et al., 2016a,b) value added catalog. The Pipe3D data products were developed using the pipeline described in Sánchez et al. (2016a) and Sánchez et al. (2016b) and applied to DR14. I use the Single Stellar Population (SSP) cubes, which provide stellar mass surface density ($\log_{10}(M_{\odot})arcsec-2$) maps of the galaxies in DR14.

I make use of the specific star formation rate maps produced in Chapter 3. In addition I have rerun the DAP to produce a additional map of each galaxy which contains a single spatial bin out to $0.125r_e$, which is used to find the core velocity dispersion, σ_0, to match the definition used in Spindler and Wake (2017).

4.2.2 Other Catalogs

I make use of two additional catalogs in the analysis of this work, the Yang Group Catalog (Yang et al., 2008, 2009, 2007, 2012) and the Baldry et al. (2006) Environment Density catalog.

The Yang Group Catalog uses a friends of friends algorithm to generate galaxy groups and clusters using SDSS DR7. Galaxies are matched into tentative groups and properties such as dark matter halo mass and group luminosity are calculated, from these properties the halo groups are recalculated to include nearby galaxies that fall within the halos. This iterative process continues until no new galaxies are added to groups. From this catalog I use the Central and Satellite galaxy classifications, the dark matter halo masses and the group luminosities. The galaxy classifications and halo masses are based on rankings of the galaxies' luminosities.

There are a small number of galaxies in the MaNGA sample that are not in the SDSS DR7 (their NSA redshifts come from other sources) and so are not included in the Yang et al. catalog. Wake et al. (2017) assign these galaxies central/satellite designations and group luminosities and halo masses by associating them with Yang et al groups where possible. If a non-DR7 MaNGA galaxy has a projected separation within r_{180} of a group centre and a velocity within $\pm$ 1.5 times the group velocity dispersion then Wake et al. (2017) associate it with the group. If there is no matching group then the galaxy becomes its own group. The galaxy is then designated as either the group central or a group satellite depending on whether or not its r-band luminosity is the largest in the group. Wake et al. (2017) then recalculate the

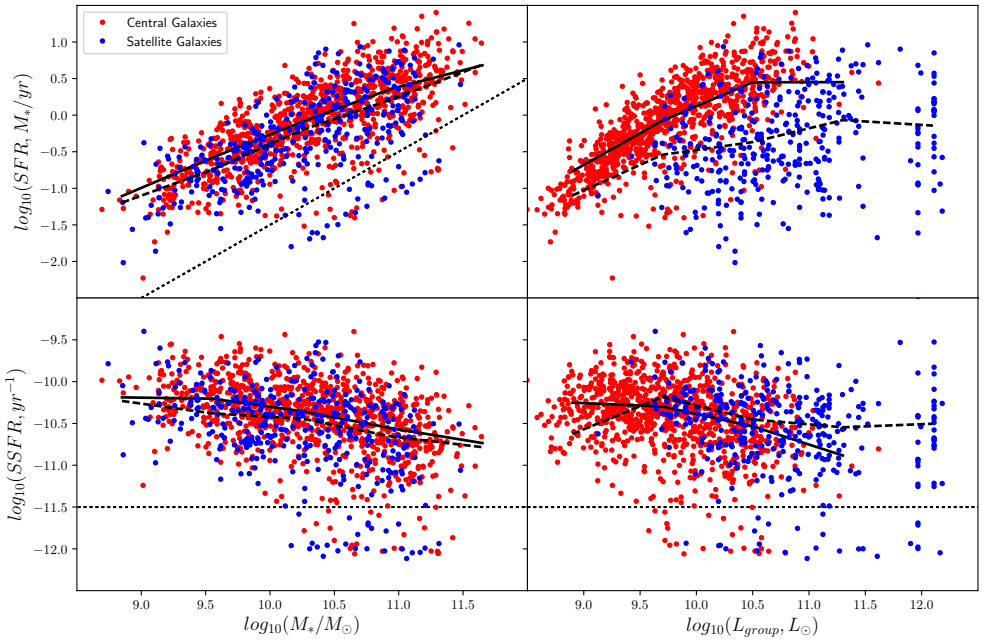

Fig. 4.2 I show the relationships between stellar mass in the left column, group luminosity in the right column, star formation rate in the top row and specific star formation rate in the bottom row. Galaxies are coloured based on their environment, with centrals in red and satellites in blue. I include the mean values of SFR and SSFR at fixed M_* and L_{group} as solid lines for centrals and dashed lines for satellites. The dotted lines indicate the position of the sample cut in specific star formation rate at $\log_{10}(SSFR) = -11.5$.

group luminosity including the new galaxy and calculate the other group properties following Yang et al. prescription.

Finally, I make use of the environment densities around galaxies calculated in Baldry et al. (2006). These densities are based on the distances to the 4th and 5th nearest neighbour galaxies with $M_r < -20(h = 0.7)$. The density is calculated as $\log_{10}(\Sigma) = 0.5 * \log_{10}(\Sigma_4) + 0.5 * \log_{10}(\Sigma_5)$, where $\Sigma_N = N/(pi * d_N^2)$ and d_N is the distance to the Nth nearest neighbour. An important note here is that the matching between this catalog and the MaNGA data is not perfect, mainly owing to the redshift limits in the Baldry et al. (2006) galaxies. Baldry et al. (2006) is limited to $0.01 < z < 0.085$, which results in 15% of our MaNGA sample not being assigned environment densities. Due to the relationship between stellar mass and redshift in MaNGA (Wake et al., 2017), this means the galaxies without densities are mainly at higher masses.

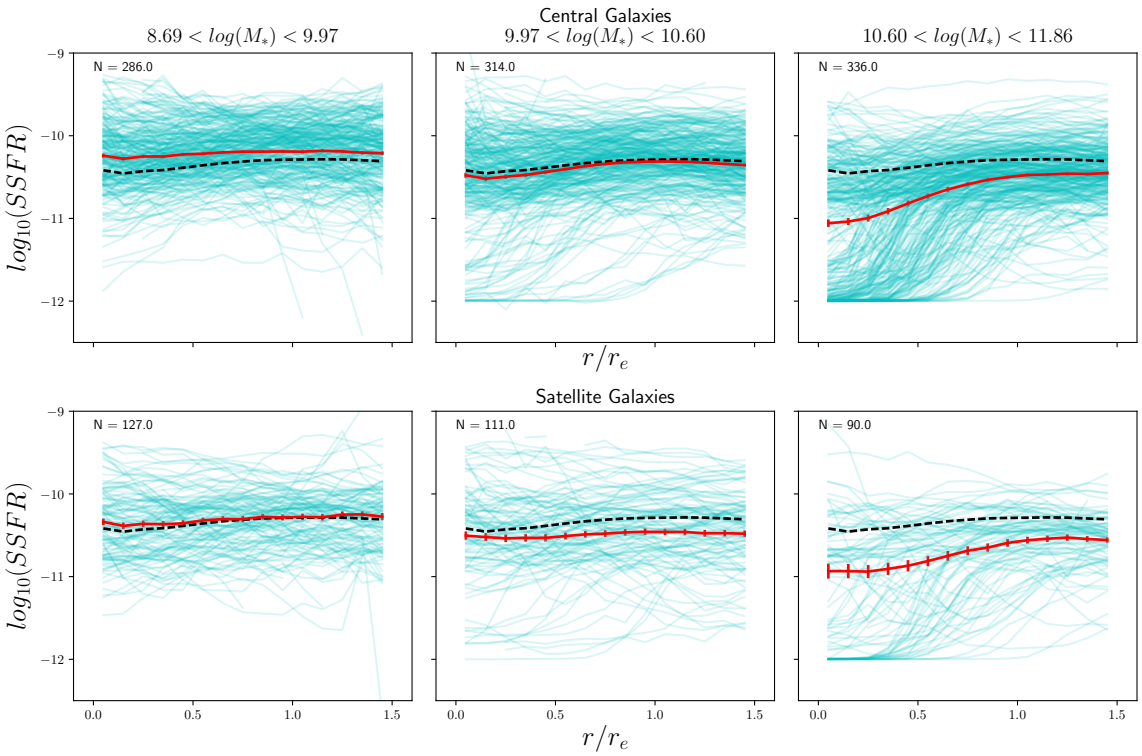

Fig. 4.3 The radial SSFR profiles in three bins of stellar mass. The individual profiles are shown by the cyan lines and the mean profile in the bin is shown by the solid red line. The dashed black line shows the mean profile of all galaxies in the sample. The number of galaxies in each bin is shown in the top left corner of each panel. The top row is the central galaxies and the bottom row is the satellite galaxies. The error bars are calculated from the scatter in 1000 bootstrap resamplings.

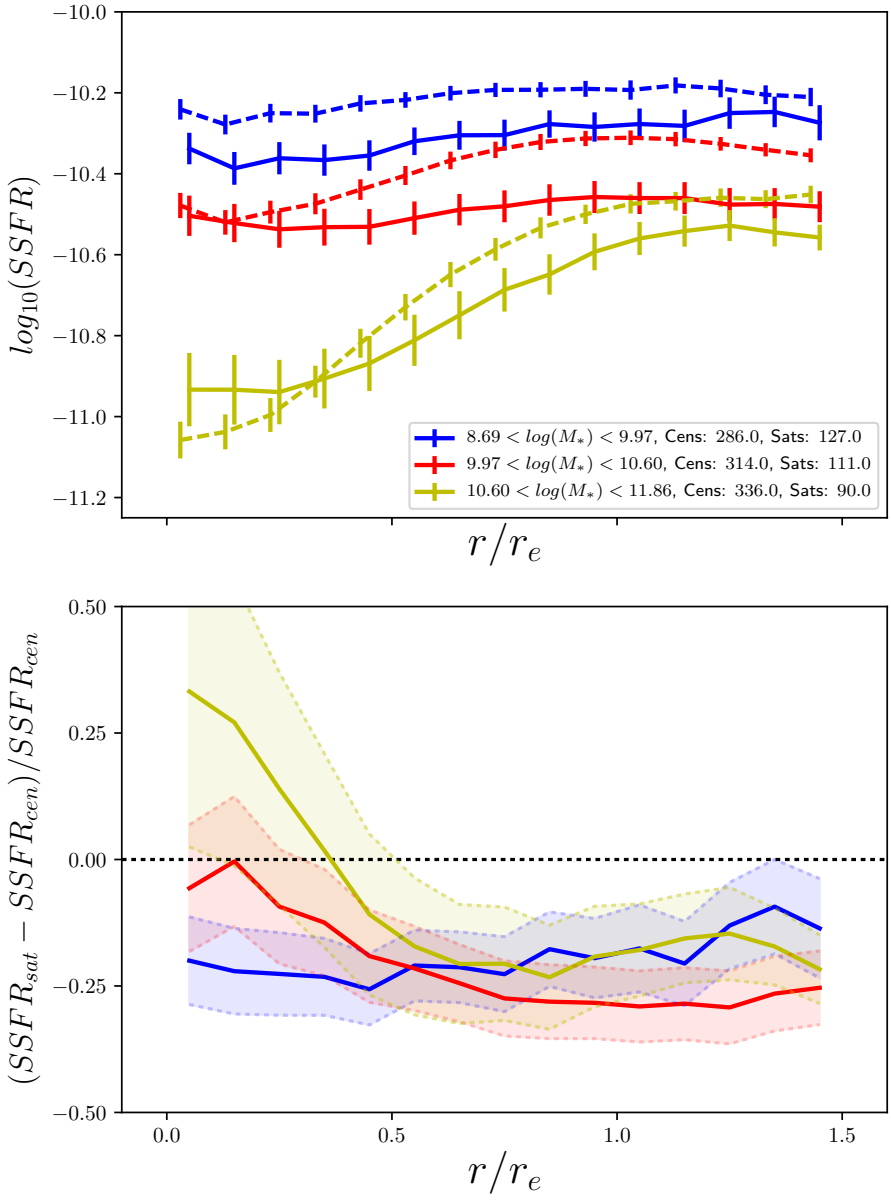

Fig. 4.4 (Top) The mean radial SSFR profiles of central (dashed) and satellite (solid) lines in bins of stellar mass. (Bottom) The fractional difference between the central and satellite mean profiles in bins of stellar mass. The shaded regions and error bars represent the $1-\sigma$ scatter in 1000 bootstrap resamplings.

4.3 Results

4.3.1 Global Properties

I begin by studying the global properties of galaxies in MaNGA. I calculate the integrated SFR, SSFR and Stellar Masses of star forming and composite galaxies from the IFUs using the ALL binned DAP MAPs, and plot their relationships along with their group luminosities from the Yang Catalogue in Figure 4.2. I plot central galaxies from Yang in red and satellites in blue and show the mean relations for those galaxies in each panel with solid and dashed lines, respectively. I include galaxies which fall below our sample cut in SSFR, which is shown by the straight dashed line in the top left and bottom panels.

In the top left panel of Figure 4.2 I show the M_*-SFR relation. I can clearly see the so-called 'Main Sequence of Star Formation' is present in this plot, as well as galaxies which fall into the 'green valley' (the region just above and below the SSFR cut). Below the SSFR cut I see galaxies with upper limit SFR which would make up the 'red sequence' of quiescent galaxies, however as these are upper limits it is important to note that this region of the plot would appear more cloud like with accurate estimates of star formation. The mean SFRs of the centrals and satellites are shown, with the satellites having lower SFR at fixed mass than the centrals, with an overal difference in the means of 0.1 ± 0.03 dex. These results are echoed in the bottom left panel, which shows the M_*-SSFR relation, with a difference in the means of 0.09 ± 0.02 dex. I again see that the satellites have lower SSFR than the central galaxies. There is a downward trend in the SSFR at fixed mass for both centrals and satellite galaxies.

In the top and bottom right panels of Figure 4.2 I show the relationships of group luminosity with SFR and SSFR. For central galaxies these relationships are broadly similar to those with mass, as the luminosity of a group is tightly correlated with stellar mass for all but the most luminous groups. The satellite galaxies however are much more spread out in the L_{group}-SFR plane, as low mass satellites with low SFR can reside in very luminous groups, compared to centrals.

More massive star forming galaxies have lower specific star formation rates that low mass star forming galaxies, as seen in Figure 4.2, and quenched galaxies are also typically found at higher masses. This raises the question, what processes are taking place within more massive galaxies that are shutting down star formation? In the next sections I will study the mean radial profiles of specific star formation rates to investigate the mechanisms of star formation shut down, particularly whether the shut-down is inside-out or outside-in.

4.3.2 SSFR Profiles at fixed M_*

I wish to study the effects of internal and external processes on the distribution of star formation in galaxies within our sample. To test the effect of internal processes, I will investigate the mean profiles of galaxies in bins of stellar mass, core velocity dispersion and Sérsic index, and to test for external environmental effects I will compare central and satellite galaxies. To investigate the distribution of star formation I choose to study the radial profiles of the specific star formation rates between $0-1.5r_e$. For each galaxy I separate the star formation maps calculated in Chapter 3 into 15 bins of elliptical radius, each $0.1r_e$ in width, from the centre of the galaxy. I calculate the mean SSFR of all the spaxels in each radius bin to find the radial profile of each galaxy.

An alternative way to calculate the radial profiles would be to integrate the light into elliptical radial bins, which can be done when processing datacubes with the DAP. I have tested this and found that it does not change the conclusions of this Chapter, so I choose to use the method described above.

I choose to calculate our radial profiles out to $1.5r_e$ to ensure that the profiles are complete for each galaxy. While it is possible to extend these profiles out beyond this point, particularly for galaxies in the Secondary MaNGA sample which are assigned an IFU to cover out to $2.5r_e$ and for edge on spirals which have radii going out to $5-6r_e$, the vast majority of galaxies do not have the signal-to-noise at these larger radii to calculate a reliable star formation rate. I find that given our signal-to-noise cuts on the emission lines and D_n4000 that 80% of galaxies are covered out to $1.5r_e$ and this number falls to 50% at $2.0r_e$. Galaxies which are covered out to these larger radii tended to be assigned one of the larger IFUs and are preferentially from the Secondary galaxy sample, they are also typically more edge on disks.

In Figure 4.3 I plot the radial SSFR profiles of central and satellite galaxies, in bins of stellar mass. The bins are chosen such that the total number of galaxies between centrals and satellites in each bin is constant. I show the individual profiles from $0-1.5r_e$ in cyan, the mean profile of each bin in red, with errors calculated from 1000 bootstrap resamplings, and the mean profile of all galaxies in the sample as a black dashed line in each panel to guide the eye and provide a point of reference.

In the lowest mass bin I see that the central and satellite profiles are largely flat, and while there are individual profiles that rise or fall with increasing radius the mean profiles remain constant. In the medium mass bin the mean profile is still rather flat, but I see that the central mean profile has been pulled down slightly by a population of galaxies which have low central SSFRs, while the satellites remain flat. The differences in the centres of galaxies are subtle, and I explore this effect further in Section 4.4.4. In the highest mass bin the galaxies with suppressed cores have significantly altered the shape of the mean profiles,

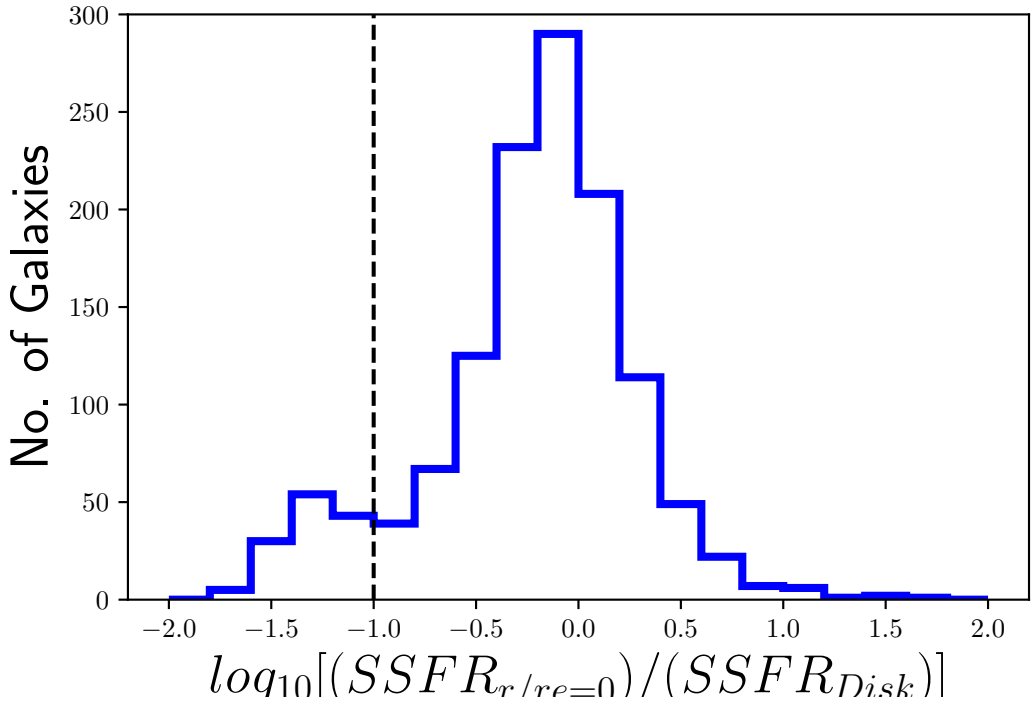

Fig. 4.5 Histogram showing the ratios between the SSFR in the centre most radial bin and the mean SSFR beyond $r/r_e = 0.75$. I show with a dashed line the cut between the centrally suppressed and unsuppressed galaxies, which marks where the disk has SSFR is approximately 10 times higher than the core of the galaxy.

which now exhibits a two-component shape with low SSFR in the centre and a flat profile outside of 1 r_e.

I can see by comparing the mean profiles in each bin with the full sample mean that the total specific star formation rate drops as stellar mass increases and that the galaxies which have suppressed star formation in their cores are mostly isolated to high masses. Figure 4.3 also displays a bimodality, particularly at high masses, between two galaxy classes, those with relatively flat profiles and those which have suppressed star formation in their centres. However there is a difference regarding the extent of the suppression from the centre of the galaxy, with some galaxies beginning to show suppression at very small radii, and others at more intermediate radii.

I show the mean profiles for centrals and satellites in the stellar mass bins in the same panel in Figure 4.4, along with the fractional differences between these profiles. The satellite galaxies have lower SSFRs than the centrals in all the stellar mass bins. In the low M_* bin the satellites have $\log_{10}(SSFR) = -10.32 \pm 0.11$ and the centrals $\log_{10}(SSFR) = -10.22 \pm 0.08$. In the medium M_* bin the satellite SSFR is $\log_{10}(SSFR) = -10.49 \pm 0.17$ compared to

$\log_{10}(SSFR) = -10.39 \pm 0.14$ for the centrals. There is a large drop in both the satellites and centrals to the high M_* bin, to $\log_{10}(SSFR) = -10.72 \pm 0.21$ and $\log_{10}(SSFR) = -10.68 \pm 0.20$, respectively. In the lowest mass galaxies the satellites have lower SSFR at all radii than the centrals. In the medium mass bin the satellite have lower SSFR at all radii, but in the cores of the galaxies it appears that the satellites are not as suppressed as the centrals. In the highest mass bin, I see that the satellites have higher SSFRs in their cores and lower SSFRs at high radii. However due to the large variance in the profiles caused by the separation of the galaxies which do and do not exhibit central suppression, it is difficult to tell whether the differences seen in the cores of these galaxies are significant. As the central suppression appears to be strongly related to mass, the differences between centrals and satellites could be due to different stellar mass distributions within each bin, however I have checked the distributions and found that this is not the case.

I desire to determine a way to split galaxies between those that have flat profiles or are 'Unsuppressed' and those that are 'Centrally Suppressed'. In Figure 4.5 I show the ratio between the SSFR in the centre radial bin and the mean SSFR beyond $r/r_e = 0.75$ (i.e. in the galaxy disk) for the full galaxy sample. This figure shows that this ratio is bimodal, with most galaxies being evenly distributed around $log_{10}[SSFR_{r/r_e=0}/SSFR_{disk}] = 0$, which represents a flat profile, and a small population of galaxies around $log_{10}[SSFR_{r/r_e=0}/SSFR_{disk}] = -1.25$. I mark on this plot with a dashed line the cut between centrally suppressed and unsuppressed galaxies, where the SSFR in the disk is approximately 10 times the SSFR in the centre of the galaxy. I also define galaxies with a central SSFR of $log_{10}(SSFR) < -11.5$ as centrally suppressed, because without this cut the lowest SSFR galaxies in the sample can be classified as unsuppressed.

The higher SSFRs in the centres of high mass satellites could be due to galaxies which have enhanced star formation in their cores, compared to their disks. This would counteract the affect of the centrally suppressed galaxies lowering the mean SSFR, leading to a higher mean SSFR in satellites compared to centrals. I investigate this possibility in Section 4.4.2.

4.3.3 SSFR Profiles at fixed σ_0

In Spindler and Wake (2017), I showed that core velocity dispersion can be a more reliable tracer of environment driven evolution of galaxies than stellar mass. σ_0 is invariant under environmental processes such as minor mergers and gas stripping, which lead to changes in the mass and size of galaxies. As such I repeat the analysis from the previous section, but instead split galaxies by their core velocity dispersions.

I show the central and satellite profiles in Figure 4.6, using the same plot style as in the previous section. In the lowest σ_0 bin, I see that the mean profile for centrals and satellites

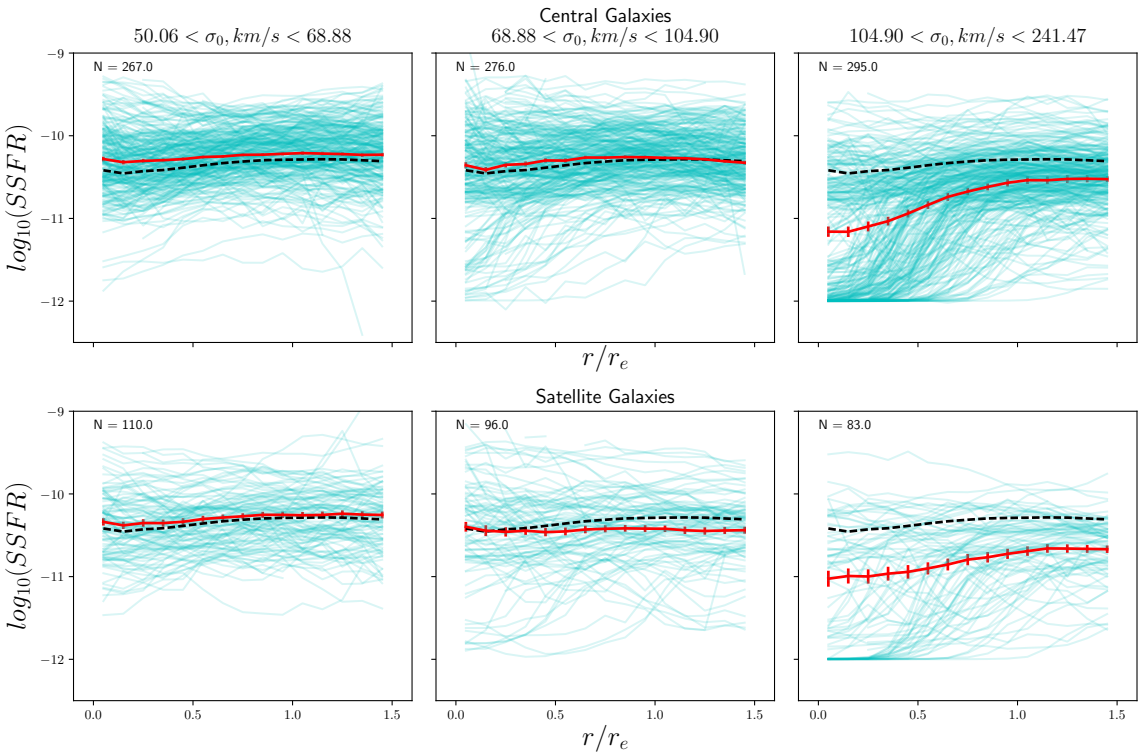

Fig. 4.6 The radial SSFR profiles in three bins of σ_0. The individual profiles are shown by the cyan lines and the mean profile in the bin is shown by the solid red line. The dashed black line shows the mean profile of all galaxies in the sample. The number of galaxies in each bin is shown in the top left corner of each panel. The top row is the central galaxies and the bottom row is the satellite galaxies. The error bars are calculated from the scatter in 1000 bootstrap resamplings.

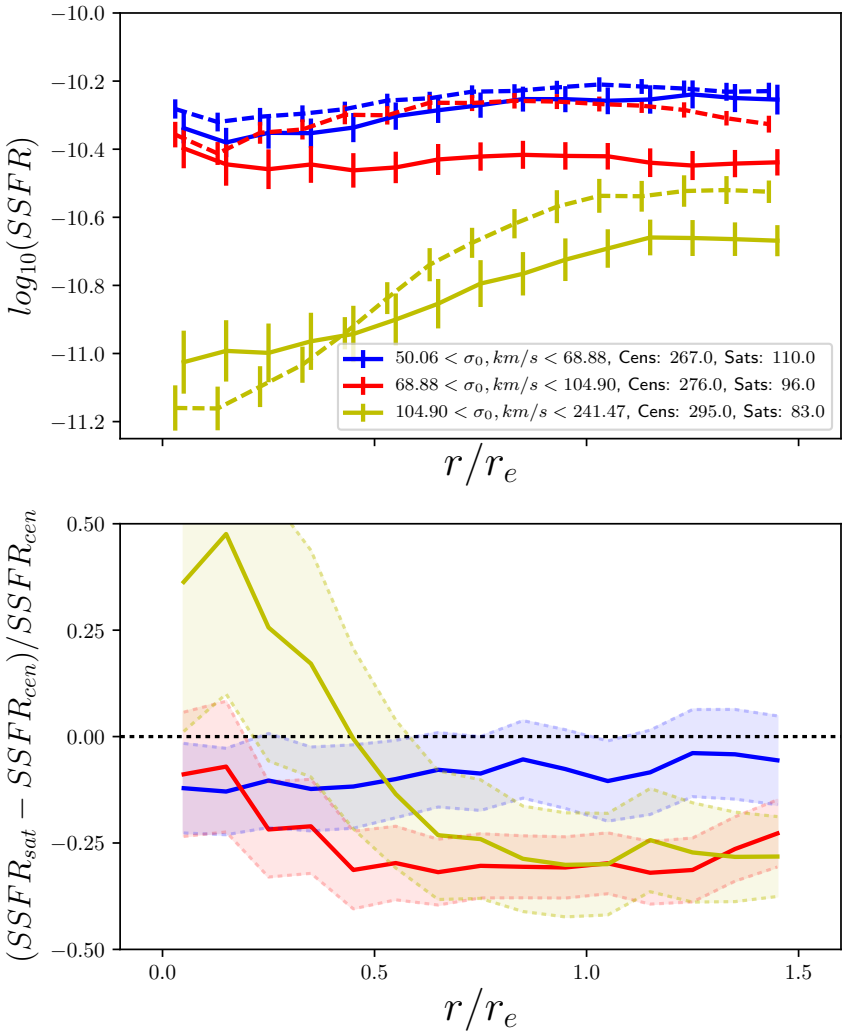

Fig. 4.7 (Top) The mean radial SSFR profiles of central (dashed) and satellite (solid) lines in bins of σ_0. (Bottom) The fractional difference between the central and satellite mean profiles in bins of σ_0. The shaded regions and error bars represent the $1-\sigma$ scatter in 1000 bootstrap resamplings.

is relatively flat, there are a small number of central galaxies with suppressed cores, but no satellites. In the medium σ_0 bin the mean profile has a slight downward trend and I once again see an increase in the number of galaxies with suppressed cores, the satellites have a flat profile. In the highest σ_0 bin there are a large number of centrally quenched galaxies which significantly affect the mean profiles of both centrals and satellites, while the outer profile has remained flat.

I compare the mean profiles and fractional differences between the mean satellite and central profiles in the three σ_0 bins in Figure 4.7. The satellite galaxies generally have lower SSFRs than the centrals. The low σ_0 bins have similar average SSFRs of $\log_{10}(SSFR) = -10.30 \pm 0.11$ and $\log_{10}(SSFR) = -10.25 \pm 0.08$, for satellites and centrals respectively. In the medium σ_0 bin the satellite SSFR is 0.1 dex lower, at $\log_{10}(SSFR) = -10.43 \pm 0.16$ for the satellites compared to $\log_{10}(SSFR) = -10.30 \pm 0.12$ for the centrals. There is a large drop in both the satellites and centrals to the high σ_0 bin, $\text{tolog}_{10}(SSFR) = -10.82 \pm 0.24$ and $\log_{10}(SSFR) = -10.76 \pm 0.27$, respectively. It appears that σ_0 is a better predictor for SSFR than stellar mass, which was also found in Wake et al. (2012).

In the low σ_0 bin, the satellites have $\sim 10\%$ less star formation out to $r/r_e = 1.5$, where the satellite profiles turn upward slightly and become more star forming than the centrals. In the medium σ_0 bin, I see that the satellites are less star forming at all radii, however at low radii it appears that the satellites exhibit less core suppression than the centrals as the fractional difference turns towards zero. In the high σ_0 bin the centrals have higher SSFRs at all radii, except in the cores where the satellites appear to have less suppression, however the scatter in the fractional difference is very high, owing to the large split in SSFRs between galaxies with and without suppressed cores.

4.4 Quenching Mechanisms

4.4.1 Centrally Suppressed Galaxies

As I have shown in the previous sections, the profile shapes seen in our sample are broadly bimodal. There are galaxies which have flat profiles, and those that have profiles which are centrally suppressed. I have also shown that in the fractional differences between the mean central and satellite SSFR profiles there appears to be two competing effects which are suppressing the star formation in different ways. There is a suppression effect at all radii upon satellite galaxies and some enhancement in the centres of satellites at high mass which may be actual enhancement of star formation or due to less satellites being centrally suppressed. In

this section I will explore the populations of centrally suppressed and unsuppressed galaxies separately.

To demonstrate this split, I plot the radial profiles of the split populations in Figure 4.8. The non-suppressed galaxies have predominantly flat profiles, however there is a subpopulation of galaxies which have enhanced SSFR in their cores and a falling profile. The centrally suppressed galaxies appear to be made of two groups, those with linear rising profiles and those which have flat profiles in their outer regions that drop off sharply towards the central bulge. There are also a small number of galaxies which are centrally suppressed by our definition, but in fact exhibit some rejuvenation in their cores.

In Figure 4.9 I show the fraction of central and satellite galaxies which are centrally suppressed in bins of stellar mass. I find that there is no difference in the fraction of centrally suppressed galaxies at fixed mass between the central and satellite population. This figure implies then that the mechanisms behind the central suppression are independent from environment completely, and depend only on the galaxy's internal properties. I also see a strong dependence on stellar mass for the fraction of suppressed galaxies, with essentially no galaxies at low mass exhibiting central suppression and 50% showing suppression at high masses. This relationship holds when the fractions are instead calculated at fixed σ_0.

One explanation for these centrally suppressed galaxies may be that I are simply tracing the existence of large bulges which formed a long time ago. This would manifest as mass profiles which increase dramatically in the centres of galaxies and SFR profiles which show a simple exponential decrease. When the mass and SFR profiles are combined to produce the SSFR profiles, I would see the characteristic centrally suppressed galaxies. To test whether this is the case I show the SFR profiles for central and satellite galaxies in Figure 4.10. This figure shows the increase in total SFR with stellar mass I demonstrated in 4.2.

I split the galaxies using the definition for centrally suppressed galaxies previously introduced and show suppressed galaxies in blue and unsuppressed galaxies in cyan. In the high and intermediate mass bins the difference between the two groups of galaxies can be clearly seen. Centrally suppressed galaxies not only exhibit decreased SFR in their cores compared to unsuppressed galaxies, but the star formation rate in their disks is also lower than in unsuppressed galaxies. This shows that the suppression of SSFR is not simply due to a much higher stellar mass in the centres of these galaxies, as if that were the case the SFR profiles of unsuppressed and centrally suppressed galaxies would be the same.

4.4.2 Comparison of Centrals and Satellite Profiles

With the population split into centrally suppressed galaxies and unsuppressed galaxies, I can revisit the SSFR profiles and determine the quenching effects operating on these different

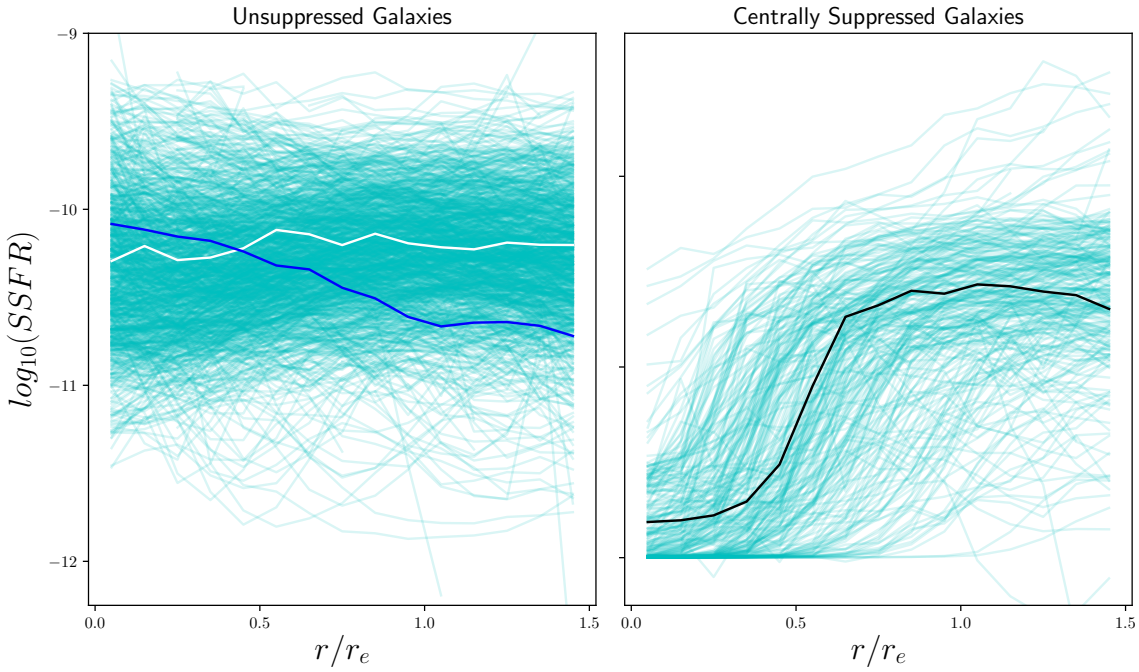

Fig. 4.8 The radial SSFR profiles of galaxies in our sample which are centrally suppressed (left) and unsuppressed (right), as defined using the classification from Figure 4.5. In the two panels, I highlight 'typical' profiles which fit the Centrally Suppressed (black), Unsuppressed (white) and Enhanced (blue). definitions.

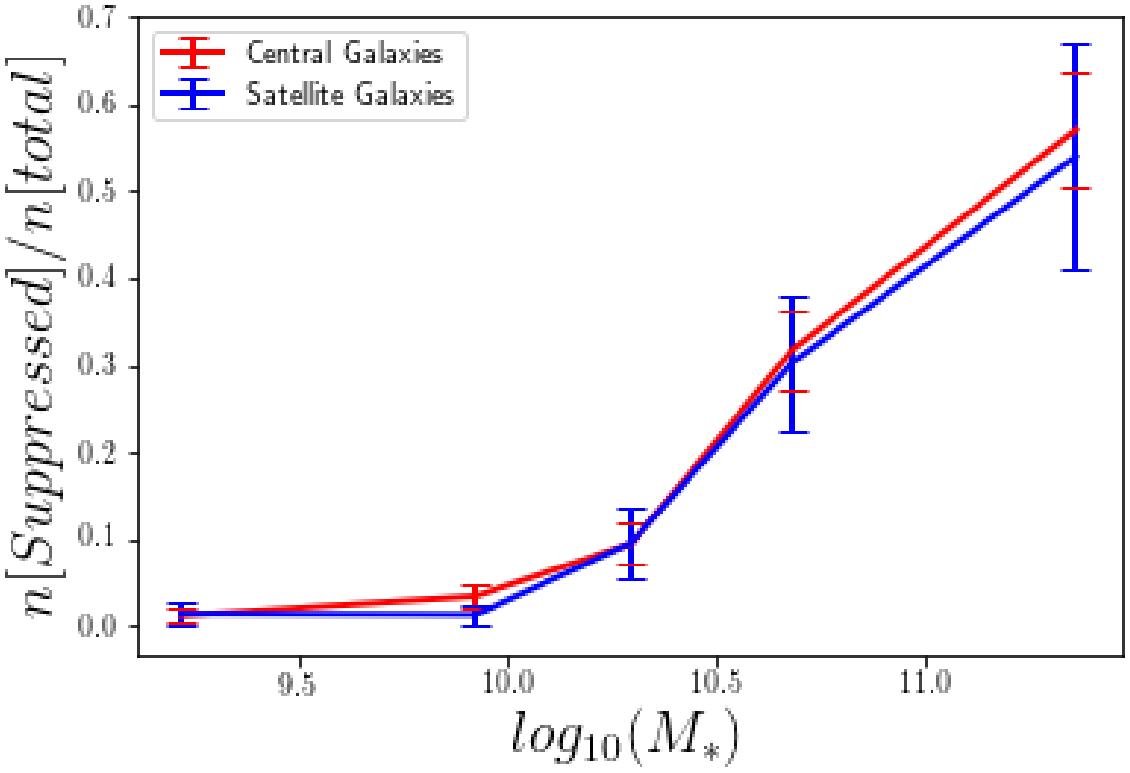

Fig. 4.9 I show the fraction of centrals (red) and satellites (blue) which are centrally suppressed, with respect to Stellar Mass.

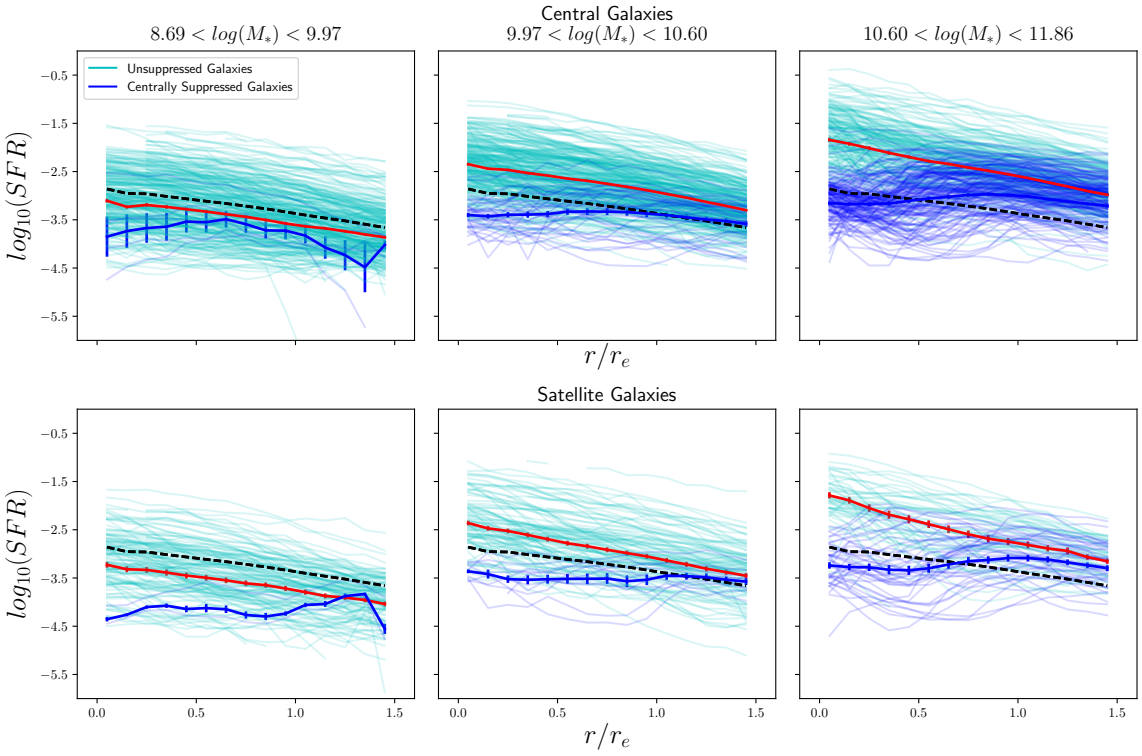

Fig. 4.10 The radial SFR profiles in three bins of stellar mass. I show the individual profiles in cyan and blue, designating unsuppressed and centrally suppressed galaxies, respectively. The mean profile for unsuppressed galaxies is shown with a red line, which the solid black line denotes the mean profile for centrally suppressed galaxies. The dashed black line shows the mean profile of all galaxies in the sample. The top row is the central galaxies and the bottom row is the satellite galaxies. The error bars are calculated from the scatter in 1000 bootstrap resamplings.

classes of galaxies. By studying the unsuppressed galaxies I can gain a better understanding of the processes which produce the reduction in SSFR at all radii in satellites compared to centrals. Studying the centrally suppressed galaxies I can find if there is a difference in the amount of core suppression which happens in satellites and centrals.

In Figure 4.11 I show the mean profiles of galaxies, split by whether they are centrally suppressed or not. Central galaxies are shown with solid lines and satellites with dashed lines, with the upper set of lines representing the unsuppressed galaxies and the lower lines the suppressed galaxies. I use the same mass binning scheme from Section 4.3.2. Note that I do not include the profiles for low mass centrally suppressed galaxies, as there are too few galaxies in this bin to draw reliable conclusions. Firstly I can see that the centrally suppressed galaxies actually have reduced SSFRs at all radii compared to the unsuppressed galaxies, not just in their cores. This is a crucial point, as it suggests that central suppression leads to external suppression, or at least that if fractional growth is low in the centre of galaxies it will be low in the outskirts. The low SSFRs in the outskirts of suppressed galaxies is not a selection effect either, as the ratio I use to divide the sample would certainly allow galaxies with SSFRs 2 or 3 dex higher in their disks, comparable to unsuppressed disks.

For the unsuppressed galaxies the low mass profiles are very similar to the profiles in the low mass bin for the full sample, due to there being very few centrally suppressed galaxies in this bin. The low mass satellites have a very flat profile, which has lower SSFR at all radii than the centrals in this bin. The central profile is also flat. In the medium mass bin the satellites appear to experience suppression at all radii compared to the centrals. In the high mass bin the satellites have higher SSFRs in their cores than the centrals, but beyond $\sim 0.5r_e$ their SSFR is consistently lower. This could be due to high mass satellites that have had some star formation driven into their centres by tidal harassment or some other instability, as it appears that the satellite profile curves upwards, while the central profile curves down.

I see that for the centrally suppressed galaxies, in both the medium and high mass bin the profiles beyond $1.0r_e$ are quite shallow and rising, and that there is a sharp drop in SSFR towards the centres of the galaxies. The drop appears to happen at a larger radii for the satellite galaxies than the centrals, however both the centrals and satellites approach similar minimum SSFRs, due to the lower limit imposed by our SSFR-D_n4000 model. I once again see that there is a suppression of satellite star formation at all radii in the medium and high mass bins.

In Figure 4.12 I show the fractional differences between the central and satellite galaxies in bins of mass, split by centrally suppressed and unsuppressed. The unsuppressed galaxies show a roughly uniform decrease in SSFR for satellites compared to centrals, except in the cores of high mass galaxies. For the centrally suppressed galaxies I also see a suppression at

all radii in the satellites, though the SSFRs in the cores of the galaxies are approaching parity due to the lower limits of our SSFR-D_n4000 model. This uniform suppression of satellites could be a signature of strangulation (Elmegreen et al., 2002; van den Bergh, 1991), which I discuss further in Section 4.4.4.

Considering the effect that galaxies with enhanced central star formation may have on these results, I devise an additional classification for those galaxies. Profiles where the SSFR in the central radial bin is 0.5 dex higher than any other radial bin are classified as centrally enhanced. I find that 183 galaxies are centrally enhanced using this classification, they are predominantly star forming galaxies, rather than composite. The fraction of enhanced galaxies decreases with stellar mass and satellites are more likely to be enhanced than centrals. At low mass $18 \pm 8\%$ of satellites are enhanced, compared to $14 \pm 5\%$ of centrals. At high mass I find that $14 \pm 3\%$ of satellites have enhancement and only $6 \pm 1\%$ of centrals do. I provide the fractional differences between central and satellite profiles of centrally suppressed and unsuppressed galaxies, with those that meet the additional enhanced criteria removed in Figure 4.13. The fractional differences for suppressed galaxies remain the same, however for the unsuppressed galaxies I see that the difference in the medium mass bin flattens and that the difference in the central radius bin of the high mass galaxies falls to zero. The exact causes of this enhancement is not clear, neither is the increased fraction in satellite galaxies. I briefly discuss this in Section 4.4.4, but would like to note that this will be the subject of further study in a future work.

4.4.3 AGN Feedback

Given that the central suppression of galaxies is highly dependent on stellar mass, one explanation may be that it is due to the activity of the central AGN, or caused by increased bulge growth in these galaxies. I address AGN feedback in this section and discuss morphological quenching in Section 4.4.5.

It is argued that radio mode AGN feedback (Bluck et al., 2014; Fabian, 2012; Wake et al., 2012) would provide a viable slow-quenching process. Such feedback would be correlated with stellar mass, as higher mass galaxies would have higher mass central black holes and be more likely to produce radio-mode episodes (Häring and Rix, 2004; Marconi and Hunt, 2003; McConnell and Ma, 2013).

To investigate the role of AGN in core quenching, I revisit the sample definition and choose to include galaxies which have a BPT classification in their integrated flux as AGN/LINER or low SNR AGN, but which have a total $log_{10}(SSFR) > 10^{-11.5}$. In Figure 4.14 I show the fraction of galaxies which are centrally quenched in three bins of stellar mass for Star Forming, Composite and AGN galaxies. At all masses, the AGN galaxies are

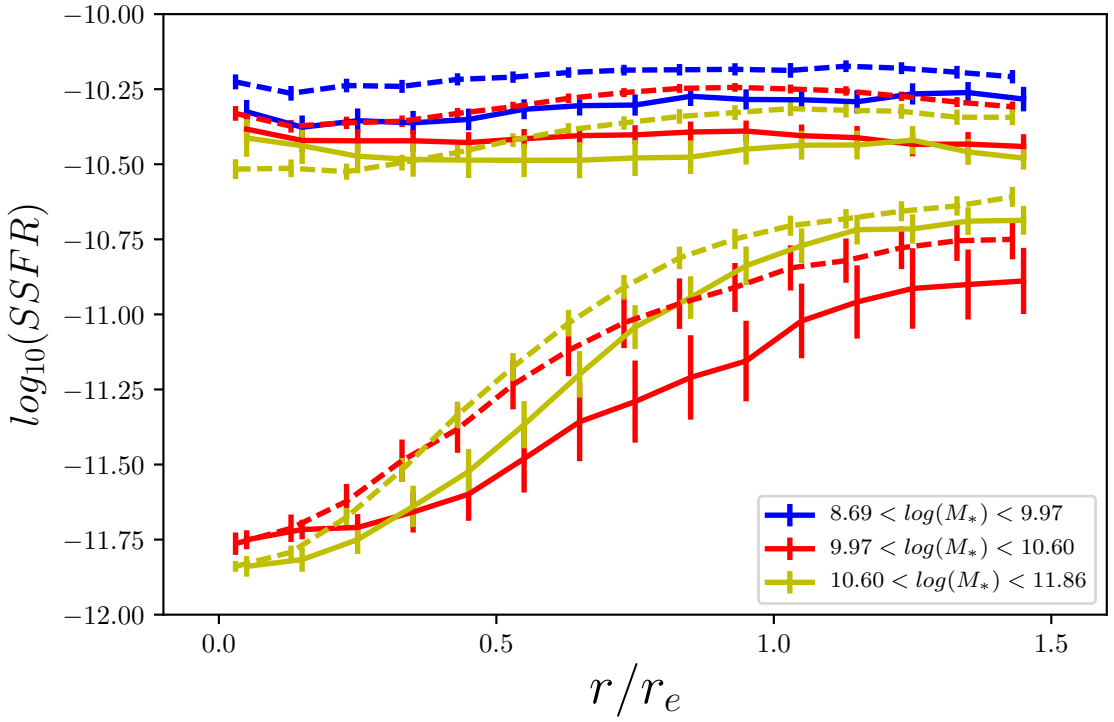

Fig. 4.11 The mean SSFR profiles of centrally suppressed and unsuppressed galaxies. The upper set of lines are the unsuppressed galaxies, while the lower lines are the suppressed galaxies. Satellite profiles use solid lines and centrals use dashing lines. I do not include the low mass bin for the suppressed galaxies. I used the same three stellar mass bins as in Figure 4.3.

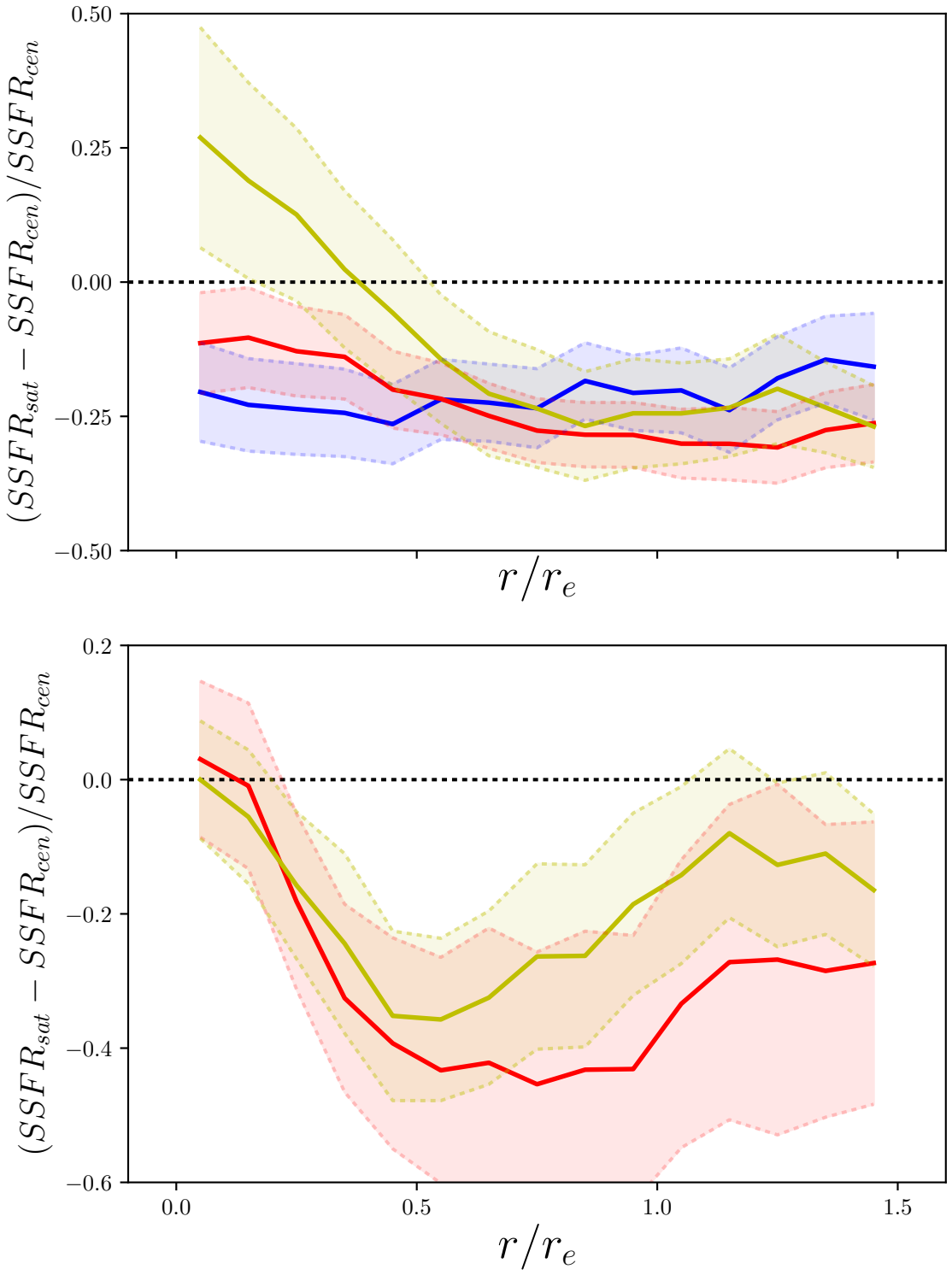

Fig. 4.12 (Top) The fractional differences between central and satellite galaxies in unsuppressed galaxies. I show the $1-\sigma$ scatter from 1000 bootstrap resamplings as the shaded area. (Bottom) The fractional differences between central and satellite galaxies in centrally suppressed galaxies. I show the $1-\sigma$ scatter from 1000 bootstrap resamplings as the shaded area.

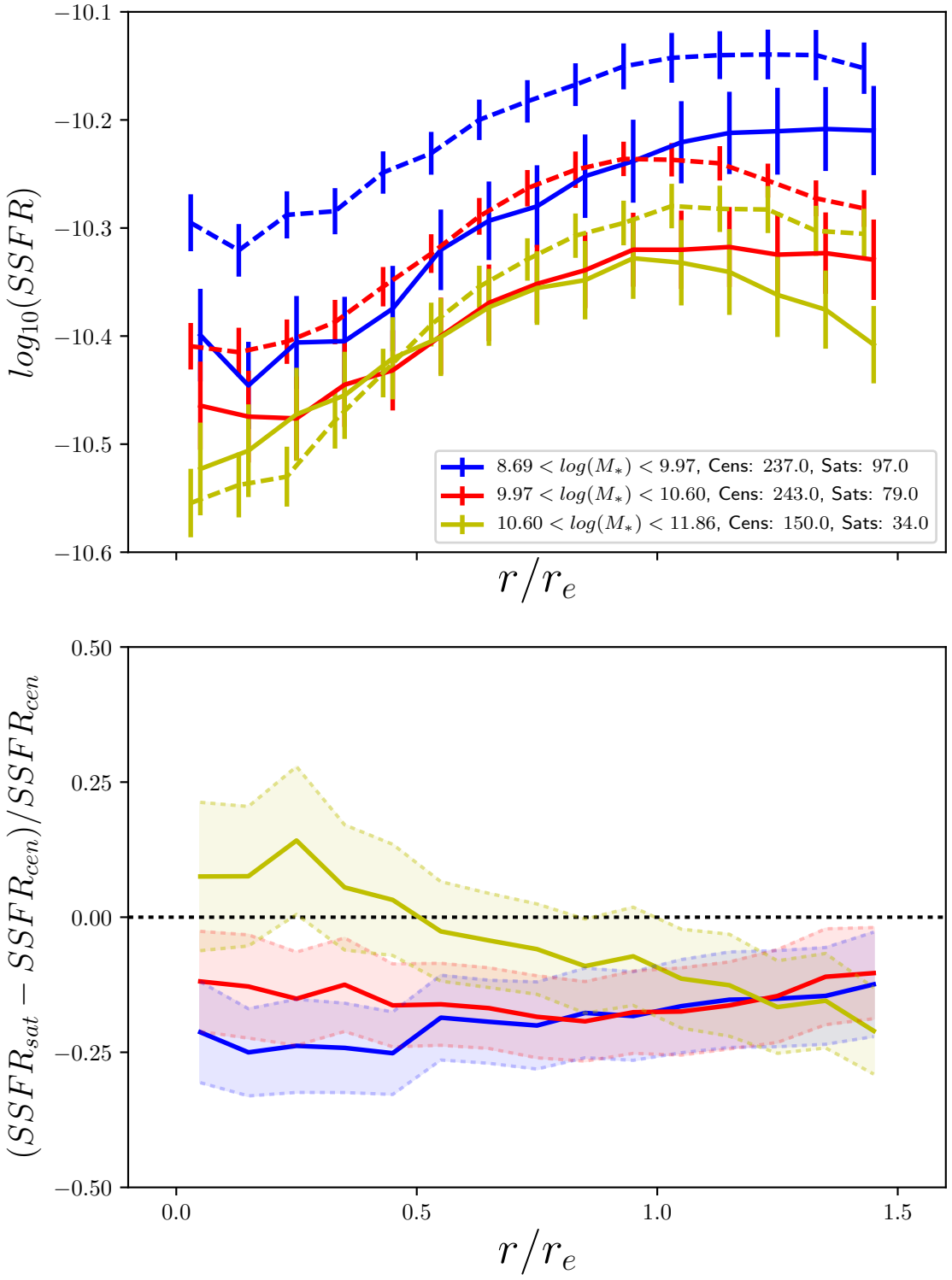

Fig. 4.13 (Top) The mean profiles for unsuppressed galaxies in bins of stellar mass, with the enhanced galaxy population removed. The error bars are calculated from the scatter in 1000 bootstrap resamplings and the stellar mass bins are the same as those from 4.3. Note the different scale in the y-axis compared to Figure 4.11 (Bottom) The fractional differences between central and satellite galaxies in unsuppressed galaxies with centrally enhanced galaxies removed. I show the $1-\sigma$ scatter from 1000 bootstrap resamplings as the shaded area.

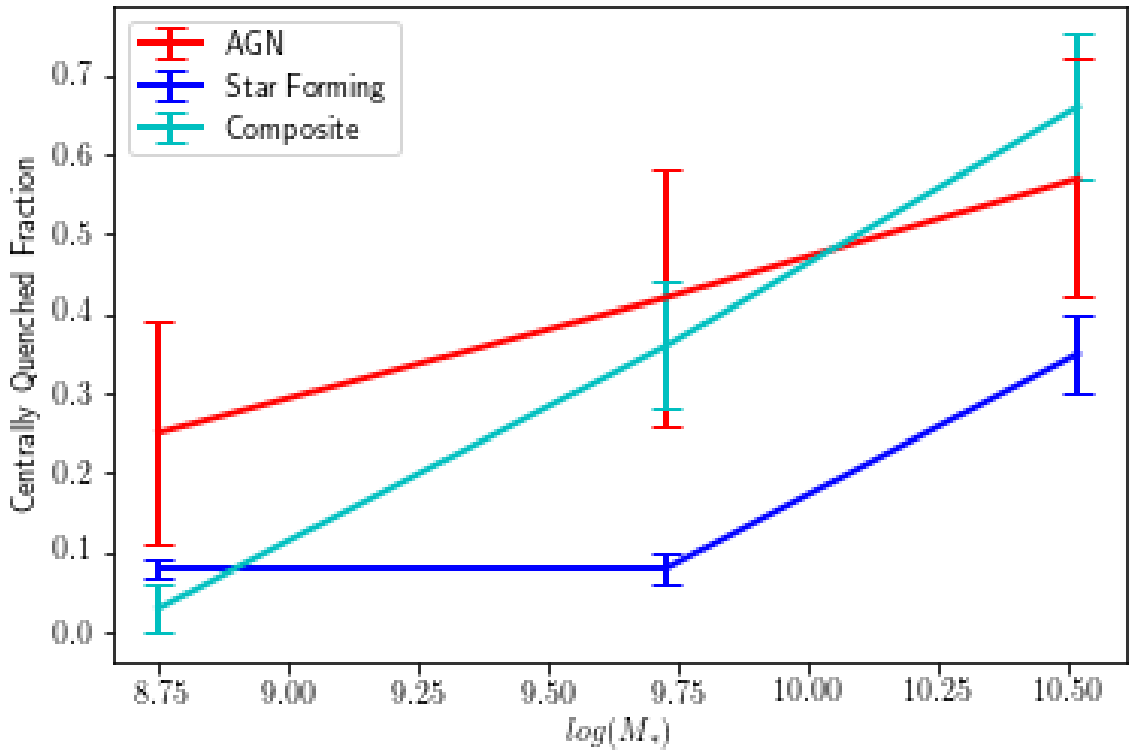

Fig. 4.14 The fraction of galaxies which are centrally quenched, for galaxies which have an integrated BPT classification of AGN, Star Forming and Composite, in three bins of Stellar Mass.

more likely to be centrally suppressed, and in the medium and high mass bins the composites are more likely to be quenched than star forming galaxies as well.

However, it should be noted that the BPT diagram does not find a significant fraction of low-excitation radio-loud AGN. These galaxies may be miss-classified as composite or star forming galaxies, or may fall into our lineless definition and not be included in this analysis. The star forming galaxies which exhibit core quenching may in fact host radio loud AGN, but without an alternative method of classifying these galaxies this cannot be checked.

4.4.4 Environmental Quenching

Throughout this Chapter I have compared the profiles of central and satellite galaxies, as they largely reside in different kinds of environments. At fixed mass, central galaxies are found in lower density environments than satellites, since a satellite of equal mass would require a more massive central to be present in the group. Satellites however are found in denser environments and are acted upon by a number of processes which can shut down star formation, such as ram pressure stripping, tidal stripping and strangulation (Abadi et al.,

1999; Balogh et al., 2000; Bialas et al., 2015; Cortese et al., 2011; Font et al., 2008; Gunn and Gott, 1972; Kauffmann et al., 2004; Koopmann and Kenney, 2004b; Lewis et al., 2002; McCarthy et al., 2008b; Peng et al., 2015; van den Bosch et al., 2008a).

Ram pressure stripping generally causes a decrease in star formation rates at large radii and a central concentration of star formation (Cortese et al., 2011; Koopmann and Kenney, 2004b). While I do see more satellites with an enhanced central SSFR compared to centrals, I do not see and increase in suppression with radii as I might expect if ram pressure stripping were important. It could be that, due to the cuts I made to effective radii in our sample, I have excluded the regions of satellites which would be most affected by ram pressure stripping. The increased fraction of centrally enhanced galaxies in the satellite population could be a signal of tidal stripping and disruption, which has been shown to drive gas into the centres of galaxies and cause an increase in circumnuclear star formation (Hernquist, 1989; Moreno et al., 2015).

Strangulation has been shown to be an effective method of quenching galaxies and it is theorised to produce a uniform suppression across a galaxy's radius, as opposed to concentrating star formation in the centre or outskirts (Elmegreen et al., 2002; Larson et al., 1980; McCarthy et al., 2008b; Peng et al., 2015; van den Bergh, 1991). I do see a roughly uniform suppression of star formation in satellite galaxies at all radii for low and medium mass galaxies, especially when I remove the effect of centrally suppressed and enhanced galaxies from the sample, indicating that strangulation may be the dominant satellite quenching mechanism. van den Bosch et al. (2008a) argued that strangulation should be the main process by which satellites quench, as opposed to ram pressure stripping or harassment which occur mainly at high dark matter halo mass. Satellites were found to be redder and more concentrated than centrals, but these differences were independent of halo mass. Similar results were found using data from the EAGLE cosmological simulations (Schaye et al., 2015) by van de Voort et al. (2017), who studied the gas accretion rates of simulated galaxies and found that satellites in dense environments are less able to replenish their cold gas than centrals, leading to a shut down of star formation. Finally, Peng et al. (2015) studied stellar metallicities and ages from local galaxies and concluded that strangulation, with an average time-scale of 4 billion years, is the dominant mechanism behind galaxy quenching.

4.4.5 Morphological Quenching

Morphological quenching occurs when a dominant spheroidal component is formed by mergers and other processes, which causes the gas within a galaxy to stabilise against fragmentation and star formation (Martig et al., 2009). The build up of the bulge then may be what is causing the centrally suppressed galaxies, and may also explain why they have

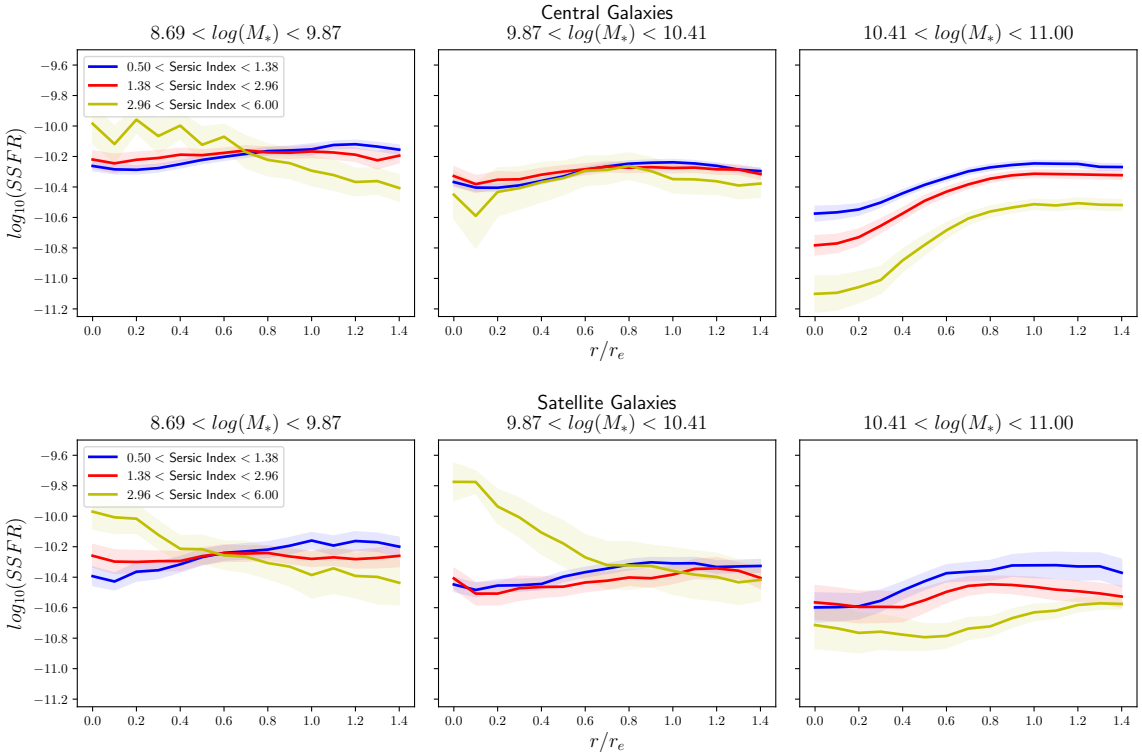

Fig. 4.15 The radial SSFR profiles for central galaxies (top) and satellite galaxies (bottom), in bins of stellar mass and Sérsic Index. In each bin the blue line represents low Sérsic index galaxies, red is medium and yellow is high Sérsic index. The shaded areas represent in the $1-\sigma$ scatter from the mean in 1000 bootstrap resamplings.

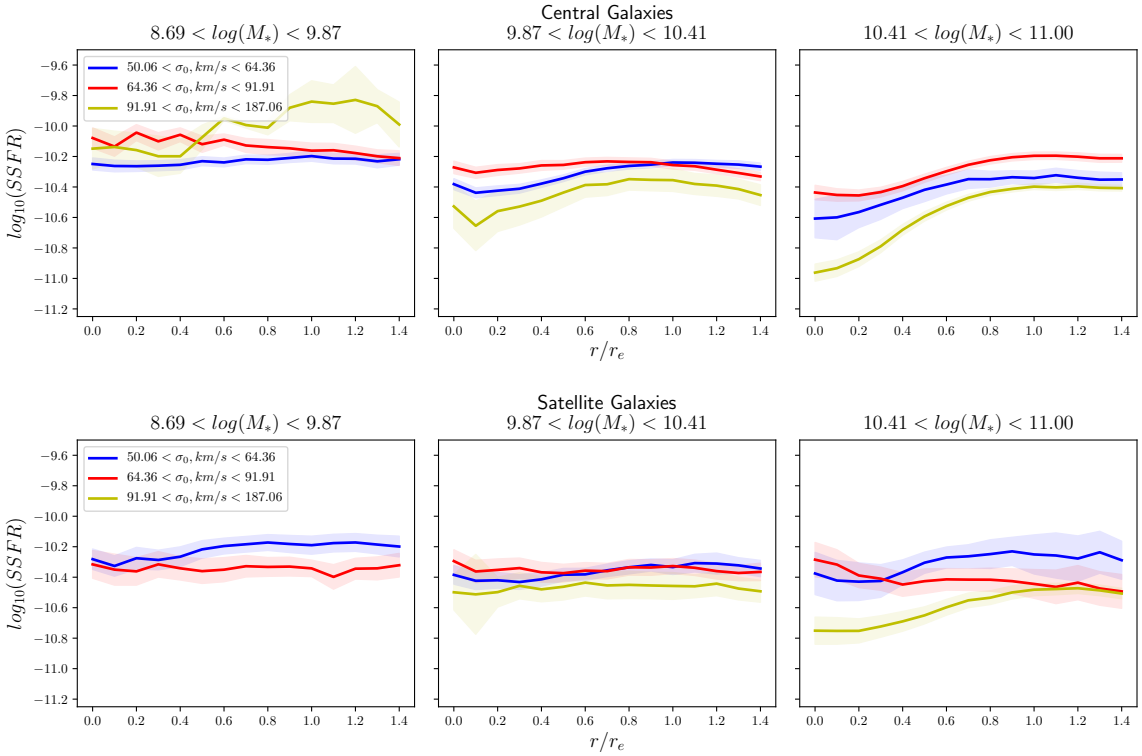

Fig. 4.16 The radial SSFR profiles for central galaxies (top) and satellite galaxies (bottom), in bins of stellar mass and σ_0. In each bin the blue line represents low σ_0 galaxies, red is medium and yellow is high σ_0. The shaded areas represent in the $1-\sigma$ scatter from the mean in 1000 bootstrap resamplings.

lower star formation rates in their outer regions than non-centrally suppressed galaxies. I now investigate the role of morphology in the suppression of star formation by studying the profiles of galaxies at fixed mass and *r*-band Sérsic index. If bulge like morphologies do in fact play a role in quenching I would expect to see lower SSFRs at high Sérsic indices.

In Figure 4.15 I show the mean profiles for central and satellite galaxies in bins of stellar mass and Sérsic index. The Sérsic index cuts are such that the lowest bin is mostly pure late type disk galaxies, the medium bin is likely made up of disks with some bulges and bars, while the high Sérsic index bin is likely dominated by early-type galaxies with large bulges or elliptical morphologies. The shaded areas around the lines represent the $1-\sigma$ scatter from the mean in 1000 bootstrap resamplings.

For the central galaxies in the low and medium mass bins, the low and medium Sérsic index profiles are very similar, as is the the high Sérsic profile in the medium mass bin. However at low masses the high Sérsic index profile is quite different, with high SSFR in the centre which falls off towards the edge of the galaxy, as opposed to the flat profiles which appear to be the standard across our sample. In the high mass bin the story is different. While all three profiles are centrally suppressed, I see that the Sérsic index strongly affects the normalisation of the profile. Higher Sérsic index galaxies, i.e. those that are more dominated by bulge-like morphologies, have lower SSFRs across their entire profiles.

For the satellite galaxies, many of the properties are the same as the centrals. The low and medium Sérsic index profiles agree well at low and medium masses, but the medium Sérsic index galaxies have slightly lower SSFRs at high mass in their disks. The high Sérsic index satellites have very different profiles compared to the centrals however. I see that the cores of these satellite galaxies are enhanced compared to the general population in both the low and medium mass bins. There also appears to be some enhancement compared to high Sérsic index centrals in the high mass bin, but not to the same extent as the other profiles. This enhancement may be due to gas being driven into their centres of galaxies by tidal interactions, however it is unclear why this would mainly affect galaxies with high Sérsic indices.

I also investigate the profiles in bins of stellar mass and σ_0 simultaneously. I show the mean profiles for central and satellites galaxies in Figure 4.16, with galaxies split by mass in the columns and into three bins of σ_0 in each panel, I omit the low mass-high σ_0 profile, as there are < 3 galaxies in this bin. Velocity dispersion has previously been found to be a better predictor of galaxy colour, bulge mass, bar strength and whether a galaxy is passive or not (Das et al., 2008; Spindler and Wake, 2017; Teimoorinia et al., 2016; Wake et al., 2012). Once again I see that as stellar mass increases the galaxies become more centrally suppressed, in addition I see that in the high mass bins the galaxies with the highest σ_0

exhibit the strongest suppression of star formation. This suppression occurs both in the cores of these galaxies, but also in the SSFR at all radii. This is particularly strong for central galaxies, where the high mass galaxies with low or medium dispersions are not significantly suppressed compared to the full sample mean and the high dispersion galaxies are very suppressed. One possible explanation for enhancement of high Sérsic satellites is that it is a selection effect. If these galaxies have very high star formation rates in their centres the light could wash out the disk when the single component fit is attempted, making them seem more bulge dominated.

Combining the results from Figures 4.15 and 4.16, I see a strong correlation between the central suppression and bulge dominated morphologies at high and intermediate masses. This suggests that in more bulge like morphologies the galaxies are more likely to be centrally suppressed and that this suppression extends beyond the bulge into the disk. This would appear to agree with the premise of morphological quenching that the large bulge stabilises the gas and prevents star formation. As I do not see an enhancement in the profiles of high σ_0 satellites, which would be expected if the enhanced galaxies did have very large bulges, this suggests that the Sérsic index may in fact be skewed higher due to the increased central star formation.

4.5 Comparison with previous works

Quenching processes have been widely studied in astronomy, in particular the role of the environments galaxies live in. I will compare our work with some previous studies and draw some conclusions as to what quenching processes may be driving our results.

Belfiore et al. (2017b) used the MaNGA survey to reveal what they refer to as extended LIER (eLIER) and central LIER (cLIER) galaxies. By studying the emission line properties, they showed that LINER emission is related to old stellar populations, and not necessarily AGN. These galaxy regions do not exhibit star formation, but still emit emission line radiation. cLIER galaxies in particular appear to be late-type spirals which populate the green valley and may be in the process of quenching inside-out. These galaxies are likely related to our centrally suppressed galaxies, which I find to be largely Composite and AGN/LI(N)ER in their BPT classification.

In Belfiore et al. (2017a) I investigated the profiles of specific star formation rate and the equivalent width of H_α of blue cloud and green valley galaxies, with particular emphasis on the properties of cLIER galaxies. I found consistent patterns of central suppression in blue cloud and green valley galaxies, as I have in this work. In addition in Belfiore et al. (submitted) I find that green valley galaxies and cLIER galaxies not only show suppression in

their central regions, but are suppressed at all radii, and that this effect is stronger for cLIER galaxies.

The uniform suppression of satellite star formation explains why in Goddard et al. (2017a) and Zheng et al. (2017) there is no environmental dependence on the gradients of stellar age in MaNGA galaxies, irrespective of whether environment is measured as an environmental density or central/satellite split. In addition, earlier work from Thomas et al. (2010) showed no dependence on environment for the stellar population properties of early type galaxies, finding that their evolution was driven purely by self-regulation processes related to stellar mass, which is echoed in our findings that the central suppression is independent of environment.

Using the SAMI survey, Schaefer et al. (2017) (S17) studied the H_α surface density gradients of 201 star forming galaxies with respect to stellar mass and environmental density. They found that the gradients of H_α surface density steepen as environmental density increases (by a factor of ~ 0.6 dex in the most massive galaxies).

I provide a direct comparison to S17 in Figure 4.17, in which I have plotted the profiles of Star Formation Surface Density, Σ_{SFR}, in bins of stellar mass and nearest neighbour environmental density for star forming galaxies. I use the environmental densities from Baldry et al. (2006), which are described in Section 4.2.2. The environment densities in Baldry et al. (2006) were calculated using SDSS galaxies, while S17 uses data from the Galaxies And Mass Assembly (GAMA, Driver et al., 2011) survey. The GAMA survey is almost two magnitudes deeper than the SDSS main sample used in Baldry et al. (2006), meaning that the local density measurements used here at not exactly equivalent. To reconcile this, I have not used the same bins in $\log_{10}(\Sigma_5)$ as S17, but instead I have constructed our bins to contain the same proportion of galaxies in each environment bin as S17. The stellar mass bins were chosen to match those in S17.

I provide the properties of a linear fit to the mean Σ_{SFR} profiles and the number of galaxies in each bin in the top corner of each panel, with errors calculated from 1000 bootstrap resamplings. I do see a steepening of the gradients with increasing $\log_{10}(\Sigma_5)$, however this steepening is only significant in the medium mass bin as the gradients in the high and low mass bins are all within $1-2\sigma$ of each other. I also do not see much central enhancement except in the highest mass and density bin.

Although I have attempted to match the analysis of Schaefer et al. (2017) there are a number of differences that may explain our discrepant findings. Of particular importance is the fact that S17 only include spaxels with detectable H_α emission, whereas I include all spaxels, making use of D_n4000 where H_α is unavailable. The exclusion of such spaxels in S17 will have the tendency to bias the Σ_{SFR} high since these will often by spaxels with low S/N H_α as a result of their low SFRs. This issue most prominently affects the profiles in

the central regions of higher mass galaxies where the SFR may be lower if there is a bulge present, our centrally suppressed galaxies. If I also exclude such spaxels then I do indeed see much more central enhancement, typically at high mass and density, which does increase the gradients, although the trend with environment remains present only in the intermediate mass bin. Another difference is that S17 do not take into account possible contamination from AGN/LI(N)ER emission in the individual spaxels in their galaxies (once they have entirely excluded AGN from their sample), which I and Belfiore et al. (2016) have shown is present. Such contamination is again more likely to be present in the central regions of galaxies with a bulge component. Finally as I have already mentioned, I are not using the same environmental definition as S17. The higher galaxy density in GAMA means that the fifth nearest neighbour density used by S17 will be probing smaller scales than the measure I have used. It is possible that at these smaller scales a relationship with local overdensity becomes more apparent.

Crucially, it is important to note that the environmental signal of the central/satellite split is much stronger and more significant than the dependence on local environmental overdensity. The relationships between environmental densities and internal properties such as stellar mass and star formation are complex, and two galaxies with similar densities may actually occupy very different conditions and be acted upon by different processes owing to their different locations in the dark matter halos. For example, as I see in Figure 4.2 a satellite and a central occupying the same environmental density can have dramatically different star formation rates, particularly at high densities where the centrals are guaranteed to be very high mass galaxies, whereas the satellites can be very low mass and have very low levels of star formation.

In addition our results show that the profiles of star formation are not linear, with many galaxies exhibiting two or more components in their profiles. In particular our centrally suppressed galaxies would be incredibly poorly fit by a linear profile. S17 argue that star formation becomes more centrally concentrated at higher environment densities

4.6 Conclusions

Using IFU data from the SDSSIV-MaNGA survey I have studied the spatial distribution of star formation 1494 galaxies in the local universe. I have used a two source model to calculate star formation rates using H_α and D_n4000, in order to account for emission line contamination in galaxies from AGN and LI(N)ER like sources. The galaxies in our sample were chosen based on their classification in the BPT diagram, using Star Forming and Composite galaxies for the bulk of the work, and introducing a small number of AGN/LI(N)ER galaxies, which

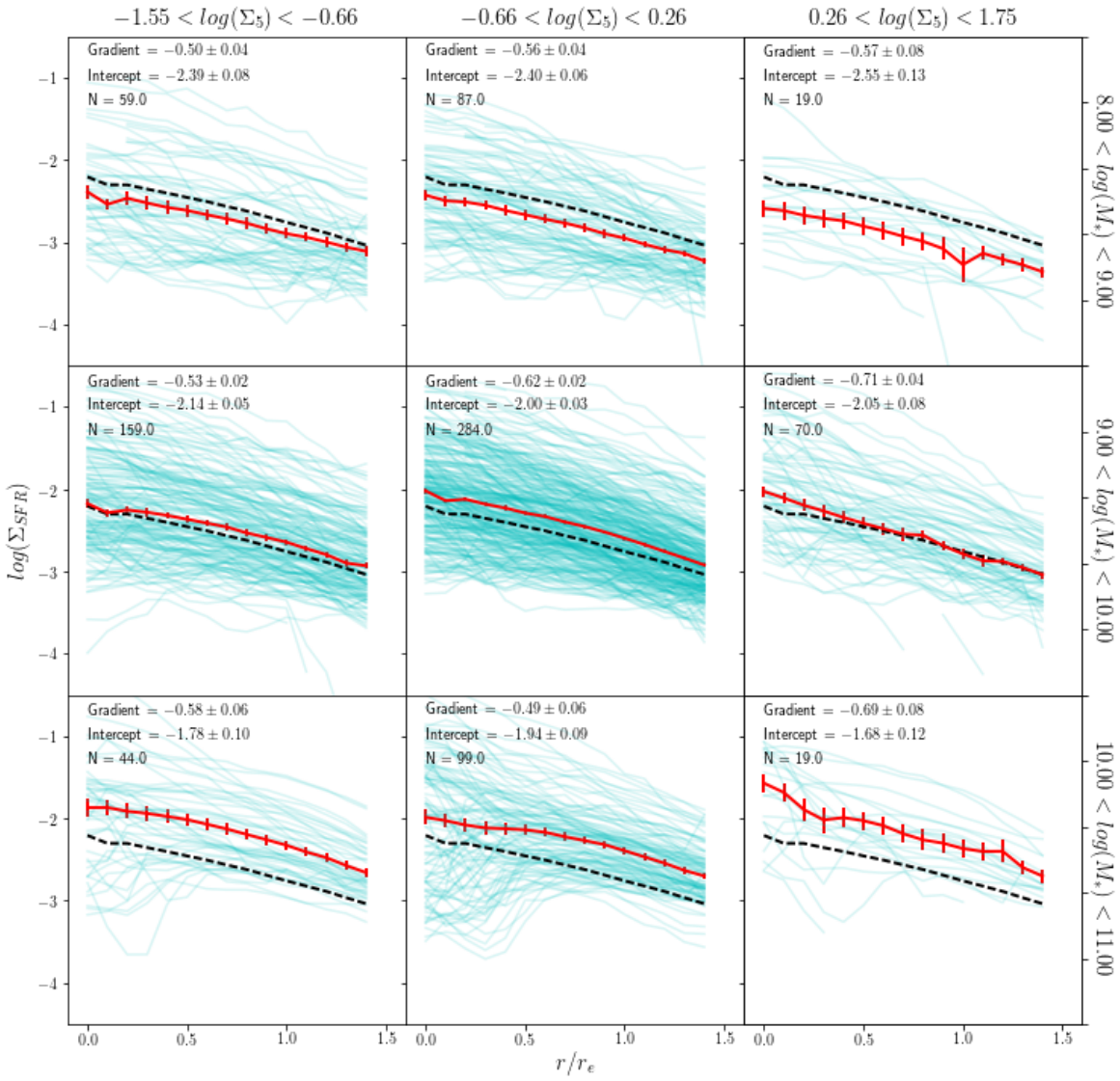

Fig. 4.17 I show the star formation rate surface density in three bins of stellar mass (rows) and three bins of environment density (columns). The cyan lines are the mean radial profiles of the individual galaxies, the solid red line represents the mean profile of all galaxies in the bin and the black dashed line is the mean profile of all galaxies in the sample. I show the properties of a linear fit to the mean profile in the top left corner of each panel.

passed our total specific star formation rate cut, to study the role of AGN in inside-out quenching.

I have shown that our star formation rate model is internally consistent, by comparing the total star formation rates measured using H_α and D_n4000. I have also shown that the total star formation rates agreed well with those calculated for the same galaxies in the MPA/JHU catalog, which use a Bayesian SED fitting method based on H_α and D_n4000 from single fibre spectroscopy, aperture corrected to global values using the broadband photometry from SDSS.

Using the radial profiles of specific star formation rate the spatial distribution of star formation was studied. I binned galaxies based on their internal and external properties and compared the mean profiles in these bins to determine the effect each property had on SSFR. Our main results are as follows:

- I found that the SSFR of galaxies decreases with mass and σ_0. This decrease occurs at both the global scale with total SSFRs, and at the local scale with higher mass and σ_0 galaxies having lower SSFR at all radii compared to galaxies with low mass and σ_0.

- I revealed the existence of two groups of galaxies, which I have named 'Centrally Suppressed' and 'Unsuppressed'. The unsuppressed galaxies have flat profiles in SSFR and can be found at all stellar masses and velocity dispersions. I have defined the centrally suppressed galaxies as having a SSFR in their disk at least 10 times higher than in their core. There is a strong relationship between stellar mass, σ_0 and whether a galaxy is centrally suppressed or not, with high mass and high σ_0 galaxies being much more likely to have suppressed SSFR in their cores.

- The profiles of the two classes of galaxies showed that the centrally suppressed galaxies have suppressed SSFR at all radii, compared to the unsuppressed galaxies. This suggests that central suppression correlates with the suppression of star formation in the outskirts of the galaxy, or at least that low fractional growth in the centre of galaxies means low growth in the outskirts. I find that the mean SSFRs of centrally suppressed galaxies within $0.5r_e$ of the galaxy centre are ~ 1.25 dex lower than unsuppressed galaxies, and ~ 0.5 dex lower beyond $1.0r_e$.

- I explored the possibility that suppression of star formation is due to AGN feedback by investigating the fractions of galaxies that were centrally suppressed for star forming galaxies, composites and AGN/LI(N)ER hosts, as characterised by the BPT diagram. I found that at all masses the AGN/LI(N)ER galaxies were more likely to have centrally suppressed SSFRs than star forming galaxies, and that composites were more likely to be suppressed at medium and high masses.

- Another possibility is that the suppression is caused by morphological quenching, which I study using the profiles binned by stellar mass and Sérsic index or σ_0 simultaneously. These profiles show that both the central suppression and suppression of the disk is strongly correlated to properties which imply large bulges, with high mass-high Sérsic and high mass-high dispersion galaxies predominantly being centrally suppressed. This result seems to suggest that morphological quenching, where a large bulge component stabilises the gas disk and prevents star formation, may be playing a major role in the lowered SSFRs in the cores and disks of the centrally suppressed galaxies.

- Throughout this Chapter I have compared central and satellite galaxies in order to determine what role environment plays in regulating star formation. I found that central and satellite galaxies are equally likely to have suppressed star formation in their cores, implying that there is no environmental component in that process. However, I did find that satellites do have suppressed SSFRs compared to central galaxies at all radii. This lowered star formation in satellite galaxies is most likely caused by strangulation, which has previously been found to be a likely candidate for satellite quenching. I do not see any suppression in the outskirts of satellites that would be related to ram pressure stripping. I do find that there are a population of galaxies with enhanced star formation in their centres which are more likely to be satellites than centrals, this may be due to tidal harassment driving gas into the centres of satellites, however this is currently unclear and will be the subject of a future study.

- Finally, I compared our work to that of Schaefer et al. (2017), who found a steepening of the SFR surface density gradients with 5-th nearest neighbour environment density. I too see a small amount steepening, however I find that it is not statistically significant.

Our results in this work show the power of IFU surveys in analysing the spatial properties of galaxies for studying the mechanisms behind the shut down of star formation. I have found evidence of inside-out quenching driven associated with AGN/LI(N)ER like emission, implying suppression of star formation via AGN feedback. In addition I have observed a uniform suppression of star formation in satellite galaxies, indicative of strangulation of cool gas supplies.

5

The Role of Bars in Suppressing and Enhancing Star Formation

"All this happened, more or less."

– Kurt Vonnegut, *Slaughterhouse Five, 1969*

5.1 Introduction

Perhaps one of the most prominent structures that form in galaxies is the bar. Bars are an orbital density wave pattern where stars in the galaxy centres develop unstable orbits, moving from circular orbits to more elongated elliptical orbits (Athanassoula et al., 2013; Athanassoula and Misiriotis, 2002; Kormendy, 2013). These structures have been the subject of much study, going back to their identification by Hubble (1926) as a distinct morphological type of galaxy. It is currently believed that up 30% of galaxies contain bars, but this fraction can rise to over 70% in studies which included infra-red data and weak bars (Eskridge and Frogel, 1999; Eskridge et al., 2000; Masters et al., 2010; Sheth et al., 2008).

The bar is important to galaxy evolution because of its ability to transfer angular momentum between different components of the galaxy. For example, they have been shown to be able to efficiently move gas and stellar material from the galaxy disk into the bulge (Bournaud et al., 2005; Friedli and Martinet, 1993; Knapen et al., 2002; Kormendy, 2013; Masters et al., 2011). Crucially, this transfer of material could lead to the build up of a pseudobulge, either through sparking star formation, or the deposition of stellar material into the centre of the galaxy (Athanassoula et al., 2013; Bournaud et al., 2005; Kormendy, 2013). While classical bulges are thought to be constructed through violent processes, such as major mergers, pseudobulges are instead built up through slow secular processes, and take on boxy

or peanut shapes, as opposed to rounder spherical bulges. Bars could also power the Active Galactic Nucleus (AGN) of a galaxy, again through the funnelling of gas into the galaxy core (Galloway et al., 2015; Lee et al., 2012b). However, little evidence has been found linking bar fraction to the presence of an AGN.

The formation of a bar has long been a subject of study in the simulations of galaxy evolution. Early simulations found that bars formed very easily in disk galaxies, and it was believed that unless some global stabilisation was present, all disk galaxies would eventually form a bar instability (Ostriker and Peebles, 1973; Toomre, 1977, 1981). Ostriker and Peebles (1973) showed that a large dark halo could act as a stabiliser, showing that disk galaxies within a dark halo are less likely to form bars, but form quickly in systems where the disk component is dominant.

The picture is of course more complicated than that, and there are many competing factors in the formation of bars. Considerable work has been done by Athanassoula et al. (2013), who show that gas fraction plays a dominant role in the formation of a bar. Gasless disks form bars quicker than gas-rich systems, and ultimately grow stronger and more prominent bars. Athanassoula et al. (2013) also show that the structure of the dark matter halo plays a role in bar formation, where triaxial haloes drive the formation of a bar earlier than spherical haloes, but that spherical systems lead to stronger bars after the long secular evolution phase. Bars, once formed, can remain very stable in a galaxy and remain over periods of Gyrs.

Bars have also been long studied in observational astronomy and are now understood to be a vital part in the secular evolution of both late and early-type disk galaxies, with evolutionary links to many galaxy properties. Masters et al. (2011) find that galaxies with bars are much more likely to have redder colours, lower luminosity and more prominent bulges (See also, Elmegreen et al., 2004; Giordano et al., 2010; Nair and Abraham, 2010). Unbarred disks on the other hand tended to be blue, and have very few classical bulges. Further to this, Masters et al. (2012) found that bars are more likely to occur in gas-poor galaxies, which agree with the later results by Athanassoula et al. (2013) mentioned above, and that this trend is still present when stellar mass is accounted for. The presence of a bar in redder galaxies poses the question of the role of a bar in the shut down of star formation in galaxies. Masters et al. (2012) discuss that the bars may be responsible for regulating disk star formation, by preventing the infall of new gas and exchanging angular momentum between the gas in the disk and the stars in the bulge. Cheung et al. (2013) find an anti-correlation between bars and the Specific Star Formation Rate (SSFR) of a galaxy, regardless of the galaxies stellar mass or bulge prominence, which suggests that bars are a very important aspect of secular evolution.

Many recent studies have concerned themselves with the question of how bars influence the ongoing star formation in galaxies. In the broader context of galaxy quenching, bar mechanisms are normally included in 'Secular Quenching', the slow shut down of galaxy star formation due to internal processes. Bars can drive gas into the centre of a galaxy, which results in circumnuclear star bursts which exhaust the cold gas supply, effectively shutting down star formation (Gavazzi et al., 2015; Kruk et al., 2017; Lin et al., 2017; Smethurst et al., 2015). They may also prevent new gas from accreting onto the disk by angular momentum regulation with the galaxy halo (Bournaud and Combes, 2002; Brooks, 2010). In addition, recent observations have been studying a phenomenon known as the 'star formation desert', a region of very low star formation in a galaxy disk which has been swept out by a strong bar (Abdurro'uf and Akiyama, 2017; Hakobyan et al., 2016; James et al., 2009; James and Percival, 2016, 2017).

Interestingly, bars have also been linked to dense group environments. Smethurst et al. (2017) find that there is an increase in bar fraction towards the centre of galaxy groups. Indeed, bars could be formed by the kinds of gravitational instabilities, such as tidal harassment, which are prevalent in the group environments. Skibba et al. (2012) also find a strong correlation between the bar fraction and environment density, disagreeing with previous studies that found that there was no correlation between bars and environment. Skibba et al. (2012) stress that their increased sample size, 20x larger than previous studies (e.g. Aguerri et al., 2009; Giordano et al., 2011; Lee et al., 2012a; Li et al., 2009; Martínez and Muriel, 2011), shows that the environment signal may have been washed out by noise in old research. The question then becomes, have these galaxies quenched due to the action of the bar, or did it form simply as a consequence of the environment? As I showed in Chapter 4, the environment can act to suppress the star formation in the disk of satellite galaxies, which may explain the reddening of some barred galaxy disks.

Kruk et al. (2017) performed a study of galaxies in the Galaxy Zoo 2 sample from the Sloan Digital Sky Survey using bulge-bar-disk decompositions. They found that the disk components of barred galaxies have significantly redder colours than the disks of unbarred galaxies, while the bulges of the two samples have similar colours. They also find evidence that the bar can lead to the build up of significant pseudobulge components and that bars may be responsible for quenching the star formation in galaxy disks.

With the advent of new Integral Field Spectroscopy (IFS) Surveys, more detailed studies of the structure and composition of barred and unbarred galaxies can be made. For example, Lin et al. (2017) study a small sample of barred galaxies in the Calar Alto Legacy Integral Field Area (CALIFA) Survey. They found that galaxies with centrally enhanced star for-

mation are more likely to host bars than to be unbarred. This suggests that the bars are responsible for driving circumnuclear star formation by driving gas into the galaxy bulge.

Given the new data available from the Mapping Nearby Galaxies at APO (MANGA) survey, and the ongoing debate on the role of bar quenching, now is the perfect time to perform a study on how bars affect the spatially resolved star formation properties of galaxies. In this Chapter, I study the SSFR maps produced in Chapter 3, and using morphologies from the citizen science project Galaxy Zoo (Lintott et al., 2008; Willett et al., 2013), investigate the differences in star formation between a sample of barred and unbarred disks. In Section 5.2 I discuss the data products used, including a brief overview of the MaNGA SSFR maps and the Galaxy Zoo 2 morphologies. Section 5.3 describes the results, where I compared the SSFR, D_n4000 and Equivalent Width of H_α profiles at fixed stellar mass. In Section 5.4 I discuss two potential bar mechanisms, the suppression of disk star formation and the enhancement of bulge star formation. Finally, I make concluding remarks in Section 5.5.

5.2 Data

5.2.1 MaNGA Dataproducts

I make use of the same data products in this chapter as in Chapters 3 & 4. To briefly recap, the MaNGA data is from Data Release 14 of the Sloan Digital Sky Survey, which contains IFU observations of 2791 galaxies. The parent sample is selected to have a flat density distribution in stellar mass. I make use of the data products from the Data Analysis Pipeline (DAP, Westfall et al. in prep), which performs fits on the continuum, emission lines, kinematics and spectral indices to the full spectral data cubes produced by the Data Reduction Pipeline (DRP, Law et al., 2016).

I utilise these spatially resolved maps of star formation throughout this chapter, finding radial profiles of specific star formation rate. I bin each map into 10 radial annuli, from $0-1.5r/r_e$, and find the mean specific star formation rate in each bin.

5.2.2 MaNGA-Galaxy Zoo Data

Citizen science, the process of asking for public volunteers to perform many simple tasks, has been used to great success in astronomy. Perhaps the greatest success is the 'Galaxy Zoo' project Lintott et al. (2008), which firmly established the role of citizen science in identifying and classifying galaxy morphologies. While there are many automated methods of measuring galaxy shapes (using computer assisted techniques, machine learning or using galaxy properties as proxies Abraham et al. 1994; Ball et al. 2004; Huertas-Company et al.

2011), image classification is still a task at which humans minds excel. With just a small amount of training and practice, a human inspector can reliably identify physical structures in galaxies, such as bars, bulges and spiral arms. However, there is a drawback in that human beings perform these tasks relatively slowly, compared to computers. Galaxy Zoo addressed this problem by opening up the morphological classification of galaxies to millions of public users online.

The first Galaxy Zoo project (GZ1, Lintott et al., 2008), tasked users with identifying the simple morphological classifications of nearly one million galaxies in SDSS. GZ1 users were asked to classify galaxies from the SDSS main galaxy sample as 'early-type', 'late-type' or 'merger'. The follow-up program to Galaxy Zoo aimed to provide more detailed examinations of the brightest and most massive Sloan galaxies. While dividing galaxies into spirals and ellipticals is perhaps the most fundamental distinction you can make, there are many more important and interesting morphological phenomena.

Galaxy Zoo 2 (GZ2, Willett et al., 2013) bases its morphological classifications on Hubble's Tuning Fork diagram. Galaxies are split into the recognisable early and late type distinctions, but there is also a split for barred and unbarred galaxies. Other prominent features including the presence and strength of a galactic bulge, rings, lens and the number of spiral arms. GZ2 constructed a decision tree, which would lead users through a series of questions to classify each galaxy image they were shown. Each *classification* is the total amount of information for the galaxy. Each step on the tree represents a *task*, which includes a *question* and a fixed number of *responses*. A users input for each task represents a single *vote*.

For the selection of our sample I use the 'debiased vote fractions', which determine the probability that a galaxy has the given morphology. This vote fraction is based on the raw number of votes for and against the particular feture, but also adjsted for both consistency from the voter, and for classification bias. Individual users have their votes weighted in order to reduce the effect of unreliable classifiers. Users that gave less accurate responses, based on the overall result for a particular question, have their answers weighted down. The classification bias is a result of redshift, galaxies at larger distances are smaller and fainter in the cut-out images, and so finer detailed morphologies are more difficult to detect. This is not an effect of evolution, in should be noted, as the sample depth is not high enough to allow for much evolution with redshift.

I use a matched catalog between the 304,122 galaxies in the GZ2 data release, with the MaNGA parent sample of 42,561 galaxies. The results is a table of morphological classifications for 38,944 MaNGA galaxies, of which 2,474 have been observed for DR14 of SDSS.

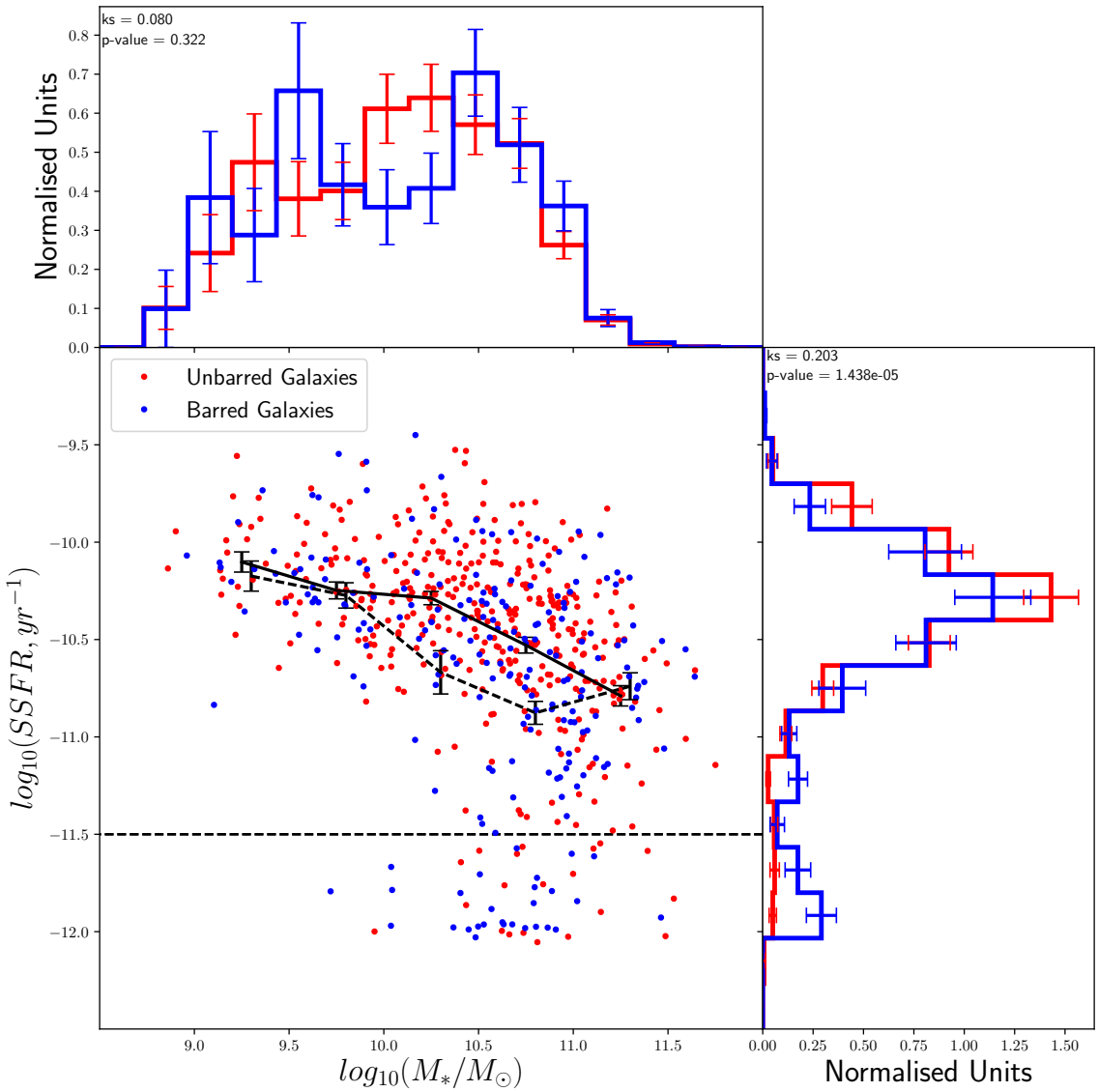

Fig. 5.1 The distribution of stellar mass versus specific star formation rate for barred (blue) and unbarred (red) galaxies, in our main sample. The normalised histograms are show in the upper and rightmost panels. In the main panel I show the mean SSFR at fixed mass for barred and unbarred galaxies with dashed and solid lines, respectively. The specific star formation rate cut of $\log_{10}(SSFR) > -11.5$ is shown using the dotted line.

5.2.3 Sample Selection

The initial sample selection follows on from Chapter 4. I select galaxies from the Primary+ and Secondary samples. IFUs with two or more galaxies are removed, as in Chapter 4, to eliminate the need to mask the individual galaxies in the pair, this removes 153 fibre bundles. I make no initial cuts on BPT-classification. I define a cut in specific star formation rate at $\log_{10}(SSFR) = -11.5$, galaxies above this cut can be safely analysed using their SSFR profiles. I shall also perform further analysis on the sample without the SSFR cut using the profiles of D_n4000 and equivalent width of H_α (EW[H_α]). I remove galaxies with an axis ratio of $b/a > 0.3$.

I use the debiased vote fractions from GZ2 to select two morphological samples, barred and unbarred disks. Throughout this chapter I may refer to these samples as barred and unbarred galaxies or spirals, but this will refer to the same sample definitions laid out in this Section. Willett et al. (2013) lay out the process for selecting morphological samples and I will follow the example for barred galaxies given therein. Our choices for barred galaxies are slightly less conservative than Willett et al. (2013), however it is noted in that paper the subsequent sample would include only the strongest bars, whereas I wish to investigate a larger sample of galaxies with a variety of bar types.

To be selected, each galaxy must have received at least 10 votes in each task, this is to prevent errors from small number statistics. The debiased vote fractions for the likelihood that a galaxy is a disk (p_{disk}), edge on (p_{edge}) and barred (p_{bar}) are used. Both of our samples require that the galaxy to have $p_{disk} > 43\%$ and $p_{edge} < 30\%$, to ensure that I are certainly looking at late-type galaxies and prevent issues in trying to identify bars in edge-on galaxies. The barred sample is chosen to have $p_{bar} > 50\%$, while the unbarred sample has $p_{bar} < 20\%$. I show the details of this sample selection in Table 5.1.

This selected sample includes 215 barred galaxies, and 402 unbarred galaxies. I show their stellar masses and specific star formation rates in Figure 5.1. In the main panel I show the star formation main sequence for barred disks in blue and unbarred disks in red. The dashed and solid lines show the mean SSFR at fixed mass for barred and unbarred galaxies. The barred galaxies have a lower SSFR than unbarred galaxies at fixed mass, at all but the highest masses. This agrees with previous works that have found that bars occupy redder and older galaxies (Masters et al., 2011). In the top panel I show the distribution of stellar masses as histograms, the unbarred galaxies have a peak mass of $log_{10}(M_*) \sim 10.3$, whereas the barred galaxies appear to have a double peaked mass distribution. The results of a two-sample KS test are shown in the top left corner, and show that we cannot reject the hypothesis that these samples are the same. In the right panel, I show the histogram distributions of SSFR. The barred galaxies exhibit a shift towards lower SSFRs, with 18% of

Sample Cut	Sample Size
DR14	2791
Primary+ and Secondary Samples	2445
Galaxy Pairs	2321
Inclination	2246
GZ2 Disks ($p_{disk} > 43\%$)	1300
GZ2 Not Edge On ($p_{edge} < 30\%$)	748
GZ2 Barred ($p_{bar} > 50\%$)	215
GZ2 Unbarred ($p_{bar} < 20\%$)	402

Table 5.1 Sample selection cuts for Chapter 5.

barred galaxies falling below the SSFR cut and compared to only 5% of unbarred galaxies. The KS test for the SSFRs supports the hypothesis that these distributions are different, with a p-value of 1.44×10^{-5} and a KS statistic of 0.203.

5.3 Radial Profiles of Star Formation, D_n4000 and EW[H_α]

5.3.1 Specific Star Formation Rate Profiles

I begin our analysis by following the procedure from Chapter 4; I study the mean SSFR profiles of the galaxy sample in bins of stellar mass, comparing the barred and unbarred galaxies in our sample. I wish to determine if there is any overall difference in the SSFR profiles, i.e. one group of galaxies having lower SSFR at all radii, or if there is a radial trend, i.e. one group of galaxies favouring bulge centric star formation.

In Figure 5.2 I show the mean SSFR profiles of barred and unbarred galaxies in three bins of stellar mass. The stellar mass bins are chosen so that there is the same number of galaxies in each bin. The individual galaxy profiles are shown with cyan lines, while the red lines display the mean SSFR profile in each panel, with errors calculated from the scatter in 1000 bootstrap resamplings.

Immediately clear from this plot is the characteristics of the 'Centrally Suppressed' galaxies which were discussed in detail in Chapter 4. Towards higher masses more galaxies exhibit suppressed star formation in their cores, with respect to their disks. In the low mass bin, both barred and unbarred galaxies experience a small drop in SSFR from the outer to inner regions, however there is a small upturn in the mean barred profile in the inner radial bins. At intermediate masses there are a small number of centrally suppressed galaxies in both the barred and unbarred samples. As was seen in Chapter 4, the increase in mass has led to a decrease in overall SSFR at all radii, compared to the lower mass bin. Both samples show

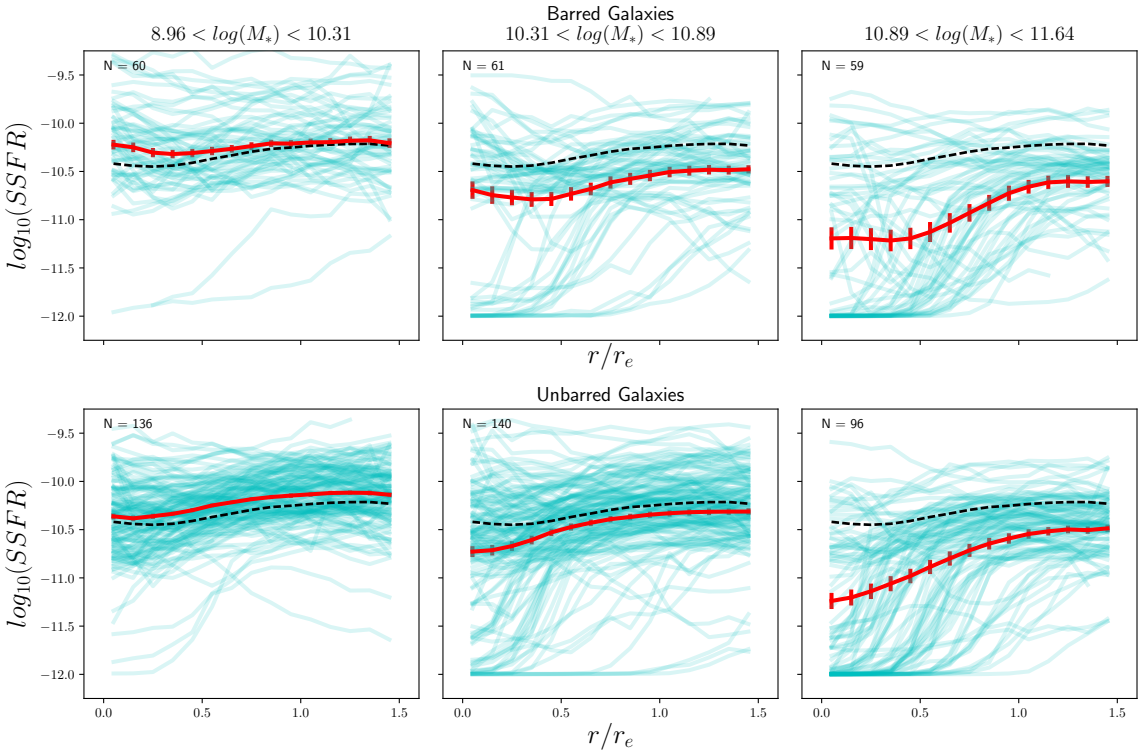

Fig. 5.2 I show the radial profiles of specific star formation rate for barred and unbarred disks. The cyan lines show the individual galaxy profiles, while the red lines show the mean profile in each panel. The galaxies are divided into three bins of stellar mass. The errors are calculated from the scatter in 1000 bootstrap resamplings. I include the mean profile for all galaxies in the sample as a dashed line in each panel to guide the eye.

a decrease in the centre of their mean profiles related to the centrally suppressed galaxies, however the barred galaxies again demonstrate an upturn of star formation in the central regions. Finally, in the highest mass bin, I again see a decrease in overall star formation, and an increase in the contribution to the mean profile from centrally suppressed galaxies. Both barred and unbarred galaxies appear to be suppressed out to larger radii than in the intermediate mass bin, and again the barred galaxies show an upturn in star formation towards the central radial bins.

I compare the mean SSFR profiles of barred and unbarred galaxies in Figure 5.3. I use solid lines for barred galaxies, and dashed lines for unbarred galaxies. At low masses the barred galaxies exhibit significantly lower SSFR than unbarred galaxies at large radii, though this difference is smaller than at other masses. The barred galaxies exhibit an upturn in SSFR inwards of $0.4r_e$ which is not present in the unbarred sample. The upturn is of the order of ~ 0.15 dex and results in the low mass barred galaxies having significantly higher bulge SSFR than the unbarred galaxies.

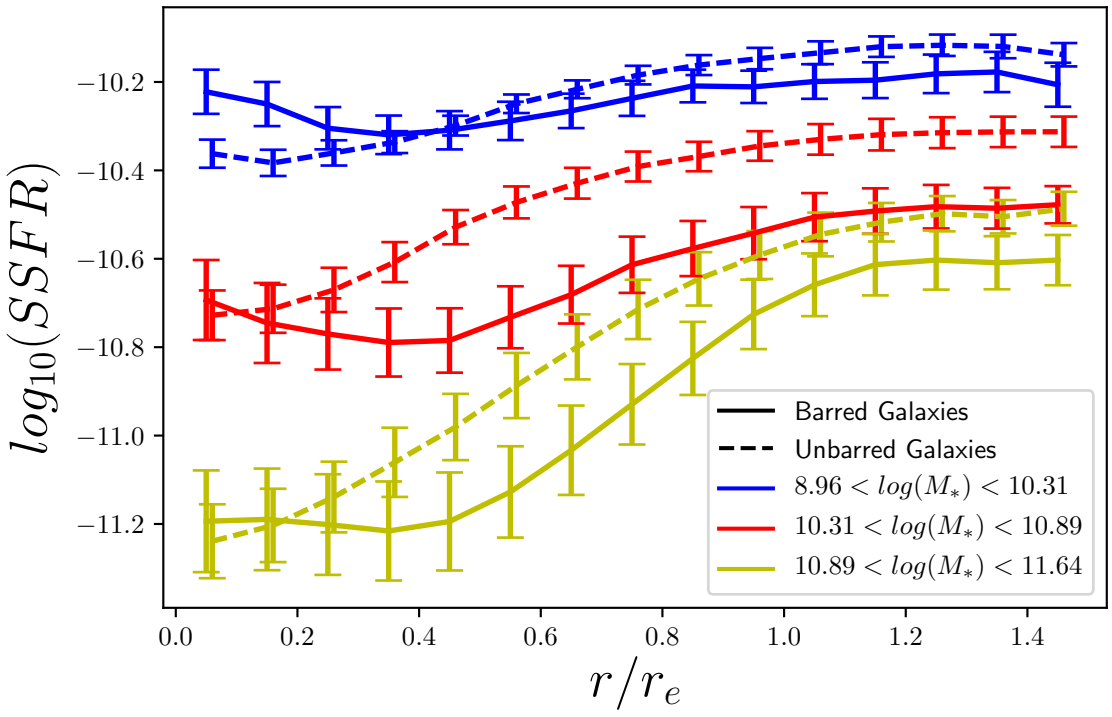

Fig. 5.3 The mean SSFR profiles in three bins of stellar mass, barred (solid lines) and unbarred galaxies (dashed lines). The errors are calculated from the scatter in 1000 bootstrap resamplings.

The intermediate mass galaxies show significant differences in the shapes of the profiles. In the disk regions, barred galaxies have much less star formation than the unbarred galaxies, with a SSFR on average 0.2 dex lower. As the profile moves inwards from the disk to the core both profiles begin to fall, however for the barred galaxies it begins to rise again inward of $0.4r_e$. This upturn implies that there are galaxies with enhanced star formation in their bulges, relative to their disks, present in the barred sample that are not present in the unbarred sample.

In the high mass bin the difference between the barred and unbarred samples is still present, but is less prominent than at intermediate masses. At this mass, the barred galaxies still have lower SSFR in their disks than the unbarred galaxies. In the cores, it may appear that the barred galaxies exhibit the same upturn as in the lower masses, however this is clouded by the SSFR limit imposed by the D_n4000-SSFR model. At high masses, many of the galaxies in both samples have SSFR profiles that decline in their centres to our imposed SSFR floor, and this dominates the mean profile. It does seem that the barred galaxies suppress at a larger radii than the unbarred galaxies, but it is unclear whether this is a different mechanism to the global suppression that I see.

5.3.2 Profiles of D_n4000 and EW[H_α]

As discussed in both Chapters 3 and 4, there is a limitation in our model for star formation rates, regarding spaxels in maps with high D_n4000. In these spaxels, I are not able to correctly assign a SSFR, and thus I use an upper limit instead of throwing these spaxels away. This means that I are not able to study galaxies with very low amounts of star formation. Since I have shown that barred galaxies have lower SSFRs on average compared to unbarred galaxies, I wish to study the properties of galaxies which would fall below our SSFR cut. To do this, I will investigate the profiles of D_n4000 and the equivalent width of H_α emission. These properties are related to the ages and properties of stars within galaxies, and will allow us to investigate low SSFR disks. As I showed in Chapter 3, D_n4000 can be used as a predictor for SSFR, as it is a tracer of long term stellar age. Sánchez et al. (2013) and Belfiore et al. (2017a) both show that EW[H_α] can be related to SSFR, using data from both MaNGA and CALIFA.

In Figure 5.4 I plot the D_n4000 profiles of barred and unbarred galaxies, with solid and dashed lines respectively. In the low mass bin, the barred galaxies have higher values of D_n4000 at all radii compared to the unbarred sample, however the lines do converge slightly towards the centre regions. The profiles are fairly flat, particularly in the disk regions, with a small upturn towards the centres of the galaxies. For the intermediate mass bin, the barred galaxies exhibit much higher values of D_n4000 than the unbarred galaxies at radii beyond

$0.5r_e$. There is a downward turn in the barred profile, which corresponds to the upturn in SSFR from Figure 5.3. The high mass galaxies follow the same trend as the intermediate galaxies, though the overall difference between the profiles is smaller. I see that the high mass barred galaxies do exhibit a downturn, which was unclear in the SSFR profiles due to the SSFR limit.

I also show the profiles of EW(H_α) in Figure 5.4. I find that the barred galaxies have lower values of EW(H_α) in their disks than unbarred galaxies. In the low mass bin, both profiles rise slightly from the outermost radii, but the unbarred galaxies turn down towards the centres while barred galaxies continue to increase. The profiles approach parity with each other in the central radial bin. In the intermediate mass bin, the unbarred galaxies fall steadily from the disk into the core, while the barred galaxies fall towards $\sim 0.5r_e$ and turn back upwards towards the centres of the galaxies. I again see that the intermediate and high mass barred galaxies are very similar, while the same cannot be said for the unbarred galaxies. The high mass barred galaxies have slightly lower EW[H_α] than the unbarred galaxies, except in the centres where the barred profile turns over.

These results have shown that barred galaxies have older stellar populations and less star formation on average than unbarred galaxies, as indicated by their SSFR, D_n4000 and EW[H_α] profiles. However, this is mainly true for the disks of these galaxies; in the cores I find that barred galaxies have enhanced star formation and younger stellar populations. This enhancement leads to barred galaxies having the same or more star formation in their cores as unbarred galaxies. In the following section I will further explore the suppression and enhancement of barred galaxies to determine what properties drive these changes.

5.4 Analysis of Bar Regulation of Star Formation

In this section I shall explore the physical processes which may be causing the differences in the profiles found previously. In particular, I focus on the role of environment in the suppression of disk star formation, and the enhancement of nuclear star formation in barred galaxies.

5.4.1 Suppression of barred disks

The suppression of disk star formation in barred galaxies implies that either the bar is responsible for quenching the galaxies' star formation, or that the process of quenching is responsible for the creation of a bar. Similar results have been found throughout the literature; most recently Kruk et al. (2017) used bulge-disk-bar decompositions of a sample

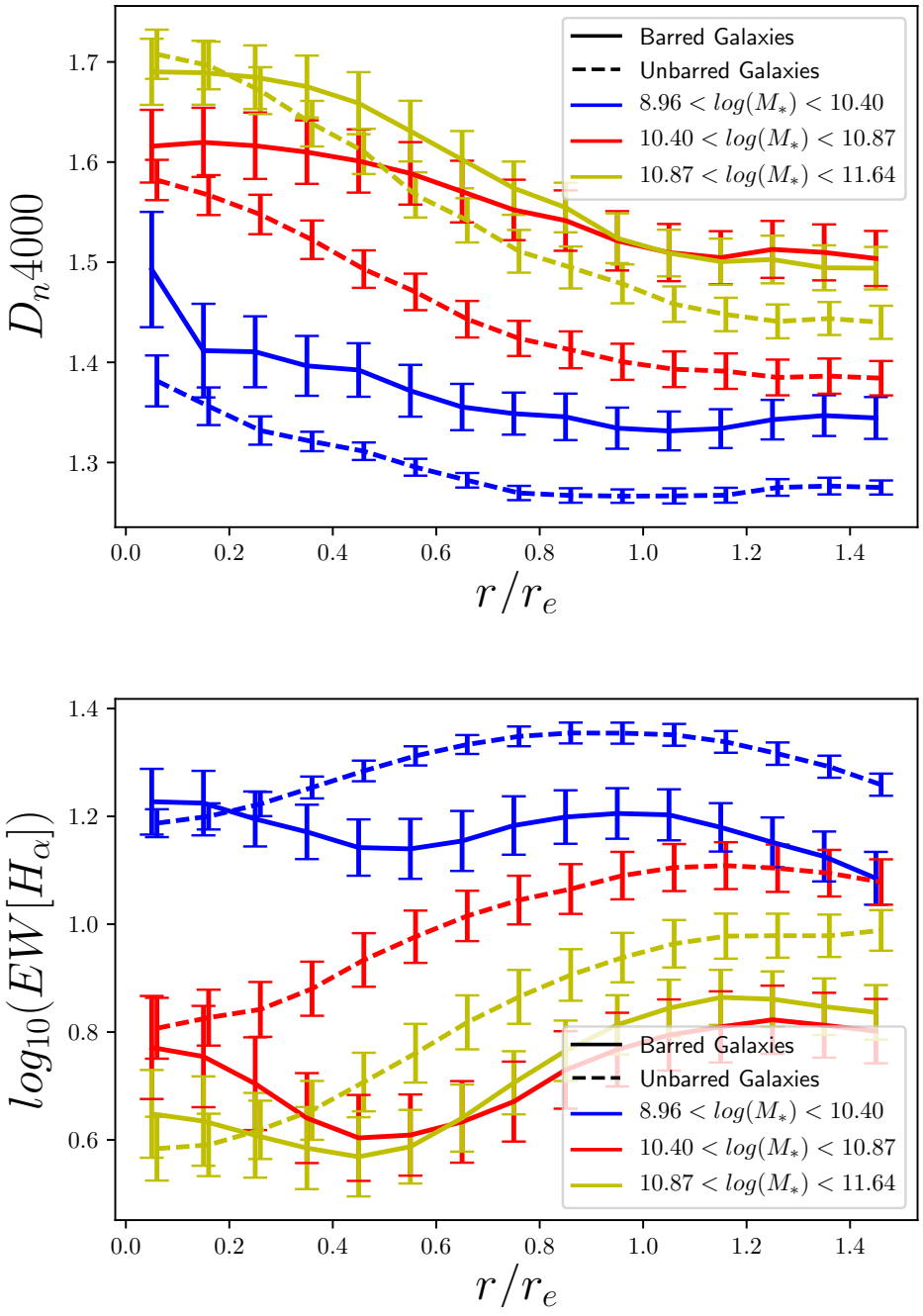

Fig. 5.4 The mean D_n4000 (top) and EW[H_α] (bottom) profiles in three bins of stellar mass, barred (solid lines) and unbarred galaxies (dashed lines). The errors are calculated from the scatter in 1000 bootstrap resamplings.

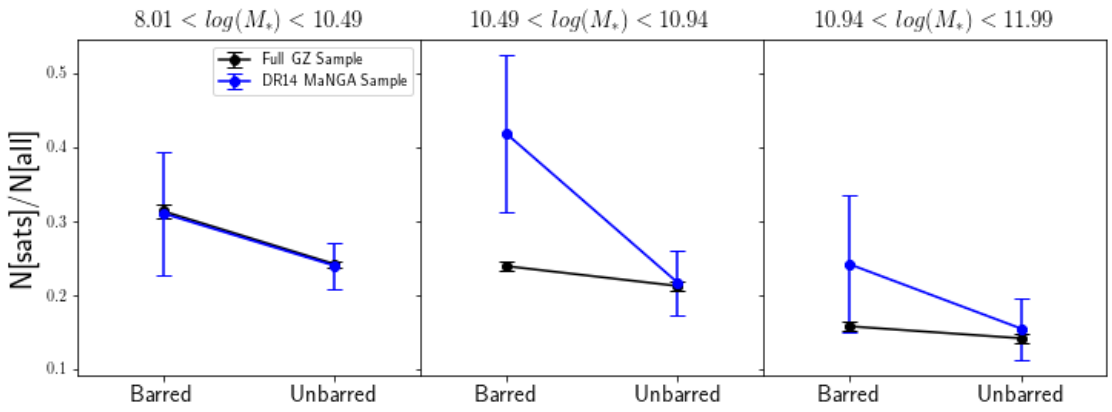

Fig. 5.5 The fraction of barred and unbarred galaxies which are satellites, for the full GZ2 sample (black) and for the DR14 MaNGA sample (blue).

of barred and unbarred galaxies from Galaxy Zoo to show that barred galaxies have redder disks than unbarred galaxies. There has been some suggestion in the literature that bar and morphological quenching may in fact be related to galaxy environments. One such study by Smethurst et al. (2017) found an increase in the fraction of satellite galaxies with bars towards the centres of galaxy groups. The increase in bars may lead to these galaxies quenching via bulge growth, though it may also be the case that it is the environment itself that triggers the formation of the bar via tidal interactions and harassment.

The interplay between morphological quenching and environmental processes is interesting, particularly when you consider both the results of this Chapter and of Chapter 4. Recall that satellite galaxies were found to have suppressed star formation in their disks compared to central galaxies at fixed mass. Satellites typically occupy higher density environments at fixed stellar mass, and so are subject more readily to environmental quenching mechanisms. The similarity between this and the comparison of barred and unbarred galaxies is thus tantalising, as it may connect the two mechanisms, as suggested by Smethurst et al. (2017).

In order to study the relationship between bar and environmental quenching, I must first understand the environments that our galaxies occupy. In Figure 5.5 I show the satellite fractions of barred and unbarred galaxies, in the full Galazy Zoo sample and for the DR14 MaNGA galaxies. Interestingly, there is a strong disagreement between the DR14 sample and the parent catalog from which the morphologies are drawn from. In all three mass bins the satellite fraction is higher for barred galaxies than unbarred galaxies, however in the Galaxy Zoo sample this appears to be particularly significant in the low mass bin. Due to the significantly smaller sample size in the DR14 galaxies ($\sim$ 2400 galaxies in DR14 vs $\sim 230,000$ Galaxy Zoo targets with environments from Yang et al. 2007) the errors in

the satellite fractions are much larger. What's more, the intermediate and high mass bins show large deviations in satellite fractions from the full Galaxy Zoo sample. Intermediate mass barred galaxies are almost twice as likely to be satellites in DR14 than in Galaxy Zoo, but with the large errors this is less than 2σ away. It seems more likely that, rather than a real physical difference, the increase in satellite fraction is due to random chance as the sample was cut down to the DR14 catalog. In the full MaNGA target catalogue, which contains $\sim 40,000$ galaxies, I find a much smaller increase in the satellite fractions. In the intermediate mass bin the barred satellite fraction is just $33 \pm 4\%$, which is lower than the DR14 sample and still within 2σ of the full GZ2 sample.

If the difference in disk star formation for barred galaxies is tied to environment, this large difference in satellite fractions may be explained by the same mechanisms I discussed in Chapter 4. On the one hand, the mass bin which shows the largest difference in disk star formation is the intermediate masses, where I see the largest difference in satellite fractions. On the other hand, the high and low mass bins have roughly the same difference in satellite fractions, while the suppression of barred galaxies is not as pronounced in the low mass bin as in the high mass galaxies.

A major issue in finding whether there is a connection between bar quenching and environment quenching appears to be one of sample size. Skibba et al. (2012) showed that there is a statistically significant relationship between the number of barred and bugle-dominated galaxies, and environment density. However, with a sample size of 15,810 galaxies from Galaxy Zoo Skibba et al. (2012) studied 20 times more galaxies than previous studies that had found no correlation between bars and environment. They argue that previous studies had been inhibited by small number statistics, and with just 215 barred galaxies, and 402 unbarred galaxies this work is certainly limited by its sample size.

All things considered, I still wish to see whether the different environments seen in Figure 5.5 are having an effect on the mean profiles. In Figure 5.6 I separate galaxies into centrals and satellites and compare the SSFR profiles of barred and unbarred galaxies. For central galaxies, the mean profiles look similar to the full sample in Figure 5.3, but the difference between the barred and unbarred galaxies is smaller in all three stellar mass bins.

For the satellites however, the profiles are quite different. In the low and medium mass bin I indeed see that barred and unbarred satellites have slightly lower SSFRs at all radii compared to the centrals, as I found in Chapter 4. In the low mass bin, the barred satellites have lower SSFRs than unbarred satellites at all radii except in their cores, and in the high mass bin the barred galaxies have the same SSFRs in their disks, but slightly higher in their cores. In the intermediate mass bin, however, things look quite different. Comparing barred centrals and satellites, I see that the satellites are dominated by a centrally suppressed profile,

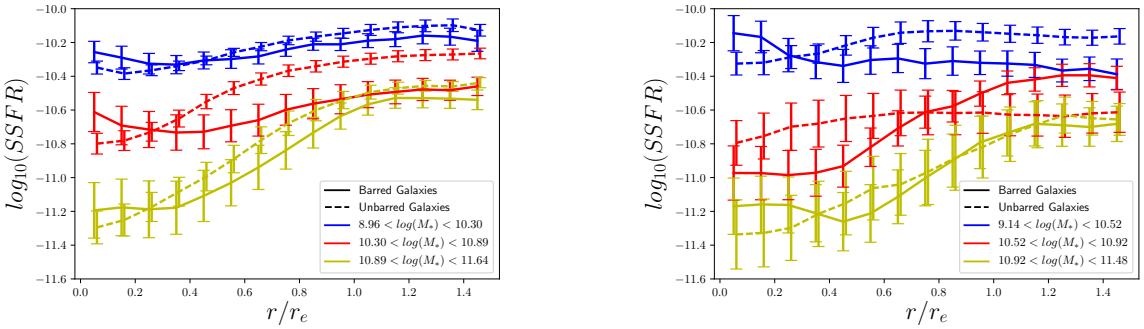

(a) Central Galaxies.

(b) Satellite Galaxies.

Fig. 5.6 I show the mean SSFR profiles of barred and unbarred galaxies, separated by their environments, in three bins of stellar mass. The errors are calculated from the scatter in 1000 bootstrap resamplings.

Table 5.2 The number of galaxies which are barred and unbarred for the central and satellite populations at fixed mass.

	$8.96 < log(M_*) < 10.30$	$10.30 < log(M_*) < 10.89$	$10.89 < log(M_*) < 11.64$
		Centrals	
Barred	40	39	39
Unbarred	100	115	78
		Satellites	
Barred	19	20	18
Unbarred	41	17	13

while the centrals are much flatter with some core enhancement. In the inner regions the satellites have lower SSFR than centrals, but higher in the outskirts. The same can be said for the comparison between barred and unbarred galaxies: the unbarred profile is quite flat, but the barred profile has lower SSFR in the core and higher in the disk.

It is unclear why the barred satellites in the intermediate mass bin appear to break all the established trends I have seen previously throughout this work. Ultimately it may simply be a matter of sample size. In Table 5.2 I show the number of centrals and satellites there are in the three mass bins for barred and unbarred galaxies. I see that the numbers of galaxies in each bin do fall quite low, compared to the previous studies I have conducted using the MaNGA SSFR profiles. At this point I cannot rule out that the mechanisms causing barred and unbarred galaxies to have different profiles are related to their environments, or if it is a purely internal process.

5.4.2 Enhancement of central star formation rates

The upturn in SSFR in the centre of barred galaxies is particularly interesting, as it indicates an enhancement of central star formation with respect to unbarred disks. In Chapter 4 I demonstrated that a simple way to distinguish between centrally suppressed and unsuppressed galaxies was to look at the ratio between SSFR in the core of the galaxy and the outer regions. Since I want to analyse the effects of the central enhancement I choose to find the ratio of mean SSFR inwards of $r/r_e = 0.4$ and outwards of that radius. I choose this radii as a rough estimate of where most of the enhanced profiles begin to turn upwards.

In Figure 5.7 I show the SSFR ratios for barred and unbarred galaxies. The barred galaxies are shown with the blue line, while the red line indicates the unbarred galaxies. For both samples I see the bimodal distribution found in Chapter 4, separating galaxies which are centrally suppressed and unsuppressed at around a factor of 10 decrease of SSFR in the centres of galaxies. However, the distribution of ratios is different between the samples: the suppressed region appears to cover a slightly larger range of SSFR for the barred galaxies, while the unsuppressed region is entirely shifted to higher ratios, indicating more central enhancement in galaxies that contain bars.

Furthermore, I investigate the bulge-to-disk ratios of D_n4000 and EW[H_α] for barred and unbarred galaxies without a cut in SSFR in Figure 5.8. Unlike the SSFR ratios, the distribution is not bimodal and I cannot distinguish between suppressed and unsuppressed cores. For both D_n4000 and EW[H_α] I see that the barred galaxies and unbarred galaxies have different distributions in ratios. The barred galaxies have a wider distribution, with a greater number of galaxies having lower D_n4000 or higher EW[H_α] in their cores compared to their disks than unbarred galaxies.

Figures 5.7 and 5.8 show that there is a significant difference between the bulge-to-disk ratios of barred and unbarred galaxies. This is not the first time barred galaxies have been shown to have more centrally concentrated star formation. For example, Lin et al. (2017), when studying a small sample of galaxies in the CALIFA survey, identified 17 of galaxies which experienced a turnover in D_n4000 and the equivalent width of H_δ absorption (EW($H_\delta A$)) and H_α emission (EW[H_α]). This turnover indicated a younger population of stars in the bulges of these galaxies. Of those 17 galaxies, 15 had bars, however only half of the barred galaxies in their sample experienced a turnover.

The ratios tell us that barred galaxies are more centrally enhanced, but they do not show how that enhancement manifests in the galaxy. For this, I can study both the profiles of these galaxies, and the SSFR maps. To begin with, I show the profiles of galaxies with $\log_{10}(SSFR_{[Bulge]}/SSFR_{[Disk]}) > 0.2$ from the barred and unbarred samples in Figure 5.9. These galaxies represent 15% of the barred galaxy sample, but just 6% of the unbarred

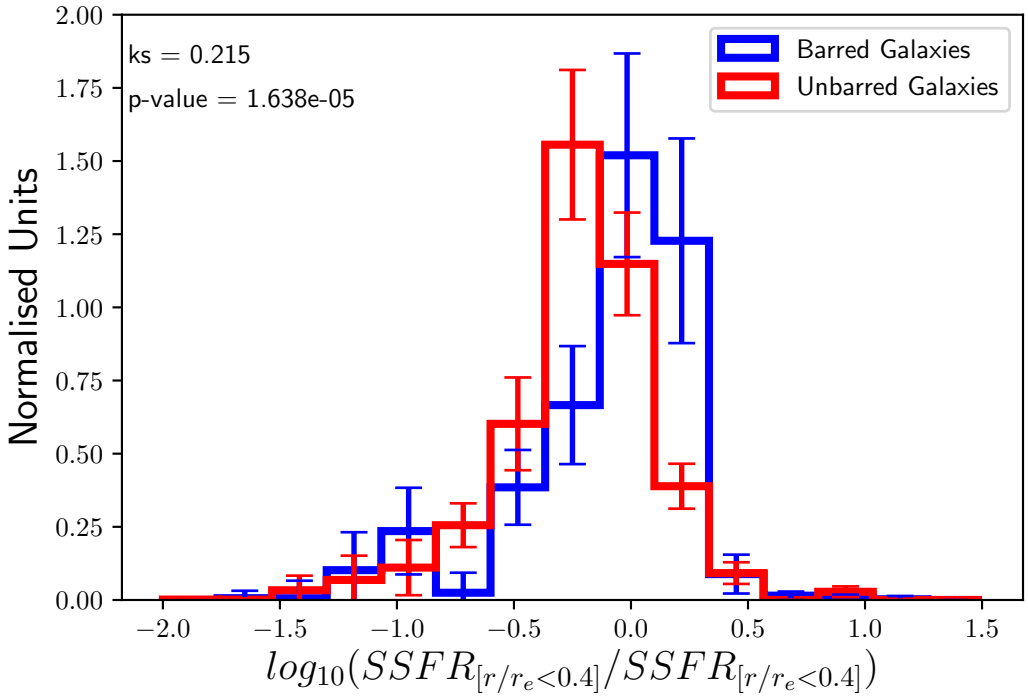

Fig. 5.7 The bulge-to-disk ratios of SSFR for barred and unbarred galaxies. The mean bulge SSFR is calculated within $0.4r_e$ of the centre of the galaxy, while the mean disk SSFR is calculated outwards from $0.4r_e$.

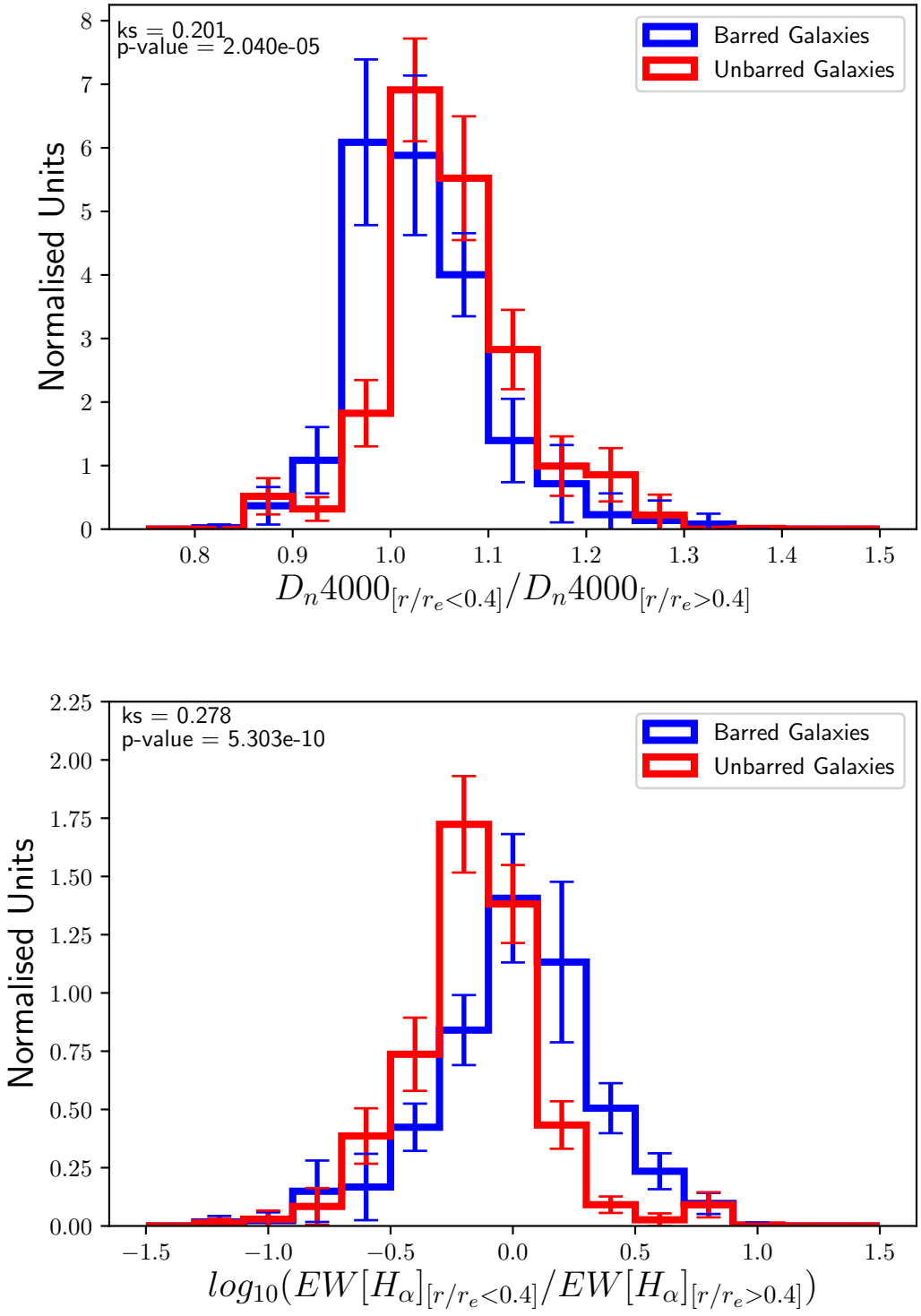

Fig. 5.8 The bulge-to-disk ratios of D_n4000 (top) and EW[H_α] (bottom) for barred and unbarred galaxies. The mean bulge values are calculated within $0.4r_e$ of the centre of the galaxy, while the mean disk values are calculated outwards from $0.4r_e$.

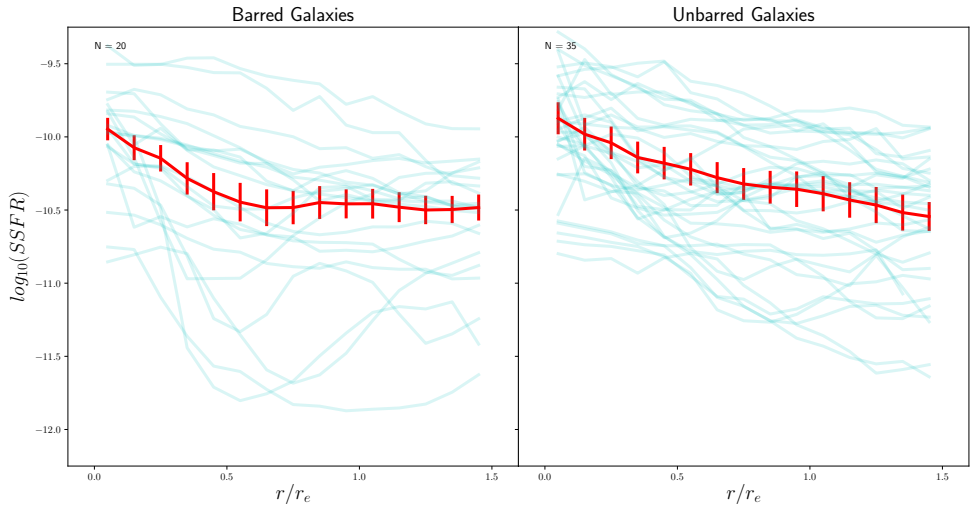

Fig. 5.9 The SSFR profiles of galaxies from the barred and unbarred samples, with $\log_{10}(SSFR_{[Bulge]} \ / \ SSFR_{[Disk]}) > 0.2$. I show the mean profile of these galaxies with the red line. The errors are calculated from the scatter in 1000 bootstrap resamplings.

galaxies. The two samples of galaxies are clearly different, with the unbarred galaxies being made up of smooth, monotonic profiles which decrease from the core to the outer disk. While these profiles also exist in the barred sample, there is also a population of galaxies that appear to be centrally suppressed, but have substantial rejuvenation in their cores. This suppression into central star formation is not present at all in the unbarred sample.

In Figure 5.10 I show the SSFR maps of the 20 barred galaxies from Figure 5.10, in order to investigate the full 2D distribution of star formation. While a number of these maps show SSFR increasing steadily from the disk to the core, as seen in Figure 5.9, I can clearly pick out the galaxies with rejuvenated cores. 8465-12705 and 8726-12701 are particularly good examples of this rejuvenation, showing star formation in the outer part of their disks and then a ring of low SSFR around the central bulge. This ring of low star formation has been coined by previous authors as the 'Star Formation Desert', and is likely a region where the strong bar has swept out the star forming material from the disk (James and Percival, 2016, 2017).

Figures 5.9 and 5.10 show clear evidence that the barred galaxies have more star formation in their cores than unbarred galaxies. This indicates that the bars are possibly responsible for channeling gas into the cores of these galaxies, providing fuel for star formation. This also may explain why the disks have lower levels of star formation, if the bar is driving gas into the bulge, it is necessarily removing gas from the disks, which would result in less star formation compared to unbarred galaxies.

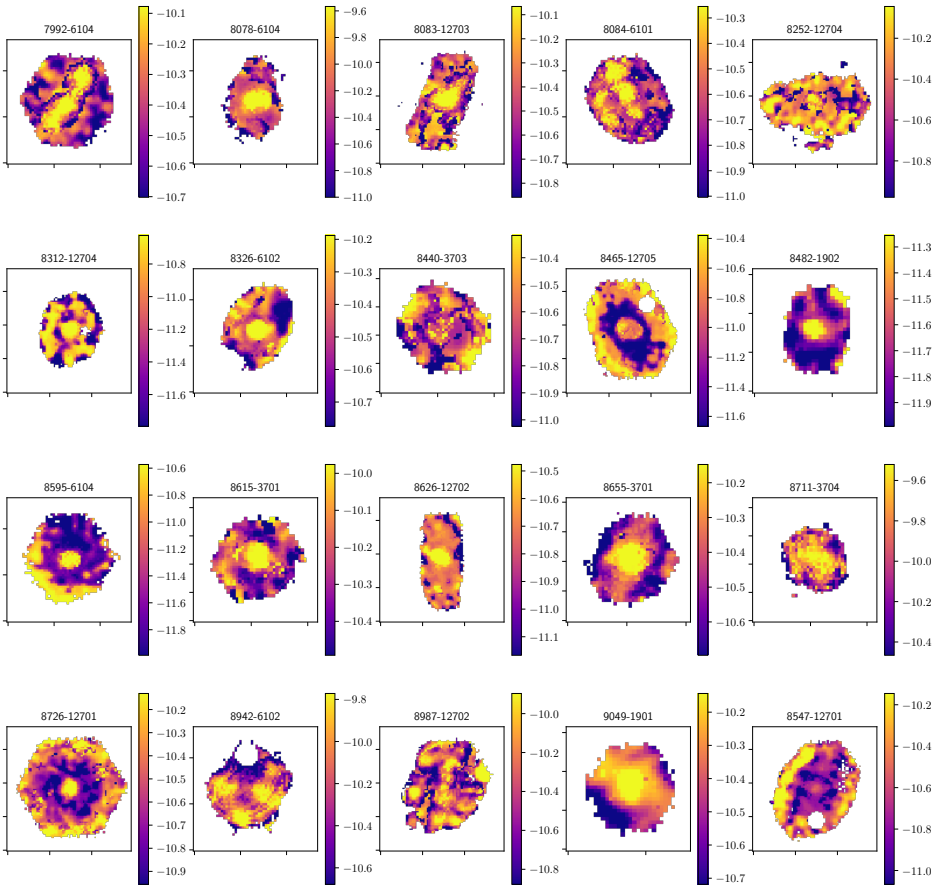

Fig. 5.10 I show the SSFR maps of 20 galaxies, selected from Figure 5.10. Each panel shows the plate and IFU number for each galaxy, which is used as an identification number. The colour bar shows the $\log_{10}(SSFR)$.

5.5 Conclusions

In this Chapter I have investigated the spatially resolved star forming properties of 215 barred and 420 unbarred galaxies in the MaNGA survey. I selected galaxies based on their morphologies from Galaxy Zoo 2 (Willett et al., 2013). I utilised the measurements of SSFR from Chapter 3 of this work, and the maps of D_n4000 and EW[H_α], to study where galaxies are growing most with respect to their stellar mass. Barred and unbarred galaxies were compared at fixed stellar mass, both producing radial profiles of the listed properties between $0-1.5r/r_e$.

- I found that barred galaxies have lower SSFR globally than unbarred galaxies, at fixed stellar mass. This decrease agrees with many previous studies that find that barred galaxies are forming fewer stars and tend to have redder colours. At the local scale, I found that barred galaxies have lower SSFR in their disks than unbarred galaxies. This lower disk star formation is likely responsible for the trends I see in the global properties. This agrees with studies of spatially resolved colours of barred galaxies which have found they have redder disks than unbarred galaxies. The difference in disk SSFR is strongest at intermediate stellar masses, and weakest at low stellar mass. I have also studied the profiles of D_n4000 and $(EW[H_\alpha])$ so that I could investigate the properties of quenched galaxies which are not well modelled by our SSFR predictions. I have found that the profiles of these properties agree well with the results from the SSFR profiles, showing that barred galaxies have older disks than unbarred galaxies.

- I investigated whether or not environment played a role in the suppression of barred galaxy star formation. I found that in the DR14 sample, barred galaxies are more likely to be satellites than unbarred galaxies, which may imply that the satellite quenching seen in Chapter 4 is partly responsible for the suppression of bars compared to disks. However, when I compared galaxies at fixed environment by comparing centrals with centrals and satellites with satellites, I found that the differences in SSFR did not vanish completely. For centrals the difference in disk SSFR between barred and unbarred galaxies decreased at all masses. For satellites, the differences increased in low mass galaxies and decreased at high masses. For intermediate mass satellites the profiles took on a dramatically different shape, with barred galaxies have higher SSFR in their outskirts, but lower SSFR in their cores. I believe that the environment signal is perhaps too weak to detect properly with such a small sample size of galaxies, as other studies have found that a large sample size is needed to detect an appreciable difference between the environments of barred and unbarred disks.

- At all masses, barred galaxies show an enhancement of central star formation compared to the unbarred galaxies. I found that the bulge-to-disk ratios of SSFR, D_n4000 and $(EW[H_\alpha])$ are shifted towards bulge centric star formation for barred galaxies compared to the unbarred sample. Barred galaxies are much more likely to have an enhanced core, with $15 \pm 3\%$ of barred galaxies having $\log_{10}(SSFR_{[Bulge]}/SSFR_{[Disk]}) > 0.2$, compared to only $6 \pm 3\%$ of unbarred galaxies. When I investigated the profiles of the centrally enhanced galaxies, I found that while enhanced unbarred galaxies display a simple monotonic increase from the outskirts of the disk to the core, there is a sub-sample of barred galaxies that look like 'centrally suppressed' galaxies but with rejuvenated bulges.

These results agree well with previous studies which have found both that the disks of barred galaxies are redder with older stellar populations, and that they have enhanced circumnuclear star formation compared to unbarred galaxies. This is likely due to the bar structure funnelling gas from the galaxy disk into the bulge, leading to a decrease in available star forming material in the former and an increase in the latter. This explains why I see lower disk star formation for barred galaxies than in unbarred galaxies, and the enhancement found in their cores. Thanks to the nature of the MaNGA survey I have managed to perform this study on a larger sample of IFU observed galaxies than previous research (five times as many barred galaxies as Lin et al. 2017). With the spectral data I have confirmed that the differences seen in the colours of barred and unbarred galaxies are in fact related to differences in levels of star formation.

However, I have not been able to rule out the role of environment in this process. Some studies have found a link between the fraction of bars and environment density, which may imply that the two processes are linked. When I tried to match our samples based on environment I found that while the differences between barred and unbarred galaxies decreased in some cases, in others they became more extreme. Skibba et al. (2012) showed that large sample sizes are needed to demonstrate the differences between barred and unbarred galaxies in different environments, as such I believe that our small sample size is at the core of why I cannot disentangle the environment and internal effects in this Chapter. However, by the end of the MaNGA survey run in 2020, there will be 4 times as many galaxies available to study. With a much larger sample size, I believe that the competing factors of secular and environmental activity can be studied in full.

6

Conclusions

"Roads? Where we're going we don't need roads."

– Dr. Emmett Brown, *Back to the Future, 1985*

In this thesis I have attempted to answer a deceptively simple question: why does the local universe look the way it does? I have presented research which studies the properties of local galaxies, using single fibre spectroscopy from SDSS I/II and Integral Field Spectroscopy from SDSS IV-MaNGA, to determine the roles of internal and external processes in shaping their structure and ongoing star formation. I will now conclude with a summary of this research, a discussion of the wider implications in modern astronomy, and a look to the future.

6.1 Summary of Research

Recall from Chapter 1, I established our science goals to answer this set of questions:

1. How are galaxies shaped by their environment? What processes drive the structural evolution of central and satellite galaxies?

2. What are the roles of internal, secular processes in the shutdown of star formation?

3. What are the roles of external, environmental processes in the shutdown of star formation?

6.1.1 How are galaxies shaped by their environment?

It has been well known for some time that galaxy environments play a role in the structural evolution of galaxies. Dressler (1980) established the Morphology-Density relation, which

shows that in dense environments, those within galaxy groups and clusters, galaxies are more likely to have early-type morphologies. Over the decades many mechanisms have been theorised to explain these relationships. Major and minor mergers provide pathways for transformative, and in some cases destructive, changes to a galaxy's shape, mass and size by adding new material. Conversely, tidal stripping, ram pressure stripping, and galaxy-galaxy harassment all provide ways for mass to be removed from a galaxy. Depending on a galaxy's environment, they may be more likely to be affected by one set of processes than another.

Many authors have established that the Size-Mass relation for galaxies was independent of environment (Baldry et al., 2006; Huertas-Company et al., 2013; Kauffmann et al., 2004; Shankar et al., 2014). That is, galaxies at fixed mass have the same average size regardless of their local environment. This is interesting, because as I stated above, galaxies in different environments are subject to different structurally transformative processes. Central galaxies, in all but the largest halos, are typically stationary in their gravitational potential wells and as such are not subject to ram pressure stripping or tidal stripping, and as the largest galaxies in the group they do not typically experience harassment. However, due to their prime position in the halo, they are perfectly poised to experience numerous mergers, and cannibalise smaller satellite galaxies to increase their size and mass (Hirschmann et al., 2013; McCavana et al., 2012). Satellites are not typically subject to minor mergers, but do experience ram pressure stripping due to their motion through intracluster medium, tidal stripping due to their offset from the centre of the gravitational potential and harassment from interactions with other satellites (Abadi et al., 1999; Balogh et al., 2004; Dekel et al., 2003; Gunn and Gott, 1972; Larson et al., 1980; Pasquali, 2015; van den Bosch et al., 2008b).

A key point to all the above processes, except major mergers, is that in theory they should preferentially act on the outskirts of a galaxy. In elliptical galaxies in particular, the galaxy core is somewhat shielded from the effects of the outer environment. Adding and removing stars and gas from the galaxy is like peeling or adding layers to an onion. In addition, these processes explicitly add or take away stellar mass, and as such pose an interesting point when you consider the Size-Mass relation. If stars are removed from a galaxy by tidal stripping, the galaxy's size must decrease as well, and vice versa for minor mergers. If the masses of galaxies are changing, is it even valid to compare galaxies in different environments based on their mass? Two galaxies that begin their lives in similar conditions may have the same mass, but if one is accreted onto a larger dark matter halo it becomes subject to dramatically different forces on its evolution. Two galaxies with similar masses now, may have had significantly different masses in the past, and so comparing galaxies at fixed mass doesn't necessarily capture the environmental aspect of the evolution. For this, I require a galaxy property that is invariant to environment.

In Chapter 2, I chose to study the relationships between core velocity dispersion (σ_0), size, mass and metallicity. σ_0 is the measure of the motion of stars in the very core of the galaxy. With the exception of major mergers, it is likely much less affected by environmental processes than stellar mass. It is perfect, then, for studying any differences in the structural evolution of central and satellite galaxies.

For star forming galaxies, I found very little difference in the masses and sizes of centrals and satellites at fixed σ_0. This suggests that star forming satellites may not have been satellites for very long. Recent studies have shown that satellites may quench their star formation quite rapidly once they are accreted onto a new dark matter halo, as such it may be the case that these satellites have not had the time to be stripped or harassed yet (Bluck et al., 2016; Knobel et al., 2015; Oman and Hudson, 2016; Smethurst et al., 2017; Wetzel, 2011; Wetzel et al., 2013). Star forming galaxies are also typically disks, which may affect how the environmental processes act on their mass and size.

For quiescent galaxies however, I see that there is a significant difference in the Mass-σ_0 and Size-σ_0 relations for centrals and satellites. At low σ_0 I find that centrals are around 5% larger than satellites, but at the high σ_0 end the centrals are about 30% larger. Centrals are also consistently more massive than satellites, but the degree to which this is the case is smaller. This is due to the shape of the Size-Mass relation; small changes of mass in high mass galaxies causes larger changes in size than in low mass galaxies. We also show that these differences are not due to residual differences in the star formation and Sérsic indices of the centrals and satellites.

We took this research a step further by investigating the radial mass profiles of centrals and satellites. We constructed mass profiles from the *r*-band and *g*-band colour profiles from SDSS photometry. In the cores of both star forming and quiescent galaxies, the stellar mass density is the same for central and satellite galaxies. However as I study the outer regions of these profiles, I see that centrals have higher mass and mass density than satellites. These profiles are crucial to the results of this study, for they confirm two things. Firstly, that the cores of central and satellite galaxies are unaffected by the different environmental processes. Secondly, that the environment acts to add and remove mass preferentially from the outer regions of centrals and satellites, respectively. The differences between the profiles follow the same trends and the Size-σ_0 and Mass-σ_0 profiles, they are stronger for quiescent galaxies than in star forming ones, and there is a dependence on σ_0 for the strength of the difference.

Finally, I studied the metallicity of central and satellites, as measured within the 3" fibre in SDSS. As this metallicity is measured within the inner regions of the galaxy, I expected to find little difference in the Mass-Metallicity and σ_0-Metallicity relations. Indeed, I found that when I accounted for specific star formation rate, there was at most a 5% difference

in metallicity between centrals and satellites in the mass-metallicity relationship. This differences was found to be entirely consistent with the Mass-σ_0 relation. Metallicity then, at least in the core of the galaxy, is also unaffected by environmental processes.

Taken together, these results suggest three possibilities. That centrals are growing due to mass deposition from minor mergers, that satellites are shrinking due to the removal of mass via ram pressure, tidal stripping and harassment, and that satellites that quench after being accreted onto new halos have different masses and sizes than those that quench as centrals.

We expect that, due to the stellar-to-halo mass relation, that more massive (higher σ_0) galaxies would accrete more mass via minor mergers than low mass (low σ_0) galaxies. This explains why I see that the differences in mass and size are larger for high σ_0. These galaxies are subject to a higher rate of mergers, and as such more of their mass comes from this process (Naab et al., 2009). Tidal stripping is perhaps consistent with our results, as the expected mass loss, between a few percent up to 20%, agrees with our results. It is expected that there would be a dependence on stellar mass, with smaller galaxies in higher mass halos losing more mass. However, the difference between the Mass-σ_0 relationships is fairly flat, which seems to be inconsistent with the mass dependent stripping fraction seen in galaxy cluster simulations (Bahe et al., 2016). Fianlly, I expect that the corrections I have made to ensure the star formation rate and Sérsic index distributions are the same in all of our samples would cancel out any differences caused by where and when satellite galaxies quench. It remains the case that different quenching mechanisms between centrals and satellites may mean that satellite galaxies that quenched as satellites are larger and more massive than satellites quenched as centrals. This is due to star forming galaxies being larger at fixed σ_0 than quiescent galaxies.

Ultimately, it appears that minor mergers providing a way for quiescent central galaxies to continue growing is the main driver for the differences in stellar mass and half-light radius I see at fixed σ_0. We expect that tidal stripping plays a small role at low σ_0, but due to the relationship between expected mass loss and total stellar mass, at high σ_0 essentially all of the differences in size and mass can be attributed to minor mergers that have occurred over the last 3 Gyr, or the average time-scale for satellite in fall (Wetzel et al., 2013).

6.1.2 What are the roles of internal and external processes in the shut down of star formation?

Star formation is arguably one of the most important processes in the Universe. Stars form galaxies, process hydrogen and helium into heavier elements and in their deaththroes spread those elements throughout the cosmos. One of the striking aspects of extragalactic astronomy

is the bimodality in star formation rates (and colour) that we see in the local universe. Galaxies at fixed mass tend to lie along the so-called 'Main Sequence of Star Formation', or significantly below the sequence. This is also seen in the Colour-Magnitude diagram, with galaxies falling in the blue cloud or red sequence. Galaxies are believed to transition from star forming to quiescent via the green valley, a region of low number density in the Mass-SFR and Colour-Magnitude spaces. This shut down of star formation, often called quenching, is an active area of study, and is the main focus of this body of work.

Through Chapters 3 to 5, I studied the spatially resolved star forming properties of galaxies in the MaNGA survey, in order to build up a picture of what processes affect the shut down of star formation, and where those processes act. To perform this analysis I constructed a two-source model for star formation rates, which relied on measurements of the dust-corrected H_α luminosity and the strength of the $4000-$Å break. The purpose of using both measurements is to build up complete maps of star formation. In many previous studies (Belfiore et al., 2017b,c; Lin et al., 2017; Schaefer et al., 2017) IFU star formation rates have been calculated in ways that either remove or ignore contamination of the H_α emission line; be this by masking out spaxels that are identified as AGN or LINER-like, or by selecting a sample that is entirely star forming by their BPT classification. This masking biases the samples towards high central star formation rates, however, as galaxies with low star formation rates in their cores and star forming disks will not be included. For example, Belfiore et al. (2016) shows that some galaxies in the MaNGA sample have central regions that fall under the LI(N)ER region of the BPT diagram, they contain gas regions that have emission lines, but do not form new stars. We attempted to circumvent this bias by constructing a SSFR-D_n4000 model, which can be used to predict SSFR in regions of a galaxy where H_α is unusable.

In Chapter 4 I used these maps to study the broad picture of quenching, by studying how the spatial distribution of star formation depended on stellar mass, structure and environment. We studied the radial profiles of SSFR for a sample of 1494 star forming, composite and AGN/LI(N)ER galaxies, with $\log_{10}(SSFR) > -11$, to investigate the roles of processes such as: ram pressure/tidal stripping, strangulation, morphological quenching and AGN feedback. This sample is double the size of previous MaNGA studies, owing to using a more up to date data release and including galaxies with AGN/LI(N)ER contamination, and seven times larger than studies which have used other IFU based surveys (Belfiore et al., 2017a; Schaefer et al., 2017).

We found that, in agreement with many previous studies (Belfiore et al., 2016; Brammer et al., 2009; Elbaz et al., 2011; Lee et al., 2015; Michałowski et al., 2012; Noeske et al., 2007; Renzini and Peng, 2015; Schreiber et al., 2015; Tacconi et al., 2013), the total SSFR

decreases with increasing mass. We extended this result to show that this occurs at the local scale as well, the mean SSFR profile drops as stellar mass and σ_0 increase, and this drop occurs evenly at all radii.

Perhaps that most important result of the work, is the classification of galaxies as 'unsuppressed' and 'centrally suppressed'. We find that as stellar mass (and σ_0) increase, a greater number of galaxies experiences a sharp decrease of SSFR in their cores. In addition, I found that galaxies that are centrally suppressed also experience a suppression of star formation in their disks. On average, the centrally suppressed galaxies have SSFR inwards of $0.5r_e$ is ~ 1.25 dex lower than unsuppressed galaxies, and outwards of $1.0r_e$ there is a ~ 0.5 dex decrease. This implies that whatever process is causing the cores of these galaxies to quench is also permeating out into the galaxy's disk.

We determined that the central suppression is likely caused by some combination of morphological quenching; the stabilisation of the gas in the bulge against collapse, and AGN feedback; radio-mode AGN disrupting the gas around the galaxy bulge and preventing it from collapsing. Both of these mechanisms agree with our findings. As stellar mass increases so does the bulge mass, which could lead to morphological quenching, but it also leads to a higher black hole mass, and thus higher chance of hosting a radio mode AGN that could suppress star formation in the core. These are further evidenced when I look at Sérsic Index and σ_0 at fixed Mass, as these properties increase at fixed mass, I find a higher fraction of centrally suppressed systems, and more suppressed systems overall. All these point towards galaxies with large central bulges having suppressed star formation in their cores, while still forming stars in their disks.

To study the role of environment, I compare the profiles of central and satellite galaxies throughout Chapter 4. Firstly, I find there is no difference in the fraction of galaxies that experience suppression of their core SSFR, implying that the process is purely secular. This seems to follow on from Chapter 2, processes that come from the environment do not affect the cores of galaxies, as such I see the same cores in centrals and satellites. Secondly, I find that at fixed stellar mass and σ_0, the SSFR of satellites is lower at all radii than it is for central galaxies. This is as opposed to seeing an outside-in quenching pattern, which would be expected if tidal stripping or ram pressure stripping were the dominant processes in quenching star formation. In fact, our results agree with recent studies that show that strangulation, the cut off of cold gas from the galaxies' gas halo and slow shut down of star formation as gas reserves are used up, is the main quenching mechanism for satellite galaxies (Larson et al., 1980; McCarthy et al., 2008b; Peng et al., 2015). Strangulation has been shown by simulations to provide a flat quenching pattern, not preferring to shut down

star formation in the cores or disks of galaxies, which agrees with our results Elmegreen et al. (2002); van den Bergh (1991).

In Chapter 5 I focussed on one particular galaxy property that has been shown to both decrease and increase the star formation in a galaxy, the presence of a bar. Previous studies have shown that bars are more often found in 'red and dead' disk galaxies, which implies they may play some role in the shut down of star formation in some galaxies (Cheung et al., 2013; Elmegreen et al., 2004; Friedli and Martinet, 1993; Giordano et al., 2010; Masters et al., 2012, 2011; Nair and Abraham, 2010). One such mechanism for this is for the bar to channel gas into the galaxy bulge via angular momentum transfer, feeding a circumnuclear starburst that exhausts the galaxies gas supplies (Bournaud et al., 2005; Friedli and Martinet, 1993; Knapen et al., 2002; Kormendy, 2013; Masters et al., 2011). Observationally, barred galaxies typically have larger bulges than unbarred galaxies, and redder disks, which supports this hypothesis. We studied the SSFR, D_n4000 and EW[H_α] profiles of galaxies in MaNGA, using a morphological selection from galaxy zoo (Lintott et al., 2008; Willett et al., 2013). In this Chapter I studied a sample of 215 barred and 402 unbarred disk galaxies, which is 5 times as many barred galaxies as were studied using IFU data from CALIFA in Lin et al. (2017).

Globally, I find that barred galaxies have lower SSFRs on average compared to unbarred disks, at fixed stellar mass. This agrees with studies showing redder colours found by Masters et al. (2011), among others. In the profiles, I find that barred galaxies have lower SSFR in their disks, again agreeing with previous studies that barred galaxies have redder colours in their disks, and thus lower star formation. We also find these same differences in the disk when I look at proxies for star formation and stellar population age, such as D_n4000 and EW[H_α], with barred galaxies having older populations. Using these properties allows us to extend this result to otherwise quenched galaxies, which I do not have reliable star formation rates for.

Based on the assumption that the disks have reduced star formation due to gas being funnelled into the bulge by the bar, I expect to see higher star formation rates in the barred galaxies core. In fact, this is exactly what I see, at all masses and for all three measured properties I find that the mean barred galaxy profile exhibits and enhancement inwards of $\sim 0.4r_e$. We also find that the bulge-to-disk ratios of SSFR, D_n4000 and EW[H_α] in barred disks are shifted towards more bulged focusses star formation rates, compared to unbarred disks. We observe two main forms of centrally enhanced SSFR profiles: those that increase monotonically from the edge of the disk to the bulge, and those that have multiple components. The multiple component galaxies look similar to centrally suppressed galaxies, with flat SSFR profiles in their disk, and a steep drop around $0.3-0.5r_e$, where they

differ however, is the enhanced galaxies show a strong rejuvenation of their star formation, which could be linked to a circumnuclear star burst. these multiple component profiles are exclusively found in the barred disk sample, and do not appear in the unbarred disks. Even including monotonically enhanced galaxies, a barred galaxy is significantly more likely to have more SSFR in its core than its disk than an unbarred galaxy.

Finally, I attempted to study whether there was a link between galaxy environments and bars. Some recent studies (for example Skibba et al. 2012 and Smethurst et al. 2017) have shown that bars are more likely to be found in dense environments, and I also find that the satellite fraction for barred galaxies is higher than unbarred galaxies. However, there is some contention between the MaNGA DR14 sample, which shows a very high satellite fraction for intermediate mass barred galaxies, compared to the full Willett et al. (2013) Galaxy Zoo 2 sample. this is likely an artefact of the very small sample size in DR14, which is 100 times smaller than the GZ2 sample.

In order to account for the differences in environments, I decided to compare satellites and centrals separately. The intention here, was that if bar formation and environment density were linked, I would expect the differences in disk star formation to decrease. This would imply that the lower SSFR in the disks of barred galaxies is partly due to the strangulation signal found in Chapter 4, and that perhaps the formation of a bar was simply a side effect of the satellite environment. However, this does not seem to be the case. For centrals, and high mass satellites, the difference in disk SSFR does indeed decrease, but does not vanish. For intermediate mass galaxies, the bar profile changes dramatically, being higher than the unbarred galaxies at large radii and lower than unbarred galaxies at small radii. Finally, for low mass satellites, the difference between barred and unbarred disks actually increases. These results are puzzling, and I have not come up with an adequate explanation for them. The mostly likely, however, is that the sample sizes I have are simply too small to identify a strong environmental correlation. Indeed, Skibba et al. (2012) suggest that the reason they found an environmental signal and previous studies did not was a matter of sample size, with their research studying 20 times more galaxies than in earlier works.

6.2 Further Remarks

Given the research presented here, what can be said about the wider picture of galaxy evolution? Ultimately, I have presented work that tries to tackle two different, but connected, fields of galaxy evolution; evolution of galaxy structure due to the environment, and quenching due to secular and environmental processes. Here are a few key take away points from this thesis:

1. Selecting the correct fixed parameter is vital. As shown in Chapter 2, when you are studying galaxy environments, the variable you choose to fix is incredibly important. By fixing stellar mass you potentially miss signals in the data, as stellar mass has been shown to evolve with the environment. By focussing on σ_0, however, I was able to reveal the evolution of mass and size, owing to the fact that σ_0 is invariant with environment. We now know that passive central galaxies are on average 20-30% larger than passive satellites, due to the higher merger rates among central galaxies.

2. Tidal and ram pressure stripping are not dominant effects on the satellite population. This was found in two cases, and they complement each other well. Firstly, from a structural sense, I see no differences in the sizes of star forming centrals and satellites that would indicate this stripping is occurring at a meaningful level in the satellite population. When I consider star formation, I don't see the tell-tale sign of stripping, an outside-in quenching pattern, in satellites compared the centrals.

3. You cannot simply ignore AGN/LI(N)ER galaxies. As I showed in Chapter 4 (& 5), the composite and AGN/LI(N)ER galaxies make up a significant portion of the galaxies that have centrally suppressed star formation. When you ignore these galaxies, either by selecting them out of your sample or removing the spaxels that are contaminated, you deliberately bias your sample to higher star formation rates. Schaefer et al. (2017), for example, select only star forming galaxies for their study with SAMI data, and do not find the suppression of bulge star formation that is present in this thesis. By using D_n4000 as a probe for SSFR in these contaminated galaxies, I have revealed previously unseen evidence of secular evolution of star formation.

4. Some recent works have shown that different quenching mechanisms may in fact be intimately linked. Schawinski et al. (2014) and Smethurst et al. (2017) argue that environmental and secular quenching may be one in the same, simply expressed differently galaxy by galaxy. This is difficult to reconcile with this work, as in some cases I see evidence of purely secular evolution, while in others the evidence is more muddled. On the one hand, the centrally suppressed galaxies in Chapter 4 are clearly a secular phenomenon, with links to galaxy mass, morphology and AGN activity, and I find no evidence that centrals and satellites are quenched in their cores at different rates. On the other hand, mass and morphology are tightly linked in environment, higher mass galaxies and early type galaxies typically show up in more dense environments, so there may be a halo mass connection. In addition, there is weak evidence of a link between bar induced quenching and environment, but I do not have the sample size to confirm this.

6.3 Future Research

In this final section, I wish to talk about the limitations and future plans for this research. Good research always asks more questions, and the work presented in this thesis certainly opens up into many wide possibilities for future studies. I will address what can be done to improve to quality of the work already presented, and then follow up with potential new threads to follow.

Firstly, I will discuss error analysis. It would not take a keen eye to notice that throughout this thesis I have relied on 'Bootstrapping' to handle errors in this work. Bootstrapping is the process of randomly resampling data, with repetition, to determine what the scatter on a particular result is, e.g. the mean or median. With a sufficiently large data set, it is possible to derive an error value that accurately describes the scatter in a dataset. I used this method throughout the thesis to remain consistent and handle the problem of calculating errors on star formation rates in MaNGA. Currently, the handling of error analysis in the D_n4000-SSFR model is not well defined, owing to issues in the currently available run of the Data Analysis Pipeline, which has trouble calculating errors in the D_n4000 values. In addition to this, the mass maps from Pipe3D have no error maps at all. In future iterations of the SFR model I intend to address this shortcoming, firstly by including the updated D_n4000 errors in future MaNGA data releases (or measuring this myself if they continue to be unavailable) and by exploring alternative sources of stellar masses. Fully propagating the errors and inverse variances from the MaNGA DAP model is an important next step to ensuring the accuracy and efficacy of this work. The final goal of course will be to release a Value Added Catalog to be included in a future SDSS Data Release including star formation maps for all 10,000 MaNGA target galaxies.

I wish to further explore the nature of environmental quenching in MaNGA, in particular by studying any relationships with dark matter halo mass and halo-centric distance. By studying the relationship between SFR suppression in satellites at different distances from their host halo centres, the nature and rate at that quenching takes place can be studied. It would also be interesting to see if halo mass affects the fraction of centrally quenched galaxies, at fixed stellar mass or morphology. As mass and morphology are closely related to halo mass (Dressler, 1980; Kauffmann et al., 2004; Yang et al., 2009), it would certainly be good to try to disentangle the centrally suppressed signal and see if it is truely secular. An issue in this case may prove to be sample size, however with the full MaNGA target catalog of 10,000 galaxies it should be able to determine any environmental properties.

There is much more to explore in the realm of galaxy bars. Firstly, the current work can be greatly improved by increasing sample sizes, the next data release doubles the number of available galaxies, and by surveys end the full 10,000 galaxies will mean I have $\sim 800-1000$

barred galaxies to study. Determining the properties of galaxies with enhanced central star formation are a priority, and finding what properties specifically relate to the rejuvenated cores seen in Chapter 5. Further studying the relationship between bars and environment is also important, particularly in finding out why the Galaxy Zoo 2 and MaNGA target catalog have different central/satellite distributions, and determining if there is a link between the satellite strangulation and bar suppression.

There is also a lot of potential to expand this work to other wavelengths, taking advantage of current legacy and follow up surveys. It would be possible to link cold molecular gas detections using the Atacama Large Millimetre Array (ALMA) to test for presence of gas in the cores of centrally suppressed galaxies, which I believe is present due to being able to measure gas emission lines. This work could also easily interface with the HI-MaNGA follow up survey, which is using the Green Bank Telescope to study MaNGA galaxies in the radio, against to study the distribution of gas in the galaxies and its relationship to star formation. These follow ups are particularly interesting in the study of galaxy bars, as they will allow us to determine how the gas is distributed, and whether it correlates with the lower disk and high bulge star formation rates that I see.

Going forward it makes sense to take this research to higher redshifts, potentially making use of the James Web Space Telescope in its IFU mode to study how star formation is distributed in the earlier universe. Studies of younger galaxies will allow us to draw conclusions regarding how quenching has evolved with time, for example I would expect to see less effects from environment in the early universe as galaxies are less densely packed. It would also be interesting to test whether I detect galaxies with centrally suppressed star formation, and at what fraction compared to the local universe.

References

Abadi, M. G., Moore, B., and Bower, R. G. (1999). Ram pressure stripping of spiral galaxies in clusters. *MNRAS*, 308:947–954.

Abazajian, K. N., Adelman-McCarthy, J. K., Agüeros, M. A., Allam, S. S., Allende Prieto, C., An, D., Anderson, K. S. J., Anderson, S. F., Annis, J., and Bahcall, N. A., e. a. (2009). The Seventh Data Release of the Sloan Digital Sky Survey. *ApJS*, 182:543–558.

Abdurro'uf and Akiyama, M. (2017). Understanding the scatter in the spatially resolved star formation main sequence of local massive spiral galaxies. *MNRAS*, 469:2806–2820.

Abolfathi, B., Aguado, D. S., Aguilar, G., Allende Prieto, C., Almeida, A., Tasnim Ananna, T., Anders, F., Anderson, S. F., Andrews, B. H., and Anguiano, B., e. a. (2017). The Fourteenth Data Release of the Sloan Digital Sky Survey: First Spectroscopic Data from the extended Baryon Oscillation Sky Survey and from the second phase of the Apache Point Observatory Galactic Evolution Experiment. *ArXiv e-prints*.

Abraham, R. G., Valdes, F., Yee, H. K. C., and van den Bergh, S. (1994). The morphologies of distant galaxies. 1: an automated classification system. *ApJ*, 432:75–90.

Aguerri, J. A. L., Méndez-Abreu, J., and Corsini, E. M. (2009). The population of barred galaxies in the local universe. I. Detection and characterisation of bars. *A&A*, 495:491–504.

Aihara, H., Allende Prieto, C., An, D., Anderson, S. F., Aubourg, É., Balbinot, E., Beers, T. C., Berlind, A. A., Bickerton, S. J., Bizyaev, D., Blanton, M. R., Bochanski, J. J., Bolton, A. S., Bovy, J., Brandt, W. N., Brinkmann, J., Brown, P. J., Brownstein, J. R., Busca, N. G., Campbell, H., and Carr, e. a. (2011). The Eighth Data Release of the Sloan Digital Sky Survey: First Data from SDSS-III. *ApJS*, 193:29.

Allen, J. T. (2015). The SAMI Galaxy Survey: first 1000 galaxies. In Ziegler, B. L., Combes, F., Dannerbauer, H., and Verdugo, M., editors, *Galaxies in 3D across the Universe*, volume 309 of *IAU Symposium*, pages 109–112.

Astropy Collaboration, Robitaille, T. P., Tollerud, E. J., Greenfield, P., Droettboom, M., Bray, E., Aldcroft, T., Davis, M., Ginsburg, A., Price-Whelan, A. M., Kerzendorf, W. E., Conley, A., Crighton, N., Barbary, K., Muna, D., Ferguson, H., Grollier, F., Parikh, M. M., Nair, P. H., Unther, H. M., Deil, C., Woillez, J., Conseil, S., Kramer, R., Turner, J. E. H., Singer, L., Fox, R., Weaver, B. A., Zabalza, V., Edwards, Z. I., Azalee Bostroem, K., Burke, D. J., Casey, A. R., Crawford, S. M., Dencheva, N., Ely, J., Jenness, T., Labrie, K., Lim, P. L., Pierfederici, F., Pontzen, A., Ptak, A., Refsdal, B., Servillat, M., and Streicher, O. (2013). Astropy: A community Python package for astronomy. *A&A*, 558:A33.

Athanassoula, E., Machado, R. E. G., and Rodionov, S. A. (2013). Bar formation and evolution in disc galaxies with gas and a triaxial halo: morphology, bar strength and halo properties. *MNRAS*, 429:1949–1969.

Athanassoula, E. and Misiriotis, A. (2002). Morphology, photometry and kinematics of N -body bars - I. Three models with different halo central concentrations. *MNRAS*, 330:35–52.

Athanassoula, E., Rodionov, S. A., Peschken, N., and Lambert, J. C. (2016). Forming Disk Galaxies in Wet Major Mergers. I. Three Fiducial Examples. *ApJ*, 821:90.

Bahe, Y. M., Schaye, J., Crain, R. A., McCarthy, I. G., Bower, R. G., Theuns, T., McGee, S. L., and Trayford, J. W. (2016). The origin of the enhanced metallicity of satellite galaxies. *ArXiv e-prints*.

Baldry, I. K., Balogh, M. L., Bower, R. G., Glazebrook, K., Nichol, R. C., Bamford, S. P., and Budavari, T. (2006). Galaxy bimodality versus stellar mass and environment. *MNRAS*, 373:469–483.

Baldry, I. K., Glazebrook, K., Brinkmann, J., Ivezić, Ž., Lupton, R. H., Nichol, R. C., and Szalay, A. S. (2004). Quantifying the Bimodal Color-Magnitude Distribution of Galaxies. *ApJ*, 600:681–694.

Baldwin, J. A., Phillips, M. M., and Terlevich, R. (1981). Classification parameters for the emission-line spectra of extragalactic objects. *PASP*, 93:5–19.

Ball, N. M., Loveday, J., Fukugita, M., Nakamura, O., Okamura, S., Brinkmann, J., and Brunner, R. J. (2004). Galaxy types in the Sloan Digital Sky Survey using supervised artificial neural networks. *MNRAS*, 348:1038–1046.

Balogh, M. L., Baldry, I. K., Nichol, R., Miller, C., Bower, R., and Glazebrook, K. (2004). The Bimodal Galaxy Color Distribution: Dependence on Luminosity and Environment. *ApJ*, 615:L101–L104.

Balogh, M. L., Morris, S. L., Yee, H. K. C., Carlberg, R. G., and Ellingson, E. (1999). Differential Galaxy Evolution in Cluster and Field Galaxies at z˜0.3. *ApJ*, 527:54–79.

Balogh, M. L., Navarro, J. F., and Morris, S. L. (2000). The Origin of Star Formation Gradients in Rich Galaxy Clusters. *ApJ*, 540:113–121.

Bamford, S. P., Nichol, R. C., Baldry, I. K., Land, K., Lintott, C. J., Schawinski, K., Slosar, A., Szalay, A. S., Thomas, D., Torki, M., Andreescu, D., Edmondson, E. M., Miller, C. J., Murray, P., Raddick, M. J., and Vandenberg, J. (2009). Galaxy Zoo: the dependence of morphology and colour on environment*. *MNRAS*, 393:1324–1352.

Barnes, J. E. and Hernquist, L. E. (1991). Fueling starburst galaxies with gas-rich mergers. *ApJ*, 370:L65–L68.

Baugh, C. M., Cole, S., Frenk, C. S., and Lacey, C. G. (1998). The Epoch of Galaxy Formation. *ApJ*, 498:504–521.

Beers, T. C. and Tonry, J. L. (1986). Density cusps in clusters of galaxies. *ApJ*, 300:557–567.

Behroozi, P. S., Wechsler, R. H., and Conroy, C. (2013). The Average Star Formation Histories of Galaxies in Dark Matter Halos from z = 0-8. *ApJ*, 770:57.

Belfiore, F., Maiolino, R., Bundy, K., Masters, K., Bershady, M., Oyarzun, G., Lin, L., Cano-Diaz, M., Wake, D., Spindler, A., Thomas, D., and Brownstein, J. R. (2017a). SDSS IV MaNGA - sSFR profiles and the slow quenching of discs in green valley galaxies. *ArXiv e-prints*.

Belfiore, F., Maiolino, R., Maraston, C., Emsellem, E., Bershady, M. A., Masters, K. L., Bizyaev, D., Boquien, M., Brownstein, J. R., Bundy, K., Diamond-Stanic, A. M., Drory, N., Heckman, T. M., Law, D. R., Malanushenko, O., Oravetz, A., Pan, K., Roman-Lopes, A., Thomas, D., Weijmans, A.-M., Westfall, K. B., and Yan, R. (2017b). SDSS-IV MaNGA - the spatially resolved transition from star formation to quiescence. *MNRAS*, 466:2570–2589.

Belfiore, F., Maiolino, R., Maraston, C., Emsellem, E., Bershady, M. A., Masters, K. L., Yan, R., Bizyaev, D., Boquien, M., Brownstein, J. R., Bundy, K., Drory, N., Heckman, T. M., Law, D. R., Roman-Lopes, A., Pan, K., Stanghellini, L., Thomas, D., Weijmans, A.-M., and Westfall, K. B. (2016). SDSS IV MaNGA - spatially resolved diagnostic diagrams: a proof that many galaxies are LIERs. *MNRAS*, 461:3111–3134.

Belfiore, F., Maiolino, R., Tremonti, C., Sánchez, S. F., Bundy, K., Bershady, M., Westfall, K., Lin, L., Drory, N., Boquien, M., Thomas, D., and Brinkmann, J. (2017c). SDSS IV MaNGA - metallicity and nitrogen abundance gradients in local galaxies. *MNRAS*, 469:151–170.

Bell, E. F. and de Jong, R. S. (2001). Stellar Mass-to-Light Ratios and the Tully-Fisher Relation. *ApJ*, 550:212–229.

Bell, E. F., van der Wel, A., Papovich, C., Kocevski, D., Lotz, J., McIntosh, D. H., Kartaltepe, J., Faber, S. M., Ferguson, H., Koekemoer, A., Grogin, N., Wuyts, S., Cheung, E., Conselice, C. J., Dekel, A., Dunlop, J. S., Giavalisco, M., Herrington, J., Koo, D. C., McGrath, E. J., de Mello, D., Rix, H.-W., Robaina, A. R., and Williams, C. C. (2012). What Turns Galaxies Off? The Different Morphologies of Star-forming and Quiescent Galaxies since z ˜ 2 from CANDELS. *ApJ*, 753:167.

Berezhiani, Z., Comelli, D., and Villante, F. L. (2001). The early mirror universe: inflation, baryogenesis, nucleosynthesis and dark matter. *Physics Letters B*, 503:362–375.

Bernardi, M., Sheth, R. K., Annis, J., Burles, S., Eisenstein, D. J., Finkbeiner, D. P., Hogg, D. W., Lupton, R. H., Schlegel, D. J., SubbaRao, M., Bahcall, N. A., Blakeslee, J. P., Brinkmann, J., Castander, F. J., Connolly, A. J., Csabai, I., Doi, M., Fukugita, M., Frieman, J., Heckman, T., Hennessy, G. S., Ivezić, Ž., Knapp, G. R., Lamb, D. Q., McKay, T., Munn, J. A., Nichol, R., Okamura, S., Schneider, D. P., Thakar, A. R., and York, D. G. (2003). Early-Type Galaxies in the Sloan Digital Sky Survey. III. The Fundamental Plane. *AJ*, 125:1866–1881.

Bershady, M. A., Verheijen, M. A. W., Swaters, R. A., Andersen, D. R., Westfall, K. B., and Martinsson, T. (2010). The DiskMass Survey. I. Overview. *ApJ*, 716:198–233.

Bertelli, G., Bressan, A., Chiosi, C., Fagotto, F., and Nasi, E. (1994). Theoretical isochrones from models with new radiative opacities. *A&AS*, 106:275–302.

Bezanson, R., Franx, M., and van Dokkum, P. G. (2015). One Plane for All: Massive Star-forming and Quiescent Galaxies Lie on the Same Mass Fundamental Plane at z ˜ 0 and z ˜ 0.7. *ApJ*, 799:148.

Bezanson, R., van Dokkum, P., and Franx, M. (2012). Evolution of Quiescent and Star-forming Galaxies since z ˜ 1.5 as a Function of their Velocity Dispersions. *ApJ*, 760:62.

Bialas, D., Lisker, T., Olczak, C., Spurzem, R., and Kotulla, R. (2015). On the occurrence of galaxy harassment. *A&A*, 576:A103.

Bianchi, L. (2011). GALEX and star formation. *APSS*, 335:51–60.

Blanton, M. R., Bershady, M. A., Abolfathi, B., Albareti, F. D., Allende Prieto, C., Almeida, A., Alonso-García, J., Anders, F., Anderson, S. F., Andrews, B., and et al. (2017). Sloan Digital Sky Survey IV: Mapping the Milky Way, Nearby Galaxies, and the Distant Universe. *AJ*, 154:28.

Blanton, M. R., Eisenstein, D., Hogg, D. W., Schlegel, D. J., and Brinkmann, J. (2005a). Relationship between Environment and the Broadband Optical Properties of Galaxies in the Sloan Digital Sky Survey. *ApJ*, 629:143–157.

Blanton, M. R., Hogg, D. W., Bahcall, N. A., Brinkmann, J., Britton, M., Connolly, A. J., Csabai, I., Fukugita, M., Loveday, J., Meiksin, A., Munn, J. A., Nichol, R. C., Okamura, S., Quinn, T., Schneider, D. P., Shimasaku, K., Strauss, M. A., Tegmark, M., Vogeley, M. S., and Weinberg, D. H. (2003). The Galaxy Luminosity Function and Luminosity Density at Redshift z = 0.1. *ApJ*, 592:819–838.

Blanton, M. R. and Moustakas, J. (2009). Physical Properties and Environments of Nearby Galaxies. *ARA&A*, 47:159–210.

Blanton, M. R., Schlegel, D. J., Strauss, M. A., Brinkmann, J., Finkbeiner, D., Fukugita, M., Gunn, J. E., Hogg, D. W., Ivezić, Ž., Knapp, G. R., Lupton, R. H., Munn, J. A., Schneider, D. P., Tegmark, M., and Zehavi, I. (2005b). New York University Value-Added Galaxy Catalog: A Galaxy Catalog Based on New Public Surveys. *AJ*, 129:2562–2578.

Bluck, A. F. L., Mendel, J. T., Ellison, S. L., Moreno, J., Simard, L., Patton, D. R., and Starkenburg, E. (2014). Bulge mass is king: the dominant role of the bulge in determining the fraction of passive galaxies in the Sloan Digital Sky Survey. *MNRAS*, 441:599–629.

Bluck, A. F. L., Mendel, J. T., Ellison, S. L., Patton, D. R., Simard, L., Henriques, B. M. B., Torrey, P., Teimoorinia, H., Moreno, J., and Starkenburg, E. (2016). The impact of galactic properties and environment on the quenching of central and satellite galaxies: a comparison between SDSS, Illustris and L-Galaxies. *MNRAS*, 462:2559–2586.

Böhringer, H., Briel, U. G., Schwarz, R. A., Voges, W., Hartner, G., and Trümper, J. (1994). The structure of the Virgo cluster of galaxies from Rosat X-ray images. *Nature*, 368:828–831.

Bournaud, F., Chapon, D., Teyssier, R., Powell, L. C., Elmegreen, B. G., Elmegreen, D. M., Duc, P.-A., Contini, T., Epinat, B., and Shapiro, K. L. (2011a). Hydrodynamics of High-redshift Galaxy Collisions: From Gas-rich Disks to Dispersion-dominated Mergers and Compact Spheroids. *ApJ*, 730:4.

Bournaud, F. and Combes, F. (2002). Gas accretion on spiral galaxies: Bar formation and renewal. *A&A*, 392:83–102.

Bournaud, F., Combes, F., and Semelin, B. (2005). The lifetime of galactic bars: central mass concentrations and gravity torques. *MNRAS*, 364:L18–L22.

Bournaud, F., Dekel, A., Teyssier, R., Cacciato, M., Daddi, E., Juneau, S., and Shankar, F. (2011b). Black Hole Growth and Active Galactic Nuclei Obscuration by Instability-driven Inflows in High-redshift Disk Galaxies Fed by Cold Streams. *ApJ*, 741:L33.

Bower, R. G., Benson, A. J., Malbon, R., Helly, J. C., Frenk, C. S., Baugh, C. M., Cole, S., and Lacey, C. G. (2006). Breaking the hierarchy of galaxy formation. *MNRAS*, 370:645–655.

Brammer, G. B., Whitaker, K. E., van Dokkum, P. G., Marchesini, D., Labbé, I., Franx, M., Kriek, M., Quadri, R. F., Illingworth, G., Lee, K.-S., Muzzin, A., and Rudnick, G. (2009). The Dead Sequence: A Clear Bimodality in Galaxy Colors from z = 0 to z = 2.5. *ApJ*, 706:L173–L177.

Brinchmann, J., Charlot, S., White, S. D. M., Tremonti, C., Kauffmann, G., Heckman, T., and Brinkmann, J. (2004). The physical properties of star-forming galaxies in the low-redshift Universe. *MNRAS*, 351:1151–1179.

Brooks, A. (2010). Toward the Formation of Realistic Galaxy Disks. In Stanford, L. M., Green, J. D., Hao, L., and Mao, Y., editors, *New Horizons in Astronomy: Frank N. Bash Symposium 2009*, volume 432 of *Astronomical Society of the Pacific Conference Series*, page 17.

Brooks, A., Governato, F., Brook, C., Mayer, L., Willman, B., Jonsson, P., Stilp, A., Pope, L., Christensen, C., Wadsley, J., and Quinn, T. (2009). The Formation of Large Galaxy Disks in Low z Major Mergers. In *American Astronomical Society Meeting Abstracts #214*, volume 214 of *American Astronomical Society Meeting Abstracts*, page 737.

Brough, S., Croom, S., Sharp, R., Hopkins, A. M., Taylor, E. N., Baldry, I. K., Gunawardhana, M. L. P., Liske, J., Norberg, P., Robotham, A. S. G., Bauer, A. E., Bland-Hawthorn, J., Colless, M., Foster, C., Kelvin, L. S., Lara-Lopez, M. A., López-Sánchez, Á. R., Loveday, J., Owers, M., Pimbblet, K. A., and Prescott, M. (2013). Galaxy And Mass Assembly: resolving the role of environment in galaxy evolution. *MNRAS*, 435:2903–2917.

Bruzual, G. and Charlot, S. (2003). Stellar population synthesis at the resolution of 2003. *MNRAS*, 344:1000–1028.

Bruzual A., G. (1983). Spectral evolution of galaxies. I - Early-type systems. *ApJ*, 273:105–127.

Bruzual A., G. and Charlot, S. (1993). Spectral evolution of stellar populations using isochrone synthesis. *ApJ*, 405:538–553.

Bryant, J. J., Owers, M. S., Robotham, A. S. G., Croom, S. M., Driver, S. P., Drinkwater, M. J., Lorente, N. P. F., Cortese, L., Scott, N., Colless, M., Schaefer, A., Taylor, E. N., Konstantopoulos, I. S., Allen, J. T., Baldry, I., Barnes, L., Bauer, A. E., Bland-Hawthorn, J., Bloom, J. V., and Brooks, e. a. (2015). The SAMI Galaxy Survey: instrument specification and target selection. *MNRAS*, 447:2857–2879.

Buat, V., Deharveng, J. M., and Donas, J. (1989). Star formation rate and gas surface density in late-type galaxies. *A&A*, 223:42–46.

Bundy, K., Bershady, M. A., Law, D. R., Yan, R., Drory, N., MacDonald, N., Wake, D. A., Cherinka, B., Sánchez-Gallego, J. R., Weijmans, A.-M., Thomas, D., Tremonti, C., Masters, K., Coccato, L., and Diamond-Stanic, e. a. (2015). Overview of the SDSS-IV MaNGA Survey: Mapping nearby Galaxies at Apache Point Observatory. *ApJ*, 798:7.

Calzetti, D. (2013). *Star Formation Rate Indicators*, page 419.

Calzetti, D., Armus, L., Bohlin, R. C., Kinney, A. L., Koornneef, J., and Storchi-Bergmann, T. (2000). The Dust Content and Opacity of Actively Star-forming Galaxies. *ApJ*, 533:682–695.

Cappellari, M. (2009). Voronoi binning: Optimal adaptive tessellations of multi-dimensional data. *ArXiv e-prints*.

Cappellari, M. (2012). pPXF: Penalized Pixel-Fitting stellar kinematics extraction. Astrophysics Source Code Library.

Cappellari, M., Bacon, R., Bureau, M., Damen, M. C., Davies, R. L., de Zeeuw, P. T., Emsellem, E., Falcón-Barroso, J., Krajnović, D., Kuntschner, H., McDermid, R. M., Peletier, R. F., Sarzi, M., van den Bosch, R. C. E., and van de Ven, G. (2006). The SAURON project - IV. The mass-to-light ratio, the virial mass estimator and the Fundamental Plane of elliptical and lenticular galaxies. *MNRAS*, 366:1126–1150.

Cappellari, M. and Copin, Y. (2003). Adaptive spatial binning of integral-field spectroscopic data using Voronoi tessellations. *MNRAS*, 342:345–354.

Cappellari, M., Emsellem, E., Krajnović, D., McDermid, R. M., Scott, N., Verdoes Kleijn, G. A., Young, L. M., Alatalo, K., Bacon, R., Blitz, L., Bois, M., Bournaud, F., Bureau, M., Davies, R. L., Davis, T. A., de Zeeuw, P. T., Duc, P.-A., Khochfar, S., Kuntschner, H., Lablanche, P.-Y., Morganti, R., Naab, T., Oosterloo, T., Sarzi, M., Serra, P., and Weijmans, A.-M. (2011). The ATLAS^{3D} project - I. A volume-limited sample of 260 nearby early-type galaxies: science goals and selection criteria. *MNRAS*, 413:813–836.

Cappellari, M., McDermid, R. M., Alatalo, K., Blitz, L., Bois, M., Bournaud, F., Bureau, M., Crocker, A. F., Davies, R. L., Davis, T. A., de Zeeuw, P. T., Duc, P.-A., Emsellem, E., Khochfar, S., Krajnović, D., Kuntschner, H., Lablanche, P.-Y., Morganti, R., Naab, T., Oosterloo, T., Sarzi, M., Scott, N., Serra, P., Weijmans, A.-M., and Young, L. M. (2012). Systematic variation of the stellar initial mass function in early-type galaxies. *Nature*, 484:485–488.

Cardelli, J. A., Clayton, G. C., and Mathis, J. S. (1989). The relationship between infrared, optical, and ultraviolet extinction. *ApJ*, 345:245–256.

Carlberg, R. G. (1984). Dissipative models for the sequence of elliptical galaxies. *ApJ*, 286:416–421.

Carlesi, E., Hoffman, Y., Sorce, J. G., and Gottlöber, S. (2017). Constraining the mass of the Local Group. *MNRAS*, 465:4886–4894.

Carniani, S., Marconi, A., Maiolino, R., Balmaverde, B., Brusa, M., Cano-Díaz, M., Cicone, C., Comastri, A., Cresci, G., Fiore, F., Feruglio, C., La Franca, F., Mainieri, V., Mannucci, F., Nagao, T., Netzer, H., Piconcelli, E., Risaliti, G., Schneider, R., and Shemmer, O. (2015). Ionised outflows in z ˜ 2.4 quasar host galaxies. *A&A*, 580:A102.

Carollo, C. M., Cibinel, A., Lilly, S. J., Pipino, A., Bonoli, S., Finoguenov, A., Miniati, F., Norberg, P., and Silverman, J. D. (2016). ZENS. IV. Similar Morphological Changes Associated with Mass Quenching and Environment Quenching and the Relative Importance of Bulge Growth versus the Fading of Disks*. *ApJ*, 818:180.

Cayatte, V., Kotanyi, C., Balkowski, C., and van Gorkom, J. H. (1994). A very large array survey of neutral hydrogen in Virgo Cluster spirals. 3: Surface density profiles of the gas. *AJ*, 107:1003–1017.

Chabrier, G. (2003). Galactic Stellar and Substellar Initial Mass Function. *PASP*, 115:763–795.

Charlot, S. and Bruzual, A. G. (1991). Stellar population synthesis revisited. *ApJ*, 367:126–140.

Chester, C. and Roberts, M. S. (1964). Properties of Galaxies: color-magnitude diagram. *AJ*, 69:635.

Cheung, E., Athanassoula, E., Masters, K. L., Nichol, R. C., Bosma, A., Bell, E. F., Faber, S. M., Koo, D. C., Lintott, C., Melvin, T., Schawinski, K., Skibba, R. A., and Willett, K. W. (2013). Galaxy Zoo: Observing Secular Evolution through Bars. *ApJ*, 779:162.

Cheung, E., Faber, S. M., Koo, D. C., Dutton, A. A., Simard, L., McGrath, E. J., Huang, J.-S., Bell, E. F., Dekel, A., Fang, J. J., Salim, S., Barro, G., Bundy, K., Coil, A. L., Cooper, M. C., Conselice, C. J., Davis, M., Domínguez, A., Kassin, S. A., Kocevski, D. D., Koekemoer, A. M., Lin, L., Lotz, J. M., Newman, J. A., Phillips, A. C., Rosario, D. J., Weiner, B. J., and Willmer, C. N. A. (2012). The Dependence of Quenching upon the Inner Structure of Galaxies at 0.5 <= z < 0.8 in the DEEP2/AEGIS Survey. *ApJ*, 760:131.

Cicone, C., Maiolino, R., Sturm, E., Graciá-Carpio, J., Feruglio, C., Neri, R., Aalto, S., Davies, R., Fiore, F., Fischer, J., García-Burillo, S., González-Alfonso, E., Hailey-Dunsheath, S., Piconcelli, E., and Veilleux, S. (2014). Massive molecular outflows and evidence for AGN feedback from CO observations. *A&A*, 562:A21.

Cimatti, A., Cassata, P., Pozzetti, L., Kurk, J., Mignoli, M., Renzini, A., Daddi, E., Bolzonella, M., Brusa, M., Rodighiero, G., Dickinson, M., Franceschini, A., Zamorani, G., Berta, S., Rosati, P., and Halliday, C. (2008). GMASS ultradeep spectroscopy of galaxies at z ˜ 2. II. Superdense passive galaxies: how did they form and evolve? *A&A*, 482:21–42.

Ciotti, L., Lanzoni, B., and Volonteri, M. (2007). The Importance of Dry and Wet Merging on the Formation and Evolution of Elliptical Galaxies. *ApJ*, 658:65–77.

Colless, M., Dalton, G., Maddox, S., Sutherland, W., Norberg, P., Cole, S., Bland-Hawthorn, J., Bridges, T., Cannon, R., Collins, C., Couch, W., Cross, N., Deeley, K., De Propris, R., Driver, S. P., Efstathiou, G., Ellis, R. S., Frenk, C. S., Glazebrook, K., Jackson, C., Lahav, O., Lewis, I., Lumsden, S., Madgwick, D., Peacock, J. A., Peterson, B. A., Price, I., Seaborne, M., and Taylor, K. (2001). The 2dF Galaxy Redshift Survey: spectra and redshifts. *MNRAS*, 328:1039–1063.

Combes, F. and Sanders, R. H. (1981). Formation and properties of persisting stellar bars. *A&A*, 96:164–173.

Conroy, C. (2013). Modeling the Panchromatic Spectral Energy Distributions of Galaxies. *ARA&A*, 51:393–455.

Conroy, C., Graves, G. J., and van Dokkum, P. G. (2014). Early-type Galaxy Archeology: Ages, Abundance Ratios, and Effective Temperatures from Full-spectrum Fitting. *ApJ*, 780:33.

Conroy, C., Shapley, A. E., Tinker, J. L., Santos, M. R., and Lemson, G. (2008). The Varied Fates of z ˜ 2 Star-forming Galaxies. *ApJ*, 679:1192–1203.

Conroy, C., van Dokkum, P. G., and Villaume, A. (2017). The Stellar Initial Mass Function in Early-type Galaxies from Absorption Line Spectroscopy. IV. A Super-Salpeter IMF in the Center of NGC 1407 from Non-parametric Models. *ApJ*, 837:166.

Conroy, C. and Wechsler, R. H. (2009). Connecting Galaxies, Halos, and Star Formation Rates Across Cosmic Time. *ApJ*, 696:620–635.

Cooper, M. C., Newman, J. A., Coil, A. L., Croton, D. J., Gerke, B. F., Yan, R., Davis, M., Faber, S. M., Guhathakurta, P., Koo, D. C., Weiner, B. J., and Willmer, C. N. A. (2007). The DEEP2 galaxy redshift survey: evolution of the colour-density relation at $0.4 < z < 1.35$. *MNRAS*, 376:1445–1459.

Copernicus, N. (1543). *De revolutionibus orbium coelestium*.

Cortese, L., Boissier, S., Boselli, A., Bendo, G. J., Buat, V., Davies, J. I., Eales, S., Heinis, S., Isaak, K. G., and Madden, S. C. (2012). The GALEX view of the Herschel Reference Survey. Ultraviolet structural properties of nearby galaxies. *A&A*, 544:A101.

Cortese, L., Catinella, B., Boissier, S., Boselli, A., and Heinis, S. (2011). The effect of the environment on the H I scaling relations. *MNRAS*, 415:1797–1806.

Courteau, S., Cappellari, M., de Jong, R. S., Dutton, A. A., Emsellem, E., Hoekstra, H., Koopmans, L. V. E., Mamon, G. A., Maraston, C., Treu, T., and Widrow, L. M. (2014). Galaxy masses. *Reviews of Modern Physics*, 86:47–119.

Cowie, L. L., Hu, E. M., Songaila, A., and Egami, E. (1997). The Evolution of the Distribution of Star Formation Rates in Galaxies. *ApJ*, 481:L9–L13.

Croom, S. M., Lawrence, J. S., Bland-Hawthorn, J., Bryant, J. J., Fogarty, L., Richards, S., Goodwin, M., Farrell, T., Miziarski, S., Heald, R., Jones, D. H., Lee, S., Colless, M., Brough, S., Hopkins, A. M., Bauer, A. E., Birchall, M. N., Ellis, S., Horton, A., Leon-Saval, S., Lewis, G., López-Sánchez, Á. R., Min, S.-S., Trinh, C., and Trowland, H. (2012). The Sydney-AAO Multi-object Integral field spectrograph. *MNRAS*, 421:872–893.

Crowe, M. J. (1990). *Theories of the World from Antiquity to the Copernican Revolution*.

Cucciati, O., Iovino, A., Marinoni, C., Ilbert, O., Bardelli, S., Franzetti, P., Le Fèvre, O., Pollo, A., Zamorani, G., Cappi, A., Guzzo, L., McCracken, H. J., Meneux, B., Scaramella, R., Scodeggio, M., Tresse, L., Zucca, E., Bottini, D., Garilli, B., Le Brun, V., Maccagni, D., Picat, J. P., Vettolani, G., Zanichelli, A., Adami, C., Arnaboldi, M., Arnouts, S., Bolzonella, M., Charlot, S., Ciliegi, P., Contini, T., Foucaud, S., Gavignaud, I., Marano, B., Mazure, A., Merighi, R., Paltani, S., Pellò, R., Pozzetti, L., Radovich, M., Bondi, M., Bongiorno, A., Busarello, G., de la Torre, S., Gregorini, L., Lamareille, F., Mathez, G., Mellier, Y., Merluzzi, P., Ripepi, V., Rizzo, D., Temporin, S., and Vergani, D. (2006). The VIMOS VLT Deep Survey: the build-up of the colour-density relation. *A&A*, 458:39–52.

Das, M., Laurikainen, E., Salo, H., and Buta, R. (2008). Variation of bar strength with central velocity dispersion in spiral galaxies. *APSS*, 317:163–168.

Dawson, K. S., Kneib, J.-P., Percival, W. J., Alam, S., Albareti, F. D., Anderson, S. F., Armengaud, E., Aubourg, É., Bailey, S., Bautista, J. E., Berlind, A. A., Bershady, M. A., Beutler, F., Bizyaev, D., Blanton, M. R., Blomqvist, M., Bolton, A. S., Bovy, J., Brandt, W. N., Brinkmann, J., and Brownstein, J. R., e. a. (2016). The SDSS-IV Extended Baryon Oscillation Spectroscopic Survey: Overview and Early Data. *AJ*, 151:44.

de Ravel, L., Kampczyk, P., Le Fèvre, O., Lilly, S. J., Tasca, L., Tresse, L., Lopez-Sanjuan, C., Bolzonella, M., Kovac, K., Abbas, U., Bardelli, S., Bongiorno, A., Caputi, K., Contini, T., Coppa, G., Cucciati, O., de la Torre, S., Dunlop, J. S., Franzetti, P., Garilli, B., Iovino, A., Kneib, J. ., Koekemoer, A. M., Knobel, C., Lamareille, F., Le Borgne, J. ., Le Brun, V., Leauthaud, A., Maier, C., Mainieri, V., Mignoli, M., Pello, R., Peng, Y., Perez Montero, E., Ricciardelli, E., Scodeggio, M., Silverman, J. D., Tanaka, M., Vergani, D., Zamorani, G., Zucca, E., Bottini, D., Cappi, A., Carollo, C. M., Cassata, P., Cimatti, A., Fumana, M., Guzzo, L., Maccagni, D., Marinoni, C., McCracken, H. J., Memeo, P., Meneux, B., Oesch, P., Porciani, C., Pozzetti, L., Renzini, A., Scaramella, R., and Scarlata, C. (2011). The zCOSMOS redshift survey : Influence of luminosity, mass and environment on the galaxy merger rate. *ArXiv e-prints*.

de Zeeuw, P. T., Bureau, M., Emsellem, E., Bacon, R., Carollo, C. M., Copin, Y., Davies, R. L., Kuntschner, H., Miller, B. W., Monnet, G., Peletier, R. F., and Verolme, E. K. (2002). The SAURON project - II. Sample and early results. *MNRAS*, 329:513–530.

Deharveng, J.-M., Sasseen, T. P., Buat, V., Bowyer, S., Lampton, M., and Wu, X. (1994). Ultraviolet observations of galaxies with the FAUST experiment. *A&A*, 289:715–728.

Dekel, A., Devor, J., and Hetzroni, G. (2003). Galactic halo cusp-core: tidal compression in mergers. *MNRAS*, 341:326–342.

Dekel, A., Sari, R., and Ceverino, D. (2009). Formation of Massive Galaxies at High Redshift: Cold Streams, Clumpy Disks, and Compact Spheroids. *ApJ*, 703:785–801.

Dobbs, C. and Baba, J. (2014). Dawes Review 4: Spiral Structures in Disc Galaxies. *PASA*, 31:e035.

Dressler, A. (1980). Galaxy morphology in rich clusters - Implications for the formation and evolution of galaxies. *ApJ*, 236:351–365.

Dressler, A. and Gunn, J. E. (1983). Spectroscopy of galaxies in distant clusters. II - The population of the 3C 295 cluster. *ApJ*, 270:7–19.

Driver, S. P., Hill, D. T., Kelvin, L. S., Robotham, A. S. G., Liske, J., Norberg, P., Baldry, I. K., Bamford, S. P., Hopkins, A. M., Loveday, J., Peacock, J. A., Andrae, E., Bland-Hawthorn, J., Brough, S., Brown, M. J. I., Cameron, E., Ching, J. H. Y., Colless, M., Conselice, C. J., Croom, S. M., Cross, N. J. G., de Propris, R., Dye, S., Drinkwater, M. J., Ellis, S., Graham, A. W., Grootes, M. W., Gunawardhana, M., Jones, D. H., van Kampen, E., Maraston, C., Nichol, R. C., Parkinson, H. R., Phillipps, S., Pimbblet, K., Popescu, C. C., Prescott, M., Roseboom, I. G., Sadler, E. M., Sansom, A. E., Sharp, R. G., Smith, D. J. B., Taylor, E., Thomas, D., Tuffs, R. J., Wijesinghe, D., Dunne, L., Frenk, C. S., Jarvis, M. J., Madore, B. F., Meyer, M. J., Seibert, M., Staveley-Smith, L., Sutherland, W. J., and Warren, S. J. (2011). Galaxy and Mass Assembly (GAMA): survey diagnostics and core data release. *MNRAS*, 413:971–995.

Drory, N., MacDonald, N., Bershady, M. A., Bundy, K., Gunn, J., Law, D. R., Smith, M., Stoll, R., Tremonti, C. A., Wake, D. A., Yan, R., Weijmans, A. M., Byler, N., Cherinka, B., Cope, F., Eigenbrot, A., Harding, P., Holder, D., Huehnerhoff, J., Jaehnig, K., Jansen, T. C., Klaene, M., Paat, A. M., Percival, J., and Sayres, C. (2015). The MaNGA Integral Field Unit Fiber Feed System for the Sloan 2.5 m Telescope. *AJ*, 149:77.

Einstein, A. (1913). Outline of a generalized theory of relativity and of a theory of gravitation: Physical part. *Zeitschrift für Mathematik und Physik*, 62.

Eisenhardt, P. R. M., Wu, J., Tsai, C.-W., Assef, R., Benford, D., Blain, A., Bridge, C., Condon, J. J., Cushing, M. C., Cutri, R., Evans, II, N. J., Gelino, C., Griffith, R. L., Grillmair, C. J., Jarrett, T., Lonsdale, C. J., Masci, F. J., Mason, B. S., Petty, S., Sayers, J., Stanford, S. A., Stern, D., Wright, E. L., and Yan, L. (2012). The First Hyper-luminous Infrared Galaxy Discovered by WISE. *ApJ*, 755:173.

Elbaz, D., Dickinson, M., Hwang, H. S., Díaz-Santos, T., Magdis, G., Magnelli, B., Le Borgne, D., Galliano, F., Pannella, M., Chanial, P., Armus, L., Charmandaris, V., Daddi, E., Aussel, H., Popesso, P., Kartaltepe, J., Altieri, B., Valtchanov, I., Coia, D., Dannerbauer, H., Dasyra, K., Leiton, R., Mazzarella, J., Alexander, D. M., Buat, V., Burgarella, D., Chary, R.-R., Gilli, R., Ivison, R. J., Juneau, S., Le Floc'h, E., Lutz, D., Morrison, G. E., Mullaney, J. R., Murphy, E., Pope, A., Scott, D., Brodwin, M., Calzetti, D., Cesarsky, C., Charlot, S., Dole, H., Eisenhardt, P., Ferguson, H. C., Förster Schreiber, N., Frayer, D., Giavalisco, M., Huynh, M., Koekemoer, A. M., Papovich, C., Reddy, N., Surace, C., Teplitz, H., Yun, M. S., and Wilson, G. (2011). GOODS-Herschel: an infrared main sequence for star-forming galaxies. *A&A*, 533:A119.

Elmegreen, B. G., Elmegreen, D. M., and Hirst, A. C. (2004). A Constant Bar Fraction out to Redshift z ˜ 1 in the Advanced Camera for Surveys Field of the Tadpole Galaxy. *ApJ*, 612:191–201.

Elmegreen, D. M., Elmegreen, B. G., Frogel, J. A., Eskridge, P. B., Pogge, R. W., Gallagher, A., and Iams, J. (2002). Arm Structure in Anemic Spiral Galaxies. *AJ*, 124:777–781.

Eskridge, P. B. and Frogel, J. A. (1999). What is the True Fraction of Barred Spiral Galaxies? *APSS*, 269:427–430.

Eskridge, P. B., Frogel, J. A., Pogge, R. W., Quillen, A. C., Davies, R. L., DePoy, D. L., Houdashelt, M. L., Kuchinski, L. E., Ramírez, S. V., Sellgren, K., Terndrup, D. M., and Tiede, G. P. (2000). The Frequency of Barred Spiral Galaxies in the Near-Infrared. *AJ*, 119:536–544.

Faber, S. M. (1972). Quadratic programming applied to the problem of galaxy population synthesis. *A&A*, 20:361–374.

Faber, S. M., Willmer, C. N. A., Wolf, C., Koo, D. C., Weiner, B. J., Newman, J. A., Im, M., Coil, A. L., Conroy, C., Cooper, M. C., Davis, M., Finkbeiner, D. P., Gerke, B. F., Gebhardt, K., Groth, E. J., Guhathakurta, P., Harker, J., Kaiser, N., Kassin, S., Kleinheinrich, M., Konidaris, N. P., Kron, R. G., Lin, L., Luppino, G., Madgwick, D. S., Meisenheimer, K., Noeske, K. G., Phillips, A. C., Sarajedini, V. L., Schiavon, R. P., Simard, L., Szalay, A. S., Vogt, N. P., and Yan, R. (2007). Galaxy Luminosity Functions to z˜1 from DEEP2 and COMBO-17: Implications for Red Galaxy Formation. *ApJ*, 665:265–294.

Fabian, A. C. (2012). Observational Evidence of Active Galactic Nuclei Feedback. *ARA&A*, 50:455–489.

Fan, L., Lapi, A., De Zotti, G., and Danese, L. (2008). The Dramatic Size Evolution of Elliptical Galaxies and the Quasar Feedback. *ApJ*, 689:L101.

Fogarty, L. M. R., Scott, N., Owers, M. S., Brough, S., Croom, S. M., Pracy, M. B., Houghton, R. C. W., Bland-Hawthorn, J., Colless, M., Davies, R. L., Jones, D. H., Allen, J. T., Bryant, J. J., Goodwin, M., Green, A. W., Konstantopoulos, I. S., Lawrence, J. S., Richards, S., Cortese, L., and Sharp, R. (2014). The SAMI Pilot Survey: the kinematic morphology-density relation in Abell 85, Abell 168 and Abell 2399. *MNRAS*, 443:485–503.

Font, A. S., Bower, R. G., McCarthy, I. G., Benson, A. J., Frenk, C. S., Helly, J. C., Lacey, C. G., Baugh, C. M., and Cole, S. (2008). The colours of satellite galaxies in groups and clusters. *MNRAS*, 389:1619–1629.

Forman, W. and Jones, C. (1982). X-ray-imaging observations of clusters of galaxies. *ARA&A*, 20:547–585.

Franx, M., van Dokkum, P. G., Förster Schreiber, N. M., Wuyts, S., Labbé, I., and Toft, S. (2008). Structure and Star Formation in Galaxies out to z = 3: Evidence for Surface Density Dependent Evolution and Upsizing. *ApJ*, 688:770–788.

Frenk, C. S., Evrard, A. E., White, S. D. M., and Summers, F. J. (1996). Galaxy Dynamics in Clusters. *ApJ*, 472:460.

Friedli, D. and Martinet, L. (1993). Bars Within Bars in Lenticular and Spiral Galaxies - a Step in Secular Evolution. *A&A*, 277:27.

Furlong, M., Bower, R. G., Crain, R. A., Schaye, J., Theuns, T., Trayford, J. W., Qu, Y., Schaller, M., Berthet, M., and Helly, J. C. (2017). Size evolution of normal and compact galaxies in the EAGLE simulation. *MNRAS*, 465:722–738.

Gaffney, C., Gaffney, V., Neubauer, W., Baldwin, E., Chapman, H., Garwood, P., Moulden, H., Sparrow, T., Bates, R., Löcker, K., Hinterleitner, A., Trinks, I., Nau, E., Zitz, T., Floery, S., Verhoeven, G., and Doneus, M. (2012). The stonehenge hidden landscapes project. *Archaeological Prospection*, 19(2):147–155.

Gallazzi, A., Charlot, S., Brinchmann, J., White, S. D. M., and Tremonti, C. A. (2005). The ages and metallicities of galaxies in the local universe. *MNRAS*, 362:41–58.

Galloway, M., Willett, K., Fortson, L., and Galaxy Zoo Science Team (2015). Galaxy Zoo: AGN may be fueled by stellar bars in the local Universe. In *American Astronomical Society Meeting Abstracts*, volume 225 of *American Astronomical Society Meeting Abstracts*, page 144.25.

Gaspari, M., Brighenti, F., and Temi, P. (2012). Mechanical AGN feedback: controlling the thermodynamical evolution of elliptical galaxies. *MNRAS*, 424:190–209.

Gavazzi, G., Consolandi, G., Dotti, M., Fanali, R., Fossati, M., Fumagalli, M., Viscardi, E., Savorgnan, G., Boselli, A., Gutiérrez, L., Hernández Toledo, H., Giovanelli, R., and Haynes, M. P. (2015). Hα3: an Hα imaging survey of HI selected galaxies from ALFALFA. VI. The role of bars in quenching star formation from z = 3 to the present epoch. *A&A*, 580:A116.

Giordano, L., Tran, K.-V. H., Moore, B., and Saintonge, A. (2010). Multi-Wavelength Properties of Barred Galaxies in the Local Universe. I: Virgo Cluster. *ArXiv e-prints*.

Giordano, L., Tran, K.-V. H., Moore, B., and Saintonge, A. (2011). Multi-Wavelength Properties of Barred Galaxies in the Local Universe: Environment and evolution across the Hubble sequence. *ArXiv e-prints*.

Giovanelli, R. and Haynes, M. P. (1985). A 21 CM survey of the Pisces-Perseus supercluster. I - The declination zone +27.5 to +33.5 degrees. *AJ*, 90:2445–2473.

Goddard, D., Thomas, D., Maraston, C., Westfall, K., Etherington, J., Riffel, R., Mallmann, N. D., Zheng, Z., Argudo-Fernández, M., Bershady, M., Bundy, K., Drory, N., Law, D., Yan, R., Wake, D., Weijmans, A., Bizyaev, D., Brownstein, J., Lane, R. R., Maiolino, R., Masters, K., Merrifield, M., Nitschelm, C., Pan, K., Roman-Lopes, A., and Storchi-Bergmann, T. (2017a). SDSS-IV MaNGA: stellar population gradients as a function of galaxy environment. *MNRAS*, 465:688–700.

Goddard, D., Thomas, D., Maraston, C., Westfall, K., Etherington, J., Riffel, R., Mallmann, N. D., Zheng, Z., Argudo-Fernández, M., Lian, J., Bershady, M., Bundy, K., Drory, N., Law, D., Yan, R., Wake, D., Weijmans, A., Bizyaev, D., Brownstein, J., Lane, R. R., Maiolino, R., Masters, K., Merrifield, M., Nitschelm, C., Pan, K., Roman-Lopes, A., Storchi-Bergmann, T., and Schneider, D. P. (2017b). SDSS-IV MaNGA: Spatially resolved star formation histories in galaxies as a function of galaxy mass and type. *MNRAS*, 466:4731–4758.

Goldreich, P. and Lynden-Bell, D. (1965). II. Spiral arms as sheared gravitational instabilities. *MNRAS*, 130:125.

González, R. E., Kravtsov, A. V., and Gnedin, N. Y. (2014). On the Mass of the Local Group. *ApJ*, 793:91.

González Delgado, R. M., Pérez, E., Cid Fernandes, R., García-Benito, R., López Fernández, R., Vale Asari, N., Cortijo-Ferrero, C., de Amorim, A. L., Lacerda, E. A. D., Sánchez, S. F., Lehnert, M. D., and Walcher, C. J. (2017). The spatially-resolved star formation histories of CALIFA galaxies: Implications for galaxy formation. *ArXiv e-prints*.

Goto, T. (2007). Abundance diagnosis of e+a (post-starburst) galaxies. *Monthly Notices of the Royal Astronomical Society*, 377(3):1222–1228.

Guiderdoni, B. and Rocca-Volmerange, B. (1987). A model of spectrophotometric evolution for high-redshift galaxies. *A&A*, 186:1–21.

Gunn, J. E. and Gott, III, J. R. (1972). On the Infall of Matter Into Clusters of Galaxies and Some Effects on Their Evolution. *ApJ*, 176:1.

Gunn, J. E., Siegmund, W. A., Mannery, E. J., Owen, R. E., Hull, C. L., Leger, R. F., Carey, L. N., Knapp, G. R., York, D. G., Boroski, W. N., Kent, S. M., Lupton, R. H., Rockosi, C. M., Evans, M. L., Waddell, P., Anderson, J. E., Annis, J., Barentine, J. C., Bartoszek, L. M., Bastian, S., Bracker, S. B., Brewington, H. J., Briegel, C. I., Brinkmann, J., Brown, Y. J., Carr, M. A., Czarapata, P. C., Drennan, C. C., Dombeck, T., Federwitz, G. R., Gillespie, B. A., Gonzales, C., Hansen, S. U., Harvanek, M., Hayes, J., Jordan, W., Kinney, E., Klaene, M., Kleinman, S. J., Kron, R. G., Kresinski, J., Lee, G., Limmongkol, S., Lindenmeyer, C. W., Long, D. C., Loomis, C. L., McGehee, P. M., Mantsch, P. M., Neilsen, Jr., E. H., Neswold, R. M., Newman, P. R., Nitta, A., Peoples, Jr., J., Pier, J. R., Prieto, P. S., Prosapio, A., Rivetta, C., Schneider, D. P., Snedden, S., and Wang, S.-i. (2006). The 2.5 m Telescope of the Sloan Digital Sky Survey. *AJ*, 131:2332–2359.

Gupta, A., Yuan, T., Martizzi, D., Tran, K.-V. H., and Kewley, L. J. (2017). Survival of Massive Star-forming Galaxies in Cluster Cores Drives Gas-Phase Metallicity Gradients : The Effects of Ram Pressure Stripping. *ArXiv e-prints*.

Hakobyan, A. A., Karapetyan, A. G., Barkhudaryan, L. V., Mamon, G. A., Kunth, D., Petrosian, A. R., Adibekyan, V., Aramyan, L. S., and Turatto, M. (2016). Supernovae and their host galaxies - III. The impact of bars and bulges on the radial distribution of supernovae in disc galaxies. *MNRAS*, 456:2848–2860.

Häring, N. and Rix, H.-W. (2004). On the Black Hole Mass-Bulge Mass Relation. *ApJ*, 604:L89–L92.

Hart, R. E., Bamford, S. P., Hayes, W. B., Cardamone, C. N., Keel, W. C., Kruk, S. J., Lintott, C. J., Masters, K. L., Simmons, B. D., and Smethurst, R. J. (2017). Galaxy Zoo and sparcfire: constraints on spiral arm formation mechanisms from spiral arm number and pitch angles. *MNRAS*, 472:2263–2279.

Heavens, A., Panter, B., Jimenez, R., and Dunlop, J. (2004). The star-formation history of the Universe from the stellar populations of nearby galaxies. *Nature*, 428:625–627.

Heckman, T. M. (1980). An optical and radio survey of the nuclei of bright galaxies - Activity in normal galactic nuclei. *A&A*, 87:152–164.

Heckman, T. M. and Best, P. N. (2014). The Coevolution of Galaxies and Supermassive Black Holes: Insights from Surveys of the Contemporary Universe. *ARA&A*, 52:589–660.

Hernquist, L. (1989). Tidal triggering of starbursts and nuclear activity in galaxies. *Nature*, 340:687–691.

Herschel, W. (1785). Xii. on the construction of the heavens. *Phil. Trans. R. Soc. Lond.*, 75:213–266.

Hirschmann, M., De Lucia, G., Iovino, A., and Cucciati, O. (2013). Isolated galaxies in hierarchical galaxy formation models - present-day properties and environmental histories. *MNRAS*, 433:1479–1491.

Ho, I.-T., Kewley, L. J., Dopita, M. A., Medling, A. M., Allen, J. T., Bland-Hawthorn, J., Bloom, J. V., Bryant, J. J., Croom, S. M., Fogarty, L. M. R., Goodwin, M., Green, A. W., Konstantopoulos, I. S., Lawrence, J. S., López-Sánchez, Á. R., Owers, M. S., Richards, S., and Sharp, R. (2014). The SAMI Galaxy Survey: shocks and outflows in a normal star-forming galaxy. *MNRAS*, 444:3894–3910.

Hopkins, A. M. and Beacom, J. F. (2006). On the Normalization of the Cosmic Star Formation History. *ApJ*, 651:142–154.

Hou, L. and Wang, Y. (2015). The fundamental plane relation of early-type galaxies: environmental dependence. *Research in Astronomy and Astrophysics*, 15:651.

Hubble, E. P. (1925). Cepheids in spiral nebulae. *The Observatory*, 48:139–142.

Hubble, E. P. (1926). Extragalactic nebulae. *ApJ*, 64:321–325.

Hubble, E. P. (1927). The classification of spiral nebulae. *The Observatory*, 50:276–281.

Huertas-Company, M., Aguerri, J. A. L., Bernardi, M., Mei, S., and Sánchez Almeida, J. (2011). Revisiting the Hubble sequence in the SDSS DR7 spectroscopic sample: a publicly available Bayesian automated classification. *A&A*, 525:A157.

Huertas-Company, M., Shankar, F., Mei, S., Bernardi, M., Aguerri, J. A. L., Meert, A., and Vikram, V. (2013). No Evidence for a Dependence of the Mass-Size Relation of Early-type Galaxies on Environment in the Local Universe. *ApJ*, 779:29.

James, P. A., Bretherton, C. F., and Knapen, J. H. (2009). The Hα galaxy survey. VII. The spatial distribution of star formation within disks and bulges. *A&A*, 501:207–220.

James, P. A. and Percival, S. M. (2016). Stellar population constraints on the ages of galactic bars. *MNRAS*, 457:917–925.

James, P. A. and Percival, S. M. (2017). Star formation suppression and bar ages in nearby barred galaxies. *ArXiv e-prints*.

Jones, E., Oliphant, T., Peterson, P., et al. (2001). SciPy: Open source scientific tools for Python. [Online; accessed 13/12/17].

Jorgensen, I., Franx, M., and Kjaergaard, P. (1995). Multicolour CCD surface photometry for E and S0 galaxies in 10 clusters. *MNRAS*, 273:1097–1128.

Kaiser, N. and Squires, G. (1993). Mapping the dark matter with weak gravitational lensing. *ApJ*, 404:441–450.

Kauffmann, G., Heckman, T. M., Tremonti, C., Brinchmann, J., Charlot, S., White, S. D. M., Ridgway, S. E., Brinkmann, J., Fukugita, M., Hall, P. B., Ivezić, Ž., Richards, G. T., and Schneider, D. P. (2003a). The host galaxies of active galactic nuclei. *MNRAS*, 346:1055–1077.

Kauffmann, G., Heckman, T. M., White, S. D. M., Charlot, S., Tremonti, C., Peng, E. W., Seibert, M., Brinkmann, J., Nichol, R. C., SubbaRao, M., and York, D. (2003b). The dependence of star formation history and internal structure on stellar mass for 10^5 low-redshift galaxies. *MNRAS*, 341:54–69.

Kauffmann, G., White, S. D. M., Heckman, T. M., Ménard, B., Brinchmann, J., Charlot, S., Tremonti, C., and Brinkmann, J. (2004). The environmental dependence of the relations between stellar mass, structure, star formation and nuclear activity in galaxies. *MNRAS*, 353:713–731.

Kennicutt, Jr., R. C. (1983). The rate of star formation in normal disk galaxies. *ApJ*, 272:54–67.

Kennicutt, Jr., R. C. (1998a). Star Formation in Galaxies Along the Hubble Sequence. *ARA&A*, 36:189–232.

Kennicutt, Jr., R. C. (1998b). The Global Schmidt Law in Star-forming Galaxies. *ApJ*, 498:541–552.

Kennicutt, Jr., R. C., Tamblyn, P., and Congdon, C. E. (1994). Past and future star formation in disk galaxies. *ApJ*, 435:22–36.

Kewley, L. J., Dopita, M. A., Sutherland, R. S., Heisler, C. A., and Trevena, J. (2001). Theoretical Modeling of Starburst Galaxies. *ApJ*, 556:121–140.

Knapen, J. H., Pérez-Ramírez, D., and Laine, S. (2002). Circumnuclear regions in barred spiral galaxies - II. Relations to host galaxies. *MNRAS*, 337:808–828.

Knobel, C., Lilly, S. J., Woo, J., and Kovač, K. (2015). Quenching of Star Formation in Sloan Digital Sky Survey Groups: Centrals, Satellites, and Galactic Conformity. *ApJ*, 800:24.

Kodama, T. and Arimoto, N. (1997). Origin of the colour-magnitude relation of elliptical galaxies. *A&A*, 320:41–53.

Koopmann, R. A. and Kenney, J. D. P. (2004a). Hα Morphologies and Environmental Effects in Virgo Cluster Spiral Galaxies. *ApJ*, 613:866–885.

Koopmann, R. A. and Kenney, J. D. P. (2004b). Massive Star Formation Rates and Radial Distributions from Hα Imaging of 84 Virgo Cluster and Isolated Spiral Galaxies. *ApJ*, 613:851–865.

Kormendy, J. (2013). *Secular Evolution in Disk Galaxies*, page 1.

Kormendy, J., Fisher, D. B., Cornell, M. E., and Bender, R. (2009). Structure and Formation of Elliptical and Spheroidal Galaxies. *ApJS*, 182:216–309.

Kravtsov, A. V. and Borgani, S. (2012). Formation of Galaxy Clusters. *ARA&A*, 50:353–409.

Kravtsov, A. V., Gnedin, O. Y., and Klypin, A. A. (2004). The Tumultuous Lives of Galactic Dwarfs and the Missing Satellites Problem. *ApJ*, 609:482–497.

Kroupa, P. (2001). On the variation of the initial mass function. *MNRAS*, 322:231–246.

Kruk, S. J., Lintott, C. J., Bamford, S. P., Masters, K. L., Simmons, B. D., Häußler, B., Cardamone, C. N., Hart, R. E., Kelvin, L., Schawinski, K., Smethurst, R. J., and Vika, M. (2017). Galaxy Zoo: Secular evolution of barred galaxies from structural decomposition of multi-band images. *ArXiv e-prints*.

Larson, R. B. and Tinsley, B. M. (1978). Star formation rates in normal and peculiar galaxies. *ApJ*, 219:46–59.

Larson, R. B., Tinsley, B. M., and Caldwell, C. N. (1980). The evolution of disk galaxies and the origin of S0 galaxies. *ApJ*, 237:692–707.

Law, D. R., Cherinka, B., Yan, R., Andrews, B. H., Bershady, M. A., Bizyaev, D., Blanc, G. A., Blanton, M. R., Bolton, A. S., Brownstein, J. R., Bundy, K., Chen, Y., Drory, N., D'Souza, R., Fu, H., Jones, A., Kauffmann, G., MacDonald, N., Masters, K. L., Newman, J. A., Parejko, J. K., Sánchez-Gallego, J. R., Sánchez, S. F., Schlegel, D. J., Thomas, D., Wake, D. A., Weijmans, A.-M., Westfall, K. B., and Zhang, K. (2016). The Data Reduction Pipeline for the SDSS-IV MaNGA IFU Galaxy Survey. *AJ*, 152:83.

Law, D. R., Yan, R., Bershady, M. A., Bundy, K., Cherinka, B., Drory, N., MacDonald, N., Sánchez-Gallego, J. R., Wake, D. A., Weijmans, A.-M., Blanton, M. R., Klaene, M. A., Moran, S. M., Sanchez, S. F., and Zhang, K. (2015). Observing Strategy for the SDSS-IV/MaNGA IFU Galaxy Survey. *AJ*, 150:19.

Lee, G.-H., Park, C., Lee, M. G., and Choi, Y.-Y. (2012a). Dependence of Barred Galaxy Fraction on Galaxy Properties and Environment. *ApJ*, 745:125.

Lee, G.-H., Woo, J.-H., Lee, M. G., Hwang, H. S., Lee, J. C., Sohn, J., and Lee, J. H. (2012b). Do Bars Trigger Activity in Galactic Nuclei? *ApJ*, 750:141.

Lee, N., Sanders, D. B., Casey, C. M., Toft, S., Scoville, N. Z., Hung, C.-L., Le Floc'h, E., Ilbert, O., Zahid, H. J., Aussel, H., Capak, P., Kartaltepe, J. S., Kewley, L. J., Li, Y., Schawinski, K., Sheth, K., and Xiao, Q. (2015). A Turnover in the Galaxy Main Sequence of Star Formation at M $_*$ $\sim$ $10^1$0 M$_\odot$ for Redshifts z $<$ 1.3. *ApJ*, 801:80.

Leitherer, C., Ferguson, H. C., Heckman, T. M., and Lowenthal, J. D. (1995). The Lyman Continuum in Starburst Galaxies Observed with the Hopkins Ultraviolet Telescope. *ApJ*, 454:L19.

Lewis, I., Balogh, M., De Propris, R., Couch, W., Bower, R., Offer, A., Bland-Hawthorn, J., Baldry, I. K., Baugh, C., Bridges, T., Cannon, R., Cole, S., Colless, M., Collins, C., Cross, N., Dalton, G., Driver, S. P., Efstathiou, G., Ellis, R. S., Frenk, C. S., Glazebrook, K., Hawkins, E., Jackson, C., Lahav, O., Lumsden, S., Maddox, S., Madgwick, D., Norberg, P., Peacock, J. A., Percival, W., Peterson, B. A., Sutherland, W., and Taylor, K. (2002). The 2dF Galaxy Redshift Survey: the environmental dependence of galaxy star formation rates near clusters. *MNRAS*, 334:673–683.

Li, C., Gadotti, D. A., Mao, S., and Kauffmann, G. (2009). The clustering of barred galaxies in the local Universe. *MNRAS*, 397:726–732.

Li, C., Wang, E., Lin, L., Bershady, M. A., Bundy, K., Tremonti, C. A., Xiao, T., Yan, R., Bizyaev, D., Blanton, M., Cales, S., Cherinka, B., Cheung, E., Drory, N., Emsellem, E., Fu, H., Gelfand, J., Law, D. R., Lin, L., MacDonald, N., Maraston, C., Masters, K. L., Merrifield, M. R., Pan, K., Sánchez, S. F., Schneider, D. P., Thomas, D., Wake, D., Wang, L., Weijmans, A.-M., Wilkinson, D., Yoachim, P., Zhang, K., and Zheng, T. (2015). P-MaNGA: Gradients in Recent Star Formation Histories as Diagnostics for Galaxy Growth and Death. *ApJ*, 804:125.

Lilly, S. J., Le Fèvre, O., Renzini, A., Zamorani, G., Scodeggio, M., Contini, T., Carollo, C. M., Hasinger, G., Kneib, J.-P., Iovino, A., Le Brun, V., Maier, C., Mainieri, V., Mignoli, M., Silverman, J., and Tasca, L. A. M., e. a. (2007). zCOSMOS: A Large VLT/VIMOS Redshift Survey Covering $0 < z < 3$ in the COSMOS Field. *ApJS*, 172:70–85.

Lin, L., Li, C., He, Y., Xiao, T., and Wang, E. (2017). Bar-induced Central Star Formation as Revealed by Integral Field Spectroscopy from CALIFA. *ApJ*, 838:105.

Lintott, C. J., Schawinski, K., Slosar, A., Land, K., Bamford, S., Thomas, D., Raddick, M. J., Nichol, R. C., Szalay, A., Andreescu, D., Murray, P., and Vandenberg, J. (2008). Galaxy Zoo: morphologies derived from visual inspection of galaxies from the Sloan Digital Sky Survey. *MNRAS*, 389:1179–1189.

Loeb, A. and Peebles, P. J. E. (2003). Cosmological Origin of the Stellar Velocity Dispersions in Massive Early-Type Galaxies. *ApJ*, 589:29–34.

Lundgren, B. F., van Dokkum, P., Franx, M., Labbe, I., Trenti, M., Bouwens, R., Gonzalez, V., Illingworth, G., Magee, D., Oesch, P., and Stiavelli, M. (2014). Tracing the Mass Growth and Star Formation Rate Evolution of Massive Galaxies from z ˜ 6 to z ˜ 1 in the Hubble Ultra-Deep Field. *ApJ*, 780:34.

Madau, P. and Dickinson, M. (2014). Cosmic Star-Formation History. *ARA&A*, 52:415–486.

Madau, P., Pozzetti, L., and Dickinson, M. (1998). The Star Formation History of Field Galaxies. *ApJ*, 498:106–116.

Maiolino, R., Gallerani, S., Neri, R., Cicone, C., Ferrara, A., Genzel, R., Lutz, D., Sturm, E., Tacconi, L. J., Walter, F., Feruglio, C., Fiore, F., and Piconcelli, E. (2012). Evidence of strong quasar feedback in the early Universe. *MNRAS*, 425:L66–L70.

Mandelbaum, R., Seljak, U., Kauffmann, G., Hirata, C. M., and Brinkmann, J. (2006). Galaxy halo masses and satellite fractions from galaxy-galaxy lensing in the Sloan Digital Sky Survey: stellar mass, luminosity, morphology and environment dependencies. *MNRAS*, 368:715–731.

Marconi, A. and Hunt, L. K. (2003). The Relation between Black Hole Mass, Bulge Mass, and Near-Infrared Luminosity. *ApJ*, 589:L21–L24.

Markevitch, M., Ponman, T. J., Nulsen, P. E. J., Bautz, M. W., Burke, D. J., David, L. P., Davis, D., Donnelly, R. H., Forman, W. R., Jones, C., Kaastra, J., Kellogg, E., Kim, D.-W., Kolodziejczak, J., Mazzotta, P., Pagliaro, A., Patel, S., Van Speybroeck, L., Vikhlinin, A., Vrtilek, J., Wise, M., and Zhao, P. (2000). Chandra Observation of Abell 2142: Survival of Dense Subcluster Cores in a Merger. *ApJ*, 541:542–549.

Martig, M., Bournaud, F., Teyssier, R., and Dekel, A. (2009). Morphological Quenching of Star Formation: Making Early-Type Galaxies Red. *ApJ*, 707:250–267.

Martin, D. C., Fanson, J., Schiminovich, D., Morrissey, P., Friedman, P. G., Barlow, T. A., Conrow, T., Grange, R., Jelinsky, P. N., Milliard, B., Siegmund, O. H. W., Bianchi, L., Byun, Y.-I., Donas, J., Forster, K., Heckman, T. M., Lee, Y.-W., Madore, B. F., Malina, R. F., Neff, S. G., Rich, R. M., Small, T., Surber, F., Szalay, A. S., Welsh, B., and Wyder, T. K. (2005). The Galaxy Evolution Explorer: A Space Ultraviolet Survey Mission. *ApJ*, 619:L1–L6.

Martínez, H. J. and Muriel, H. (2011). Relating bars with the environment in the nearby Universe. *MNRAS*, 418:L148–L151.

Masters, K. L., Mosleh, M., Romer, A. K., Nichol, R. C., Bamford, S. P., Schawinski, K., Lintott, C. J., Andreescu, D., Campbell, H. C., Crowcroft, B., Doyle, I., Edmondson, E. M., Murray, P., Raddick, M. J., Slosar, A., Szalay, A. S., and Vandenberg, J. (2010). Galaxy Zoo: passive red spirals. *MNRAS*, 405:783–799.

Masters, K. L., Nichol, R. C., Haynes, M. P., Keel, W. C., Lintott, C., Simmons, B., Skibba, R., Bamford, S., Giovanelli, R., and Schawinski, K. (2012). Galaxy Zoo and ALFALFA: atomic gas and the regulation of star formation in barred disc galaxies. *MNRAS*, 424:2180–2192.

Masters, K. L., Nichol, R. C., Hoyle, B., Lintott, C., Bamford, S. P., Edmondson, E. M., Fortson, L., Keel, W. C., Schawinski, K., Smith, A. M., and Thomas, D. (2011). Galaxy Zoo: bars in disc galaxies. *MNRAS*, 411:2026–2034.

McCarthy, I. G., Babul, A., Bower, R. G., and Balogh, M. L. (2008a). Towards a holistic view of the heating and cooling of the intracluster medium. *MNRAS*, 386:1309–1331.

McCarthy, I. G., Frenk, C. S., Font, A. S., Lacey, C. G., Bower, R. G., Mitchell, N. L., Balogh, M. L., and Theuns, T. (2008b). Ram pressure stripping the hot gaseous haloes of galaxies in groups and clusters. *MNRAS*, 383:593–605.

McCavana, T., Micic, M., Lewis, G. F., Sinha, M., Sharma, S., Holley-Bockelmann, K., and Bland-Hawthorn, J. (2012). The lives of high-redshift mergers. *MNRAS*, 424:361–371.

McConnell, N. J. and Ma, C.-P. (2013). Revisiting the Scaling Relations of Black Hole Masses and Host Galaxy Properties. *ApJ*, 764:184.

McLure, R. J., Pearce, H. J., Dunlop, J. S., Cirasuolo, M., Curtis-Lake, E., Bruce, V. A., Caputi, K. I., Almaini, O., Bonfield, D. G., Bradshaw, E. J., Buitrago, F., Chuter, R., Foucaud, S., Hartley, W. G., and Jarvis, M. J. (2013). The sizes, masses and specific star formation rates of massive galaxies at $1.3 < z < 1.5$: strong evidence in favour of evolution via minor mergers. *MNRAS*, 428:1088–1106.

Meert, A., Vikram, V., and Bernardi, M. (2013). Simulations of single- and two-component galaxy decompositions for spectroscopically selected galaxies from the Sloan Digital Sky Survey. *MNRAS*, 433:1344–1361.

Meert, A., Vikram, V., and Bernardi, M. (2015). A catalogue of 2D photometric decompositions in the SDSS-DR7 spectroscopic main galaxy sample: preferred models and systematics. *MNRAS*, 446:3943–3974.

Meert, A., Vikram, V., and Bernardi, M. (2016). A catalogue of two-dimensional photometric decompositions in the SDSS-DR7 spectroscopic main galaxy sample: extension to g and i bands. *MNRAS*, 455:2440–2452.

Mehlert, D., Thomas, D., Saglia, R. P., Bender, R., and Wegner, G. (2003). Spatially resolved spectroscopy of Coma cluster early-type galaxies. III. The stellar population gradients. *A&A*, 407:423–435.

Mendel, J. T., Simard, L., Ellison, S. L., and Patton, D. R. (2013). Towards a physical picture of star formation quenching: the photometric properties of recently quenched galaxies in the Sloan Digital Sky Survey. *MNRAS*, 429:2212–2227.

Merritt, D. (1984). Relaxation and tidal stripping in rich clusters of galaxies. II. Evolution of the luminosity distribution. *ApJ*, 276:26–37.

Meurer, G. R., Heckman, T. M., Leitherer, C., Kinney, A., Robert, C., and Garnett, D. R. (1995). Starbursts and Star Clusters in the Ultraviolet. *AJ*, 110:2665.

Michałowski, M. J., Dunlop, J. S., Cirasuolo, M., Hjorth, J., Hayward, C. C., and Watson, D. (2012). The stellar masses and specific star-formation rates of submillimetre galaxies. *A&A*, 541:A85.

Mittal, R., Hudson, D. S., Reiprich, T. H., and Clarke, T. (2009). AGN heating and ICM cooling in the HIFLUGCS sample of galaxy clusters. *A&A*, 501:835–850.

Mocz, P., Green, A., Malacari, M., and Glazebrook, K. (2012). The Tully-Fisher relation for 25 000 Sloan Digital Sky Survey galaxies as a function of environment. *MNRAS*, 425:296–310.

Moore, B., Katz, N., Lake, G., Dressler, A., and Oemler, A. (1996). Galaxy harassment and the evolution of clusters of galaxies. *Nature*, 379:613–616.

Moore, B., Lake, G., and Katz, N. (1998). Morphological Transformation from Galaxy Harassment. *ApJ*, 495:139–151.

Moreno, J., Torrey, P., Ellison, S. L., Patton, D. R., Bluck, A. F. L., Bansal, G., and Hernquist, L. (2015). Mapping galaxy encounters in numerical simulations: the spatial extent of induced star formation. *MNRAS*, 448:1107–1117.

Moster, B. P., Naab, T., and White, S. D. M. (2013). Galactic star formation and accretion histories from matching galaxies to dark matter haloes. *MNRAS*, 428:3121–3138.

Naab, T., Johansson, P. H., and Ostriker, J. P. (2009). Minor Mergers and the Size Evolution of Elliptical Galaxies. *ApJ*, 699:L178–L182.

Nagai, D. and Kravtsov, A. V. (2005). The Radial Distribution of Galaxies in Λ Cold Dark Matter Clusters. *ApJ*, 618:557–568.

Nair, P. B. and Abraham, R. G. (2010). On the Fraction of Barred Spiral Galaxies. *ApJ*, 714:L260–L264.

Navarro, J. F., Frenk, C. S., and White, S. D. M. (1997). A Universal Density Profile from Hierarchical Clustering. *ApJ*, 490:493–508.

Noeske, K. G., Weiner, B. J., Faber, S. M., Papovich, C., Koo, D. C., Somerville, R. S., Bundy, K., Conselice, C. J., Newman, J. A., Schiminovich, D., Le Floc'h, E., Coil, A. L., Rieke, G. H., Lotz, J. M., Primack, J. R., Barmby, P., Cooper, M. C., Davis, M., Ellis, R. S., Fazio, G. G., Guhathakurta, P., Huang, J., Kassin, S. A., Martin, D. C., Phillips, A. C., Rich, R. M., Small, T. A., Willmer, C. N. A., and Wilson, G. (2007). Star Formation in AEGIS Field Galaxies since z=1.1: The Dominance of Gradually Declining Star Formation, and the Main Sequence of Star-forming Galaxies. *ApJ*, 660:L43–L46.

Noll, S., Burgarella, D., Giovannoli, E., Buat, V., Marcillac, D., and Muñoz-Mateos, J. C. (2009). Analysis of galaxy spectral energy distributions from far-UV to far-IR with CIGALE: studying a SINGS test sample. *A&A*, 507:1793–1813.

North, J. (1997). *Stonehenge: Ritual Origins and Astronomy*.

Oman, K. A. and Hudson, M. J. (2016). Satellite quenching time-scales in clusters from projected phase space measurements matched to simulated orbits. *MNRAS*, 463:3083–3095.

O'Mill, A. L., Padilla, N., and García Lambas, D. (2008). Evolution of environment-dependent galaxy properties in the Sloan Digital Sky Survey. *MNRAS*, 389:1763–1770.

Ostriker, J. P. and Peebles, P. J. E. (1973). A Numerical Study of the Stability of Flattened Galaxies: or, can Cold Galaxies Survive? *ApJ*, 186:467–480.

Ouchi, M., Shimasaku, K., Akiyama, M., Sekiguchi, K., Furusawa, H., Okamura, S., Kashikawa, N., Iye, M., Kodama, T., Saito, T., Sasaki, T., Simpson, C., Takata, T., Yamada, T., Yamanoi, H., Yoshida, M., and Yoshida, M. (2005). The Discovery of Primeval Large-Scale Structures with Forming Clusters at Redshift 6. *ApJ*, 620:L1–L4.

Page, M. J., Symeonidis, M., and Vieira, J. D., e. a. (2012). The suppression of star formation by powerful active galactic nuclei. *Nature*, 485:213–216.

Papovich, C., Finkelstein, S. L., Ferguson, H. C., Lotz, J. M., and Giavalisco, M. (2011). The rising star formation histories of distant galaxies and implications for gas accretion with time. *MNRAS*, 412:1123–1136.

Pasquali, A. (2015). How environment drives galaxy evolution: Lessons learnt from satellite galaxies. *Astronomische Nachrichten*, 336:505.

Pasquali, A., Gallazzi, A., Fontanot, F., van den Bosch, F. C., De Lucia, G., Mo, H. J., and Yang, X. (2010). Ages and metallicities of central and satellite galaxies: implications for galaxy formation and evolution. *MNRAS*, 407:937–954.

Pasquali, A., Gallazzi, A., and van den Bosch, F. C. (2012). The gas-phase metallicity of central and satellite galaxies in the Sloan Digital Sky Survey. *MNRAS*, 425:273–286.

Patel, S. G., Fumagalli, M., Franx, M., van Dokkum, P. G., van der Wel, A., Leja, J., Labbé, I., Brammer, G., Skelton, R. E., Momcheva, I., Whitaker, K. E., Lundgren, B., Muzzin, A., Quadri, R. F., Nelson, E. J., Wake, D. A., and Rix, H.-W. (2013). The Structural Evolution of Milky-Way-like Star-forming Galaxies since z ˜ 1.3. *ApJ*, 778:115.

Peng, C. Y., Ho, L. C., Impey, C. D., and Rix, H.-W. (2010a). Detailed Decomposition of Galaxy Images. II. Beyond Axisymmetric Models. *AJ*, 139:2097–2129.

Peng, Y., Maiolino, R., and Cochrane, R. (2015). Strangulation as the primary mechanism for shutting down star formation in galaxies. *Nature*, 521:192–195.

Peng, Y.-j., Lilly, S. J., Kovač, K., Bolzonella, M., Pozzetti, L., Renzini, A., Zamorani, G., Ilbert, O., Knobel, C., Iovino, A., Maier, C., Cucciati, O., Tasca, L., Carollo, C. M., Silverman, J., Kampczyk, P., de Ravel, L., Sanders, D., Scoville, N., Contini, T., Mainieri, V., Scodeggio, M., Kneib, J.-P., and Le Fèvre, O., e. a. (2010b). Mass and Environment as Drivers of Galaxy Evolution in SDSS and zCOSMOS and the Origin of the Schechter Function. *ApJ*, 721:193–221.

Pérez, E., Cid Fernandes, R., González Delgado, R. M., García-Benito, R., Sánchez, S. F., Husemann, B., Mast, D., Rodón, J. R., Kupko, D., Backsmann, N., de Amorim, A. L., van de Ven, G., Walcher, J., Wisotzki, L., Cortijo-Ferrero, C., and CALIFA Collaboration (2013). The Evolution of Galaxies Resolved in Space and Time: A View of Inside-out Growth from the CALIFA Survey. *ApJ*, 764:L1.

Poggianti, B. M. and Barbaro, G. (1997). Indicators of star formation: 4000 Å break and Balmer lines. *A&A*, 325:1025–1030.

Rafferty, D. A., McNamara, B. R., and Nulsen, P. E. J. (2008). The Regulation of Cooling and Star Formation in Luminous Galaxies by Active Galactic Nucleus Feedback and the Cooling-Time/Entropy Threshold for the Onset of Star Formation. *ApJ*, 687:899–918.

Rees, M. J. and Ostriker, J. P. (1977). Cooling, dynamics and fragmentation of massive gas clouds - Clues to the masses and radii of galaxies and clusters. *MNRAS*, 179:541–559.

Renzini, A. and Buzzoni, A. (1986). Global properties of stellar populations and the spectral evolution of galaxies. In Chiosi, C. and Renzini, A., editors, *Spectral Evolution of Galaxies*, volume 122 of *Astrophysics and Space Science Library*, pages 195–231.

Renzini, A. and Peng, Y.-j. (2015). An Objective Definition for the Main Sequence of Star-forming Galaxies. *ApJ*, 801:L29.

Riechers, D. A., Leung, T. K. D., Ivison, R. J., Pérez-Fournon, I., Lewis, A. J. R., Marques-Chaves, R., Oteo, I., Clements, D. L., Cooray, A., Greenslade, J., Martínez-Navajas, P., Oliver, S., Rigopoulou, D., Scott, D., and Weiss, A. (2017). Rise of the Titans: A Dusty, Hyper-luminous "870 μm Riser" Galaxy at $z \sim 6$. *ApJ*, 850:1.

Riess, A. G., Filippenko, A. V., Challis, P., Clocchiatti, A., Diercks, A., Garnavich, P. M., Gilliland, R. L., Hogan, C. J., Jha, S., Kirshner, R. P., Leibundgut, B., Phillips, M. M., Reiss, D., Schmidt, B. P., Schommer, R. A., Smith, R. C., Spyromilio, J., Stubbs, C., Suntzeff, N. B., and Tonry, J. (1998). Observational Evidence from Supernovae for an Accelerating Universe and a Cosmological Constant. *AJ*, 116:1009–1038.

Roberts, I. (1899). *A Selection of Photographs of Stars, Star-clusters and Nebulae*. The Universal Press, London.

Rubin, V. C., Ford, Jr., W. K., and Thonnard, N. (1980). Rotational properties of 21 SC galaxies with a large range of luminosities and radii, from NGC 4605 /R = 4kpc/ to UGC 2885 /R = 122 kpc/. *ApJ*, 238:471–487.

Salim, S., Lee, J. C., Janowiecki, S., da Cunha, E., Dickinson, M., Boquien, M., Burgarella, D., Salzer, J. J., and Charlot, S. (2016). GALEX-SDSS-WISE Legacy Catalog (GSWLC): Star Formation Rates, Stellar Masses, and Dust Attenuations of 700,000 Low-redshift Galaxies. *ApJS*, 227:2.

Salim, S., Rich, R. M., Charlot, S., Brinchmann, J., Johnson, B. D., Schiminovich, D., Seibert, M., Mallery, R., Heckman, T. M., Forster, K., Friedman, P. G., Martin, D. C., Morrissey, P., Neff, S. G., Small, T., Wyder, T. K., Bianchi, L., Donas, J., Lee, Y.-W., Madore, B. F., Milliard, B., Szalay, A. S., Welsh, B. Y., and Yi, S. K. (2007). UV Star Formation Rates in the Local Universe. *ApJS*, 173:267–292.

Salpeter, E. E. (1955). The Luminosity Function and Stellar Evolution. *ApJ*, 121:161.

Sánchez, S. F., Kennicutt, R. C., Gil de Paz, A., van de Ven, G., Vílchez, J. M., Wisotzki, L., Walcher, C. J., Mast, D., and Aguerri, J. A. L., e. a. (2012). CALIFA, the Calar Alto Legacy Integral Field Area survey. I. Survey presentation. *A&A*, 538:A8.

Sánchez, S. F., Pérez, E., Sánchez-Blázquez, P., García-Benito, R., Ibarra-Mede, H. J., González, J. J., Rosales-Ortega, F. F., Sánchez-Menguiano, L., Ascasibar, Y., Bitsakis, T., Law, D., Cano-Díaz, M., López-Cobá, C., Marino, R. A., Gil de Paz, A., López-Sánchez, A. R., Barrera-Ballesteros, J., Galbany, L., Mast, D., Abril-Melgarejo, V., and Roman-Lopes, A. (2016a). Pipe3D, a pipeline to analyze Integral Field Spectroscopy Data: II. Analysis sequence and CALIFA dataproducts. *Rev. Mex. Astron. Astrofis.*, 52:171–220.

Sánchez, S. F., Pérez, E., Sánchez-Blázquez, P., González, J. J., Rosález-Ortega, F. F., Cano-Dí az, M., López-Cobá, C., Marino, R. A., Gil de Paz, A., Mollá, M., López-Sánchez, A. R., Ascasibar, Y., and Barrera-Ballesteros, J. (2016b). Pipe3D, a pipeline to analyze Integral Field Spectroscopy Data: I. New fitting philosophy of FIT3D. *Rev. Mex. Astron. Astrofis.*, 52:21–53.

Sánchez, S. F., Rosales-Ortega, F. F., Jungwiert, B., Iglesias-Páramo, J., Vílchez, J. M., Marino, R. A., Walcher, C. J., Husemann, B., Mast, D., Monreal-Ibero, A., Cid Fernandes, R., Pérez, E., González Delgado, R., García-Benito, R., Galbany, L., van de Ven, G., Jahnke, K., Flores, H., Bland-Hawthorn, J., López-Sánchez, A. R., Stanishev, V., Miralles-Caballero, D., Díaz, A. I., Sánchez-Blazquez, P., Mollá, M., Gallazzi, A., Papaderos, P., Gomes, J. M., Gruel, N., Pérez, I., Ruiz-Lara, T., Florido, E., de Lorenzo-Cáceres, A., Mendez-Abreu, J., Kehrig, C., Roth, M. M., Ziegler, B., Alves, J., Wisotzki, L., Kupko, D., Quirrenbach, A., Bomans, D., and Califa Collaboration (2013). Mass-metallicity

relation explored with CALIFA. I. Is there a dependence on the star-formation rate? *A&A*, 554:A58.

Sánchez Almeida, J., Elmegreen, B. G., Muñoz-Tuñón, C., and Elmegreen, D. M. (2014). Star formation sustained by gas accretion. *AAPR*, 22:71.

Schaefer, A. L., Croom, S. M., Allen, J. T., Brough, S., Medling, A. M., Ho, I.-T., Scott, N., Richards, S. N., Pracy, M. B., Gunawardhana, M. L. P., Norberg, P., Alpaslan, M., Bauer, A. E., Bekki, K., Bland-Hawthorn, J., Bloom, J. V., Bryant, J. J., Couch, W. J., Driver, S. P., Fogarty, L. M. R., Foster, C., Goldstein, G., Green, A. W., Hopkins, A. M., Konstantopoulos, I. S., Lawrence, J. S., López-Sánchez, A. R., Lorente, N. P. F., Owers, M. S., Sharp, R., Sweet, S. M., Taylor, E. N., van de Sande, J., Walcher, C. J., and Wong, O. I. (2017). The SAMI Galaxy Survey: spatially resolving the environmental quenching of star formation in GAMA galaxies. *MNRAS*, 464:121–142.

Schawinski, K., Thomas, D., Sarzi, M., Maraston, C., Kaviraj, S., Joo, S.-J., Yi, S. K., and Silk, J. (2007). Observational evidence for AGN feedback in early-type galaxies. *MNRAS*, 382:1415–1431.

Schawinski, K., Urry, C. M., Simmons, B. D., Fortson, L., Kaviraj, S., Keel, W. C., Lintott, C. J., Masters, K. L., Nichol, R. C., Sarzi, M., Skibba, R., Treister, E., Willett, K. W., Wong, O. I., and Yi, S. K. (2014). The green valley is a red herring: Galaxy Zoo reveals two evolutionary pathways towards quenching of star formation in early- and late-type galaxies. *MNRAS*, 440:889–907.

Schaye, J., Crain, R. A., Bower, R. G., Furlong, M., Schaller, M., Theuns, T., Dalla Vecchia, C., Frenk, C. S., McCarthy, I. G., Helly, J. C., Jenkins, A., Rosas-Guevara, Y. M., White, S. D. M., Baes, M., Booth, C. M., Camps, P., Navarro, J. F., Qu, Y., Rahmati, A., Sawala, T., Thomas, P. A., and Trayford, J. (2015). The EAGLE project: simulating the evolution and assembly of galaxies and their environments. *MNRAS*, 446:521–554.

Schaye, J., Dalla Vecchia, C., Booth, C. M., Wiersma, R. P. C., Theuns, T., Haas, M. R., Bertone, S., Duffy, A. R., McCarthy, I. G., and van de Voort, F. (2010). The physics driving the cosmic star formation history. *MNRAS*, 402:1536–1560.

Schreiber, C., Pannella, M., Elbaz, D., Béthermin, M., Inami, H., Dickinson, M., Magnelli, B., Wang, T., Aussel, H., Daddi, E., Juneau, S., Shu, X., Sargent, M. T., Buat, V., Faber, S. M., Ferguson, H. C., Giavalisco, M., Koekemoer, A. M., Magdis, G., Morrison, G. E., Papovich, C., Santini, P., and Scott, D. (2015). The Herschel view of the dominant mode of galaxy growth from z = 4 to the present day. *A&A*, 575:A74.

Searle, L., Sargent, W. L. W., and Bagnuolo, W. G. (1973). The History of Star Formation and the Colors of Late-Type Galaxies. *ApJ*, 179:427–438.

Shankar, F., Mei, S., Huertas-Company, M., Moreno, J., Fontanot, F., Monaco, P., Bernardi, M., Cattaneo, A., Sheth, R., Licitra, R., Delaye, L., and Raichoor, A. (2014). Environmental dependence of bulge-dominated galaxy sizes in hierarchical models of galaxy formation. Comparison with the local Universe. *MNRAS*, 439:3189–3212.

Sheth, K., Elmegreen, D. M., Elmegreen, B. G., Capak, P., Abraham, R. G., Athanassoula, E., Ellis, R. S., Mobasher, B., Salvato, M., Schinnerer, E., Scoville, N. Z., Spalsbury, L., Strubbe, L., Carollo, M., Rich, M., and West, A. A. (2008). Evolution of the Bar Fraction in COSMOS: Quantifying the Assembly of the Hubble Sequence. *ApJ*, 675:1141–1155.

Silk, J. (1977). On the fragmentation of cosmic gas clouds. I - The formation of galaxies and the first generation of stars. *ApJ*, 211:638–648.

Skibba, R. A., Masters, K. L., Nichol, R. C., Zehavi, I., Hoyle, B., Edmondson, E. M., Bamford, S. P., Cardamone, C. N., Keel, W. C., Lintott, C., and Schawinski, K. (2012). Galaxy Zoo: the environmental dependence of bars and bulges in disc galaxies. *MNRAS*, 423:1485–1502.

Skibba, R. A., van den Bosch, F. C., Yang, X., More, S., Mo, H., and Fontanot, F. (2011). Are brightest halo galaxies central galaxies? *MNRAS*, 410:417–431.

Skrutskie, M. F., Cutri, R. M., Stiening, R., Weinberg, M. D., Schneider, S., Carpenter, J. M., Beichman, C., Capps, R., Chester, T., Elias, J., Huchra, J., Liebert, J., Lonsdale, C., Monet, D. G., Price, S., Seitzer, P., Jarrett, T., Kirkpatrick, J. D., Gizis, J. E., Howard, E., Evans, T., Fowler, J., Fullmer, L., Hurt, R., Light, R., Kopan, E. L., Marsh, K. A., McCallon, H. L., Tam, R., Van Dyk, S., and Wheelock, S. (2006). The Two Micron All Sky Survey (2MASS). *AJ*, 131:1163–1183.

Smee, S. A., Gunn, J. E., Uomoto, A., Roe, N., Schlegel, D., Rockosi, C. M., Carr, M. A., Leger, F., Dawson, K. S., Olmstead, M. D., Brinkmann, J., Owen, R., Barkhouser, R. H., Honscheid, K., Harding, P., Long, D., Lupton, R. H., and Loomis, C., e. a. (2013). The Multi-object, Fiber-fed Spectrographs for the Sloan Digital Sky Survey and the Baryon Oscillation Spectroscopic Survey. *AJ*, 146:32.

Smethurst, R. J., Lintott, C. J., Bamford, S. P., Hart, R. E., Kruk, S. J., Masters, K. L., Nichol, R. C., and Simmons, B. D. (2017). Galaxy Zoo: the interplay of quenching mechanisms in the group environment. *MNRAS*, 469:3670–3687.

Smethurst, R. J., Lintott, C. J., Simmons, B. D., Schawinski, K., Marshall, P. J., Bamford, S., Fortson, L., Kaviraj, S., Masters, K. L., Melvin, T., Nichol, R. C., Skibba, R. A., and Willett, K. W. (2015). Galaxy Zoo: evidence for diverse star formation histories through the green valley. *MNRAS*, 450:435–453.

Solanes, J. M., Manrique, A., García-Gómez, C., González-Casado, G., Giovanelli, R., and Haynes, M. P. (2001). The H I Content of Spirals. II. Gas Deficiency in Cluster Galaxies. *ApJ*, 548:97–113.

Spindler, A. and Wake, D. (2017). The differing relationships between size, mass, metallicity and core velocity dispersion of central and satellite galaxies. *MNRAS*, 468:333–345.

Spindler, A., Wake, D., Belfiore, F., Bershady, M., Bundy, K., Drory, N., Law, D. R., Masters, K., Sánchez-Gallego, J. R., Thomas, D., Westfall, K., and Wild, V. (2017). SDSS-IV MaNGA: The Spatial Distribution of Star Formation and its Dependence on Mass, Structure and Environment. *ArXiv e-prints*.

Springel, V., Yoshida, N., and White, S. D. M. (2001). GADGET: a code for collisionless and gasdynamical cosmological simulations. *NA*, 6:79–117.

Steidel, C. C., Giavalisco, M., Pettini, M., Dickinson, M., and Adelberger, K. L. (1996). Spectroscopic Confirmation of a Population of Normal Star-forming Galaxies at Redshifts $Z > 3$. *ApJ*, 462:L17.

Stoughton, C., Lupton, R. H., Bernardi, M., Blanton, M. R., Burles, S., Castander, F. J., Connolly, A. J., Eisenstein, D. J., Frieman, J. A., Hennessy, G. S., Hindsley, R. B., Ivezić, Ž., Kent, S., Kunszt, P. Z., Lee, B. C., Meiksin, A., Munn, J. A., Newberg, H. J., Nichol, R. C., Nicinski, T., Pier, J. R., Richards, G. T., Richmond, M. W., Schlegel, D. J., Smith, J. A., Strauss, M. A., SubbaRao, M., Szalay, A. S., Thakar, A. R., Tucker, D. L., Vanden Berk, D. E., and Yanny, B., e. a. (2002). Sloan Digital Sky Survey: Early Data Release. *AJ*, 123:485–548.

Strateva, I., Ivezić, Ž., Knapp, G. R., Narayanan, V. K., Strauss, M. A., Gunn, J. E., Lupton, R. H., Schlegel, D., Bahcall, N. A., Brinkmann, J., Brunner, R. J., Budavári, T., Csabai, I., Castander, F. J., Doi, M., Fukugita, M., Győry, Z., Hamabe, M., Hennessy, G., Ichikawa, T., Kunszt, P. Z., Lamb, D. Q., McKay, T. A., Okamura, S., Racusin, J., Sekiguchi, M., Schneider, D. P., Shimasaku, K., and York, D. (2001). Color Separation of Galaxy Types in the Sloan Digital Sky Survey Imaging Data. *AJ*, 122:1861–1874.

Tacchella, S., Carollo, C. M., Renzini, A., Schreiber, N. M. F., Lang, P., Wuyts, S., Cresci, G., Dekel, A., Genzel, R., Lilly, S. J., Mancini, C., Newman, S., Onodera, M., Shapley, A., Tacconi, L., Woo, J., and Zamorani, G. (2015). Evidence for mature bulges and an inside-out quenching phase 3 billion years after the Big Bang. *Science*, 348:314–317.

Tacconi, L. J., Neri, R., Genzel, R., Combes, F., Bolatto, A., Cooper, M. C., Wuyts, S., Bournaud, F., Burkert, A., Comerford, J., Cox, P., Davis, M., Förster Schreiber, N. M., García-Burillo, S., Gracia-Carpio, J., Lutz, D., Naab, T., Newman, S., Omont, A., Saintonge, A., Shapiro Griffin, K., Shapley, A., Sternberg, A., and Weiner, B. (2013). Phibss: Molecular Gas Content and Scaling Relations in z ˜ 1-3 Massive, Main-sequence Star-forming Galaxies. *ApJ*, 768:74.

Teimoorinia, H., Bluck, A. F. L., and Ellison, S. L. (2016). An artificial neural network approach for ranking quenching parameters in central galaxies. *MNRAS*, 457:2086–2106.

The, L. S. and White, S. D. M. (1986). The mass of the Coma cluster. *AJ*, 92:1248–1253.

Thomas, D., Maraston, C., Bender, R., and Mendes de Oliveira, C. (2005). The Epochs of Early-Type Galaxy Formation as a Function of Environment. *ApJ*, 621:673–694.

Thomas, D., Maraston, C., Schawinski, K., Sarzi, M., and Silk, J. (2010). Environment and self-regulation in galaxy formation. *MNRAS*, 404:1775–1789.

Tinsley, B. M. and Gunn, J. E. (1976). Evolutionary synthesis of the stellar population in elliptical galaxies. I - Ingredients, broad-band colors, and infrared features. *ApJ*, 203:52–62.

Toomre, A. (1977). Theories of spiral structure. *ARA&A*, 15:437–478.

Toomre, A. (1981). What amplifies the spirals. In Fall, S. M. and Lynden-Bell, D., editors, *Structure and Evolution of Normal Galaxies*, pages 111–136.

Torrey, P., Wellons, S., Machado, F., Griffen, B., Nelson, D., Rodriguez-Gomez, V., McKinnon, R., Pillepich, A., Ma, C.-P., Vogelsberger, M., Springel, V., and Hernquist, L. (2015). An analysis of the evolving comoving number density of galaxies in hydrodynamical simulations. *MNRAS*, 454:2770–2786.

Tran, Q. D., Lutz, D., Genzel, R., Rigopoulou, D., Spoon, H. W. W., Sturm, E., Gerin, M., Hines, D. C., Moorwood, A. F. M., Sanders, D. B., Scoville, N., Taniguchi, Y., and Ward, M. (2001). Isocam-Cvf 5-12 Micron Spectroscopy of Ultraluminous Infrared Galaxies. *ApJ*, 552:527–543.

Tully, R. B. and Fisher, J. R. (1977). A new method of determining distances to galaxies. *A&A*, 54:661–673.

Tully, R. B. and Shaya, E. J. (1984). Infall of galaxies into the Virgo cluster and some cosmological constraints. *ApJ*, 281:31–55.

Ulmer, M. P., Wirth, G. D., and Kowalski, M. P. (1992). Clusters in collision? *ApJ*, 397:430–437.

van de Voort, F., Bahé, Y. M., Bower, R. G., Correa, C. A., Crain, R. A., Schaye, J., and Theuns, T. (2017). The environmental dependence of gas accretion on to galaxies: quenching satellites through starvation. *MNRAS*, 466:3460–3471.

van den Bergh, S. (1991). What are anemic galaxies? *PASP*, 103:390.

van den Bosch, F. C., Aquino, D., Yang, X., Mo, H. J., Pasquali, A., McIntosh, D. H., Weinmann, S. M., and Kang, X. (2008a). The importance of satellite quenching for the build-up of the red sequence of present-day galaxies. *MNRAS*, 387:79–91.

van den Bosch, F. C., Pasquali, A., Yang, X., Mo, H. J., Weinmann, S., McIntosh, D. H., and Aquino, D. (2008b). Satellite Ecology: The Dearth of Environment Dependence. *ArXiv e-prints*.

van der Walt, S., Colbert, S. C., and Varoquaux, G. (2011). The numpy array: A structure for efficient numerical computation. *Computing in Science & Engineering*, 13(2):22–30.

van Dokkum, P., Conroy, C., Villaume, A., Brodie, J., and Romanowsky, A. J. (2017). The Stellar Initial Mass Function in Early-type Galaxies from Absorption Line Spectroscopy. III. Radial Gradients. *ApJ*, 841:68.

van Dokkum, P. G., Whitaker, K. E., Brammer, G., Franx, M., Kriek, M., Labbé, I., Marchesini, D., Quadri, R., Bezanson, R., Illingworth, G. D., Muzzin, A., Rudnick, G., Tal, T., and Wake, D. (2010). The Growth of Massive Galaxies Since z = 2. *ApJ*, 709:1018–1041.

Vergani, D., Scodeggio, M., Pozzetti, L., Iovino, A., Franzetti, P., Garilli, B., Zamorani, G., Maccagni, D., Lamareille, F., Le Fèvre, O., Charlot, S., Contini, T., Guzzo, L., Bottini, D., Le Brun, V., Picat, J. P., Scaramella, R., Tresse, L., Vettolani, G., Zanichelli, A., Adami, C., Arnouts, S., Bardelli, S., Bolzonella, M., Cappi, A., Ciliegi, P., Foucaud, S., Gavignaud, I., Ilbert, O., McCracken, H. J., Marano, B., Marinoni, C., Mazure, A., Meneux, B., Merighi, R., Paltani, S., Pellò, R., Pollo, A., Radovich, M., Zucca, E., Bondi, M., Bongiorno, A., Brinchmann, J., Cucciati, O., de la Torre, S., Gregorini, L., Perez-Montero, E., Mellier, Y.,

Merluzzi, P., and Temporin, S. (2008). The VIMOS VLT Deep Survey. Tracing the galaxy stellar mass assembly history over the last 8 Gyr. *A&A*, 487:89–101.

Vieira, J. D., Marrone, D. P., Chapman, S. C., De Breuck, C., Hezaveh, Y. D., Weiβ, A., Aguirre, J. E., Aird, K. A., Aravena, M., Ashby, M. L. N., Bayliss, M., Benson, B. A., Biggs, A. D., Bleem, L. E., Bock, J. J., Bothwell, M., Bradford, C. M., Brodwin, M., Carlstrom, J. E., Chang, C. L., Crawford, T. M., Crites, A. T., de Haan, T., Dobbs, M. A., Fomalont, E. B., Fassnacht, C. D., George, E. M., Gladders, M. D., Gonzalez, A. H., Greve, T. R., Gullberg, B., Halverson, N. W., High, F. W., Holder, G. P., Holzapfel, W. L., Hoover, S., Hrubes, J. D., Hunter, T. R., Keisler, R., Lee, A. T., Leitch, E. M., Lueker, M., Luong-van, D., Malkan, M., McIntyre, V., McMahon, J. J., Mehl, J., Menten, K. M., Meyer, S. S., Mocanu, L. M., Murphy, E. J., Natoli, T., Padin, S., Plagge, T., Reichardt, C. L., Rest, A., Ruel, J., Ruhl, J. E., Sharon, K., Schaffer, K. K., Shaw, L., Shirokoff, E., Spilker, J. S., Stalder, B., Staniszewski, Z., Stark, A. A., Story, K., Vanderlinde, K., Welikala, N., and Williamson, R. (2013). Dusty starburst galaxies in the early Universe as revealed by gravitational lensing. *Nature*, 495:344–347.

Visvanathan, N. (1981). Colour-absolute magnitude relation for spiral galaxies. *A&A*, 100:L20–L22.

Visvanathan, N. and Griersmith, D. (1977). Absolute magnitude-color relation for early type spirals. *A&A*, 59:317–328.

Vorobyov, E. I. and Basu, S. (2005). The Origin of Episodic Accretion Bursts in the Early Stages of Star Formation. *ApJ*, 633:L137–L140.

Wake, D. A., Bundy, K., Diamond-Stanic, A. M., Yan, R., Blanton, M. R., Bershady, M. A., Sánchez-Gallego, J. R., Drory, N., Jones, A., Kauffmann, G., Law, D. R., Li, C., MacDonald, N., Masters, K., Thomas, D., Tinker, J., Weijmans, A.-M., and Brownstein, J. R. (2017). The SDSS-IV MaNGA Sample: Design, Optimization, and Usage Considerations. *AJ*, 154:86.

Wake, D. A., Sheth, R. K., Nichol, R. C., Baugh, C. M., Bland-Hawthorn, J., Colless, M., Couch, W. J., Croom, S. M., de Propris, R., Drinkwater, M. J., Edge, A. C., Loveday, J., Lam, T. Y., Pimbblet, K. A., Roseboom, I. G., Ross, N. P., Schneider, D. P., Shanks, T., and Sharp, R. G. (2008). The 2dF-SDSS LRG and QSO Survey: evolution of the clustering of luminous red galaxies since z = 0.6. *MNRAS*, 387:1045–1062.

Wake, D. A., van Dokkum, P. G., and Franx, M. (2012). Revealing Velocity Dispersion as the Best Indicator of a Galaxy's Color, Compared to Stellar Mass, Surface Mass Density, or Morphology. *ApJ*, 751:L44.

Weinmann, S. M., Kauffmann, G., van den Bosch, F. C., Pasquali, A., McIntosh, D. H., Mo, H., Yang, X., and Guo, Y. (2009). Environmental effects on satellite galaxies: the link between concentration, size and colour profile. *MNRAS*, 394:1213–1228.

Weisz, D. R., Dalcanton, J. J., Williams, B. F., Gilbert, K. M., Skillman, E. D., Seth, A. C., Dolphin, A. E., McQuinn, K. B. W., Gogarten, S. M., Holtzman, J., Rosema, K., Cole, A., Karachentsev, I. D., and Zaritsky, D. (2011). The ACS Nearby Galaxy Survey Treasury. VIII. The Global Star Formation Histories of 60 Dwarf Galaxies in the Local Volume. *ApJ*, 739:5.

Wetzel, A. R. (2011). On the orbits of infalling satellite haloes. *MNRAS*, 412:49–58.

Wetzel, A. R., Tinker, J. L., and Conroy, C. (2012). Galaxy evolution in groups and clusters: star formation rates, red sequence fractions and the persistent bimodality. *MNRAS*, 424:232–243.

Wetzel, A. R., Tinker, J. L., Conroy, C., and van den Bosch, F. C. (2013). Galaxy evolution in groups and clusters: satellite star formation histories and quenching time-scales in a hierarchical Universe. *MNRAS*, 432:336–358.

White, M., Zheng, Z., Brown, M. J. I., Dey, A., and Jannuzi, B. T. (2007). Evidence for Merging or Disruption of Red Galaxies from the Evolution of Their Clustering. *ApJ*, 655:L69–L72.

White, S. D. M. and Frenk, C. S. (1991). Galaxy formation through hierarchical clustering. *ApJ*, 379:52–79.

Willett, K. W., Lintott, C. J., Bamford, S. P., Masters, K. L., Simmons, B. D., Casteels, K. R. V., Edmondson, E. M., Fortson, L. F., Kaviraj, S., Keel, W. C., Melvin, T., Nichol, R. C., Raddick, M. J., Schawinski, K., Simpson, R. J., Skibba, R. A., Smith, A. M., and Thomas, D. (2013). Galaxy Zoo 2: detailed morphological classifications for 304 122 galaxies from the Sloan Digital Sky Survey. *MNRAS*, 435:2835–2860.

Wright, E. L., Eisenhardt, P. R. M., Mainzer, A. K., Ressler, M. E., Cutri, R. M., Jarrett, T., Kirkpatrick, J. D., Padgett, D., McMillan, R. S., Skrutskie, M., Stanford, S. A., Cohen, M., Walker, R. G., Mather, J. C., Leisawitz, D., Gautier, III, T. N., McLean, I., Benford, D., Lonsdale, C. J., Blain, A., Mendez, B., Irace, W. R., Duval, V., Liu, F., Royer, D., Heinrichsen, I., Howard, J., Shannon, M., Kendall, M., Walsh, A. L., Larsen, M., Cardon, J. G., Schick, S., Schwalm, M., Abid, M., Fabinsky, B., Naes, L., and Tsai, C.-W. (2010). The Wide-field Infrared Survey Explorer (WISE): Mission Description and Initial On-orbit Performance. *AJ*, 140:1868–1881.

Yan, R., Bundy, K., Law, D. R., Bershady, M. A., Andrews, B., Cherinka, B., Diamond-Stanic, A. M., Drory, N., MacDonald, N., Sánchez-Gallego, J. R., Thomas, D., Wake, D. A., Weijmans, A.-M., Westfall, K. B., Zhang, K., Aragón-Salamanca, A., Belfiore, F., Bizyaev, D., Blanc, G. A., Blanton, M. R., Brownstein, J., Cappellari, M., D'Souza, R., Emsellem, E., Fu, H., Gaulme, P., Graham, M. T., Goddard, D., Gunn, J. E., Harding, P., Jones, A., Kinemuchi, K., Li, C., Li, H., Maiolino, R., Mao, S., Maraston, C., Masters, K., Merrifield, M. R., Oravetz, D., Pan, K., Parejko, J. K., Sanchez, S. F., Schlegel, D., Simmons, A., Thanjavur, K., Tinker, J., Tremonti, C., van den Bosch, R., and Zheng, Z. (2016a). SDSS-IV MaNGA IFS Galaxy Survey - Survey Design, Execution, and Initial Data Quality. *AJ*, 152:197.

Yan, R., Tremonti, C., Bershady, M. A., Law, D. R., Schlegel, D. J., Bundy, K., Drory, N., MacDonald, N., Bizyaev, D., Blanc, G. A., Blanton, M. R., Cherinka, B., Eigenbrot, A., Gunn, J. E., Harding, P., Hogg, D. W., Sánchez-Gallego, J. R., Sánchez, S. F., Wake, D. A., Weijmans, A.-M., Xiao, T., and Zhang, K. (2016b). SDSS-IV/MaNGA: Spectrophotometric Calibration Technique. *AJ*, 151:8.

Yang, X., Mo, H. J., and van den Bosch, F. C. (2008). Galaxy Groups in the SDSS DR4. II. Halo Occupation Statistics. *ApJ*, 676:248–261.

Yang, X., Mo, H. J., and van den Bosch, F. C. (2009). Galaxy Groups in the SDSS DR4. III. The Luminosity and Stellar Mass Functions. *ApJ*, 695:900–916.

Yang, X., Mo, H. J., van den Bosch, F. C., Pasquali, A., Li, C., and Barden, M. (2007). Galaxy Groups in the SDSS DR4. I. The Catalog and Basic Properties. *ApJ*, 671:153–170.

Yang, X., Mo, H. J., van den Bosch, F. C., Zhang, Y., and Han, J. (2012). Evolution of the Galaxy-Dark Matter Connection and the Assembly of Galaxies in Dark Matter Halos. *ApJ*, 752:41.

York, D. G. and SDSS Collaboration (2000). The Sloan Digital Sky Survey: Technical Summary. *AJ*, 120:1579–1587.

Zana, T., Dotti, M., Capelo, P. R., Bonoli, S., Haardt, F., Mayer, L., and Spinoso, D. (2018). External versus internal triggers of bar formation in cosmological zoom-in simulations. *MNRAS*, 473:2608–2621.

Zheng, Z., Coil, A. L., and Zehavi, I. (2007). Galaxy Evolution from Halo Occupation Distribution Modeling of DEEP2 and SDSS Galaxy Clustering. *ApJ*, 667:760–779.

Zheng, Z., Wang, H., Ge, J., Mao, S., Li, C., Li, R., Mo, H., Goddard, D., Bundy, K., Li, H., Nair, P., Lin, L., Long, R. J., Riffel, R., Thomas, D., Masters, K., Bizyaev, D., Brownstein, J. R., Zhang, K., Law, D. R., Drory, N., Roman Lopes, A., and Malanushenko, O. (2017). SDSS-IV MaNGA: environmental dependence of stellar age and metallicity gradients in nearby galaxies. *MNRAS*, 465:4572–4588.

Appendix A

Two-Source Star Formation Rate Data Model

Here we describe the data structure for the output of the two-source star formation rate model. The following tables show how the data is formatted into the standard FITS file format. Each of the HDUs (except the primary) contains a number of NxN maps of different properties, where N depends on the size of the IFU bundle.

HDU No.	Name	Size	Description
0	Primary	1x1	Contains identifying properties of the galaxy, including RA, DEC, Plate Number, IFU Number. Also contains integrated galaxy properties: Total SFR from H_α, total SFR from D_n4000, total SFR from two-source model, total SSFR, total Stellar Mass, synthetic 3" fibre measurements of SFR, SSFR and Mass, and percentage of spaxels which are Star Forming or AGN/LI(N)ER.
1	SFR_DATA	NxNx9	SFR Maps, in three sets of three. For H_α, D_n4000 and the two-source model, we provide SFR, Star Formation Rate Surface Densities and SSFR.
2	SFR_ERRORS	NxNx9	Propogated errors for each of the SFR Maps in SFR_Data.
3	SFR_MASKS	NxNx9	Bad pixel masks for each of the Maps in SFR_Data.
4	BPT_CLASS	NxNx4	Contains BPT classifications, a map showing which source of SFR is used in the two-source model and a Bitmask detailing the SNR cuts made.
5	RADIAL_MAPS	NxNx4	Radial maps for the galaxy, in units of kpc and r_e.
6	MASS_DATA	NxNx2	Stellar Mass map from Pipe3D and the associated bad pixel mask.
7	Dn4000_DATA	NxNx3	Measurements of D_n4000 from the DAP, with associated errors and bad pixel mask.

Table A.1 Data Model for the FITS files generated in the two-source SFR Model. We detail the structure of the FITS file and what each HDU contains. N is the length of the FITS image and depends on the IFU size.

SFR_DATA		
Channel	Units	Description
SFR_Ha	$M_\odot yr^{-1}$	Star Formation Rate using H_α
SFR_spec_Ha	yr^{-1}	Specific Star Formation Rate using H_α
SFR_surf_Ha	$M_\odot yr^{-1} kpc^{-2}$	Star Formation Rate Surface Density using H_α
SFR_d4000	$M_\odot yr^{-1}$	Star Formation Rate using D_n4000
SFR_spec_d4000	yr^{-1}	Specific Star Formation Rate using D_n4000
SFR_surf_d4000	$M_\odot yr^{-1} kpc^{-2}$	Star Formation Rate Surface Density using D_n4000
SFR_comb	$M_\odot yr^{-1}$	Star Formation Rate using the two-source model
SFR_spec_comb	yr^{-1}	Specific Star Formation Rate using the two-source model
SFR_surf_comb	$M_\odot yr^{-1} kpc^{-2}$	Star Formation Rate Surface Density using the two-source model

Table A.2 Structure of the SFR_Data HDU, which contains the various maps of star formation, as calculated using H_α, D_n4000 and the two-source model. The SFR_ERRORS and SFR_MASKS HDUs follow the same structure.

BPT_CLASS	
Channel	Description
BPT Classification	1,3 = Excess Emission, 2 = Star Forming, 4 = low SNR
BPT Mask	0 = Good pixel, 1 = Bad pixel
SFR Source	1=H_α, 2=D_n4000
SNR Mask	Bitmask: 0=Ha, 1=Hb, 2=OIII, 3=NII, 4=AGN, 5=Low SNR AGN, 6=low SNR

Table A.3 Structure of the BPT_CLASS HDU, which contains information for the emission source of spaxels determined by the BPT diagram, and a bit mask showing which spaxels have low SNR in certain emission lines.

RADIAL_MAPS		
Channel	Units	Description
Raidal_kpc	kpc	Raidal map of the galaxy, in units of kpc.
Raidal_r50	r/r_e	Radial map of the galaxy, in units of effective radii.
Raidal_kpc_mask	N/A	0 = Good pixel, 1 = Bad pixel
Raidal_r50_mask	N/A	0 = Good pixel, 1 = Bad pixel

Table A.4 Structure of the RADIAL_MAPS HDU, which contains maps of the distance form the centre of the galaxy, in units of kpc and effective radii.

MASS_DATA		
Channel	Units	Description
Stellar_Mass	$M_\odot$	Stellar Mass map from Pipe3D.
Mass_Mask	N/A	0 = Good pixel, 1 = Bad pixel

Table A.5 Structure of the MASS_DATA HDU, which contains the stellar mass maps from Pipe3D, in units of solar masses.

D4000_DATA		
Channel	Units	Description
Dn4000	N/A	D_n4000, from the DAP.
Dn4000_Mask	N/A	0 = Good pixel, 1 = Bad pixel
Dn4000_Err	N/A	Inverse Variance of D_n4000 from the DAP.

Table A.6 Structure of the D4000_DATA HDU, which contains the strength of the 4000Å-break, from the Data Analysis Pipeline, and it's associated mask and inverse variances.